



1 **Global Carbon Budget 2023**

2 Pierre Friedlingstein 1,2, Michael O'Sullivan 1, Matthew W. Jones 3, Robbie M. Andrew 4, Dorothee C. E.
3 Bakker 5, Judith Hauck 6, Peter Landschützer 7, Corinne Le Quéré 3, Ingrid T. Lujikx 8, Glen P. Peters 4,
4 Wouter Peters 8,9, Julia Pongratz 10,11, Clemens Schwingshackl 10, Stephen Sitch 1, Josep G. Canadell 12,
5 Philippe Ciais 13, Robert B. Jackson 14, Simone R. Alin 15, Peter Anthoni 16, Leticia Barbero 17, Nicholas R.
6 Bates 18,19, Meike Becker 20,21, Nicolas Bellouin 22, Bertrand Decharme 23, Laurent Bopp 2, Ida Bagus
7 Mandhara Brasika 1,24, Patricia Cadule 25, Matthew A. Chamberlain 26, Naveen Chandra 27, Thi-Tuyet-Trang
8 Chau 13, Frédéric Chevallier 13, Louise P. Chini 28, Margot Cronin 29, Xinyu Dou 30, Kazutaka Enyo 31,
9 Wiley Evans 32, Stefanie Falk 10, Richard A. Feely 15, Liang Feng 33,34, Daniel. J. Ford 1, Thomas Gasser 35,
10 Josefina Ghattas 13, Thanos Gkritzalis 7, Giacomo Grassi 36, Luke Gregor 37, Nicolas Gruber 38, Özgür
11 Gürses 6, Ian Harris 39, Matthew Hefner 40,41, Jens Heinke 42, Richard A. Houghton 43, George C. Hurtt 44,
12 Yosuke Iida 31, Tatiana Ilyina 11, Andrew R. Jacobson 45,46, Atul Jain 47, Tereza Jarníková 48, Annika Jersild
13 11, Fei Jiang 49, Zhe Jin 50,51, Fortunat Joos 52,53, Etsushi Kato 54, Ralph F. Keeling 55, Daniel Kennedy 56,
14 Kees Klein Goldewijk 57, Jürgen Knauer 58,12, Jan Ivar Korsbakken 4, Arne Körtzinger 59, Xin Lan 45,46,
15 Nathalie Lefèvre 60, Hongmei Li 11, Junjie Liu 61,62, Zhiqiang Liu 63, Lei Ma 28, Greg Marland 40,41,
16 Nicolas Mayot 64, Patrick C. McGuire 65, Galen A. McKinley 66, Gesa Meyer 67, Eric J. Morgan 55, David R.
17 Munro 45,68, Shin-Ichiro Nakaoka 69, Yosuke Niwa 69,70, Kevin M. O'Brien 71,15, Are Olsen 20,21,
18 Abdurahman M. Omar 72,21, Tsuneo Ono 73, Melf E. Paulsen 59, Denis Pierrot 74, Katie Pocock 75, Benjamin
19 Poulter 76, Carter M. Powis 77, Gregor Rehder 78, Laure Resplandy 79, Eddy Robertson 80, Christian
20 Rödenbeck 81, Thais M Rosan 1, Jörg Schwinger 21,82, Roland Séférian 83, T. Luke Smallman 33, Stephen M.
21 Smith 77, Reinel Sospedra-Alfonso 84, Qing Sun 52,53, Adrienne J. Sutton 15, Colm Sweeney 46, Shintaro
22 Takao 69, Pieter P. Tans 85, Hanqin Tian 86, Bronte Tilbrook 87,88, Hiroyuki Tsujino 89, Francesco Tubiello
23 90, Guido R. van der Werf 8, Erik van Ooijen 87, Rik Wanninkhof 74, Michio Watanabe 91, Cathy Wilmart-
24 Rousseau 59, Dongxu Yang 92, Xiaojuan Yang 93, Wenping Yuan 94, Xu Yue 95, Sönke Zaehle 81, Jiye Zeng
25 69, Bo Zheng 96

26

27 1 Faculty of Environment, Science and Economy, University of Exeter, Exeter EX4 4QF, UK

28 2 Laboratoire de Météorologie Dynamique / Institut Pierre-Simon Laplace, CNRS, Ecole Normale Supérieure /
29 Université PSL, Sorbonne Université, Ecole Polytechnique, Paris, France

30 3 Tyndall Centre for Climate Change Research, School of Environmental Sciences, University of East Anglia,
31 Norwich Research Park, Norwich NR4 7TJ, UK

32 4 CICERO Center for International Climate Research, Oslo 0349, Norway

33 5 School of Environmental Sciences, University of East Anglia, Norwich NR4 7TJ, UK

34 6 Alfred-Wegener-Institut, Helmholtz-Zentrum für Polar- und Meeresforschung, Am Handelshafen 12, 27570
35 Bremerhaven

36 7 VLIZ Flanders Marine Institute, Jacobsenstraat 1, 8400, Ostend, Belgium

37 8 Wageningen University, Environmental Sciences Group, P.O. Box 47, 6700AA, Wageningen, The
38 Netherlands



- 39 9 University of Groningen, Centre for Isotope Research, Groningen, The Netherlands
40 10 Ludwig-Maximilians-Universität München, Luisenstr. 37, 80333 München, Germany
41 11 Max Planck Institute for Meteorology, Bundesstraße 53, 20146 Hamburg, Germany
42 12 CSIRO Environment, Canberra, ACT 2101, Australia
43 13 Laboratoire des Sciences du Climat et de l'Environnement, LSCE/IPSL, CEA-CNRS-UVSQ, Université
44 Paris-Saclay, F-91198 Gif-sur-Yvette, France
45 14 Department of Earth System Science, Woods Institute for the Environment, and Precourt Institute for
46 Energy, Stanford University, Stanford, CA 94305–2210, United States of America
47 15 National Oceanic and Atmospheric Administration, Pacific Marine Environmental Laboratory
48 (NOAA/PMEL), 7600 Sand Point Way NE, Seattle, WA 98115, USA
49 16 Karlsruhe Institute of Technology, Institute of Meteorology and Climate Research/Atmospheric
50 Environmental Research, 82467 Garmisch-Partenkirchen, Germany
51 17 Rosenstiel School of Marine Atmospheric and Earth Science, Cooperative Institute for Marine and
52 Atmospheric Studies (CIMAS), University of Miami, 4600 Rickenbacker Causeway, Miami, FL, USA
53 18 School of Ocean Futures, Julie Ann Wrigley Global Futures Laboratory, Arizona State University, Tempe,
54 Arizona, AZ 85287-5502, USA
55 19 Bermuda Institute of Ocean Sciences (BIOS), 17 Biological Lane, St. Georges, GE01, Bermuda
56 20 Geophysical Institute, University of Bergen, Allégaten 70, 5007 Bergen, Norway
57 21 Bjerknes Centre for Climate Research, Bergen, Norway
58 22 Department of Meteorology, University of Reading, Reading, RG6 6BB, UK
59 23 CNRM, Université de Toulouse, Météo-France, CNRS, Toulouse, France
60 24 Faculty of Marine Science & Fisheries, University of Udayana, Bali 80361, Indonesia
61 25 CNRS, Institut Pierre-Simon Laplace, Sorbonne Université, Paris, France
62 26 CSIRO Environment, Hobart, TAS, Australia
63 27 Research Institute for Global Change, JAMSTEC, 3173-25 Showa-machi, Kanazawa, Yokohama, 236-0001,
64 Japan
65 28 Department of Geographical Sciences, University of Maryland, College Park, MD 20742, USA
66 29 Marine Institute, Rinville, Oranmore, Co Galway H91 R673, Ireland
67 30 Department of Earth System Science, Tsinghua University, Beijing, China
68 31 Japan Meteorological Agency, 3-6-9 Toranomon, Minato City, Tokyo 105-8431, Japan
69 32 Hakai Institute, 1713 Hyacinthe Bay Rd, Heriot Bay, BC, V0P 1H0, Canada
70 33 National Centre for Earth Observation, University of Edinburgh, Edinburgh, EH9 3FE, UK
71 34 School of Geosciences, University of Edinburgh, UK
72 35 International Institute for Applied Systems Analysis (IIASA), Schlossplatz 1, A-2361 Laxenburg, Austria
73 36 European Commission, Joint Research Centre, 21027 Ispra (VA), Italy
74 37 ETH Zürich, Switzerland
75 38 Environmental Physics Group, Institute of Biogeochemistry and Pollutant Dynamics and Center for Climate
76 Systems Modeling (C2SM), ETH Zürich, Switzerland
77 39 NCAS-Climate, Climatic Research Unit, School of Environmental Sciences, University of East Anglia,
78 Norwich Research Park, Norwich, NR4 7TJ, UK



- 79 40 Research Institute for Environment, Energy, and Economics, Appalachian State University, Boone, North
80 Carolina, USA
81 41 Department of Geological and Environmental Sciences, Appalachian State University, Boone, North
82 Carolina, USA
83 42 Potsdam Institute for Climate Impact Research (PIK), member of the Leibniz Association, P.O. Box 60 12
84 03, 14412 Potsdam, Germany
85 43 Woodwell Climate Research Center, Falmouth, MA 02540, USA
86 44 Department of Geographical Sciences, University of Maryland, College Park, Maryland 20742, USA
87 45 Cooperative Institute for Research in Environmental Sciences (CIRES), University of Colorado, Boulder, CO
88 80305, USA
89 46 National Oceanic and Atmospheric Administration, Global Monitoring Laboratory (NOAA/GML), 325
90 Broadway R/GML, Boulder, CO 80305, USA
91 47 Department of Atmospheric Sciences, University of Illinois, Urbana, IL 61821, USA
92 48 School of Environmental Sciences, University of East Anglia, Norwich Research Park, Norwich NR4 7TJ,
93 UK
94 49 Jiangsu Provincial Key Laboratory of Geographic Information Science and Technology, International
95 Institute for Earth System Science, Nanjing University, Nanjing, 210023, China
96 50 State Key Laboratory of Tibetan Plateau Earth System and Resource Environment, Institute of Tibetan
97 Plateau Research, Chinese Academy of Sciences, Beijing 100101, China
98 51 Institute of Carbon Neutrality, Peking University, Beijing 100871, China
99 52 Climate and Environmental Physics, Physics Institute, University of Bern, Bern, Switzerland
100 53 Oeschger Centre for Climate Change Research, University of Bern, Bern, Switzerland
101 54 Institute of Applied Energy (IAE), Minato-ku, Tokyo 105-0003, Japan
102 55 University of California, San Diego, Scripps Institution of Oceanography, La Jolla, CA 92093-0244, USA
103 56 National Center for Atmospheric Research, Climate and Global Dynamics, Terrestrial Sciences Section,
104 Boulder, CO 80305, USA
105 57 Utrecht University, Faculty of Geosciences, Department IMEW, Copernicus Institute of Sustainable
106 Development, Heidelberglaan 2, P.O. Box 80115, 3508 TC, Utrecht, the Netherlands
107 58 Hawkesbury Institute for the Environment, Western Sydney University, Penrith, New South Wales, Australia
108 59 GEOMAR Helmholtz Centre for Ocean Research, Wischhofstr. 1-3, 24148 Kiel, Germany
109 60 LOCEAN/IPSL laboratory, Sorbonne Université, CNRS/IRD/MNHN, Paris, France
110 61 NASA JPL, USA
111 62 Caltech, USA
112 63 CMA Key Open Laboratory of Transforming Climate Resources to Economy, Chongqing Institute of
113 Meteorological Sciences, Chongqing 401147, China
114 64 University of East Anglia, Norwich, UK
115 65 Department of Meteorology & National Centre for Atmospheric Science (NCAS), University of Reading,
116 Reading, United Kingdom
117 66 Columbia University, USA
118 67 Climate Research Division, Environment and Climate Change Canada, Victoria, BC, Canada



- 119 68 National Oceanic and Atmospheric Administration/Global Monitoring Laboratory (NOAA/GML), 325
120 Broadway R/GML, Boulder, CO 80305, USA
121 69 Earth System Division, National Institute for Environmental Studies, 16-2 Onogawa, Tsukuba, Ibaraki, 305-
122 8506 Japan
123 70 Department of Climate and Geochemistry Research, Meteorological Research Institute, 1-1 Nagamine,
124 Tsukuba, Ibaraki 305-0052, Japan
125 71 Cooperative Institute for Climate, Ocean and Ecosystem Studies (CICOES), University of Washington,
126 Seattle, WA 98105, USA
127 72 NORCE Norwegian Research Centre, Jahnebakken 5, 5007 Bergen, Norway
128 73 Marine Environment Division, Fisheries Resources Institute, Japan Fisheries Research and Education
129 Agency, 2-12-4 Fukuura, Kanazawa-Ku, Yokohama 236-8648, Japan
130 74 National Oceanic & Atmospheric Administration, Atlantic Oceanographic & Meteorological Laboratory
131 (NOAA/AOML), 4301 Rickenbacker Causeway, Miami, FL 33149, USA
132 75 Hakai Institute, 1713 Hyacinthe Bay Rd, Heriot Bay, BC, V0P 1H0, Canada
133 76 NASA Goddard Space Flight Center, Biospheric Sciences Laboratory, Greenbelt, Maryland 20771, USA
134 77 Smith School for Enterprise and the Environment, University of Oxford, Oxford, UK
135 78 Leibniz Institute for Baltic Sea Research Warnemünde (IOW), Seestrasse 15, 18119 Rostock, Germany
136 79 Princeton University, Department of Geosciences and Princeton Environmental Institute, Princeton, NJ, USA
137 80 Met Office Hadley Centre, FitzRoy Road, Exeter EX1 3PB, UK
138 81 Max Planck Institute for Biogeochemistry, P.O. Box 600164, Hans-Knöll-Str. 10, 07745 Jena, Germany
139 82 NORCE Climate & Environment, Jahnebakken 5, 5007 Bergen, Norway
140 83 CNRM (Météo-France/CNRS)-UMR 3589, Toulouse, France
141 84 Canadian Centre for Climate Modelling and Analysis, Victoria BC, Canada
142 85 Institute of Arctic and Alpine Research, University of Colorado, Boulder, CO 80309, USA
143 86 Schiller Institute of Integrated Science and Society, Department of Earth and Environmental Sciences,
144 Boston College, Chestnut Hill, MA 02467, USA
145 87 CSIRO Environment, Castray Esplanade, Hobart, Tasmania 7004, Australia
146 88 Australian Antarctic Partnership Program, University of Tasmania, Hobart, Australia
147 89 JMA Meteorological Research Institute, Japan
148 90 Statistics Division, Food and Agriculture Organization of the United Nations, Via Terme di Caracalla, Rome
149 00153, Italy
150 91 Japan Agency for Marine-Earth Science and Technology (JAMSTEC), 3173-25, Showa-machi, Kanazawa-
151 ku, Yokohama, 236-0001, Japan
152 92 Institute of Atmospheric Physics, Chinese Academy of Sciences
153 93 Environmental Sciences Division and Climate Change Science Institute, Oak Ridge National Laboratory,
154 Oak Ridge, TN, 37831, USA
155 94 School of Atmospheric Sciences, Sun Yat-sen University, Zhuhai, Guangdong 510245, China
156 95 School of Environmental Science and Engineering, Nanjing University of Information Science and
157 Technology (NUIST)



158 96 Shenzhen Key Laboratory of Ecological Remediation and Carbon Sequestration, Institute of Environment
159 and Ecology, Tsinghua Shenzhen International Graduate School, Tsinghua University, Shenzhen 518055, China
160

161 *Correspondence to:* Pierre Friedlingstein (p.friedlingstein@exeter.ac.uk)

162 **Abstract**

163 Accurate assessment of anthropogenic carbon dioxide (CO₂) emissions and their redistribution among the
164 atmosphere, ocean, and terrestrial biosphere in a changing climate is critical to better understand the global
165 carbon cycle, support the development of climate policies, and project future climate change. Here we describe
166 and synthesise data sets and methodology to quantify the five major components of the global carbon budget
167 and their uncertainties. Fossil CO₂ emissions (E_{FOS}) are based on energy statistics and cement production data,
168 while emissions from land-use change (E_{LUC}), mainly deforestation, are based on land-use and land-use change
169 data and bookkeeping models. Atmospheric CO₂ concentration is measured directly, and its growth rate (G_{ATM})
170 is computed from the annual changes in concentration. The ocean CO₂ sink (S_{OCEAN}) is estimated with global
171 ocean biogeochemistry models and observation-based *f*CO₂-products. The terrestrial CO₂ sink (S_{LAND}) is
172 estimated with dynamic global vegetation models. Additional lines of evidence on land and ocean sinks are
173 provided by atmospheric inversions, atmospheric oxygen measurements and Earth System Models. The
174 resulting carbon budget imbalance (B_{IM}), the difference between the estimated total emissions and the
175 estimated changes in the atmosphere, ocean, and terrestrial biosphere, is a measure of imperfect data and
176 understanding of the contemporary carbon cycle. All uncertainties are reported as ±1σ.

177 For the year 2022, E_{FOS} increased by 1.0% relative to 2021, with fossil emissions at 10.2 ± 0.5 GtC yr⁻¹ (9.9 ±
178 0.5 GtC yr⁻¹ when the cement carbonation sink is included), E_{LUC} was 1.2 ± 0.7 GtC yr⁻¹, for a total
179 anthropogenic CO₂ emission (including the cement carbonation sink) of 11.1 ± 0.8 GtC yr⁻¹ (40.7 ± 3.2 GtCO₂
180 yr⁻¹). Also, for 2022, G_{ATM} was 4.6 ± 0.2 GtC yr⁻¹ (2.18 ± 0.1 ppm yr⁻¹), S_{OCEAN} was 2.8 ± 0.4 GtC yr⁻¹ and
181 S_{LAND} was 3.8 ± 0.8 GtC yr⁻¹, with a B_{IM} of -0.1 GtC yr⁻¹ (i.e. total estimated sources marginally too low or
182 sinks too high). The global atmospheric CO₂ concentration averaged over 2022 reached 417.1 ± 0.1 ppm.
183 Preliminary data for 2023, suggest an increase in E_{FOS} relative to 2022 of +1.2% (0.2% to 2.2%) globally, and
184 atmospheric CO₂ concentration reaching 419.2 ppm, more than 50% above pre-industrial level (around 278
185 ppm in 1750). Overall, the mean and trend in the components of the global carbon budget are consistently
186 estimated over the period 1959-2022, with a near-zero overall budget imbalance, although discrepancies of up
187 to around 1 GtC yr⁻¹ persist for the representation of annual to semi-decadal variability in CO₂ fluxes.
188 Comparison of estimates from multiple approaches and observations shows: (1) a persistent large uncertainty
189 in the estimate of land-use changes emissions, (2) a low agreement between the different methods on the
190 magnitude of the land CO₂ flux in the northern extra-tropics, and (3) a discrepancy between the different
191 methods on the strength of the ocean sink over the last decade. This living data update documents changes in
192 the methods and data sets used in this new global carbon budget and the progress in understanding of the
193 global carbon cycle compared with previous publications of this data set.



195 **Executive Summary**

196 **Global fossil CO₂ emissions (including cement carbonation) are expected to further increase in 2023, to**
197 **1.5% above their pre-COVID-19 pandemic 2019 level.** The 2022 emission increase was 0.08 GtC yr⁻¹ (0.31
198 GtCO₂ yr⁻¹) relative to 2021, bringing 2022 fossil CO₂ emissions to 9.9 ± 0.5 GtC yr⁻¹ (36.3 ± 1.8 GtCO₂ yr⁻¹),
199 virtually equal to the emissions level of 2019. Preliminary estimates based on data available suggest fossil CO₂
200 emissions to increase further in 2023, by 1.2% relative to 2022 (0.2% to 2.2%), bringing emissions to 10.0 GtC
201 yr⁻¹ (36.8 GtCO₂ yr⁻¹), 1.5% above the 2019 level.

202 Emissions from coal, oil, and gas in 2023 are expected to be slightly above their 2022 levels (by 1.1%, 1.8% and
203 0.3% respectively). Regionally, fossil emissions in 2022 are expected to decrease by 7.1% in the European
204 Union (0.7 GtC, 2.6 GtCO₂), and by 3.4% in the United States (1.3 GtC, 4.9 GtCO₂), but to increase by 4.0% in
205 China (3.2 GtC, 11.9 GtCO₂), 8.0% in India (0.8 GtC, 3.1 GtCO₂) and 0.9% for the rest of the world (4.2 GtC,
206 15.2 GtCO₂).

207 **Fossil CO₂ emissions decreased in 18 countries during the decade 2013-2022.** Altogether, these 18 countries
208 contribute about 1.9 GtC yr⁻¹ (7.1 GtCO₂) fossil fuel CO₂ emissions over the last decade, representing about
209 20% of world CO₂ fossil emissions.

210 **Global CO₂ emissions from land-use, land-use change, and forestry (LUC) averaged 1.3 ± 0.7 GtC yr⁻¹**
211 **(4.7 ± 2.6 GtCO₂ yr⁻¹) for the 2013-2022 period with a preliminary projection for 2023 of 1.1 ± 0.7 GtC yr⁻¹**
212 **(4.0 ± 2.6 GtCO₂ yr⁻¹). A small decrease over the past two decades is not robust given the large model**
213 **uncertainty.** Emissions from deforestation, the main driver of global gross sources, remain high at around 1.9
214 GtC yr⁻¹ over the 2013-2022 period, highlighting the strong potential of halting deforestation for emissions
215 reductions. Sequestration of 1.3 GtC yr⁻¹ through re-/afforestation and forestry offsets two third of the
216 deforestation emissions. Emissions from other land-use transitions and from peat drainage and peat fire add
217 further, smaller contributions. The highest emitters during 2013-2022 in descending order were Brazil,
218 Indonesia, and the Democratic Republic of the Congo, with these 3 countries contributing more than half of
219 global land-use CO₂ emissions.

220 **The remaining carbon budget for a 50% likelihood to limit global warming to 1.5°C, 1.7°C and 2°C has**
221 **respectively reduced to 75 GtC (275 GtCO₂), 175 GtC (625 GtCO₂) and 315 GtC (1150 GtCO₂) from the**
222 **beginning of 2024, equivalent to around 7, 15 and 28 years, assuming 2023 emissions levels.** Total
223 anthropogenic emissions were 11.1 GtC yr⁻¹ (40.7 GtCO₂ yr⁻¹) in 2022, with a similar preliminary estimate of
224 11.2 GtC yr⁻¹ (40.9 GtCO₂ yr⁻¹) for 2023.

225 **The concentration of CO₂ in the atmosphere is set to reach 419.2 ppm in 2023, 51% above pre-industrial**
226 **levels.** The atmospheric CO₂ growth was 5.2 ± 0.02 GtC yr⁻¹ during the decade 2013-2022 (47% of total CO₂
227 emissions) with a preliminary 2023 growth rate estimate of around 4.0 GtC (1.89 ppm).

228 **The ocean CO₂ sink resumed a more rapid growth in the past two decades after low or no growth during**
229 **the 1991-2002 period, overlaid with imprints of climate variability.** The estimates based on *f*CO₂-products
230 and models diverge with the growth of the ocean CO₂ sink in the past decade being a factor 2.5 larger than in the



231 models. This discrepancy in the trend originates from all latitudes but is largest in the Southern Ocean. The
232 ocean CO₂ sink was 2.9 ± 0.4 GtC yr⁻¹ during the decade 2013-2022 (26% of total CO₂ emissions), and did not
233 grow since 2019 due to a triple La Niña event. A similar value of 2.9 GtC yr⁻¹ is preliminarily estimated for
234 2023, which marks an increase in the sink compared to the last two years due to the transition from La Niña to
235 El Niño conditions in 2023.

236 **The land CO₂ sink continued to increase during the 2013-2022 period primarily in response to increased**
237 **atmospheric CO₂, albeit with large interannual variability.** The land CO₂ sink was 3.3 ± 0.8 GtC yr⁻¹ during
238 the 2013-2022 decade (31% of total CO₂ emissions), 0.4 GtC yr⁻¹ larger than during the previous decade (2000-
239 2009), with a preliminary 2023 estimate of around 3.0 GtC yr⁻¹. Year to year variability in the land sink is about
240 1 GtC yr⁻¹ and dominates the year-to-year changes in the global atmospheric CO₂ concentration, implying that
241 small annual changes in anthropogenic emissions (such as the fossil fuel emission decrease in 2020) are hard to
242 detect in the atmospheric CO₂ observations.

243



244

245 **1 Introduction**

246 The concentration of carbon dioxide (CO₂) in the atmosphere has increased from approximately 278 parts per
247 million (ppm) in 1750 (Gulev et al., 2021), the beginning of the Industrial Era, to 417.1 ± 0.1 ppm in 2022 (Lan
248 et al., 2023; Figure 1). The atmospheric CO₂ increase above pre-industrial levels was, initially, primarily caused
249 by the release of carbon to the atmosphere from deforestation and other land-use change activities (Canadell et
250 al., 2021). While emissions from fossil fuels started before the Industrial Era, they became the dominant source
251 of anthropogenic emissions to the atmosphere from around 1950 and their relative share has continued to
252 increase until present. Anthropogenic emissions occur on top of an active natural carbon cycle that circulates
253 carbon between the reservoirs of the atmosphere, ocean, and terrestrial biosphere on time scales from sub-daily
254 to millennia, while exchanges with geologic reservoirs occur at longer timescales (Archer et al., 2009).

255 The global carbon budget (GCB) presented here refers to the mean, variations, and trends in the perturbation of
256 CO₂ in the environment, referenced to the beginning of the Industrial Era (defined here as 1750). This paper
257 describes the components of the global carbon cycle over the historical period with a stronger focus on the
258 recent period (since 1958, onset of robust atmospheric CO₂ measurements), the last decade (2013-2022), the last
259 year (2022) and the current year (2023). Finally, it provides cumulative emissions from fossil fuels and land-use
260 change since the year 1750 (the pre-industrial period), and since the year 1850 (the reference year for historical
261 simulations in IPCC AR6) (Eyring et al., 2016).

262 We quantify the input of CO₂ to the atmosphere by emissions from human activities, the growth rate of
263 atmospheric CO₂ concentration, and the resulting changes in the storage of carbon in the land and ocean
264 reservoirs in response to increasing atmospheric CO₂ levels, climate change and variability, and other
265 anthropogenic and natural changes (Figure 2). An understanding of this perturbation budget over time and the
266 underlying variability and trends of the natural carbon cycle is necessary to understand the response of natural
267 sinks to changes in climate, CO₂ and land-use change drivers, and to quantify emissions compatible with a given
268 climate stabilisation target.

269 The components of the CO₂ budget that are reported annually in this paper include separate and independent
270 estimates for the CO₂ emissions from (1) fossil fuel combustion and oxidation from all energy and industrial
271 processes; also including cement production and carbonation (E_{FOS} ; GtC yr⁻¹) and (2) the emissions resulting
272 from deliberate human activities on land, including those leading to land-use change (E_{LUC} ; GtC yr⁻¹); and their
273 partitioning among (3) the growth rate of atmospheric CO₂ concentration (G_{ATM} ; GtC yr⁻¹), and the uptake of
274 CO₂ (the ‘CO₂ sinks’) in (4) the ocean (S_{OCEAN} ; GtC yr⁻¹) and (5) on land (S_{LAND} ; GtC yr⁻¹). The CO₂ sinks as
275 defined here conceptually include the response of the land (including inland waters and estuaries) and ocean
276 (including coastal and marginal seas) to elevated CO₂ and changes in climate and other environmental
277 conditions, although in practice not all processes are fully accounted for (see Section 2.10). Global emissions
278 and their partitioning among the atmosphere, ocean and land are in balance in the real world. Due to the
279 combination of imperfect spatial and/or temporal data coverage, errors in each estimate, and smaller terms not
280 included in our budget estimate (discussed in Section 2.10), the independent estimates (1) to (5) above do not



281 necessarily add up to zero. We therefore assess a set of additional lines of evidence derived from global
282 atmospheric inversion system results (Section 2.7), observed changes in oxygen concentration (Section 2.8) and
283 Earth System Models (ESMs) simulations (Section 2.9), all of which closing the global carbon balance. We also
284 estimate a budget imbalance (B_{IM}), which is a measure of the mismatch between the estimated emissions and the
285 estimated changes in the atmosphere, land and ocean, as follows:

$$286 \quad B_{IM} = E_{FOS} + E_{LUC} - (G_{ATM} + S_{OCEAN} + S_{LAND}) \quad (1)$$

287 G_{ATM} is usually reported in ppm yr^{-1} , which we convert to units of carbon mass per year, GtC yr^{-1} , using 1 ppm
288 $= 2.124 \text{ GtC}$ (Ballantyne et al., 2012; Table 1). All quantities are presented in units of gigatonnes of carbon
289 (GtC , 10^{15} gC), which is the same as petagrams of carbon (PgC ; Table 1). Units of gigatonnes of CO_2 (or billion
290 tonnes of CO_2) used in policy are equal to 3.664 multiplied by the value in units of GtC .

291 We also quantify E_{FOS} and E_{LUC} by country, including both territorial and consumption-based accounting for
292 E_{FOS} (see Section 2), and discuss missing terms from sources other than the combustion of fossil fuels (see
293 Section 2.10, Supplement S1 and S2).

294 We now assess carbon dioxide removal (CDR) (see Sect. 2.2 and 2.3). Land-based CDR is significant, but
295 already accounted for in E_{LUC} in equation (1) (Sect 3.2.2). Other CDR methods, not based on vegetation, are
296 currently several orders of magnitude smaller than the other components of the budget (Sect. 3.3), hence these
297 are not included in equation (1), or in the global carbon budget tables or figures (with the exception of Figure 2
298 where CDR is shown primarily for illustrative purpose).

299 The global CO_2 budget has been assessed by the Intergovernmental Panel on Climate Change (IPCC) in all
300 assessment reports (Prentice et al., 2001; Schimel et al., 1995; Watson et al., 1990; Denman et al., 2007; Ciais et
301 al., 2013; Canadell et al., 2021), and by others (e.g. Ballantyne et al., 2012). The Global Carbon Project (GCP,
302 www.globalcarbonproject.org, last access: 27 September 2023) has coordinated this cooperative community
303 effort for the annual publication of global carbon budgets for the year 2005 (Raupach et al., 2007; including
304 fossil emissions only), year 2006 (Canadell et al., 2007), year 2007 (GCP, 2008), year 2008 (Le Quéré et al.,
305 2009), year 2009 (Friedlingstein et al., 2010), year 2010 (Peters et al., 2012a), year 2012 (Le Quéré et al., 2013;
306 Peters et al., 2013), year 2013 (Le Quéré et al., 2014), year 2014 (Le Quéré et al., 2015a; Friedlingstein et al.,
307 2014), year 2015 (Jackson et al., 2016; Le Quéré et al., 2015b), year 2016 (Le Quéré et al., 2016), year 2017 (Le
308 Quéré et al., 2018a; Peters et al., 2017), year 2018 (Le Quéré et al., 2018b; Jackson et al., 2018), year 2019
309 (Friedlingstein et al., 2019; Jackson et al., 2019; Peters et al., 2020), year 2020 (Friedlingstein et al., 2020; Le
310 Quéré et al., 2021), year 2021 (Friedlingstein et al., 2022a; Jackson et al., 2022) and most recently the year 2022
311 (Friedlingstein et al., 2022b). Each of these papers updated previous estimates with the latest available
312 information for the entire time series.

313 We adopt a range of ± 1 standard deviation (σ) to report the uncertainties in our global estimates, representing a
314 likelihood of 68% that the true value will be within the provided range if the errors have a gaussian distribution,
315 and no bias is assumed. This choice reflects the difficulty of characterising the uncertainty in the CO_2 fluxes
316 between the atmosphere and the ocean and land reservoirs individually, particularly on an annual basis, as well
317 as the difficulty of updating the CO_2 emissions from land-use change. A likelihood of 68% provides an



318 indication of our current capability to quantify each term and its uncertainty given the available information.
319 The uncertainties reported here combine statistical analysis of the underlying data, assessments of uncertainties
320 in the generation of the data sets, and expert judgement of the likelihood of results lying outside this range. The
321 limitations of current information are discussed in the paper and have been examined in detail elsewhere
322 (Ballantyne et al., 2015; Zscheischler et al., 2017). We also use a qualitative assessment of confidence level to
323 characterise the annual estimates from each term based on the type, amount, quality, and consistency of the
324 different lines of evidence as defined by the IPCC (Stocker et al., 2013).

325 This paper provides a detailed description of the data sets and methodology used to compute the global carbon
326 budget estimates for the industrial period, from 1750 to 2023, and in more detail for the period since 1959. This
327 paper is updated every year using the format of ‘living data’ to keep a record of budget versions and the changes
328 in new data, revision of data, and changes in methodology that lead to changes in estimates of the carbon
329 budget. Additional materials associated with the release of each new version will be posted at the Global Carbon
330 Project (GCP) website (<http://www.globalcarbonproject.org/carbonbudget>, last access: 27 September 2023),
331 with fossil fuel emissions also available through the Global Carbon Atlas (<http://www.globalcarbonatlas.org>,
332 last access: 27 September 2023). All underlying data used to produce the budget can also be found at
333 <https://globalcarbonbudget.org/> (last access: 27 September 2023). With this approach, we aim to provide the
334 highest transparency and traceability in the reporting of CO₂, the key driver of climate change.

335 2 Methods

336 Multiple organisations and research groups around the world generated the original measurements and data used
337 to complete the global carbon budget. The effort presented here is thus mainly one of synthesis, where results
338 from individual groups are collated, analysed, and evaluated for consistency. We facilitate access to original
339 data with the understanding that primary data sets will be referenced in future work (see Table 2 for how to cite
340 the data sets, and Section on data availability). Descriptions of the measurements, models, and methodologies
341 follow below, with more detailed descriptions of each component provided as Supplementary Information (S1 to
342 S5).

343 This is the 18th version of the global carbon budget and the 12th revised version in the format of a living data
344 update in Earth System Science Data. It builds on the latest published global carbon budget of Friedlingstein et
345 al. (2022b). The main changes this year are: the inclusion of (1) data to year 2022 and a projection for the global
346 carbon budget for year 2023; (2) CO₂ uptake from Carbon Dioxide Removal (CDR); (3) land and ocean net
347 carbon fluxes estimates from changes in atmospheric oxygen concentration; (4) land and ocean net carbon
348 fluxes estimates from ESMS; and (5) revised method to estimate the current year (2023) atmospheric CO₂. The
349 main methodological differences between recent annual carbon budgets (2019 to 2023) are summarised in Table
350 3 and previous changes since 2006 are provided in Table S8.



351 **2.1 Fossil CO₂ emissions (E_{FOS})**

352 **2.1.1 Historical period 1850-2022**

353 The estimates of global and national fossil CO₂ emissions (E_{FOS}) include the oxidation of fossil fuels through
354 both combustion (e.g., transport, heating) and chemical oxidation (e.g. carbon anode decomposition in
355 aluminium refining) activities, and the decomposition of carbonates in industrial processes (e.g. the production
356 of cement). We also include CO₂ uptake from the cement carbonation process. Several emissions sources are not
357 estimated or not fully covered: coverage of emissions from lime production are not global, and decomposition of
358 carbonates in glass and ceramic production are included only for the “Annex 1” countries of the United Nations
359 Framework Convention on Climate Change (UNFCCC) for lack of activity data. These omissions are
360 considered to be minor. Short-cycle carbon emissions - for example from combustion of biomass - are not
361 included here but are accounted for in the CO₂ emissions from land use (see Section 2.2).

362 Our estimates of fossil CO₂ emissions rely on data collection by many other parties. Our goal is to produce the
363 best estimate of this flux, and we therefore use a prioritisation framework to combine data from different
364 sources that have used different methods, while being careful to avoid double counting and undercounting of
365 emissions sources. The CDIAC-FF emissions dataset, derived largely from UN energy data, forms the
366 foundation, and we extend emissions to year Y-1 using energy growth rates reported by the Energy Institute (a
367 dataset formally produced by BP). We then proceed to replace estimates using data from what we consider to be
368 superior sources, for example Annex 1 countries’ official submissions to the UNFCCC. All data points are
369 potentially subject to revision, not just the latest year. For full details see Andrew and Peters (2022).

370 Other estimates of global fossil CO₂ emissions exist, and these are compared by Andrew (2020a). The most
371 common reason for differences in estimates of global fossil CO₂ emissions is a difference in which emissions
372 sources are included in the datasets. Datasets such as those published by the energy company BP, the US Energy
373 Information Administration, and the International Energy Agency’s ‘CO₂ emissions from fuel combustion’ are
374 all generally limited to emissions from combustion of fossil fuels. In contrast, datasets such as PRIMAP-hist,
375 CEDS, EDGAR, and GCP’s dataset aim to include all sources of fossil CO₂ emissions. See Andrew (2020a) for
376 detailed comparisons and discussion.

377 Cement absorbs CO₂ from the atmosphere over its lifetime, a process known as ‘cement carbonation’. We
378 estimate this CO₂ sink, from 1931, onwards as the average of two studies in the literature (Cao et al., 2020; Guo
379 et al., 2021). Both studies use the same model, developed by Xi et al. (2016), with different parameterisations
380 and input data, with the estimate of Guo and colleagues being a revision of Xi et al. (2016). The trends of the
381 two studies are very similar. Since carbonation is a function of both current and previous cement production, we
382 extend these estimates to 2022 by using the growth rate derived from the smoothed cement emissions (10-year
383 smoothing) fitted to the carbonation data. In the present budget, we always include the cement carbonation
384 carbon sink in the fossil CO₂ emission component (E_{FOS}).

385 We use the Kaya Identity for a simple decomposition of CO₂ emissions into the key drivers (Raupach et al.,
386 2007). While there are variations (Peters et al., 2017), we focus here on a decomposition of CO₂ emissions into
387 population, GDP per person, energy use per GDP, and CO₂ emissions per energy. Multiplying these individual



388 components together returns the CO₂ emissions. Using the decomposition, it is possible to attribute the change
389 in CO₂ emissions to the change in each of the drivers. This method gives a first-order understanding of what
390 causes CO₂ emissions to change each year.

391 **2.1.2 2023 projection**

392 We provide a projection of global fossil CO₂ emissions in 2022 by combining separate projections for China,
393 USA, EU, India, and for all other countries combined. The methods are different for each of these. For China we
394 combine monthly fossil fuel production data from the National Bureau of Statistics and trade data from the
395 Customs Administration, giving us partial data for the growth rates to date of natural gas, petroleum, and
396 cement, and of the apparent consumption itself for raw coal. We then use a regression model to project full-year
397 emissions based on historical observations. For the USA our projection is taken directly from the Energy
398 Information Administration's (EIA) Short-Term Energy Outlook (EIA, 2023), combined with the year-to-date
399 growth rate of cement clinker production. For the EU we use monthly energy data from Eurostat to derive
400 estimates of monthly CO₂ emissions through July, with coal emissions extended through September using a
401 statistical relationship with reported electricity generation from coal and other factors. For natural gas we use
402 Holt-Winters to project the last four months of the year. EU emissions from oil are derived using the EIA's
403 projection of oil consumption for Europe. EU cement emissions are based on available year-to-date data from
404 three of the largest producers, Germany, Poland, and Spain. India's projected emissions are derived from
405 estimates through August (July for coal) using the methods of Andrew (2020b) and extrapolated assuming
406 seasonal patterns from before 2019. Emissions for the rest of the world are derived using projected growth in
407 economic production from the IMF (2023) combined with extrapolated changes in emissions intensity of
408 economic production. More details on the E_{FOS} methodology and its 2023 projection can be found in
409 Supplement S.1.

410 **2.2 CO₂ emissions from land-use, land-use change and forestry (E_{LUC})**

411 **2.2.1 Historical period 1850-2022**

412 The net CO₂ flux from land-use, land-use change and forestry (E_{LUC}, called land-use change emissions in the
413 rest of the text) includes CO₂ fluxes from deforestation, afforestation, logging and forest degradation (including
414 harvest activity), shifting cultivation (cycle of cutting forest for agriculture, then abandoning), and regrowth of
415 forests (following wood harvest or agriculture abandonment). Emissions from peat burning and peat drainage
416 are added from external datasets, peat drainage being averaged from three spatially explicit independent datasets
417 (see Supplement S.2.1).

418 Three bookkeeping approaches (updated estimates each of BLUE (Hansis et al., 2015), OSCAR (Gasser et al.,
419 2020), and H&C2023 (Houghton and Castanho, 2023)) were used to quantify gross emissions and gross
420 removals and the resulting net E_{LUC}. Uncertainty estimates were derived from the Dynamic Global Vegetation
421 Models (DGVMs) ensemble for the time period prior to 1960, and using for the recent decades an uncertainty
422 range of ±0.7 GtC yr⁻¹, which is a semi-quantitative measure for annual and decadal emissions and reflects our



423 best value judgement that there is at least 68% chance ($\pm 1\sigma$) that the true land-use change emission lies within
424 the given range, for the range of processes considered here.

425 Our E_{LUC} estimates follow the definition of global carbon cycle models of CO_2 fluxes related to land use and
426 land management and differ from IPCC definitions adopted in National GHG Inventories (NGHGI) for
427 reporting under the UNFCCC, which additionally generally include, through adoption of the IPCC so-called
428 managed land proxy approach, the terrestrial fluxes occurring on all land that countries define as managed. This
429 partly includes fluxes due to environmental change (e.g. atmospheric CO_2 increase), which are part of S_{LAND} in
430 our definition. This causes the global emission estimates to be smaller for NGHGI than for the global carbon
431 budget definition (Grassi et al., 2018). The same is the case for the Food Agriculture Organization (FAO)
432 estimates of carbon fluxes on forest land, which include both anthropogenic and natural sources on managed
433 land (Tubiello et al., 2021). We translate the two definitions to each other, to provide a comparison of the
434 anthropogenic carbon budget to the official country reporting to the climate convention.

435 E_{LUC} contains a range of fluxes that are related to Carbon Dioxide Removal (CDR). CDR can be defined as the
436 set of anthropogenic activities that remove CO_2 from the atmosphere and store it in durable form, such as in
437 forest biomass and soils, long-lived products, or in geological or ocean reservoirs. We quantify vegetation-based
438 CDR that is implicitly or explicitly captured by land-use fluxes consistent with our updated model estimates
439 (CDR not based on vegetation is discussed in Section 2.3; IPCC, 2023). We quantify re/afforestation from the
440 three bookkeeping estimates by separating forest regrowth in shifting cultivation cycles from permanent
441 increases in forest cover (see Supplement C.2.1). The latter count as CDR, but it should be noted that the
442 permanence of the storage under climate risks such as fire is increasingly questioned. Other CDR activities
443 contained in E_{LUC} include the transfer of carbon to harvested wood products (HWP), which is represented by the
444 bookkeeping models with varying details concerning product usage and their lifetimes; bioenergy with carbon
445 capture and storage (BECCS); and biochar production. Bookkeeping and TRENDY models currently only
446 represent BECCS and biochar with regard to the CO_2 removal through photosynthesis, but not for the durable
447 storage. HWP, BECCS, and biochar are typically counted as CDR when the transfer to the durable storage site
448 occurs and not when the CO_2 is removed from the atmosphere, which complicates a direct comparison to the
449 global carbon budgets approach to quantify annual fluxes to and from the atmosphere. Estimates for CDR
450 through HWP, BECCS, and biochar are thus not indicated in this budget, but can be found elsewhere (see
451 Section 3.2.2).

452 **2.2.2 2023 Projection**

453 We project the 2023 land-use emissions for BLUE, H&C2023, and OSCAR based on their E_{LUC} estimates for
454 2022 and adding the change in carbon emissions from peat fires and tropical deforestation and degradation fires
455 (2023 emissions relative to 2022 emissions) estimated using active fire data (MCD14ML; Giglio et al., 2016).
456 Peat drainage is assumed to be unaltered as it has low interannual variability. More details on the E_{LUC}
457 methodology can be found in Supplement S.2.



458 **2.3 Carbon Dioxide Removal (CDR) not based on vegetation**

459 CDR not based on terrestrial vegetation currently relies on enhanced rock weathering and Direct Air Carbon
460 Capture and Storage (DACCS) projects. The majority of this (58%) derives from a single project: Climeworks'
461 Orca DACCS plant based in Hellisheidi, Iceland. The remainder is generated by 13 small-scale projects
462 including, for example, 500 tons of carbon dioxide sequestered through the spreading of crushed olivine on
463 agricultural areas by Eion Carbon. We use data from the State of CDR Report (Smith et al., 2023), which
464 quantifies all currently deployed CDR methods, including the land-use related activities already covered by
465 Section 2.2. The State of CDR Report (Smith et al., 2023) combines estimates of carbon storage in managed
466 land derived from NGHGI data with project-by-project storage rates obtained through 20 extant CDR databases
467 and registries (status as of mid-year 2022) by Powis et al. (2023). They assessed the data quality on existing
468 CDR projects to be poor, suffering from fragmentation, different reporting standards, limited geographical
469 coverage, and inclusion of a number of pilot plants with uncertain lifespans. As a consequence, these numbers
470 could change substantially from year-to-year in the near-term.

471 **2.4 Growth rate in atmospheric CO₂ concentration (G_{ATM})**

472 **2.4.1 Historical period 1850-2022**

473 The rate of growth of the atmospheric CO₂ concentration is provided for years 1959-2022 by the US National
474 Oceanic and Atmospheric Administration Global Monitoring Laboratory (NOAA/GML; Lan et al., 2023),
475 which is updated from Ballantyne et al. (2012) and includes recent revisions to the calibration scale of
476 atmospheric CO₂ measurements (Hall et al., 2021). For the 1959-1979 period, the global growth rate is based on
477 measurements of atmospheric CO₂ concentration averaged from the Mauna Loa and South Pole stations, as
478 observed by the CO₂ Program at Scripps Institution of Oceanography (Keeling et al., 1976). For the 1980-2021
479 time period, the global growth rate is based on the average of multiple stations selected from the marine
480 boundary layer sites with well-mixed background air (Ballantyne et al., 2012), after fitting a smooth curve
481 through the data for each station as a function of time, and averaging by latitude band (Masarie and Tans, 1995).
482 The annual growth rate is estimated by Lan et al. (2023) from atmospheric CO₂ concentration by taking the
483 average of the most recent December-January months corrected for the average seasonal cycle and subtracting
484 this same average one year earlier. The growth rate in units of ppm yr⁻¹ is converted to units of GtC yr⁻¹ by
485 multiplying by a factor of 2.124 GtC per ppm, assuming instantaneous mixing of CO₂ throughout the
486 atmosphere (Ballantyne et al., 2012; Table 1).

487 Since 2020, NOAA/GML provides estimates of atmospheric CO₂ concentrations with respect to a new
488 calibration scale, referred to as WMO-CO₂-X2019, in line with a recalibration agreed by the World
489 Meteorological Organization (WMO) Global Atmosphere Watch (GAW) community (Hall et al., 2021). The re-
490 calibrated data were first used to estimate G_{ATM} in the 2021 edition of the global carbon budget (Friedlingstein
491 et al., 2022a). Friedlingstein et al. (2022a) verified that the change of scales from WMO-CO₂-X2007 to WMO-
492 CO₂-X2019 made a negligible difference to the value of G_{ATM} (-0.06 GtC yr⁻¹ during 2010-2019 and -0.01 GtC
493 yr⁻¹ during 1959-2019, well within the uncertainty range reported below).



494 The uncertainty around the atmospheric growth rate is due to four main factors. First, the long-term
495 reproducibility of reference gas standards (around 0.03 ppm for 1σ from the 1980s; Lan et al., 2023). Second,
496 small unexplained systematic analytical errors that may have a duration of several months to two years come
497 and go. They have been simulated by randomising both the duration and the magnitude (determined from the
498 existing evidence) in a Monte Carlo procedure. Third, the network composition of the marine boundary layer
499 with some sites coming or going, gaps in the time series at each site, etc (Lan et al., 2023). The latter uncertainty
500 was estimated by NOAA/GML with a Monte Carlo method by constructing 100 "alternative" networks (Masarie
501 and Tans, 1995; NOAA/GML, 2019). The second and third uncertainties, summed in quadrature, add up to
502 0.085 ppm on average (Lan et al., 2023). Fourth, the uncertainty associated with using the average CO₂
503 concentration from a surface network to approximate the true atmospheric average CO₂ concentration (mass-
504 weighted, in 3 dimensions) as needed to assess the total atmospheric CO₂ burden. In reality, CO₂ variations
505 measured at the stations will not exactly track changes in total atmospheric burden, with offsets in magnitude
506 and phasing due to vertical and horizontal mixing. This effect must be very small on decadal and longer time
507 scales, when the atmosphere can be considered well mixed. The CO₂ increase in the stratosphere lags the
508 increase (meaning lower concentrations) that we observe in the marine boundary layer, while the continental
509 boundary layer (where most of the emissions take place) leads the marine boundary layer with higher
510 concentrations. These effects nearly cancel each other. In addition the growth rate is nearly the same everywhere
511 (Ballantyne et al, 2012). We therefore maintain an uncertainty around the annual growth rate based on the
512 multiple stations data set ranges between 0.11 and 0.72 GtC yr⁻¹, with a mean of 0.61 GtC yr⁻¹ for 1959-1979
513 and 0.17 GtC yr⁻¹ for 1980-2022, when a larger set of stations were available as provided by Lan et al. (2023).
514 We estimate the uncertainty of the decadal averaged growth rate after 1980 at 0.02 GtC yr⁻¹ based on the
515 calibration and the annual growth rate uncertainty but stretched over a 10-year interval. For years prior to 1980,
516 we estimate the decadal averaged uncertainty to be 0.07 GtC yr⁻¹ based on a factor proportional to the annual
517 uncertainty prior and after 1980 ($0.02 * [0.61/0.17]$ GtC yr⁻¹).

518 We assign a high confidence to the annual estimates of G_{ATM} because they are based on direct measurements
519 from multiple and consistent instruments and stations distributed around the world (Ballantyne et al., 2012; Hall
520 et al., 2021).

521 To estimate the total carbon accumulated in the atmosphere since 1750 or 1850, we use an atmospheric CO₂
522 concentration of 278.3 ± 3 ppm or 285.1 ± 3 ppm, respectively (Gulev et al., 2021). For the construction of the
523 cumulative budget shown in Figure 3, we use the fitted estimates of CO₂ concentration from Joos and Spahni
524 (2008) to estimate the annual atmospheric growth rate using the conversion factors shown in Table 1. The
525 uncertainty of ± 3 ppm (converted to $\pm 1\sigma$) is taken directly from the IPCC's AR5 assessment (Ciais et al., 2013).
526 Typical uncertainties in the growth rate in atmospheric CO₂ concentration from ice core data are equivalent to
527 ± 0.1 - 0.15 GtC yr⁻¹ as evaluated from the Law Dome data (Etheridge et al., 1996) for individual 20-year intervals
528 over the period from 1850 to 1960 (Bruno and Joos, 1997).

529 **2.4.2 2023 projection**

530 We provide an assessment of G_{ATM} for 2023 as the average of two methods. As in previous GCB releases, we
531 use the observed monthly global atmospheric CO₂ concentration (GLO) through June 2023 (Lan et al., 2023),



532 and the bias-adjusted Holt–Winters exponential smoothing with additive seasonality (Chatfield, 1978) to project
533 to January 2024. The uncertainty is estimated from past variability using the standard deviation of the last 5
534 years' monthly growth rates. For the first time this year, we also use the multi-model mean and uncertainty of
535 the 2023 G_{ATM} estimated by the ESMs prediction system (see Section 2.9). We then take the average of the
536 Holt–Winters and ESMs G_{ATM} estimates, with their respective uncertainty combined quadratically.

537 Similarly, the projection of the 2023 global average CO_2 concentration (in ppm), is calculated as the average of
538 the estimates from the two methods. For Holt–Winters method, it is the annual average of global concentration
539 over the 12 months; for the ESMs, it is the observed global average CO_2 concentration for 2022 plus the annual
540 increase in 2023 predicted by the ESMs multi-model mean.

541 2.5 Ocean CO_2 sink

542 2.5.1 Historical period 1850-2022

543 The reported estimate of the global ocean anthropogenic CO_2 sink S_{OCEAN} is derived as the average of two
544 estimates. The first estimate is derived as the mean over an ensemble of ten global ocean biogeochemistry
545 models (GOBMs, Table 4 and Table S2). The second estimate is obtained as the mean over an ensemble of
546 seven surface ocean fCO_2 -observation-based data-products (Table 4 and Table S3). An eighth fCO_2 -product
547 (Watson et al., 2020) is shown, but is not included in the ensemble average as it differs from the other products
548 by adjusting the flux to a cool, salty ocean surface skin (see Supplement S.3.1 for a discussion of the Watson
549 product). The GOBMs simulate both the natural and anthropogenic CO_2 cycles in the ocean. They constrain the
550 anthropogenic air-sea CO_2 flux (the dominant component of S_{OCEAN}) by the transport of carbon into the ocean
551 interior, which is also the controlling factor of present-day ocean carbon uptake in the real world. They cover
552 the full globe and all seasons and were recently evaluated against surface ocean carbon observations, suggesting
553 they are suitable to estimate the annual ocean carbon sink (Hauck et al., 2020). The fCO_2 -products are tightly
554 linked to observations of fCO_2 (fugacity of CO_2 , which equals pCO_2 corrected for the non-ideal behaviour of the
555 gas; Pfeil et al., 2013), which carry imprints of temporal and spatial variability, but are also sensitive to
556 uncertainties in gas-exchange parameterizations and data-sparsity (Gloeger et al., 2021, Hauck et al., 2023).
557 Their asset is the assessment of the mean spatial pattern of variability and its seasonality (Hauck et al., 2020,
558 Gloeger et al. 2021, Hauck et al., 2023). We further use two diagnostic ocean models to estimate S_{OCEAN} over the
559 industrial era (1781-1958).

560 The global fCO_2 -based flux estimates were adjusted to remove the pre-industrial ocean source of CO_2 to the
561 atmosphere of 0.65 ± 0.3 GtC yr⁻¹ from river input to the ocean (Regnier et al., 2022), to satisfy our definition of
562 S_{OCEAN} (Hauck et al., 2020). The river flux adjustment was distributed over the latitudinal bands using the
563 regional distribution of Lacroix et al. (2020; North: 0.14 GtC yr⁻¹, Tropics: 0.42 GtC yr⁻¹, South: 0.09 GtC yr⁻¹).
564 Acknowledging that this distribution is based on only one model, the advantage is that a gridded field is
565 available and the river flux adjustment can be calculated for the three latitudinal bands and the RECCAP regions
566 (REgional Carbon Cycle Assessment and Processes (RECCAP2; Ciais et al., 2020). This data set suggests that
567 more of the riverine outgassing is located in the tropics than in the Southern Ocean, and is thus opposed to the
568 previously used data set of Aumont et al. (2001). Accordingly, the regional distribution is associated with a



569 major uncertainty in addition to the large uncertainty around the global estimate (Crisp et al., 2022; Gruber et
570 al., 2023). Anthropogenic perturbations of river carbon and nutrient transport to the ocean are not considered
571 (see Section 2.10 and Supplement S.6.3).

572 We derive S_{OCEAN} from GOBMs by using a simulation (sim A) with historical forcing of climate and
573 atmospheric CO_2 , accounting for model biases and drift from a control simulation (sim B) with constant
574 atmospheric CO_2 and normal year climate forcing. A third simulation (sim C) with historical atmospheric CO_2
575 increase and normal year climate forcing is used to attribute the ocean sink to CO_2 (sim C minus sim B) and
576 climate (sim A minus sim C) effects. A fourth simulation (sim D; historical climate forcing and constant
577 atmospheric CO_2) is used to compare the change in anthropogenic carbon inventory in the interior ocean (sim A
578 minus sim D) to the observational estimate of Gruber et al. (2019) with the same flux components (steady state
579 and non-steady state anthropogenic carbon flux). The fCO_2 -products are adjusted with respect to their original
580 publications to represent the full ice-free ocean area, including coastal zones and marginal seas, when the area
581 coverage is below 99%. This is done by either area filling following Fay et al. (2021) or a simple scaling
582 approach. GOBMs and fCO_2 -products fall within the observational constraints over the 1990s (2.2 ± 0.7 GtC yr⁻¹,
583 Ciais et al., 2013) after applying adjustments.

584 S_{OCEAN} is calculated as the average of the GOBM ensemble mean and the fCO_2 -product ensemble mean from
585 1990 onwards. Prior to 1990, it is calculated as the GOBM ensemble mean plus half of the offset between
586 GOBMs and fCO_2 -products ensemble means over 1990-2001.

587 We assign an uncertainty of ± 0.4 GtC yr⁻¹ to the ocean sink based on a combination of random (ensemble
588 standard deviation) and systematic uncertainties (GOBMs bias in anthropogenic carbon accumulation,
589 previously reported uncertainties in fCO_2 -products; see Supplement S.3.4). We assess a medium confidence
590 level to the annual ocean CO_2 sink and its uncertainty because it is based on multiple lines of evidence, it is
591 consistent with ocean interior carbon estimates (Gruber et al., 2019, see Section 3.6.5) and the interannual
592 variability in the GOBMs and data-based estimates is largely consistent and can be explained by climate
593 variability. We refrain from assigning a high confidence because of the systematic deviation between the
594 GOBM and fCO_2 -product trends since around 2002. More details on the S_{OCEAN} methodology can be found in
595 Supplement S.3.

596 **2.5.2 2023 Projection**

597 The ocean CO_2 sink forecast for the year 2023 is based on the annual historical (Lan et al., 2023) and our
598 estimated 2023 atmospheric CO_2 concentration growth rate, the historical and our estimated 2023 annual global
599 fossil fuel emissions from this year's carbon budget, and the spring (March, April, May) Oceanic Niño Index
600 (ONI) (NCEP, 2023). Using a non-linear regression approach, i.e., a feed-forward neural network, atmospheric
601 CO_2 , ONI, and the fossil fuel emissions are used as training data to best match the annual ocean CO_2 sink (i.e.
602 combined S_{OCEAN} estimate from GOBMs and data products) from 1959 through 2022 from this year's carbon
603 budget. Using this relationship, the 2023 S_{OCEAN} can then be estimated from the projected 2022 input data using
604 the non-linear relationship established during the network training. To avoid overfitting, the neural network was
605 trained with a variable number of hidden neurons (varying between 2-5) and 20% of the randomly selected



606 training data were withheld for independent internal testing. Based on the best output performance (tested using
607 the 20% withheld input data), the best performing number of neurons was selected. In a second step, we trained
608 the network 10 times using the best number of neurons identified in step 1 and different sets of randomly
609 selected training data. The mean of the 10 trainings is considered our best forecast, whereas the standard
610 deviation of the 10 ensembles provides a first order estimate of the forecast uncertainty. This uncertainty is then
611 combined with the S_{OCEAN} uncertainty (0.4 GtC yr^{-1}) to estimate the overall uncertainty of the 2023 projection.
612 As an additional line of evidence, we also assess the 2023 atmosphere-ocean carbon flux from the ESM
613 prediction system (see Section 2.9).

614 2.6 Land CO_2 sink

615 2.6.1 Historical Period 1850-2022

616 The terrestrial land sink (S_{LAND}) is thought to be due to the combined effects of fertilisation by rising
617 atmospheric CO_2 and N inputs on plant growth, as well as the effects of climate change such as the lengthening
618 of the growing season in northern temperate and boreal areas. S_{LAND} does not include land sinks directly
619 resulting from land-use and land-use change (e.g., regrowth of vegetation) as these are part of the land-use flux
620 (E_{LUC}), although system boundaries make it difficult to attribute exactly CO_2 fluxes on land between S_{LAND} and
621 E_{LUC} (Erb et al., 2013).

622 S_{LAND} is estimated from the multi-model mean of 20 DGVMs (Table S1) with an additional comparison of
623 DGVMs with a data-driven, carbon data model framework (CARDAMOM) (Bloom and Williams, 2015; Bloom
624 et al., 2016), see Supplement S4. DGVMs simulations include all climate variability and CO_2 effects over land.
625 In addition to the carbon cycle represented in all DGVMs, 14 models also account for the nitrogen cycle and
626 hence can include the effect of N inputs on S_{LAND} . The DGVMs estimate of S_{LAND} does not include the export of
627 carbon to aquatic systems or its historical perturbation, which is discussed in Supplement S.6.3. See Supplement
628 S.4.2 for DGVMs evaluation and uncertainty assessment for S_{LAND} , using the International Land Model
629 Benchmarking system (ILAMB; Collier et al., 2018). More details on the S_{LAND} methodology can be found in
630 Supplement S.4.

631 2.6.2 2023 Projection

632 Like for the ocean forecast, the land CO_2 sink (S_{LAND}) forecast is based on the annual historical (Lan et al.,
633 2023) and our estimated 2023 atmospheric CO_2 concentration, historical and our estimated 2023 annual global
634 fossil fuel emissions from this year's carbon budget, and the summer (June, July, August) ONI (NCEP, 2022).
635 All training data are again used to best match S_{LAND} from 1959 through 2022 from this year's carbon budget
636 using a feed-forward neural network. To avoid overfitting, the neural network was trained with a variable
637 number of hidden neurons (varying between 2-15), larger than for S_{OCEAN} prediction due to the stronger land
638 carbon interannual variability. As done for S_{OCEAN} , a pre-training selects the optimal number of hidden neurons
639 based on 20% withheld input data, and in a second step, an ensemble of 10 forecasts is produced to provide the
640 mean forecast plus uncertainty. This uncertainty is then combined with the S_{LAND} uncertainty for 2022 (0.9 GtC
641 yr^{-1}) to estimate the overall uncertainty of the 2023 projection.



642 **2.7 Atmospheric inversion estimate**

643 The world-wide network of in-situ atmospheric measurements and satellite derived atmospheric CO₂ column
644 (xCO₂) observations put a strong constraint on changes in the atmospheric abundance of CO₂. This is true
645 globally (hence our large confidence in G_{ATM}), but also regionally in regions with sufficient observational
646 density found mostly in the extra-tropics. This allows atmospheric inversion methods to constrain the magnitude
647 and location of the combined total surface CO₂ fluxes from all sources, including fossil and land-use change
648 emissions and land and ocean CO₂ fluxes. The inversions assume E_{FOS} to be well known, and they solve for the
649 spatial and temporal distribution of land and ocean fluxes from the residual gradients of CO₂ between stations
650 that are not explained by fossil fuel emissions. By design, such systems thus close the carbon balance (B_{IM} = 0)
651 and thus provide an additional perspective on the independent estimates of the ocean and land fluxes.

652 This year's release includes fourteen inversion systems that are described in Table S4, of which thirteen are
653 included in the ensemble of inverse estimates presented in the text and figures. Each system is rooted in
654 Bayesian inversion principles but uses different methodologies. These differences concern the selection of
655 atmospheric CO₂ data or xCO₂, and the choice of a-priori fluxes to refine. They also differ in spatial and
656 temporal resolution, assumed correlation structures, and mathematical approach of the models (see references in
657 Table S4 for details). Importantly, the systems use a variety of transport models, which was demonstrated to be
658 a driving factor behind differences in atmospheric inversion-based flux estimates, and specifically their
659 distribution across latitudinal bands (Gaubert et al., 2019; Schuh et al., 2019). Six inversion systems (CAM5-
660 FT23r1, CMS-flux, GONGGA, THU, COLA, GCASv2) used satellite xCO₂ retrievals from GOSAT and/or
661 OCO-2, scaled to the WMO 2019 calibration scale. Two inversions this year (CMS-Flux, COLA) used these
662 xCO₂ datasets in addition to the in-situ observational CO₂ mole fraction records.

663 The original products delivered by the inverse modellers were modified to facilitate the comparison to the other
664 elements of the budget, specifically on two accounts: (1) global total fossil fuel emissions including cement
665 carbonation CO₂ uptake, and (2) riverine CO₂ transport. Details are given below. We note that with these
666 adjustments the inverse results no longer represent the net atmosphere-surface exchange over land/ocean areas
667 as sensed by atmospheric observations. Instead, for land, they become the net uptake of CO₂ by vegetation and
668 soils that is not exported by fluvial systems, similar to the DGVMs estimates. For oceans, they become the net
669 uptake of anthropogenic CO₂, similar to the GOBMs estimates.

670 The inversion systems prescribe global fossil fuel emissions based on e.g. the GCP's Gridded Fossil Emissions
671 Dataset versions 2023.1 (GCP-GridFED; Jones et al., 2023), which are updates to GCP-GridFEDv2021
672 presented by Jones et al. (2021b). GCP-GridFEDv2023 scales gridded estimates of CO₂ emissions from
673 EDGARv4.3.2 (Janssens-Maenhout et al., 2019) within national territories to match national emissions
674 estimates provided by the GCB for the years 1959-2022, which were compiled following the methodology
675 described in Section 2.1. Small differences between the systems due to for instance regridding to the transport
676 model resolution, or use of different fossil fuel emissions, are adjusted in the latitudinal partitioning we present,
677 to ensure agreement with the estimate of E_{FOS} in this budget. We also note that the ocean fluxes used as prior by
678 8 out of 14 inversions are part of the suite of the ocean process model or f /CO₂-products listed in Section 2.5.



679 Although these fluxes are further adjusted by the atmospheric inversions, it makes the inversion estimates of the
680 ocean fluxes not completely independent of S_{OCEAN} assessed here.

681 To facilitate comparisons to the independent S_{OCEAN} and S_{LAND} , we used the same corrections for transport and
682 outgassing of carbon transported from land to ocean, as done for the observation-based estimates of S_{OCEAN} (see
683 Supplement S.3).

684 The atmospheric inversions are evaluated using vertical profiles of atmospheric CO_2 concentrations (Figure S4).
685 More than 30 aircraft programs over the globe, either regular programs or repeated surveys over at least 9
686 months (except for SH programs), have been used to assess system performance (with space-time observational
687 coverage sparse in the SH and tropics, and denser in NH mid-latitudes; Table S7). The fourteen systems are
688 compared to the independent aircraft CO_2 measurements between 2 and 7 km above sea level between 2001 and
689 2022. Results are shown in Figure S4 and discussed in Supplement S.5.2. One inversion was flagged for
690 concerns after quality control with these observations, as well as assessment of their global growth rate. This
691 makes the number of systems included in the ensemble to be $N=13$.

692 With a relatively small ensemble of systems that cover at least one full decade ($N=9$), and which moreover share
693 some a-priori fluxes used with one another, or with the process-based models, it is difficult to justify using their
694 mean and standard deviation as a metric for uncertainty across the ensemble. We therefore report their full range
695 (min-max) without their mean. More details on the atmospheric inversions methodology can be found in
696 Supplement S.5.

697 **2.8 Atmospheric oxygen based estimate**

698 Long-term atmospheric O_2 and CO_2 observations allow estimation of the global ocean and land carbon sinks,
699 due to the coupling of O_2 and CO_2 with distinct exchange ratios for fossil fuel emissions and land uptake, and
700 uncoupled O_2 and CO_2 ocean exchange (Keeling and Manning, 2014). The global ocean and net land carbon
701 sinks were calculated following methods and constants used in Keeling and Manning (2014), but modified to
702 also include the effective O_2 source from metal refining (Battle et al., 2023), and using a value of 1.05 for the
703 exchange ratio of the net land sink, following Resplandy et al. (2019). Atmospheric O_2 is observed as $\delta(\text{O}_2/\text{N}_2)$
704 and combined with CO_2 mole fraction observations into Atmospheric Potential Oxygen (APO, Stephens et al.,
705 1998). The APO observations from 1990 to 2022 were taken from a weighted average of flask records from the
706 three stations in the Scripps O_2 program network (Alert, Canada (ALT), La Jolla, California (LJO), and Cape
707 Grim, Australia (CGO), weighted per Keeling and Manning (2020). Observed CO_2 was taken from the globally
708 averaged marine surface annual mean growth rate from the NOAA/ESRL Global Greenhouse Gas Reference
709 Network (Lan et al., 2023). The O_2 source from ocean warming is based on ocean heat content from updated
710 data from NOAA/NCEI (Levitus et al., 2012). The effective O_2 source from metal refining is based on
711 production data from Bray (2020), Flanagan (2021), and Tuck (2022). Uncertainty was determined through a
712 Monte Carlo approach with 5,000 iterations, using uncertainties prescribed in Keeling and Manning (2014),
713 including observational uncertainties from Keeling et al. (2007) and autoregressive errors in fossil fuel
714 emissions (Ballantyne et al., 2015). The reported uncertainty is one standard deviation of the ensemble.



715 2.9 Earth System Models estimate

716 Reconstructions and predictions from decadal prediction systems based on Earth system models (ESMs) provide
717 a novel line of evidence in assessing the atmosphere-land and atmosphere-ocean carbon fluxes in the past
718 decades and predicting their changes for the current year. The decadal prediction systems based on ESMs used
719 here consist of three sets of simulations: (i) uninitialized freely evolving historical simulations (1850-2014); (ii)
720 assimilation reconstruction incorporating observational data into the model (1980-2022); (iii) initialized
721 prediction simulations for the 1981-2023 period, starting every year from initial states obtained from the above
722 assimilation simulations. The assimilations are designed to reconstruct the actual evolution of the Earth system
723 by assimilating essential fields from data products. The assimilations' states, which are expected to be close to
724 observations, are used to start the initialized prediction simulations used for the current year (2023) global
725 carbon budget. Similar initialized prediction simulations starting every year (Nov. 1st or Jan. 1st) over the 1981-
726 2022 period (i.e., hindcasts) are also performed for predictive skill quantification and for bias correction. More
727 details on the illustration of a decadal prediction system based on an ESM can refer to Figure 1 of Li et al.
728 (2023).

729 By assimilating physical atmospheric and oceanic data products into the ESMs, the models are able to reproduce
730 the historical variations of the atmosphere-sea CO₂ fluxes, atmosphere-land CO₂ fluxes, and atmospheric CO₂
731 growth rate (Li et al., 2016, 2019; Lovenduski et al., 2019a,b; Ilyina et al., 2021; Li et al., 2023). Furthermore,
732 the ESM-based predictions have proven their skill in predicting the air-sea CO₂ fluxes for up to 6 years, the air-
733 land CO₂ fluxes and atmospheric CO₂ growth for 2 years (Lovenduski et al., 2019a,b; Ilyina et al., 2021; Li et
734 al., 2023). The reconstructions from the fully coupled model simulations ensure a closed budget within the Earth
735 system, i.e., no budget imbalance term.

736 Four ESMs, i.e., CanESM5 (Swart et al., 2019; Sospedra-Alfonso et al., 2021), IPSL-CM6A-CO2-LR (Boucher
737 et al., 2020), MIROC-ES2L (Watanabe et al., 2020), and MPI-ESM1-2-LR (Mauritsen et al., 2019; Li et al., 2023),
738 have performed the set of prediction simulations. Each ESM uses a different assimilation method and combination
739 of data products incorporated in the system, more details on the models configuration can be found in Table 4.
740 The ESMs use external forcings from the Coupled Model Intercomparison Project Phase 6 (CMIP6) historical
741 (1980-2014) plus SSP2-4.5 baseline and CovidMIP two year blip scenario (2015-2023) (Eyring et al., 2016; Jones
742 et al., 2021a). The CO₂ emissions forcing from 2015-2023 are substituted by GCB-GridFED (v2023.1, Jones et
743 al., 2023) to provide a more realistic forcing. Reconstructions of atmosphere-ocean CO₂ fluxes (SOCEAN) and
744 atmosphere-land CO₂ fluxes (SLAND-ELUC) for the time period from 1980-2022 are assessed here. Predictions of
745 the atmosphere-ocean CO₂ flux, atmosphere-land CO₂ flux, and atmospheric CO₂ growth for 2023 are calculated
746 based on the predictions at a lead time of 1 year. The predictions are bias-corrected using the 1985-2014
747 climatology mean of GCB2022 (Friedlingstein et al., 2022), more details on methods can be found in Boer et al.
748 (2016) and Li et al. (2023). The ensemble size of initialized prediction simulations is 10, and the ensemble mean
749 for each individual model is used here. The ESMs are used here to support the assessment of SOCEAN and net
750 atmosphere-land CO₂ flux (SLAND - ELUC) over the 1980-2022 period, and to provide an estimate of the 2023
751 projection of G_{ATM}.



752 **2.10 Processes not included in the global carbon budget**

753 The contribution of anthropogenic CO and CH₄ to the global carbon budget is not fully accounted for in Eq. (1)
754 and is described in Supplement S.6.1. The contributions to CO₂ emissions of decomposition of carbonates not
755 accounted for is described in Supplement S.6.2. The contribution of anthropogenic changes in river fluxes is
756 conceptually included in Eq. (1) in S_{OCEAN} and in S_{LAND}, but it is not represented in the process models used to
757 quantify these fluxes. This effect is discussed in Supplement S.6.3. Similarly, the loss of additional sink capacity
758 from reduced forest cover is missing in the combination of approaches used here to estimate both land fluxes
759 (E_{LUC} and S_{LAND}) and its potential effect is discussed and quantified in Supplement S.6.4.

760 **3 Results**

761 For each component of the global carbon budget, we present results for three different time periods: the full
762 historical period, from 1850 to 2022, the decades in which we have atmospheric concentration records from
763 Mauna Loa (1960-2022), a specific focus on last year (2022), and the projection for the current year (2023).
764 Subsequently, we assess the estimates of the budget components of the last decades against the top-down
765 constraints from inverse modelling of atmospheric observations, the land/ocean partitioning derived from the
766 atmospheric O₂ measurements, and the budget components estimates from the ESMs assimilation simulations.
767 Atmospheric inversions further allow for an assessment of the budget components with a regional breakdown of
768 land and ocean sinks.

769 **3.1 Fossil CO₂ Emissions**

770 **3.1.1 Historical period 1850-2022**

771 Cumulative fossil CO₂ emissions for 1850-2022 were 477 ± 25 GtC, including the cement carbonation sink
772 (Figure 3, Table 8, with all cumulative numbers rounded to the nearest 5GtC). In this period, 46% of global
773 fossil CO₂ emissions came from coal, 35% from oil, 15% from natural gas, 3% from decomposition of
774 carbonates, and 1% from flaring. In 1850, the UK stood for 62% of global fossil CO₂ emissions. In 1891 the
775 combined cumulative emissions of the current members of the European Union reached and subsequently
776 surpassed the level of the UK. Since 1917 US cumulative emissions have been the largest. Over the entire
777 period 1850-2022, US cumulative emissions amounted to 115GtC (24% of world total), the EU's to 80 GtC
778 (17%), and China's to 70 GtC (15%).

779 In addition to the estimates of fossil CO₂ emissions that we provide here (see Methods), there are three global
780 datasets with long time series that include all sources of fossil CO₂ emissions: CDIAC-FF (Gilfillan and
781 Marland, 2021), CEDS version v_2021_04_21 (Hoesly et al., 2018; O'Rourke et al., 2021) and PRIMAP-hist
782 version 2.4.2 (Gütschow et al., 2016; Gütschow and Pflüger, 2023), although these datasets are not entirely
783 independent from each other (Andrew, 2020a). CDIAC-FF has the lowest cumulative emissions over 1750-2018
784 at 440 GtC, GCP has 444 GtC, CEDS 445 GtC, PRIMAP-hist TP 453 GtC, and PRIMAP-hist CR 452 GtC.
785 CDIAC-FF excludes emissions from lime production. CEDS has higher emissions from international shipping
786 in recent years, while PRIMAP-hist has higher fugitive emissions than the other datasets. However, in general
787 these four datasets are in relative agreement as to total historical global emissions of fossil CO₂.



788 **3.1.2 Recent period 1960-2022**

789 Global fossil CO₂ emissions, E_{FOS} (including the cement carbonation sink), have increased every decade from an
790 average of 3.0 ± 0.2 GtC yr⁻¹ for the decade of the 1960s to an average of 9.6 ± 0.5 GtC yr⁻¹ during 2013-2022
791 (Table 7, Figure 2 and Figure 5). The growth rate in these emissions decreased between the 1960s and the
792 1990s, from 4.3% yr⁻¹ in the 1960s (1960-1969), 3.2% yr⁻¹ in the 1970s (1970-1979), 1.6% yr⁻¹ in the 1980s
793 (1980-1989), to 1.0% yr⁻¹ in the 1990s (1990-1999). After this period, the growth rate began increasing again in
794 the 2000s at an average growth rate of 2.8% yr⁻¹, decreasing to 0.5% yr⁻¹ for the last decade (2013-2022).
795 China's emissions increased by +1.6% yr⁻¹ on average over the last 10 years dominating the global trend, and
796 India's emissions increased by +3.5% yr⁻¹, while emissions decreased in EU27 by -1.7% yr⁻¹, and in the USA
797 by -1.0% yr⁻¹. Figure 6 illustrates the spatial distribution of fossil fuel emissions for the 2013-2022 period.

798 E_{FOS} reported here includes the uptake of CO₂ by cement via carbonation which has increased with increasing
799 stocks of cement products, from an average of 20 MtC yr⁻¹ (0.02 GtC yr⁻¹) in the 1960s to an average of 206
800 MtC yr⁻¹ (0.21 GtC yr⁻¹) during 2013-2022 (Figure 5).

801 **3.1.3 Final year 2022**

802 Global fossil CO₂ emissions were slightly higher, 0.85%, in 2022 than in 2021, with an increase of less than 0.1
803 GtC to reach 9.9 ± 0.5 GtC (including the 0.2 GtC cement carbonation sink) in 2022 (Figure 5), distributed
804 among coal (41%), oil (32%), natural gas (21%), cement (4%), flaring (1%), and others (1%). Compared to the
805 previous year, 2022 emissions from coal and oil increased by 1.6% and 3.3% respectively, while emissions from
806 gas and cement respectively decreased by 2.2% and 5.7%. All growth rates presented are adjusted for the leap
807 year, unless stated otherwise.

808 In 2022, the largest absolute contributions to global fossil CO₂ emissions were from China (31%), the USA
809 (14%), India (8%), and the EU27 (7%). These four regions account for 59% of global fossil CO₂ emissions,
810 while the rest of the world contributed 41%, including international aviation and marine bunker fuels (2.6% of
811 the total). Growth rates for these countries from 2021 to 2022 were 0.9% (China), 1% (USA), -1.9% (EU27),
812 and 5.8% (India), with +0.6% for the rest of the world. The per-capita fossil CO₂ emissions in 2022 were 1.3 tC
813 person⁻¹ yr⁻¹ for the globe, and were 4.1 (USA), 2.2 (China), 1.7 (EU27) and 0.5 (India) tC person⁻¹ yr⁻¹ for the
814 four highest emitters (Figure 5).

815 **3.1.4 Year 2023 Projection**

816 Globally, we estimate that global fossil CO₂ emissions (including cement carbonation) will grow by 1.2% in
817 2023 (0.2% to 2.3%) to 10.0 GtC (36.8 GtCO₂), exceeding the pre-COVID19 2019 emission levels of 9.9 GtC
818 (36.3 GtCO₂). Global increase in 2023 emissions per fuel types are projected to be +1.1% (range -0.2% to 2.4%)
819 for coal, +1.8% (range 0.8% to 2.9%) for oil, +0.3% (range -0.6% to 1.3%) for natural gas, and 1.8% (range
820 0.2% to 3.4%) for cement.



821 For China, projected fossil emissions in 2023 are expected to increase by 4% (range 1.9% to 6.2%) compared
822 with 2022 emissions, bringing 2023 emissions for China around 3.2 GtC yr⁻¹ (11.9 GtCO₂ yr⁻¹). Changes in fuel
823 specific projections for China are 3.5% for coal, 7.7% for oil, 6.4% natural gas, and 0.2% for cement.

824 For the USA, the Energy Information Administration (EIA) emissions projection for 2023 combined with
825 cement clinker data from USGS gives an decrease of 3.4% (range -5.9% to -0.9%) compared to 2022, bringing
826 USA 2023 emissions to around 1.3 GtC yr⁻¹ (4.9 GtCO₂ yr⁻¹). This is based on separate projections for coal -
827 19.9%, oil -0.7%, natural gas +1.7%, and cement -3.2%.

828 For the European Union, our projection for 2023 is for a decrease of 7.1% (range -9.6% to -4.6%) over 2022,
829 with 2023 emissions around 0.7 GtC yr⁻¹ (2.6 GtCO₂ yr⁻¹). This is based on separate projections for coal of -
830 19.6%, oil -0.9%, natural gas -6.6%, and cement unchanged.

831 For India, our projection for 2023 is an increase of 8% (range of 7.9% to 8.0%) over 2022, with 2023 emissions
832 around 0.8 GtC yr⁻¹ (3.1 GtCO₂ yr⁻¹). This is based on separate projections for coal of +9.2%, oil +5.2%, natural
833 gas +4.4%, and cement +8.1%.

834 For the rest of the world, the expected growth rate for 2023 is 0.9% (range -0.8% to 2.6%) with 2023 emissions
835 around 4.2 GtC yr⁻¹ (15.2 GtCO₂ yr⁻¹). The fuel-specific projected 2023 growth rates for the rest of the world
836 are: +1% for coal, +1.5% for oil, -0.3% for natural gas, +2.6% for cement.

837 **3.2 Emissions from Land Use Changes**

838 **3.2.1 Historical period 1850-2022**

839 Cumulative CO₂ emissions from land-use changes (ELUC) for 1850-2022 were 220 ± 65 GtC (Table 8; Figure 3;
840 Figure 15). The cumulative emissions from ELUC show a large spread among individual estimates of 150 GtC
841 (H&C2023), 290 GtC (BLUE), and 215 GtC (OSCAR) for the three bookkeeping models and a similar wide
842 estimate of 210 ± 65 GtC for the DGVMs (all cumulative numbers are rounded to the nearest 5 GtC). These
843 estimates are broadly consistent with indirect constraints from vegetation biomass observations, giving
844 cumulative emissions of 155 ± 50 GtC over the 1901-2012 period (Li et al., 2017). However, given the large
845 spread, a best estimate is difficult to ascertain.

846 **3.2.2 Recent period 1960-2022**

847 In contrast to growing fossil emissions, CO₂ emissions from land-use, land-use change, and forestry remained
848 relatively constant over the 1960-1999 period. Since the 1990s they have shown a slight decrease of about 0.1
849 GtC per decade, reaching 1.3 ± 0.7 GtC yr⁻¹ for the 2013-2022 period (Table 7), but with large spread across
850 estimates (Table 5, Figure 7). Different from the bookkeeping average, the DGVMs average grows slightly
851 larger over the 1970-2022 period and shows no sign of decreasing emissions in the recent decades (Table 5,
852 Figure 7). This is, however, expected as DGVM-based estimates include the loss of additional sink capacity,
853 which grows with time, while the bookkeeping estimates do not (Supplement S.6.4).



854 We separate net E_{LUC} into five component fluxes to gain further insight into the drivers of net emissions:
855 deforestation, forest (re-)growth, wood harvest and other forest management, peat drainage and peat fires, and
856 all other transitions (Figure 7c; Sec. C.2.1). We further decompose the deforestation and the forest (re-)growth
857 term into contributions from shifting cultivation vs permanent forest cover changes (Figure 7d). Averaged over
858 the 2013-2022 period and over the three bookkeeping estimates, fluxes from deforestation amount to 1.9 [1.5 to
859 2.4] GtC yr^{-1} (Table 5), of which 1.1 [1.0, 1.2] GtC yr^{-1} are from permanent deforestation. Fluxes from forest
860 (re-)growth amount to -1.3 [-1.5, -0.9] GtC yr^{-1} (Table 5), of which -0.5 [-0.8 to -0.2] GtC yr^{-1} are from
861 re/afforestation and the remainder from forest regrowth in shifting cultivation cycles. Emissions from wood
862 harvest and other forest management (0.2 [0.0, 0.6] GtC yr^{-1}), peat drainage and peat fires (0.3 [0.3, 0.3] GtC yr^{-1})
863 and the net flux from other transitions (0.1 [0.0, 0.3] GtC yr^{-1}) are substantially less important globally (Table
864 5). However, the small net flux from wood harvest and other forest management contains substantial gross
865 fluxes that largely compensate each other (see Figure S7): 1.3 [0.9, 2.0] GtC yr^{-1} emissions result from the
866 decomposition of slash and the decay of wood products and -1.1 [-1.3, -0.8] GtC yr^{-1} removals result from
867 regrowth after wood harvesting. This split into component fluxes clarifies the potentials for emission reduction
868 and carbon dioxide removal: the emissions from permanent deforestation - the largest of our component fluxes -
869 could be halted (largely) without compromising carbon uptake by forests, contributing substantially to emissions
870 reduction. By contrast, reducing wood harvesting would have limited potential to reduce emissions as it would
871 be associated with less forest regrowth; removals and emissions cannot be decoupled here on long timescales. A
872 similar conclusion applies to removals and emissions from shifting cultivation, which we have therefore
873 separated out. Carbon Dioxide Removal (CDR) in forests could instead be increased by permanently increasing
874 the forest cover through re/afforestation. Our estimate of about -0.5 [-0.8, -0.2] GtC yr^{-1} (of which about two
875 thirds are located in non-Annex-I countries, in particular in China) removed on average each year during 2013-
876 2022 by re/afforestation is very similar to independent estimates that were derived from NGHGs for 2022.
877 Re/afforestation constitutes the vast majority of all current CDR (Powis et al., 2023). Though they cannot be
878 compared directly to annual fluxes from the atmosphere, CDR through transfers between non-atmospheric
879 reservoirs such as in durable HWPs, biochar or BECCS comprise much smaller amounts of carbon. 61 MtC yr^{-1}
880 have been estimated to be transferred to HWPs in 2022, and BECCS projects have been estimated to store 0.5
881 MtC yr^{-1} in geological projects worldwide (Powis et al., 2023). “Blue carbon”, i.e. coastal wetland management
882 such as restoration of mangrove forests, saltmarshes and seagrass meadows, though at the interface of land and
883 ocean carbon fluxes, are counted towards the land-use sector as well. Currently, bookkeeping models do not
884 include blue carbon; however, current CDR deployment in coastal wetlands is small globally.

885 The small declining trend of E_{LUC} over the last three decades is a result of total deforestation emissions showing
886 no clear trend, while forest regrowth has provided steadily increasing removals. Since the processes behind
887 gross removals, foremost forest regrowth and soil recovery, are all slow, while gross emissions include a large
888 instantaneous component, short-term changes in land-use dynamics, such as a temporary decrease in
889 deforestation, influences gross emissions dynamics more than gross removals dynamics, which rather are a
890 response to longer-term dynamics. Component fluxes often differ more across the three bookkeeping estimates
891 than the net flux, which is expected due to different process representation; in particular, treatment of shifting
892 cultivation, which increases both gross emissions and removals, differs across models, but also net and gross



893 wood harvest fluxes show high uncertainty. By contrast, models agree relatively well for emissions from
894 permanent deforestation emissions and removals by re/afforestation.

895 Overall, highest land-use emissions occur in the tropical regions of all three continents. The top three emitters
896 (both cumulatively 1959-2022 and on average over 2013-2022) are Brazil (in particular the Amazon Arc of
897 Deforestation), Indonesia and the Democratic Republic of the Congo, with these 3 countries contributing 0.7
898 GtC yr⁻¹ or 55% of the global net land-use emissions (average over 2013-2022) (Figure 6b). This is related to
899 massive expansion of cropland, particularly in the last few decades in Latin America, Southeast Asia, and sub-
900 Saharan Africa (Hong et al., 2021), to a substantial part for export of agricultural products (Pendrill et al., 2019).
901 Emission intensity is high in many tropical countries, particularly of Southeast Asia, due to high rates of land
902 conversion in regions of carbon-dense and often still pristine, undegraded natural forests (Hong et al., 2021).
903 Emissions are further increased by peat fires in equatorial Asia (GFED4s, van der Werf et al., 2017). Uptake due
904 to land-use change occurs, particularly in Europe, partly related to expanding forest area as a consequence of the
905 forest transition in the 19th and 20th century and subsequent regrowth of forest (Figure 6b) (Mather 2001;
906 McGrath et al., 2015).

907 While the mentioned patterns are robust and supported by independent literature, we acknowledge that model
908 spread is substantially larger on regional than global levels, as has been shown for bookkeeping models (Bastos
909 et al., 2021) as well as DGVMs (Obermeier et al., 2021). Assessments for individual regions will be performed
910 as part of REgional Carbon Cycle Assessment and Processes (RECCAP2; Ciais et al., 2020) or already exist for
911 selected regions (e.g., for Europe by Petrescu et al., 2020, for Brazil by Rosan et al., 2021, for 8 selected
912 countries/regions in comparison to inventory data by Schwingshackl et al., 2022).

913 National GHG inventory data (NGHGI) under the LULUCF sector or data submitted by countries to FAOSTAT
914 differ from the global models' definition of ELUC. In the NGHGI reporting, the natural fluxes (S_{LAND}) are
915 counted towards ELUC when they occur on managed land (Grassi et al., 2018). In order to compare our results to
916 the NGHGI approach, we perform a translation of our ELUC estimates by subtracting S_{LAND} in managed forest
917 from the DGVMs simulations (following Grassi et al., 2021) from the bookkeeping ELUC estimate (see
918 Supplement S.2.3). For the 2013-2022 period, we estimate that 2.0 GtC yr⁻¹ of S_{LAND} occurred in managed
919 forests. Subtracting this value from ELUC changes ELUC from being a source of 1.3 GtC yr⁻¹ to a sink of 0.8 GtC
920 yr⁻¹, very similar to the NGHGI estimate that yields a sink of 0.7 GtC yr⁻¹ (Table 9). The translation approach
921 has been shown to be generally applicable also on country-level (Grassi et al., 2023; Schwingshackl et al.,
922 2022). Country-level analysis suggests, e.g., that the bookkeeping method estimates higher deforestation
923 emissions than the national report in Indonesia, but less CO₂ removal by afforestation than the national report in
924 China. The fraction of the natural CO₂ sinks that the NGHGI estimates include differs substantially across
925 countries, related to varying proportions of managed vs total forest areas (Schwingshackl et al., 2022). By
926 comparing ELUC and NGHGI on the basis of the component fluxes used above, we find that our estimates
927 reproduce very closely the NGHGI estimates for emissions from permanent deforestation (1.1 GtC yr⁻¹ averaged
928 over 2013-2022). Forest fluxes, that is, (re-)growth from re/afforestation plus the net flux from wood harvesting
929 and other forest management, constitute a large sink in the NGHGI (-1.9 GtC yr⁻¹ averaged over 2013-2022),
930 since they also include S_{LAND} in managed forests. Summing up the bookkeeping estimates of (re-)growth from
931 re/afforestation and the net flux from wood harvesting and other forest management and adding S_{LAND} in



932 managed forests yields a flux of -2.3 GtC yr^{-1} (averaged over 2013-2022), which compares well with the
933 NGHGI estimate. Emissions from organic soils in NGHGI are similar to the estimates based on the bookkeeping
934 approach and the external peat drainage and burning datasets. The net flux from other transitions is small in both
935 NGHGI and bookkeeping estimates, but a difference in sign (small source in bookkeeping estimates, small sink
936 in NGHGI) creates a notable difference between NGHGI and bookkeeping estimates. Though estimates between
937 NGHGI, FAOSTAT and the translated budget estimates still differ in value and need further analysis, the
938 approach suggested by Grassi et al. (2023), which we adopt here, provides a feasible way to relate the global
939 models' and NGHGI approach to each other and thus link the anthropogenic carbon budget estimates of land
940 CO_2 fluxes directly to the Global Stocktake, as part of UNFCCC Paris Agreement.

941 **3.2.3 Final year 2022**

942 The global CO_2 emissions from land-use change are estimated as $1.2 \pm 0.7 \text{ GtC}$ in 2022, similar to the 2020 and
943 2021 estimates. However, confidence in the annual change remains low. Effects of the COVID-19 pandemic on
944 land-use change have turned out to be country-specific as global market mechanisms, national economics and
945 changes in household income all could act to curb or enhance deforestation (Wunder et al., 2021). Concerns
946 about enhanced deforestation due to weakened environmental protection and monitoring in tropical countries
947 (Brancalion et al., 2020, Vale et al., 2021) have been confirmed only for some countries (Cespedes et al., 2023).
948 For example, a recent study suggests slightly increased deforestation rates for the Democratic Republic of
949 Congo linked in particular to post-pandemic economic recovery in the mining sector, while deforestation trends
950 in Brazil seem to have been unaffected. Land use dynamics may be further altered by the Russian invasion of
951 Ukraine, but scientific evidence related to international dependencies (like a shift to tropical palm oil to alleviate
952 dependencies on sunflower oil) so far is very limited and recent changes will not be reflected by the land-use
953 forcing applied in the global models. High food prices, which preceded but were exacerbated by the war (FAO,
954 2022), are generally linked to higher deforestation (Angelsen and Kaimowitz, 1999). A new wave of cropland
955 abandonment in the conflict region may increase the substantial Eastern European carbon sink due to land-use
956 changes, but sanctions being placed on trade may also incentivise domestic agricultural production, thus leading
957 to recultivation of abandoned areas in Russia (Winkler et al., 2023).

958 **3.2.4 Year 2023 Projection**

959 In Indonesia, peat fire emissions are below average (12 Tg C through September 29 2023) despite El Niño
960 conditions, which in general lead to more fires. Tropical deforestation and degradation fires in Indonesia are
961 around average (13 Tg C through September 29 2023), but higher than in the previous year, which had a
962 relatively wet dry season (GFED4.1s, van der Werf et al., 2017; see also
963 https://www.geo.vu.nl/~gwerf/GFED/GFED4/tables/GFED4.1s_C.txt). In South America, emissions from
964 tropical deforestation and degradation fires are among the lowest over the last decades (64 Tg C through
965 September 29 2023). Effects of the El Niño in the Amazon, such as droughts, are not expected before 2024.
966 Disentangling the degree to which interannual variability in rainfall patterns and stronger environmental
967 protection measures in both Indonesia after their 2015 high fire season and in Brazil after the change in
968 government in Brazil play a role in this is an important research topic. Cumulative fire emission estimates



969 through September 29 2023 are 155 Tg C for global deforestation and degradation fires and 12 Tg C for
970 peatland fires in Indonesia (https://www.geo.vu.nl/~gwerf/GFED/GFED4/tables/GFED4.1s_C.txt).

971 Based on these estimates, we expect E_{LUC} emissions of around 1.1 GtC (4.1 GtCO₂) in 2023. Our preliminary
972 estimate of E_{LUC} for 2023 is substantially lower than the 2013-2022 average, which saw years of anomalously
973 dry conditions in Indonesia and high deforestation fires in South America (Friedlingstein et al., 2022b). Note
974 that although our extrapolation includes tropical deforestation and degradation fires, degradation attributable to
975 selective logging, edge-effects or fragmentation is not captured. Further, deforestation and fires in deforestation
976 zones may become more disconnected, partly due to changes in legislation in some regions. For example, Van
977 Wees et al. (2021) found that the contribution from fires to forest loss decreased in the Amazon and in Indonesia
978 over the period of 2003-2018.

979 3.3 CDR not based on vegetation

980 Besides the CDR through land-use (Sec. 3.2), the atmosphere to geosphere flux of carbon resulting from carbon
981 dioxide removal (CDR) activity is currently 0.003 MtC/yr, with 0.002 MtC/yr of DACCS and 0.001 MtC/yr of
982 enhanced weathering projects. This represents an offset of about 0.03% of current fossil fuel emissions.

983 3.4 Total anthropogenic emissions

984 Cumulative anthropogenic CO₂ emissions for 1850-2022 totalled 695 ± 70 GtC (2550 ± 260 GtCO₂), of which
985 70% (485 GtC) occurred since 1960 and 33% (235 GtC) since 2000 (Table 7 and 8). Total anthropogenic
986 emissions more than doubled over the last 60 years, from 4.6 ± 0.7 GtC yr⁻¹ for the decade of the 1960s to an
987 average of 10.9 ± 0.8 GtC yr⁻¹ during 2013-2022, and reaching 11.1 ± 0.9 GtC (40.7 ± 3.3 GtCO₂) in 2022. For
988 2023, we project global total anthropogenic CO₂ emissions from fossil and land use changes to be also around
989 11.2 GtC (40.9 GtCO₂). All values here include the cement carbonation sink (currently about 0.2 GtC yr⁻¹).

990 During the historical period 1850-2022, 31% of historical emissions were from land use change and 69% from
991 fossil emissions. However, fossil emissions have grown significantly since 1960 while land use changes have
992 not, and consequently the contributions of land use change to total anthropogenic emissions were smaller during
993 recent periods (18% during the period 1960-2022 and down to 12% over the 2013-2022 period).

994 3.5 Atmospheric CO₂

995 3.5.1 Historical period 1850-2022

996 Atmospheric CO₂ concentration was approximately 278 parts per million (ppm) in 1750, reaching 300 ppm in
997 the 1910s, 350 ppm in the late 1980s, and reaching 417.07 ± 0.1 ppm in 2022 (Lan et al., 2023; Figure 1). The
998 mass of carbon in the atmosphere increased by 48% from 590 GtC in 1750 to 886 GtC in 2022. Current CO₂
999 concentrations in the atmosphere are unprecedented in the last 2 million years and the current rate of
1000 atmospheric CO₂ increase is at least 10 times faster than at any other time during the last 800,000 years
1001 (Canadell et al., 2021).



1002 **3.5.2 Recent period 1960-2022**

1003 The growth rate in atmospheric CO₂ level increased from 1.7 ± 0.07 GtC yr⁻¹ in the 1960s to 5.2 ± 0.02 GtC yr⁻¹
1004 during 2013-2022 with important decadal variations (Table 7, Figure 3 and Figure 4). During the last decade
1005 (2013-2022), the growth rate in atmospheric CO₂ concentration continued to increase, albeit with large
1006 interannual variability (Figure 4).

1007 The airborne fraction (AF), defined as the ratio of atmospheric CO₂ growth rate to total anthropogenic
1008 emissions:

$$1009 \quad AF = G_{ATM} / (E_{FOS} + E_{LUC}) \quad (2)$$

1010 provides a diagnostic of the relative strength of the land and ocean carbon sinks in removing part of the
1011 anthropogenic CO₂ perturbation. The evolution of AF over the last 60 years shows no significant trend,
1012 remaining at around 44%, albeit showing a large interannual and decadal variability driven by the year-to-year
1013 variability in G_{ATM} (Figure 9). The observed stability of the airborne fraction over the 1960-2020 period
1014 indicates that the ocean and land CO₂ sinks have been removing on average about 56% of the anthropogenic
1015 emissions (see Sections 3.6.2 and 3.7.2).

1016 **3.5.3 Final year 2022**

1017 The growth rate in atmospheric CO₂ concentration was 4.6 ± 0.2 GtC (2.18 ± 0.08 ppm) in 2022 (Figure 4; Lan
1018 et al., 2023), below the 2021 growth rate (5.2 ± 0.2 GtC) or the 2013-2022 average (5.2 ± 0.02 GtC).

1019 **3.5.4 Year 2023 Projection**

1020 The 2023 growth in atmospheric CO₂ concentration (G_{ATM}) is projected to be about 4.0 GtC (1.89 ppm). This is
1021 the average of the Holt–Winters method (3.7 GtC, 1.73 ppm) and ESMs the multi-model mean (4.4 GtC, 2.05
1022 ppm). The 2023 atmospheric CO₂ concentration, averaged over the year, is expected to reach the level of 419.2
1023 ppm, 51% over the pre-industrial level.

1024 **3.6 Ocean Sink**

1025 **3.6.1 Historical period 1850-2022**

1026 Cumulated since 1850, the ocean sink adds up to 180 ± 35 GtC, with more than two thirds of this amount (125
1027 GtC) being taken up by the global ocean since 1960. Over the historical period, the ocean sink increased in pace
1028 with the anthropogenic emissions exponential increase (Figure 3). Since 1850, the ocean has removed 26% of
1029 total anthropogenic emissions.

1030 **3.6.2 Recent period 1960-2022**

1031 The ocean CO₂ sink increased from 1.1 ± 0.4 GtC yr⁻¹ in the 1960s to 2.8 ± 0.4 GtC yr⁻¹ during 2013-2022
1032 (Table 7), with interannual variations of the order of a few tenths of GtC yr⁻¹ (Figure 10). The ocean-borne
1033 fraction ($S_{OCEAN}/(E_{FOS}+E_{LUC})$) has been remarkably constant around 25% on average (Figure 9c), with variations



1034 around this mean illustrating the decadal variability of the ocean carbon sink. So far, there is no indication of a
1035 decrease in the ocean-borne fraction from 1960 to 2022. The increase of the ocean sink is primarily driven by
1036 the increased atmospheric CO₂ concentration, with the strongest CO₂ induced signal in the North Atlantic and
1037 the Southern Ocean (Figure 11a). The effect of climate change is much weaker, reducing the ocean sink globally
1038 by $0.16 \pm 0.04 \text{ GtC yr}^{-1}$ (-6.7% of SO_{CEAN}) during 2013-2022 (all models simulate a weakening of the ocean sink
1039 by climate change, range -4.3 to -10.3%), and does not show clear spatial patterns across the GOBMs ensemble
1040 (Figure 11b). This is the combined effect of change and variability in all atmospheric forcing fields, previously
1041 attributed, in one model, to wind and temperature changes (LeQuéré et al., 2010).

1042 The global net air-sea CO₂ flux is a residual of large natural and anthropogenic CO₂ fluxes into and out of the
1043 ocean with distinct regional and seasonal variations (Figure 6 and B1). Natural fluxes dominate on regional
1044 scales, but largely cancel out when integrated globally (Gruber et al., 2009). Mid-latitudes in all basins and the
1045 high-latitude North Atlantic dominate the ocean CO₂ uptake where low temperatures and high wind speeds
1046 facilitate CO₂ uptake at the surface (Takahashi et al., 2009). In these regions, formation of mode, intermediate
1047 and deep-water masses transport anthropogenic carbon into the ocean interior, thus allowing for continued CO₂
1048 uptake at the surface. Outgassing of natural CO₂ occurs mostly in the tropics, especially in the equatorial
1049 upwelling region, and to a lesser extent in the North Pacific and polar Southern Ocean, mirroring a well-
1050 established understanding of regional patterns of air-sea CO₂ exchange (e.g., Takahashi et al., 2009, Gruber et
1051 al., 2009). These patterns are also noticeable in the Surface Ocean CO₂ Atlas (SOCAT) dataset, where an ocean
1052 $f\text{CO}_2$ value above the atmospheric level indicates outgassing (Figure S1). This map further illustrates the data-
1053 sparsity in the Indian Ocean and the southern hemisphere in general.

1054 Interannual variability of the ocean carbon sink is driven by climate variability with a first-order effect from a
1055 stronger ocean sink during large El Niño events (e.g., 1997-1998) (Figure 10; Rödenbeck et al., 2014, Hauck et
1056 al., 2020; McKinley et al. 2017). The GOBMs show the same patterns of decadal variability as the mean of the
1057 $f\text{CO}_2$ -products, with a stagnation of the ocean sink in the 1990s and a strengthening since the early 2000s
1058 (Figure 10; Le Quéré et al., 2007; Landschützer et al., 2015, 2016; DeVries et al., 2017; Hauck et al., 2020;
1059 McKinley et al., 2020, Gruber et al., 2023). Different explanations have been proposed for this decadal
1060 variability, ranging from the ocean's response to changes in atmospheric wind and pressure systems (e.g., Le
1061 Quéré et al., 2007, Keppler and Landschützer, 2019), including variations in upper ocean overturning circulation
1062 (DeVries et al., 2017) to the eruption of Mount Pinatubo and its effects on sea surface temperature and slowed
1063 atmospheric CO₂ growth rate in the 1990s (McKinley et al., 2020). The main origin of the decadal variability is
1064 a matter of debate with a number of studies initially pointing to the Southern Ocean (see review in Canadell et
1065 al., 2021), but also contributions from the North Atlantic and North Pacific (Landschützer et al., 2016, DeVries
1066 et al., 2019), or a global signal (McKinley et al., 2020) were proposed.

1067 Although all individual GOBMs and $f\text{CO}_2$ -products fall within the observational constraint, the ensemble means
1068 of GOBMs, and $f\text{CO}_2$ -products adjusted for the riverine flux diverge over time with a mean offset increasing
1069 from 0.30 GtC yr^{-1} in the 1990s to 0.57 GtC yr^{-1} in the decade 2013-2022 and reaching 0.61 GtC yr^{-1} in 2022.
1070 The SO_{CEAN} positive trend over time diverges by a factor two since 2002 (GOBMs: $0.24 \pm 0.07 \text{ GtC yr}^{-1}$ per
1071 decade, $f\text{CO}_2$ -products: $0.48 \pm 0.11 \text{ GtC yr}^{-1}$ per decade, SO_{CEAN} : 0.36 GtC yr^{-1} per decade) and by a factor of 2.5
1072 since 2010 (GOBMs: $0.16 \pm 0.15 \text{ GtC yr}^{-1}$ per decade, $f\text{CO}_2$ -products: $0.42 \pm 0.18 \text{ GtC yr}^{-1}$ per decade SO_{CEAN} :



1073 0.29 GtC yr⁻¹ per decade). The $f\text{CO}_2$ -product estimate is slightly different compared to Friedlingstein et al.
1074 (2022b) as a result of an updated submission of the NIES-ML3 product (previously NIES-NN), however the
1075 difference in the integrated mean flux is small.

1076 The discrepancy between the two types of estimates stems from a larger SO_{OCEAN} trend in the northern and
1077 southern extra-tropics since around 2002 (Figure 13). Note that the discrepancy in the mean flux, which was
1078 located in the Southern Ocean in previous versions of the GCB, has been reduced due to the choice of the
1079 regional river flux adjustment (Lacroix et al., 2020 instead of Aumont et al., 2001). This comes at the expense of
1080 a new discrepancy in the mean SO_{OCEAN} of about 0.2 GtC yr⁻¹ in the tropics. Likely explanations for the
1081 discrepancy in the trends in the high-latitudes are data sparsity and uneven data distribution (Bushinsky et al.,
1082 2019, Gloege et al., 2021, Hauck et al., 2023). In particular, two $f\text{CO}_2$ -products that are part of the GCB
1083 ensemble were shown to overestimate the Southern Ocean CO_2 flux trend by 50 and 130% based on current
1084 sampling in a model subsampling experiment (Hauck et al., 2023). Another likely contributor to the discrepancy
1085 between GOBMs and $f\text{CO}_2$ -products are model biases (as indicated by the large model spread in the South,
1086 Figure 13, and the larger model-data $f\text{CO}_2$ mismatch, Figure S2).

1087 In previous GCB releases, the ocean sink 1959-1989 was only estimated by GOBMs due to the absence of $f\text{CO}_2$
1088 observations. Now, the first data-based estimates extending back to 1957/58 are becoming available (Jena-MLS,
1089 Rödenbeck et al., 2022, LDEO-HPD, Bennington et al., 2022; Gloege et al., 2022). These are based on a multi-
1090 linear regression of $p\text{CO}_2$ with environmental predictors (Rödenbeck et al., 2022) or on model-data $p\text{CO}_2$ misfits
1091 and their relation to environmental predictors (Bennington et al., 2022). The Jena-MLS and LDEO-HPD
1092 estimates fall well within the range of GOBM estimates and have a correlation of 0.99 and 0.98 respectively
1093 with SO_{OCEAN} for the period 1959-2022 (and 0.98 and 0.97 for the 1959-1989 period). They agree well on the
1094 mean SO_{OCEAN} estimate since 1977 with a slightly higher amplitude of variability (Figure 10). Until 1976, Jena-
1095 MLS and LDEO-HPD are respectively about 0.25 GtCyr⁻¹ and about 0.1 GtCyr⁻¹ below the central SO_{OCEAN}
1096 estimate. The agreement especially on phasing of variability is impressive in both products, and the
1097 discrepancies in the mean flux 1959-1976 could be explained by an overestimated trend of Jena-MLS
1098 (Rödenbeck et al., 2022). Bennington et al. (2022) report a larger flux into the pre-1990 ocean than in Jena-
1099 MLS, although lower than SO_{OCEAN} .

1100 The reported SO_{OCEAN} estimate from GOBMs and $f\text{CO}_2$ -products is 2.2 ± 0.4 GtC yr⁻¹ over the period 1994 to
1101 2007, which is in excellent agreement with the ocean interior estimate of 2.2 ± 0.4 GtC yr⁻¹, which accounts for
1102 the climate effect on the natural CO_2 flux of -0.4 ± 0.24 GtC yr⁻¹ (Gruber et al., 2019) to match the definition of
1103 SO_{OCEAN} used here (Hauck et al., 2020). This comparison depends critically on the estimate of the climate effect
1104 on the natural CO_2 flux, which is smaller from the GOBMs (-0.1 GtC yr⁻¹) than in Gruber et al. (2019).
1105 Uncertainties of these two estimates would also overlap when using the GOBM estimate of the climate effect on
1106 the natural CO_2 flux.

1107 During 2010-2016, the ocean CO_2 sink appears to have intensified in line with the expected increase from
1108 atmospheric CO_2 (McKinley et al., 2020). This effect is slightly stronger in the $f\text{CO}_2$ -products (Figure 10, ocean
1109 sink 2016 minus 2010, GOBMs: $+0.42 \pm 0.10$ GtC yr⁻¹, $f\text{CO}_2$ -products: $+0.48 \pm 0.10$ GtC yr⁻¹). The reduction of
1110 -0.14 GtC yr⁻¹ (range: -0.39 to $+0.01$ GtC yr⁻¹) in the ocean CO_2 sink in 2017 is consistent with the return to



1111 normal conditions after the El Niño in 2015/16, which caused an enhanced sink in previous years. After an
1112 increasing S_{OCEAN} in 2018 and 2019, 2017, the GOBM and fCO_2 -product ensemble means suggest a decrease of
1113 S_{OCEAN} , related to the triple La Niña event 2020-2023.

1114 **3.6.3 Final year 2022**

1115 The estimated ocean CO_2 sink is 2.8 ± 0.4 GtC for 2022. This is a small decrease of 0.05 GtC compared to 2021,
1116 in line with the expected sink weakening from persistent La Niña conditions. GOBM and fCO_2 -product
1117 estimates consistently result in a near-stagnation of S_{OCEAN} (GOBMs: -0.01 ± 0.05 GtC, fCO_2 -products: -0.09
1118 ± 0.10 GtC). Four models and six fCO_2 -products show a decrease in S_{OCEAN} (GOBMs down to -0.09 GtC, fCO_2 -
1119 products down to -0.25 GtC), while one model shows no change and five models and two fCO_2 -products show
1120 an increase in S_{OCEAN} (GOBMs up to 0.07 GtC, fCO_2 -products up to 0.15 GtC; Figure 10). The fCO_2 -products
1121 have a larger uncertainty at the end of the reconstructed time series (tail effect, e.g., Watson et al., 2020).
1122 Specifically, the fCO_2 -products' estimate of the last year is regularly adjusted in the following release owing to
1123 the tail effect and an incrementally increasing data availability. While the monthly grid cells covered may have a
1124 lag of only about a year (Figure 10 inset), the values within grid cells may change with 1-5 years lag (see
1125 absolute number of observations plotted in previous GCB releases).

1126 **3.6.4 Year 2023 Projection**

1127 Using a feed-forward neural network method (see Section 2.5.2) we project an ocean sink of 2.9 GtC for 2023.
1128 This is slightly higher than for the year 2022 and could mark a reversal of the decreasing S_{OCEAN} sink trend of
1129 the past three years, due to the transition from persisting La Niña conditions to emerging El Niño conditions in
1130 2023. The new set of ESMs predictions support this estimate with a 2023 ocean sink of around 3.1 [2.9, 3.2]
1131 GtC.

1132 **3.6.5 Ocean Models Evaluation**

1133 The process-based model evaluation draws a generally positive picture with GOBMs scattered around the
1134 observational values for Southern Ocean sea-surface salinity, Southern Ocean stratification index and surface
1135 ocean Revelle factor (Section C3.3 and Table S10). However, the Atlantic Meridional Overturning Circulation
1136 at $26^\circ N$ is underestimated by 8 out of 10 GOBMs. It is planned to derive skill scores for the GOBMs in future
1137 releases based on these metrics.

1138 The model simulations allow to separate the anthropogenic carbon component (steady state and non-steady
1139 state, $sim D - sim A$) and to compare the model flux and DIC inventory change directly to the interior ocean
1140 estimate of Gruber et al. (2019) without further assumptions (Table S10). The GOBMs ensemble average of
1141 anthropogenic carbon inventory changes 1994-2007 amounts to 2.4 GtC yr^{-1} and is thus lower than the 2.6 ± 0.3
1142 GtC yr^{-1} estimated by Gruber et al. (2019) although within the uncertainty. Only four models with the highest
1143 sink estimate fall within the range reported by Gruber et al. (2019). This suggests that the majority of the
1144 GOBMs underestimate anthropogenic carbon uptake by 10-20%. Analysis of Earth System Models indicate that
1145 an underestimation by about 10% may be due to biases in ocean carbon transport and mixing from the surface
1146 mixed layer to the ocean interior (Goris et al., 2018, Terhaar et al., 2021, Bourgeois et al., 2022, Terhaar et al.,



1147 2022), biases in the chemical buffer capacity (Revelle factor) of the ocean (Vaittinada Ayar et al., 2022; Terhaar
1148 et al., 2022) and partly due to a late starting date of the simulations (mirrored in atmospheric CO₂ chosen for the
1149 preindustrial control simulation, Table S2, Bronselaer et al., 2017, Terhaar et al., 2022). Interestingly, and in
1150 contrast to the uncertainties in the surface CO₂ flux, we find the largest mismatch in interior ocean carbon
1151 accumulation in the tropics (96% of the mismatch), with minor contributions from the north (3%) and the south
1152 (<1%). These numbers deviate slightly from GCB2021 because of submission of the ACCESS model with a
1153 high anthropogenic carbon accumulation, particularly in the Southern Ocean. The large discrepancy in
1154 accumulation in the tropics highlights the role of interior ocean carbon redistribution for those inventories
1155 (Khatiwala et al., 2009, DeVries et al., 2023).

1156 The evaluation of the ocean estimates with the *f*CO₂ observations from the SOCAT v2023 dataset for the period
1157 1990-2022 shows an RMSE from annually detrended data of 0.4 to 2.4 μatm for the seven *f*CO₂-products over
1158 the globe (Figure S2). The GOBMs RMSEs are larger and range from 2.9 to 5.4 μatm. The RMSEs are
1159 generally larger at high latitudes compared to the tropics, for both the *f*CO₂-products and the GOBMs. The
1160 *f*CO₂-products have RMSEs of 0.3 to 2.8 μatm in the tropics, 0.7 to 2.3 μatm in the north, and 0.7 to 2.8 μatm in
1161 the south. Note that the *f*CO₂-products are based on the SOCAT v2023 database, hence the SOCAT is not an
1162 independent dataset for the evaluation of the *f*CO₂-products. The GOBMs RMSEs are more spread across
1163 regions, ranging from 2.5 to 5.0 μatm in the tropics, 3.0 to 7.2 μatm in the North, and 3.7 to 8.5 μatm in the
1164 South. The higher RMSEs occur in regions with stronger climate variability, such as the northern and southern
1165 high latitudes (poleward of the subtropical gyres). The upper range of the model RMSEs have increased
1166 somewhat relative to Friedlingstein et al. (2022b).

1167 **3.7 Land Sink**

1168 **3.7.1 Historical period 1850-2022**

1169 Cumulated since 1850, the terrestrial CO₂ sink amounts to 225 ± 55 GtC, 32% of total anthropogenic emissions.
1170 Over the historical period, the sink increased in pace with the anthropogenic emissions exponential increase
1171 (Figure 3).

1172 **3.7.2 Recent period 1960-2022**

1173 The terrestrial CO₂ sink *S*_{LAND} increased from 1.3 ± 0.5 GtC yr⁻¹ in the 1960s to 3.3 ± 0.8 GtC yr⁻¹ during 2013-
1174 2022, with important interannual variations of up to 2 GtC yr⁻¹ generally showing a decreased land sink during
1175 El Niño events (Figure 8), responsible for the corresponding enhanced growth rate in atmospheric CO₂
1176 concentration. The larger land CO₂ sink during 2013-2022 compared to the 1960s is reproduced by all the
1177 DGVMs in response to the increase in both atmospheric CO₂, nitrogen deposition, and the changes in climate,
1178 and is consistent with constraints from the other budget terms (Table 5).

1179 Over the period 1960 to present the increase in the global terrestrial CO₂ sink is largely attributed to the CO₂
1180 fertilisation effect (Prentice et al., 2001, Piao et al., 2009, Schimel et al., 2015) and increased nitrogen
1181 deposition (Huntzinger et al., 2017, O'Sullivan et al., 2019), directly stimulating plant photosynthesis and
1182 increased plant water use in water limited systems, with a small negative contribution of climate change (Figure



1183 11). There is a range of evidence to support a positive terrestrial carbon sink in response to increasing
1184 atmospheric CO₂, albeit with uncertain magnitude (Walker et al., 2021). As expected from theory, the greatest
1185 CO₂ effect is simulated in the tropical forest regions, associated with warm temperatures and long growing
1186 seasons (Hickler et al., 2008) (Figure 11a). However, evidence from tropical intact forest plots indicate an
1187 overall decline in the land sink across Amazonia (1985-2011), attributed to enhanced mortality offsetting
1188 productivity gains (Brienen et al., 2015, Hubau et al., 2020). During 2013-2022 the land sink is positive in all
1189 regions (Figure 6) with the exception of eastern Brazil, Bolivia, Paraguay, northern Venezuela, Southwest USA,
1190 central Europe and Central Asia, North and South Africa, and eastern Australia, where the negative effects of
1191 climate variability and change (i.e. reduced rainfall and/or increased temperature) counterbalance CO₂ effects.
1192 This is clearly visible on Figure 11 where the effects of CO₂ (Figure 11a) and climate (Figure 11b) as simulated
1193 by the DGVMs are isolated. The negative effect of climate is the strongest in most of South America, Central
1194 America, Southwest US, Central Europe, western Sahel, southern Africa, Southeast Asia and southern China,
1195 and eastern Australia (Figure 11b). Globally, over the 2013-2022 period, climate change reduces the land sink
1196 by 0.68 ± 0.62 GtC yr⁻¹ (20% of S_{LAND}).

1197 Most DGVMs have similar S_{LAND} averaged over 2013-2022, and 14/20 models fall within the 1σ range of the
1198 residual land sink [2.0-3.8 GtC yr⁻¹] (see Table 5), and all but one model are within the 2σ range [1.1-4.7 GtC yr
1199 ⁻¹]. The ED model is an outlier, with a land sink estimate of 5.7 GtC yr⁻¹, driven by a strong CO₂ fertilisation
1200 effect (6.6 GtC yr⁻¹ in the CO₂ only (S1) simulation), that is offset by correspondingly high land-use emissions.
1201 There are no direct global observations of the land sink, or the CO₂ fertilisation effect, and so we are not yet in a
1202 position to rule out models based on component fluxes if the net land sink (S_{LAND-ELUC}) is within the
1203 observational uncertainty provided by atmospheric O₂ measurements (Table 5). Overall, therefore the spread
1204 among models for the estimate of S_{LAND} over the last decade has increased this year (0.8 GtC yr⁻¹) compared to
1205 GCB2022 (0.6 GtC yr⁻¹).

1206 Furthermore, DGVMs were compared against a data-constrained intermediate complexity model of the land
1207 carbon cycle (CARDAMOM) (Bloom and Williams, 2015; Bloom et al., 2016). Results suggest good
1208 correspondence between approaches at the interannual timescales, but divergence in the recent trend with
1209 CARDAMOM simulating a stronger trend than the DGVMs (Figure S8).

1210 Since 2020 the globe has experienced La Niña conditions which would be expected to lead to an increased land
1211 carbon sink. A clear peak in the global land sink is not evident in S_{LAND}, and we find that a La Niña- driven
1212 increase in tropical land sink is offset by a reduced high latitude extra-tropical land sink, which may be linked to
1213 the land response to recent climate extremes. A notable difference from GCB2022 (2012-2021 S_{LAND} mean) is
1214 the reduced carbon losses across tropical drylands. Further, central Europe has switched from a sink of carbon to
1215 a source, with the summer heatwave of 2022 (and associated drought and wildfire) causing widespread losses
1216 (Peters et al., 2023). In the past years several regions experienced record-setting fire events. While global
1217 burned area has declined over the past decades mostly due to declining fire activity in savannas (Andela et al.,
1218 2017), forest fire emissions are rising and have the potential to counter the negative fire trend in savannas
1219 (Zheng et al., 2021). Noteworthy events include the 2019-2020 Black Summer event in Australia (emissions of
1220 roughly 0.2 GtC; van der Velde et al., 2021) and Siberia in 2021 where emissions approached 0.4 GtC or three



1221 times the 1997-2020 average according to GFED4s. While other regions, including Western US and
1222 Mediterranean Europe, also experienced intense fire seasons in 2021 their emissions are substantially lower.

1223 Despite these regional negative effects of climate change on S_{LAND} , the efficiency of land to remove
1224 anthropogenic CO_2 emissions has remained broadly constant over the last six decades, with a land-borne
1225 fraction ($S_{\text{LAND}}/(E_{\text{FOS}}+E_{\text{LUC}})$) of around 30% (Figure 9b).

1226 **3.7.3 Final year 2022**

1227 The terrestrial CO_2 sink from the DGVMs ensemble was 3.8 ± 0.8 GtC in 2022, above the decadal average of
1228 3.3 ± 0.8 GtC yr^{-1} (Figure 4, Table 7), and slightly above the 2021 sink of 3.5 ± 1.0 GtC, likely driven by the
1229 persistent La Niña conditions. We note that the DGVMs estimate for 2022 is similar to the 3.7 ± 1.0 GtC yr^{-1}
1230 estimate from the residual sink from the global budget ($E_{\text{FOS}}+E_{\text{LUC}}-G_{\text{ATM}}-S_{\text{OCEAN}}$) (Table 5).

1231 **3.7.4 Year 2023 Projection**

1232 Using a feed-forward neural network method we project a land sink of 3.0 GtC for 2023, 0.8 GtC smaller than
1233 the 2022 estimate. As for the ocean sink, we attribute this to the emerging El Niño conditions in 2023, leading to
1234 a reduced land sink. The ESMs do not provide an additional estimate of S_{LAND} as they only simulate the net
1235 atmosphere-land carbon flux ($S_{\text{LAND}}-E_{\text{LUC}}$).

1236 **3.7.5 Land Models Evaluation**

1237 The evaluation of the DGVMs shows generally high skill scores across models for runoff, and to a lesser extent
1238 for vegetation biomass, GPP, and ecosystem respiration. These conclusions are supported by a more
1239 comprehensive analysis of DGVM performance in comparison with benchmark data (Seiler et al., 2022). A
1240 relative comparison of DGVM performance (Figure S3) suggests several DGVMs (CABLE-POP, CLASSIC,
1241 OCN, ORCHIDEE) may outperform others at multiple carbon and water cycle benchmarks. However, results
1242 from Seiler et al., 2022, also show how DGVM differences are often of similar magnitude compared with the
1243 range across observational datasets.

1244 **3.8 Partitioning the carbon sinks**

1245 **3.8.1 Global sinks and spread of estimates**

1246 In the period 2013-2022, the bottom-up view of global net ocean and land carbon sinks provided by the GCB,
1247 S_{OCEAN} for the ocean and $S_{\text{LAND}}-E_{\text{LUC}}$ for the land, agrees closely with the top-down global carbon sinks
1248 delivered by the atmospheric inversions. This is shown in Figure 12, which visualises the individual decadal
1249 mean atmosphere-land and atmosphere-ocean fluxes from each, along with the constraints on their sum offered
1250 by the global fossil CO_2 emissions flux minus the atmospheric growth rate ($E_{\text{FOS}}-G_{\text{ATM}}$, 4.5 ± 0.5 Gt C yr^{-1} ,
1251 Table 7, shown as diagonal line on Figure 12). The GCB estimate for net atmosphere-to-surface flux ($S_{\text{OCEAN}}+$
1252 $S_{\text{LAND}}-E_{\text{LUC}}$) during 2013-2022 is 4.9 ± 1.2 Gt C yr^{-1} (Table 7), with the difference to the diagonal representing
1253 the budget imbalance (B_{IM}) of 0.4 GtC yr^{-1} discussed in Section 3.9. By virtue of the inversion methodology, the



1254 imbalance of the top-down estimates is $< 0.1 \text{ GtC yr}^{-1}$ and thus scatter across the diagonal, inverse models
1255 trading land for ocean fluxes in their solution. The independent constraint on the net atmosphere-to-surface flux
1256 based on atmospheric O_2 is $4.4 \pm 1.4 \text{ GtC yr}^{-1}$ over the 2013-2022 period (orange symbol on Figure 12), while
1257 the ESMs estimate for the net atmosphere-to-surface flux over that period is $5.0 [4.2, 5.5] \text{ GtC yr}^{-1}$, consistent
1258 with the GCB estimate (Tables 5 and 6).

1259 The distributions based on the individual models and data products reveal substantial spread but converge near
1260 the decadal means quoted in Tables 5 to 7. Sink estimates for SOCEAN and from inverse systems are mostly non-
1261 Gaussian, while the ensemble of DGVMs appears more normally distributed justifying the use of a multi-model
1262 mean and standard deviation for their errors in the budget. Noteworthy is that the tails of the distributions
1263 provided by the land and ocean bottom-up estimates would not agree with the global constraint provided by the
1264 fossil fuel emissions and the observed atmospheric CO_2 growth rate. This illustrates the power of the
1265 atmospheric joint constraint from G_{ATM} and the global CO_2 observation network it derives from.

1266 3.8.1.1 Net atmosphere-to-land fluxes

1267 The GCB net atmosphere-to-land fluxes ($S_{\text{LAND}} - E_{\text{LUC}}$), calculated as the difference between S_{LAND} from the
1268 DGVMs and E_{LUC} from the bookkeeping models, amounts to a $2.1 \pm 1.1 \text{ GtC yr}^{-1}$ sink during 2013-2022 (Table
1269 5). Estimates of net atmosphere-to-land fluxes ($S_{\text{LAND}} - E_{\text{LUC}}$) from the DGVMs alone ($1.7 \pm 0.6 \text{ GtC yr}^{-1}$, Table
1270 5, green symbol on Figure 12) are slightly lower, within the uncertainty of the GCB estimate and also with the
1271 global carbon budget constraint from the ocean sink ($E_{\text{FOS}} - G_{\text{ATM}} - \text{SOCEAN}$, $1.6 \pm 0.6 \text{ GtC yr}^{-1}$; Table 7). For the
1272 last decade (2013-2022), the inversions estimate the net atmosphere-to-land uptake to be $1.6 [0.5, 2.3] \text{ GtC yr}^{-1}$,
1273 similar to the DGVMs estimates (purple symbol on Figure 12). The ESMs estimate for the net atmosphere-to-
1274 land uptake during 2013-2022 is $2.4 [1.8, 3.3] \text{ GtC yr}^{-1}$, consistent with the GCB and DGVMs estimates of
1275 $S_{\text{LAND}} - E_{\text{LUC}}$ (Figure 13 top row). The independent constraint based on atmospheric O_2 is significantly lower,
1276 $1.1 \pm 1.3 \text{ GtC yr}^{-1}$, although its relatively high uncertainty range overlaps with the central estimates from other
1277 approaches.

1278 3.8.1.2 Net atmosphere-to-ocean fluxes

1279 For the 2013-2022 period, the GOBMs ($2.6 \pm 0.4 \text{ GtC yr}^{-1}$) produce a lower estimate for the ocean sink than the
1280 $f\text{CO}_2$ -products ($3.1 [2.6, 3.3] \text{ GtC yr}^{-1}$), which shows up in Figure 12 as separate peaks in the distribution from
1281 the GOBMs (dark blue symbols) and from the $f\text{CO}_2$ -products (light blue symbols). Atmospheric inversions (3.0
1282 $[2.4, 4.1] \text{ GtC yr}^{-1}$) suggest an ocean uptake more in line with the $f\text{CO}_2$ -products for the recent decade (Table 7),
1283 although the inversions range includes both the GOBMs and $f\text{CO}_2$ -products estimates (Figure 13 top row). The
1284 ESMs $2.6 [2.2, 3.4] \text{ GtC yr}^{-1}$ suggest a moderate estimate for the ocean carbon sink, comparable to the GOBMs
1285 estimate with regard to mean and spread. Conversely, the independent constraint based on atmospheric O_2
1286 suggests a larger ocean sink ($3.3 \pm 0.6 \text{ GtC yr}^{-1}$), more consistent with the $f\text{CO}_2$ -products and atmospheric
1287 inversions. We caution that the riverine transport of carbon taken up on land and outgassing from the ocean is a
1288 substantial ($0.65 \pm 0.3 \text{ GtC yr}^{-1}$) and uncertain term (Crisp et al., 2022; Gruber et al., 2023; DeVries et al., 2023)
1289 that separates the GOBMs, ESMs and oxygen-based estimates on the one hand from the $f\text{CO}_2$ -products and
1290 atmospheric inversions on the other hand. However, the high ocean sink estimate based on atmospheric oxygen



1291 that is not subject to river flux adjustment, provides another line of evidence that most GOBMs and ESMS
1292 underestimate the ocean sink.

1293 **3.8.2 Regional partitioning**

1294 Figure 13 shows the latitudinal partitioning of the global atmosphere-to-ocean (S_{OCEAN}), atmosphere-to-land
1295 ($S_{\text{LAND}} - E_{\text{LUC}}$), and their sum ($S_{\text{OCEAN}} + S_{\text{LAND}} - E_{\text{LUC}}$) according to the estimates from GOBMs and ocean
1296 $f\text{CO}_2$ -products (S_{OCEAN}), DGVMs ($S_{\text{LAND}} - E_{\text{LUC}}$), and from atmospheric inversions (S_{OCEAN} and $S_{\text{LAND}} - E_{\text{LUC}}$).

1297 **3.8.2.1 North**

1298 Despite being one of the most densely observed and studied regions of our globe, annual mean carbon sink
1299 estimates in the northern extra-tropics (north of 30°N) continue to differ. The atmospheric inversions suggest an
1300 atmosphere-to-surface sink ($S_{\text{OCEAN}} + S_{\text{LAND}} - E_{\text{LUC}}$) for 2013-2022 of $2.8[1.7 \text{ to } 3.3] \text{ GtC yr}^{-1}$, which is higher
1301 than the process models' estimate of $2.2 \pm 0.4 \text{ GtC yr}^{-1}$ (Figure 13). The GOBMs ($1.2 \pm 0.2 \text{ GtC yr}^{-1}$), $f\text{CO}_2$ -
1302 products ($1.3[1.2-1.4] \text{ GtC yr}^{-1}$), and inversion systems ($1.2[0.7 \text{ to } 1.4] \text{ GtC yr}^{-1}$) produce consistent estimates of
1303 the ocean sink. Thus, the difference mainly arises from the net land flux ($S_{\text{LAND}} - E_{\text{LUC}}$) estimate, which is $1.0 \pm$
1304 0.4 GtC yr^{-1} in the DGVMs compared to $1.6[0.4 \text{ to } 2.6] \text{ GtC yr}^{-1}$ in the atmospheric inversions (Figure 13,
1305 second row). We note that the range among inversions driven by OCO-2 satellite data is smaller though ($1.6 -$
1306 2.2 GtC yr^{-1} $N=6$), supporting the notion that northern extra-tropics land uptake was larger than suggested by the
1307 DGVMs at least in the 2015-2022 period covered by this data product.

1308 Discrepancies in the northern land fluxes conforms with persistent issues surrounding the quantification of the
1309 drivers of the global net land CO_2 flux (Armeth et al., 2017; Huntzinger et al., 2017; O'Sullivan et al., 2022) and
1310 the distribution of atmosphere-to-land fluxes between the tropics and high northern latitudes (Baccini et al.,
1311 2017; Schimel et al., 2015; Stephens et al., 2007; Ciais et al., 2019; Gaubert et al., 2019).

1312 In the northern extra-tropics, the process models, inversions, and $f\text{CO}_2$ -products consistently suggest that most
1313 of the variability stems from the land (Figure 13). Inversions generally estimate similar interannual variations
1314 (IAV) over land to DGVMs ($0.28-0.35$ vs $0.8-0.64 \text{ GtC yr}^{-1}$, averaged over 1990-2022), and they have higher
1315 IAV in ocean fluxes ($0.05-0.10 \text{ GtC yr}^{-1}$) relative to GOBMs ($0.02-0.06 \text{ GtC yr}^{-1}$, Figure S2), and $f\text{CO}_2$ -
1316 products ($0.03-0.10 \text{ GtC yr}^{-1}$).

1317 **3.8.2.2 Tropics**

1318 In the tropics ($30^\circ\text{S}-30^\circ\text{N}$), both the atmospheric inversions and process models estimate a net carbon balance
1319 ($S_{\text{OCEAN}} + S_{\text{LAND}} - E_{\text{LUC}}$) that is close to neutral over the past decade. The GOBMs ($-0.03 \pm 0.24 \text{ GtC yr}^{-1}$), $f\text{CO}_2$ -
1320 products ($0.2 [0.2, 0.3] \text{ GtC yr}^{-1}$), and inversion systems ($-0.3 [-0.1, 0.8] \text{ GtC yr}^{-1}$) all indicate an approximately
1321 neutral tropical ocean flux (see Figure S1 for spatial patterns). DGVMs indicate a net land sink ($S_{\text{LAND}} - E_{\text{LUC}}$) of
1322 $0.6 \pm 0.4 \text{ GtC yr}^{-1}$, whereas the inversion systems indicate a net land flux of $0.03 [-0.8, 1.1] \text{ GtC yr}^{-1}$, though with
1323 high uncertainty (Figure 13, third row).



1324 The tropical lands are the origin of most of the atmospheric CO₂ interannual variability (Ahlström et al., 2015),
1325 consistently among the process models and inversions (Figure 13). The interannual variability in the tropics is
1326 similar among the ocean f CO₂-products (0.07-0.16 GtC yr⁻¹) and the GOBMs (0.07-0.16 GtC yr⁻¹,
1327 Figure S2), which is the highest ocean sink variability of all regions. The DGVMs and inversions indicate that
1328 atmosphere-to-land CO₂ fluxes are more variable than atmosphere-to-ocean CO₂ fluxes in the tropics, with
1329 interannual variability of 0.35 to 1.61 and 0.77-0.92 GtC yr⁻¹ for DGVMs and inversions, respectively.

1330 3.8.2.3 South

1331 In the southern extra-tropics (south of 30°S), the atmospheric inversions suggest a net atmosphere-to-surface
1332 sink (SOCEAN+SLAND-ELUC) for 2013-2022 of 1.5 [1.2, 1.9] GtC yr⁻¹, slightly higher than the process models'
1333 estimate of 1.5 ± 0.4 GtC yr⁻¹ (Figure 13). An approximately neutral net land flux (SLAND-ELUC) for the southern
1334 extra-tropics is estimated by both the DGVMs (0.05 ± 0.07 GtC yr⁻¹) and the inversion systems (sink of 0.02 [-
1335 0.2, 0.2] GtC yr⁻¹). This means nearly all carbon uptake is due to oceanic sinks south of 30°S. The Southern
1336 Ocean flux in the f CO₂-products (1.6 [1.3, 1.7 GtC yr⁻¹) and inversion estimates (1.5 [1.3, 1.9] GtCyr-1) is
1337 slightly higher than in the GOBMs (1.4 ± 0.3 GtC yr⁻¹) (Figure 13, bottom row). This discrepancy in the mean
1338 flux is smaller this year than in previous releases due to the change in data set of the regional distribution of the
1339 river flux adjustment applied to f CO₂-products and inverse systems to isolate the anthropogenic SOCEAN flux.
1340 The data set used (Lacroix et al., 2020) has less river-induced carbon outgassing in the Southern Ocean than the
1341 previously used data set (Aumont et al., 2001). Nevertheless, the time-series of atmospheric inversions and
1342 f CO₂-products diverge from the GOBMs. A substantial overestimation of the trends in the f CO₂-products could
1343 be explained by sparse and unevenly distributed observations, especially in wintertime (Figure S1; Hauck et al.,
1344 2023; Gloege et al., 2021). Model biases may contribute as well, with biases in mode water formation,
1345 stratification, and the chemical buffer capacity known to play a role in Earth System Models (Terhaar et al.,
1346 2021, Bourgeois et al., 2022, Terhaar et al., 2022).

1347 The interannual variability in the southern extra-tropics is low because of the dominance of ocean areas with
1348 low variability compared to land areas. The split between land (SLAND-ELUC) and ocean (SOCEAN) shows a
1349 substantial contribution to variability in the south coming from the land, with no consistency between the
1350 DGVMs and the inversions or among inversions. This is expected due to the difficulty of separating exactly the
1351 land and oceanic fluxes when viewed from atmospheric observations alone. The SOCEAN interannual variability
1352 was found to be higher in the f CO₂-products (0.04-0.18 GtC yr⁻¹) compared to GOBMs (0.03 to 0.06 GtC yr⁻¹)
1353 in 1990-2022 (Figure S2). Model subsampling experiments recently illustrated that f CO₂-products may
1354 overestimate decadal variability in the Southern Ocean carbon sink by 30% and the trend since 2000 by 50-
1355 130% due to data sparsity, based on one and two f CO₂-products with strong variability (Gloege et al., 2021,
1356 Hauck et al., 2023).

1357 3.8.2.4 RECCAP2 regions

1358 Aligning with the RECCAP-2 initiative (Ciais et al., 2022; Poulter et al., 2022; DeVries et al., 2023), we
1359 provide an overview of ELUC, SLAND, Net land (SLAND - ELUC), and SOCEAN fluxes for 10 land regions, and 5 ocean
1360 regions, averaged over the period 2013-2022. The DGVMs and inversions suggest a positive net land sink in all



1361 regions, except for South America and Africa, where the inversions indicate a small net source of respectively -
1362 $0.1 [-0.5, 0.3]$ GtC yr^{-1} and $-0.3 [-0.6, -0.1]$ GtC yr^{-1} , compared to a small sink of 0.1 ± 0.3 GtC yr^{-1} and
1363 0.3 ± 0.2 GtC yr^{-1} for the DGVMs. However, for South America, there is substantial uncertainty in both products
1364 (ensembles span zero). For the DGVMs, this is driven by uncertainty in both S_{LAND} (0.6 ± 0.5 GtC yr^{-1}) and E_{LUC}
1365 (0.4 ± 0.2 GtC yr^{-1}). The bookkeeping models also suggest an E_{LUC} source of around 0.4 GtC yr^{-1} in South
1366 America and Africa, in line with the DGVMs estimates. Bookkeeping models and DGVMs similarly estimate a
1367 loss of 0.4 GtC yr^{-1} in Southeast Asia, with DGVMs suggesting a near neutral net land sink (0.03 ± 0.12 GtC
1368 yr^{-1}). This contrasts the inversion estimate of a $0.2 [-0.3, 0.6]$ GtC yr^{-1} sink, although the ensemble spread is
1369 substantial. The inversions suggest the largest net land sinks are located in North America ($0.5 [-0.1, 0.8]$ GtC
1370 yr^{-1}), Russia ($0.7 [0.5, 1.1]$ GtC yr^{-1}), and East Asia ($0.3 [0.0, 0.9]$ GtC yr^{-1}). This agrees well with the DGVMs
1371 in North America (0.4 ± 0.2 GtC yr^{-1}), which indicate a large natural land sink (S_{LAND}) of 0.6 ± 0.2 GtC yr^{-1} ,
1372 being slightly reduced by land-use related carbon losses (0.2 ± 0.1 GtC yr^{-1}). The DGVMs suggest a smaller net
1373 land sink in Russia compared to inversions (0.4 ± 0.2 GtC yr^{-1}), and a similar net sink in East Asia (0.2 ± 0.1 GtC
1374 yr^{-1}).

1375 There is generally a higher level of agreement in regional S_{OCEAN} estimates between the different data streams
1376 (GOBMs, $f\text{CO}_2$ -products and atmospheric inversions) on decadal scale, compared to the land flux estimates. All
1377 data streams agree that the largest contribution to S_{OCEAN} stems from the Southern Ocean, with important
1378 contributions also from the vast ocean basins in the Atlantic and Pacific oceans. In the Southern Ocean, GOBMs
1379 suggest a sink of 1.0 ± 0.3 GtC yr^{-1} , in line with the $f\text{CO}_2$ -products ($1.1 [0.9, 1.2]$ GtC yr^{-1}) and atmospheric
1380 inversions ($1.0 [0.8, 1.4]$ GtC yr^{-1}). There is similar agreement in the Pacific ocean, with GOBMs, $f\text{CO}_2$ -
1381 products, and atmospheric inversions indicating a sink of 0.5 ± 0.1 GtC yr^{-1} , $0.7 [0.5, 0.9]$ GtC yr^{-1} , and 0.6
1382 $[0.2, 1.0]$ GtC yr^{-1} , respectively. However, in the Atlantic ocean, GOBMs simulate a sink of 0.5 ± 0.1 GtC yr^{-1} ,
1383 noticeably lower than both the $f\text{CO}_2$ -products ($0.8 [0.7, 0.9]$ GtC yr^{-1}) and atmospheric inversions ($0.8 [0.5, 1.2]$
1384 GtC yr^{-1}). It is important to note the $f\text{CO}_2$ -products and atmospheric inversions have a substantial and uncertain
1385 river flux adjustment in the Atlantic ocean (0.3 GtC yr^{-1}) that also leads to a mean offset between GOBMs and
1386 $f\text{CO}_2$ -products/inversions in the latitude band of the tropics (Figure 13). The Indian Ocean due its smaller size
1387 and the Arctic Ocean due to its size and sea-ice cover that prevents air-sea gas-exchange are responsible for
1388 smaller but non negligible S_{OCEAN} fluxes (Indian Ocean: ($0.3 [0.2, 0.4]$ GtC yr^{-1} , $0.3 [0.3, 0.4]$ GtC yr^{-1} , and 0.4
1389 $[0.3, 0.6]$ GtC yr^{-1} for GOBMs, $f\text{CO}_2$ -products, and atmospheric inversions, respectively, and Arctic Ocean: (0.1
1390 $[0.1, 0.1]$ GtC yr^{-1} , $0.2 [0.2, 0.2]$ GtC yr^{-1} , and $0.1 [0.1, 0.1]$ GtC yr^{-1} for GOBMs, $f\text{CO}_2$ -products, and
1391 atmospheric inversions, respectively). Note that the S_{OCEAN} numbers presented here deviate from numbers
1392 reported in RECCAP-2 where the net air-sea CO_2 flux is reported (i.e. without river flux adjustment for $f\text{CO}_2$ -
1393 products and inversions, and with river flux adjustment subtracted from GOBMs in most chapters, or comparing
1394 unadjusted data sets with discussion of uncertain regional riverine fluxes as major uncertainty, e.g. Sarma et al.,
1395 2023, DeVries et al., 2023).



1396 **3.8.2.5 Tropical vs northern land uptake**

1397 A continuing conundrum is the partitioning of the global atmosphere-land flux between the northern hemisphere
1398 land and the tropical land (Stephens et al., 2017; Pan et al., 2011; Gaubert et al., 2019). It is of importance
1399 because each region has its own history of land-use change, climate drivers, and impact of increasing
1400 atmospheric CO₂ and nitrogen deposition. Quantifying the magnitude of each sink is a prerequisite to
1401 understanding how each individual driver impacts the tropical and mid/high-latitude carbon balance.

1402 We define the North-South (N-S) difference as net atmosphere-land flux north of 30°N minus the net
1403 atmosphere-land flux south of 30°N. For the inversions, the N-S difference ranges from -0.5 GtC yr⁻¹ to +3.0
1404 GtC yr⁻¹ across this year's inversion ensemble, but with a clear cluster of solutions driven by the OCO-2 satellite
1405 product with a NH land sink of 1.6-2.2 GtC yr⁻¹, along with a tropical land flux of -0.6 to +0.2 GtC yr⁻¹, and a
1406 dipole between +1.4 and +2.8 GtC yr⁻¹ for the period 2015-2022. Whether this tighter clustering relative to the
1407 surface-observation based inversions is driven by (a) additional information on tropical fluxes delivered by
1408 tropical retrievals contained in OCO-2, (b) a tighter constraint on the NH land sink from that same product, or
1409 (c) a reduced sensitivity to vertical transport differences between models when using CO₂ column integrals,
1410 requires further investigation.

1411 In the ensemble of DGVMs the N-S difference is 0.5 ± 0.6 GtC yr⁻¹, a much narrower range than the one from
1412 atmospheric inversions. Five DGVMs have a N-S difference larger than 1.0 GtC yr⁻¹, compared to only two
1413 from last year's ensemble. This is still only 25% of DGVMs, compared to most inversion systems simulating a
1414 difference at least this large. The smaller spread across DGVMs than across inversions is to be expected as there
1415 is no correlation between Northern and Tropical land sinks in the DGVMs as opposed to the inversions where
1416 the sum of the two regions being well-constrained by atmospheric observations leads to an anti-correlation
1417 between these two regions. This atmospheric N-S gradient could be used as an additional way to evaluate
1418 tropical and NH uptake in DGVMs, if their fluxes were combined with multiple transport models. Vice versa,
1419 the much smaller spread in the N-S difference between the DGVMs could help to scrutinise the inverse systems
1420 further. For example, a large northern land sink and a tropical land source in an inversion would suggest a large
1421 sensitivity to CO₂ fertilisation (the dominant factor driving the land sinks) for Northern ecosystems, which
1422 would be not mirrored by tropical ecosystems. Such a combination could be hard to reconcile with the process
1423 understanding gained from the DGVM ensembles and independent measurements (e.g. Free Air CO₂
1424 Enrichment experiments).

1425 **3.8.3 Forest Fires in 2023**

1426 Fire emissions so far in 2023 have been above the average of recent decades, due to an extreme wildfire season
1427 in North America. Figure S9 shows global and regional emissions estimates for the period 1st Jan-30th
1428 September in each year 2003-2023. Estimates derive from two global fire emissions products: the global fire
1429 emissions database (GFED, version 4.1s; van der Werf et al., 2017), and; the global fire assimilation system
1430 (GFAS, operated by the Copernicus Atmosphere Service; Di Giuseppe et al., 2018). The two products estimate
1431 that global emissions from fires were 1.5-1.8 GtC yr⁻¹ during January-September 2023. These estimates are 13-



1432 15% above the 2013-2022 average for the same months (1.3-1.6 GtC yr⁻¹) and 7-9% above the 2003-2022
1433 average (1.4-1.6 GtC yr⁻¹).

1434 The above-average global fire emissions during January-September 2023 have occurred despite below-average
1435 fire emissions from major source regions. On average during 2013-2022, 72-79% of global fire emissions
1436 through September occur in the tropics (0.9-1.3 GtC yr⁻¹) and around half of global fire emissions through
1437 September occur in Africa (0.6-0.8 GtC yr⁻¹). This year, through September, fire emissions in the tropics (0.7-
1438 0.9 GtC yr⁻¹) were 7-23% below the 2013-2022 average and fire emissions in Africa (0.5-0.7 GtC yr⁻¹) were 7-
1439 17% below the 2013-2022 average.

1440 In contrast, fire emissions from the Northern extra-tropics so far in 2023 have exceeded the values of all
1441 previous years 2003-2022. Northern extra-tropical emissions during January-September 2023 (0.6-0.8 GtC yr⁻¹)
1442 were 80-160% above the average for the same months in the past decade (0.3 GtC yr⁻¹ for both global fire
1443 emissions products). Fire emissions in North America alone (0.5-0.7 GtC yr⁻¹) were 220-380% above the
1444 average of the past decade (0.1 GtC yr⁻¹ for both products). In both products, North America was the only
1445 RECCAP2 region with above-average fire C emissions for January-September in 2023.

1446 While the fire emission fluxes presented above point towards a highly unusual Northern Hemisphere fire season
1447 so far in 2023, we caution that the fluxes presented should not be compared directly with other fluxes of the
1448 budget (e.g. S_{LAND} or E_{LUC}) due to incompatibilities between the observable fire emission fluxes and what is
1449 quantified in the S_{LAND} and E_{LUC} components of the budget. The fire emission estimates from global fire
1450 products relate to all fire types that can be observed in Earth Observations (Giglio et al., 2018; Randerson et al.,
1451 2012; Kaiser et al., 2012), including (i) fires occurring as part of natural disturbance-recovery cycles that would
1452 also have occurred in the pre-industrial period (Yue et al., 2016; Keeley and Pausas, 2019; Zou et al., 2019), (ii)
1453 fires occurring above and beyond natural disturbance-recovery cycle due to changes in climate, CO₂ and N
1454 fertilisation and to an increased frequency of extreme drought and heatwave events (Abatzoglou et al., 2019;
1455 Jones et al., 2022; Zheng et al., 2021; Burton et al., 2023), and (iii) fires occurring in relation to land use and
1456 land use change, such as deforestation fires and agricultural fires (van der Werf et al., 2010; Magi et al., 2012).
1457 In the context of the global carbon budget, only the portion of fire emissions associated with (ii) should be
1458 included in the S_{LAND} component, and fire emissions associated with (iii) should already be accounted for in the
1459 E_{LUC} component. Emissions associated with (i) should not be included in the global carbon budget. It is not
1460 currently possible to derive specific estimates for fluxes (i), (ii), and (iii) using global fire emission products
1461 such as GFED or GFAS. In addition, the fire emissions estimates from global fire emissions products represent
1462 a gross flux of carbon to the atmosphere, whereas the S_{LAND} component of the budget is a net flux that should
1463 also include post-fire recovery fluxes. Even if emissions from fires of type (ii) could be separated from those of
1464 type (i), these fluxes may be partially or wholly offset in subsequent years by post-fire fluxes as vegetation
1465 recovers, sequestering carbon from the atmosphere to the terrestrial biosphere (Yue et al., 2016).



1466 **3.9 Closing the Global Carbon Cycle**

1467 **3.9.1 Partitioning of Cumulative Emissions and Sink Fluxes**

1468 The global carbon budget over the historical period (1850-2021) is shown in Figure 3.

1469 Emissions during the period 1850-2022 amounted to 695 ± 70 GtC and were partitioned among the atmosphere
1470 (280 ± 5 GtC; 40%), ocean (180 ± 35 GtC; 26%), and land (225 ± 55 GtC; 32%). The cumulative land sink is
1471 almost equal to the cumulative land-use emissions (220 ± 70 GtC), making the global land nearly neutral over
1472 the whole 1850-2022 period.

1473 The use of nearly independent estimates for the individual terms of the global carbon budget shows a cumulative
1474 budget imbalance of 15 GtC (2% of total emissions) during 1850-2022 (Figure 3, Table 8), which, if correct,
1475 suggests that emissions could be slightly too high by the same proportion (2%) or that the combined land and
1476 ocean sinks are slightly underestimated (by about 3%), although these are well within the uncertainty range of
1477 each component of the budget. Nevertheless, part of the imbalance could originate from the estimation of
1478 significant increase in E_{FOS} and E_{LUC} between the mid 1920s and the mid 1960s which is unmatched by a similar
1479 growth in atmospheric CO_2 concentration as recorded in ice cores (Figure 3). However, the known loss of
1480 additional sink capacity of 30-40 GtC (over the 1850-2020 period) due to reduced forest cover has not been
1481 accounted for in our method and would exacerbate the budget imbalance (see Section 2.10 and Supplement
1482 S.6.4).

1483 For the more recent 1960-2022 period where direct atmospheric CO_2 measurements are available, total
1484 emissions ($E_{\text{FOS}} + E_{\text{LUC}}$) amounted to 485 ± 50 GtC, of which 395 ± 20 GtC (82%) were caused by fossil CO_2
1485 emissions, and 90 ± 45 GtC (18%) by land-use change (Table 8). The total emissions were partitioned among
1486 the atmosphere (215 ± 5 GtC; 44%), ocean (125 ± 25 GtC; 25%), and the land (150 ± 35 GtC; 31%), with a near
1487 zero (-5 GtC) unattributed budget imbalance. All components except land-use change emissions have
1488 significantly grown since 1960, with important interannual variability in the growth rate in atmospheric CO_2
1489 concentration and in the land CO_2 sink (Figure 4), and some decadal variability in all terms (Table 7).
1490 Differences with previous budget releases are documented in Figure S5.

1491 The global carbon budget averaged over the last decade (2013-2022) is shown in Figure 2, Figure 14 (right
1492 panel) and Table 7. For this period, 88% of the total emissions ($E_{\text{FOS}} + E_{\text{LUC}}$) were from fossil CO_2 emissions
1493 (E_{FOS}), and 12% from land-use change (E_{LUC}). The total emissions were partitioned among the atmosphere
1494 (47%), ocean (26%) and land (31%), with a small unattributed budget imbalance ($\sim 4\%$). For single years, the
1495 budget imbalance can be larger (Figure 4). For 2022, the combination of our estimated sources (11.1 ± 0.9 GtC
1496 yr^{-1}) and sinks (11.2 ± 0.9 GtC yr^{-1}) leads to a B_{IM} of -0.09 GtC, suggesting a near closure of the global carbon
1497 budget, although there is relatively high uncertainty on B_{IM} (± 1.3 GtC for 2022) as this is calculated as the
1498 residual of the five budget terms.



1499 **3.9.2 Trend and Variability in the Carbon Budget Imbalance**

1500 The carbon budget imbalance (B_{IM} ; Eq. 1, Figure 4) quantifies the mismatch between the estimated total
1501 emissions and the estimated changes in the atmosphere, land, and ocean reservoirs. The budget imbalance from
1502 1960 to 2022 is very small (-3.0 GtC over the period, i.e. average of 0.05 GtC yr^{-1}) and shows no trend over the
1503 full time series (Figure 4e). The process models (GOBMs and DGVMs) and data-products have been selected to
1504 match observational constraints in the 1990s, but no further constraints have been applied to their representation
1505 of trend and variability. Therefore, the near-zero mean and trend in the budget imbalance is seen as evidence of
1506 a coherent community understanding of the emissions and their partitioning on those time scales (Figure 4).
1507 However, the budget imbalance shows substantial variability of the order of $\pm 1 \text{ GtC yr}^{-1}$, particularly over semi-
1508 decadal time scales, although most of the variability is within the uncertainty of the estimates. The positive
1509 carbon imbalance during the 1960s, and early 1990s, indicates that either the emissions were overestimated, or
1510 the sinks were underestimated during these periods. The reverse is true for the 1970s, and to a lesser extent for
1511 the 1980s and 2013-2022 period (Figure 4, Table 7).

1512 We cannot attribute the cause of the variability in the budget imbalance with our analysis, we only note that the
1513 budget imbalance is unlikely to be explained by errors or biases in the emissions alone because of its large semi-
1514 decadal variability component, a variability that is atypical of emissions and has not changed in the past 60 years
1515 despite a near tripling in emissions (Figure 4). Errors in S_{LAND} and S_{OCEAN} are more likely to be the main cause
1516 for the budget imbalance, especially on interannual to semi-decadal timescales. For example, underestimation of
1517 the S_{LAND} by DGVMs has been reported following the eruption of Mount Pinatubo in 1991 possibly due to
1518 missing responses to changes in diffuse radiation (Mercado et al., 2009). Although since GCB2021 we
1519 accounted for aerosol effects on solar radiation quantity and quality (diffuse vs direct), most DGVMs only used
1520 the former as input (i.e., total solar radiation) (Table S1). Thus, the ensemble mean may not capture the full
1521 effects of volcanic eruptions, i.e. associated with high light scattering sulphate aerosols, on the land carbon sink
1522 (O'Sullivan et al., 2021). DGVMs are suspected to overestimate the land sink in response to the wet decade of
1523 the 1970s (Sitch et al., 2008). Quasi-decadal variability in the ocean sink has also been reported, with all
1524 methods agreeing on a smaller than expected ocean CO_2 sink in the 1990s and a larger than expected sink in the
1525 2000s (Figure 10; Landschützer et al., 2016, DeVries et al., 2019, Hauck et al., 2020, McKinley et al., 2020,
1526 Gruber et al., 2023) and the climate-driven variability could be substantial but is not well constrained (DeVries
1527 et al., 2023, Müller et al., 2023). Errors in sink estimates could also be driven by errors in the climatic forcing
1528 data, particularly precipitation for S_{LAND} and wind for S_{OCEAN} . Also, the B_{IM} shows substantial departure from
1529 zero on yearly time scales (Figure 4e), highlighting unresolved variability of the carbon cycle, likely in the land
1530 sink (S_{LAND}), given its large year to year variability (Figure 4d and 8).

1531 Both the budget imbalance (B_{IM} , Table 7) and the residual land sink from the global budget ($E_{FOS}+E_{LUC}-G_{ATM}-$
1532 S_{OCEAN} , Table 5) include an error term due to the inconsistencies that arises from combining E_{LUC} from
1533 bookkeeping models with S_{LAND} from DGVMs, most notably the loss of additional sink capacity (see Section
1534 2.10 and Supplement S.6.4). Other differences include a better accounting of land use changes practices and
1535 processes in bookkeeping models than in DGVMs, or the bookkeeping models error of having present-day
1536 observed carbon densities fixed in the past. That the budget imbalance shows no clear trend towards larger



1537 values over time is an indication that these inconsistencies probably play a minor role compared to other errors
1538 in S_{LAND} or S_{OCEAN} .

1539 Although the budget imbalance is near zero for the recent decades, it could be due to a compensation of errors.
1540 We cannot exclude an overestimation of CO_2 emissions, particularly from land-use change, given their large
1541 uncertainty, as has been suggested elsewhere (Piao et al., 2018), combined with an underestimate of the sinks. A
1542 larger DGVM ($S_{\text{LAND-ELUC}}$) over the extra-tropics would reconcile model results with inversion estimates for
1543 fluxes in the total land during the past decade (Figure 13; Table 5). Likewise, a larger S_{OCEAN} is also possible
1544 given the higher estimates from the $f\text{CO}_2$ -products (see Section 3.6.2, Figure 10 and Figure 13), the
1545 underestimation of interior ocean anthropogenic carbon accumulation in the GOBMs (Section 3.6.5), and the
1546 recently suggested upward adjustments of the ocean carbon sink in Earth System Models (Terhaar et al., 2022),
1547 and in $f\text{CO}_2$ -products, here related to a potential temperature bias and skin effects (Watson et al., 2020; Dong et
1548 al., 2022; Figure 10). If S_{OCEAN} were to be based on $f\text{CO}_2$ -products alone, with all $f\text{CO}_2$ -products including this
1549 adjustment, this would result in a 2013-2022 S_{OCEAN} of 3.7 GtC yr⁻¹ (Dong et al., 2022) or >3.9 GtC yr⁻¹
1550 (Watson et al., 2020), i.e., outside of the range supported by the atmospheric inversions and with an implied
1551 negative B_{IM} of more than -1 GtC yr⁻¹ indicating that a closure of the budget could only be achieved with either
1552 anthropogenic emissions being significantly larger and/or the net land sink being substantially smaller than
1553 estimated here. A recent model study suggests that the skin effect is smaller (about 0.1 GtC yr⁻¹ or 5%) due to
1554 feedbacks with surface carbon concentration (Bellenger et al., 2023), which would nevertheless lead to a larger
1555 S_{OCEAN} even in the GOBMs. More integrated use of observations in the Global Carbon Budget, either on their
1556 own or for further constraining model results, should help resolve some of the budget imbalance (Peters et al.,
1557 2017).

1558 **4 Tracking progress towards mitigation targets**

1559 The average growth in global fossil CO_2 emissions peaked at nearly +3% per year during the 2000s, driven by
1560 the rapid growth in emissions in China. In the last decade, however, the global growth rate has slowly declined,
1561 reaching a low +0.5% per year over 2013-2022. While this slowdown in global fossil CO_2 emissions growth is
1562 welcome, global fossil CO_2 emissions continue to grow, far from the rapid emission decreases needed to be
1563 consistent with the temperature goals of the Paris Agreement.

1564 Since the 1990s, the average growth rate of fossil CO_2 emissions has continuously declined across the group of
1565 developed countries of the Organisation for Economic Co-operation and Development (OECD), with emissions
1566 peaking in around 2005 and now declining at around 1% yr⁻¹ (Le Quéré et al., 2021). In the decade 2013-2022,
1567 territorial fossil CO_2 emissions decreased significantly (at the 95% confidence level) in 18 countries/economies
1568 whose economies grew significantly (also at the 95% confidence level): Belgium, Brazil, Croatia, Czechia,
1569 Denmark, Estonia, Finland, France, Germany, Greece, Hong Kong, Israel, Italy, Jamaica, Japan, Luxembourg,
1570 Netherlands, Norway, Portugal, Romania, Slovenia, South Africa, Sweden, Switzerland, United Kingdom,
1571 USA, Zimbabwe (updated from Le Quéré et al., 2019). Altogether, these 18 countries emitted 1.9 GtC yr⁻¹ (7.1
1572 GtCO₂ yr⁻¹) on average over the last decade, about 20% of world CO_2 fossil emissions. Figure 16 shows that the
1573 emission declines in the USA and the EU27 are primarily driven by slightly weaker economic growth in the last
1574 decade compared to the 1990s, sustained declines in energy per GDP (though, weakening in the USA), and



1575 sustained declines in CO₂ emissions per unit energy (decarbonisation) with a slight acceleration in the US in the
1576 last decade.

1577 In contrast, fossil CO₂ emissions continue to grow in non-OECD countries, although the growth rate has slowed
1578 from almost 6% yr⁻¹ during the 2000s to less than 2% yr⁻¹ in the last decade. Representing 47% of non-OECD
1579 emissions in 2022, a large part of this slowdown is due to China, which has seen emissions growth decline from
1580 9% yr⁻¹ in the 2000s to 2.2% yr⁻¹ in the last decade. Excluding China, non-OECD emissions grew at 3.1% yr⁻¹ in
1581 the 2000s compared to 1.5% yr⁻¹ in the last decade. Figure 16 shows that China has had weaker economic
1582 growth in the 2000s compared to the 2010s and a higher decarbonisation rate from 2005 to 2015 comparable to
1583 the highs in the 1990s, though the decarbonisation rate has slowed considerably since 2016. India and the rest of
1584 the world have strong economic growth that is not offset by decarbonisation or declines in energy per GDP,
1585 driving up fossil CO₂ emissions. Despite the high deployment of renewables in some countries (e.g., India),
1586 fossil energy sources continue to grow to meet growing energy demand (Le Quéré et al., 2019).

1587 Globally, fossil CO₂ emissions growth is slowing, and this is due in part to the emergence of climate policy
1588 (Eskander and Fankhauser 2020; Le Quere et al 2019) and technological change, which is leading to a shift from
1589 coal to gas and growth in renewable energies, and reduced expansion of coal capacity. At the aggregated global
1590 level, decarbonisation shows a strong and growing signal in the last decade, with smaller contributions from
1591 lower economic growth and declines in energy per GDP. Despite the slowing growth in global fossil CO₂
1592 emissions, emissions are still growing, far from the reductions needed to meet the ambitious climate goals of the
1593 UNFCCC Paris agreement.

1594 This year we updated the remaining carbon budget (RCB) based on two studies, the IPCC AR6 (Canadell et al,
1595 2021) as used in GCB2022, and a recent revision of the IPCC AR6 estimates (Forster et al 2023). We update the
1596 RCB assessed by the IPCC AR6 (Canadell et al., 2021), accounting for the 2020 to 2023 estimated emissions
1597 from fossil fuel combustion (E_{FOS}) and land use changes (E_{LUC}). From January 2024, the IPCC AR6 RCB (50%
1598 likelihood) for limiting global warming to 1.5°C, 1.7°C and 2°C is estimated to amount to 95, 190, and 325 GtC
1599 (340, 690, 1190 GtCO₂). The Forster et al. (2023) study proposed a significantly lower RCB than IPCC AR6,
1600 with the largest reduction being due to an update of the climate emulator (MAGICC) used to estimate the
1601 warming contribution of non-CO₂ agents, and to the warming (i.e. emissions) that occurred over the 2020-2022
1602 period. We update the Forster et al., budget accounting for the 2023 estimated emissions from fossil fuel
1603 combustion (E_{FOS}) and land use changes (E_{LUC}). From January 2024, the Forster et al., (2023) RCB (50%
1604 likelihood) for limiting global warming to 1.5°C, 1.7°C and 2°C is estimated to amount to 55, 155, and 305 GtC
1605 (210, 560, 1110 GtCO₂), significantly smaller than the updated IPCC AR6 estimate. Both the original IPCC
1606 AR6 and Forster et al. (2023) estimates include an uncertainty due to the climate response to cumulative CO₂
1607 emissions, which is reflected through the percent likelihood of exceeding the given temperature threshold, an
1608 additional uncertainty of 220GtCO₂ due to alternative non-CO₂ emission scenarios, and other sources of
1609 uncertainties (see Canadell et al., 2021). The two sets of estimates overlap when considering all uncertainties.
1610 The IPCC AR6 estimates have the advantage of a consensus building approach, while the Forster et al. (2023)
1611 estimates include significant update estimates but without the backing of the IPCC yet. Here, we take the
1612 average of our update of both IPCC AR6 and Forster et al. (2023) estimates, giving a remaining carbon (50%
1613 likelihood) for limiting global warming to 1.5°C, 1.7°C and 2°C of respectively 75, 175, and 315 GtC (275, 625,



1614 1150 GtCO₂) starting from January 2024. We emphasise the large uncertainties, particularly when close to the
1615 global warming limit of 1.5°C. These 1.5°C, 1.7°C and 2°C average remaining carbon budgets correspond
1616 respectively to about 7, 15 and 28 years from the beginning of 2024, at the 2023 level of total anthropogenic
1617 CO₂ emissions. Reaching net-zero CO₂ emissions by 2050 entails cutting total anthropogenic CO₂ emissions by
1618 about 0.4 GtC (1.5 GtCO₂) each year on average, comparable to the decrease in E_{FOS} observed in 2020 during
1619 the COVID-19 pandemic. However, this would lead to cumulative emissions over 2024-2050 of 150 GtC (550
1620 GtCO₂), well above the remaining carbon budget of 75 GtC to limit global warming to 1.5°C, but still below the
1621 remaining budget of 175 GtC to limit warming to 1.7°C (in phase with the “well below 2°C” ambition of the
1622 Paris Agreement). Even reaching net zero CO₂ globally by 2040, which would require annual emissions cuts of
1623 0.7 GtC (2.4 GtCO₂) on average, would still exceed the remaining carbon budget, with 95 GtC (350 GtCO₂)
1624 cumulative emissions over 2024-2050, unless the global emissions trajectory becomes net negative (i.e. more
1625 anthropogenic CO₂ sinks than emissions) after 2040.

1626 **5 Discussion**

1627 Each year when the global carbon budget is published, each flux component is updated for all previous years to
1628 consider corrections that are the result of further scrutiny and verification of the underlying data in the primary
1629 input data sets. Annual estimates may be updated with improvements in data quality and timeliness (e.g., to
1630 eliminate the need for extrapolation of forcing data such as land-use). Of all terms in the global budget, only the
1631 fossil CO₂ emissions and the growth rate in atmospheric CO₂ concentration are based primarily on empirical
1632 inputs supporting annual estimates in this carbon budget. The carbon budget imbalance, yet an imperfect
1633 measure, provides a strong indication of the limitations in observations, in understanding and representing
1634 processes in models, and/or in the integration of the carbon budget components.

1635 The persistent unexplained variability in the carbon budget imbalance limits our ability to verify reported
1636 emissions (Peters et al., 2017) and suggests we do not yet have a complete understanding of the underlying
1637 carbon cycle dynamics on annual to decadal timescales. Resolving most of this unexplained variability should
1638 be possible through different and complementary approaches. First, as intended with our annual updates, the
1639 imbalance as an error term should be reduced by improvements of individual components of the global carbon
1640 budget that follow from improving the underlying data and statistics and by improving the models through the
1641 resolution of some of the key uncertainties detailed in Table 10. Second, additional clues to the origin and
1642 processes responsible for the variability in the budget imbalance could be obtained through a closer scrutiny of
1643 carbon variability in light of other Earth system data (e.g., heat balance, water balance), and the use of a wider
1644 range of biogeochemical observations to better understand the land-ocean partitioning of the carbon imbalance
1645 such as the constraint from atmospheric oxygen included this year. Finally, additional information could also be
1646 obtained through better inclusion of process knowledge at the regional level, and through the introduction of
1647 inferred fluxes such as those based on satellite xCO₂ retrievals. The limit of the resolution of the carbon budget
1648 imbalance is yet unclear, but most certainly not yet reached given the possibilities for improvements that lie
1649 ahead.

1650 Estimates of global fossil CO₂ emissions from different datasets are in relatively good agreement when the
1651 different system boundaries of these datasets are considered (Andrew, 2020a). But while estimates of E_{FOS} are



1652 derived from reported activity data requiring much fewer complex transformations than some other components
1653 of the budget, uncertainties remain, and one reason for the apparently low variation between datasets is precisely
1654 the reliance on the same underlying reported energy data. The budget excludes some sources of fossil CO₂
1655 emissions, which available evidence suggests are relatively small (<1%). We have added emissions from lime
1656 production in China and the US, but these are still absent in most other non-Annex I countries, and before 1990
1657 in other Annex I countries.

1658 Estimates of E_{LUC} suffer from a range of intertwined issues, including the poor quality of historical land-cover
1659 and land-use change maps, the rudimentary representation of management processes in most models, and the
1660 confusion in methodologies and boundary conditions used across methods (e.g., Arneeth et al., 2017; Pongratz et
1661 al., 2014, see also Supplement S.6.4 on the loss of sink capacity; Bastos et al., 2021). Uncertainties in current
1662 and historical carbon stocks in soils and vegetation also add uncertainty in the E_{LUC} estimates. Unless a major
1663 effort to resolve these issues is made, little progress is expected in the resolution of E_{LUC}. This is particularly
1664 concerning given the growing importance of E_{LUC} for climate mitigation strategies, and the large issues in the
1665 quantification of the cumulative emissions over the historical period that arise from large uncertainties in E_{LUC}.

1666 By adding the DGVMs estimates of CO₂ fluxes due to environmental change from countries' managed forest
1667 areas (part of S_{LAND} in this budget) to the budget E_{LUC} estimate, we successfully reconciled the large gap
1668 between our E_{LUC} estimate and the land use flux from NGHGs using the approach described in Grassi et al.
1669 (2021) for future scenarios and in Grassi et al. (2023) using data from the Global Carbon Budget 2021. The
1670 updated data presented here can be used as potential adjustment in the policy context, e.g., to help assess the
1671 collective countries' progress towards the goal of the Paris Agreement and avoiding double-accounting for the
1672 sink in managed forests. In the absence of this adjustment, collective progress would hence appear better than it
1673 is (Grassi et al., 2021). The application of this adjustment is also recommended in the UNFCCC Synthesis
1674 report for the first Global Stocktake (UNFCCC, 2022) whenever a comparison between LULUCF fluxes
1675 reported by countries and the global emission estimates of the IPCC is conducted. However, this adjustment
1676 should be seen as a short-term and pragmatic fix based on existing data, rather than a definitive solution to
1677 bridge the differences between global models and national inventories. Additional steps are needed to
1678 understand and reconcile the remaining differences, some of which are relevant at the country level (Grassi, et
1679 al., 2023, Schwingshackl, et al., 2022).

1680 The comparison of GOBMs, *f*CO₂-products, and inversions highlights substantial discrepancy in the temporal
1681 evolution of S_{OCEAN} in the Southern Ocean and northern high-latitudes (Figure 13, Hauck et al., 2023) and in the
1682 mean S_{OCEAN} in the tropics. A large part of the uncertainty in the mean fluxes stems from the regional
1683 distribution of the river flux adjustment term. The current distribution simulates the largest share of the
1684 outgassing to occur in the tropics (Lacroix et al., 2020) in contrast to the regional distribution previously used
1685 with the largest riverine outgassing flux south of 20°S (Aumont et al., 2001). The long-standing sparse data
1686 coverage of *f*CO₂ observations in the Southern compared to the Northern Hemisphere (e.g., Takahashi et al.,
1687 2009) continues to exist (Bakker et al., 2016, 2022, Figure S1) and to lead to substantially higher uncertainty in
1688 the S_{OCEAN} estimate for the Southern Hemisphere (Watson et al., 2020, Gloege et al., 2021, Hauck et al., 2023).
1689 This discrepancy, which also hampers model improvement, points to the need for increased high-quality *f*CO₂
1690 observations especially in the Southern Ocean. At the same time, model uncertainty is illustrated by the large



1691 spread of individual GOBM estimates (indicated by shading in Figure 13) and highlights the need for model
1692 improvement. The diverging trends in SOCEAN from different methods is a matter of concern. Recent and on-
1693 going work suggests that the $f\text{CO}_2$ -products may overestimate the trend (Hauck et al., 2023), though many
1694 products remain to be tested, whereas evidence is accumulating that GOBMs likely underestimate the mean flux
1695 (Section 3.6.2, Terhaar et al., 2022, DeVries et al., 2023, Müller et al., 2023). The independent constraint from
1696 atmospheric oxygen measurements is consistent within errors with the relatively larger ocean sink in the $f\text{CO}_2$ -
1697 products. The assessment of the net land-atmosphere exchange from DGVMs and atmospheric inversions also
1698 shows substantial discrepancy, particularly for the estimate of the net land flux over the northern extra-tropic.
1699 This discrepancy highlights the difficulty to quantify complex processes (CO_2 fertilisation, nitrogen deposition
1700 and fertilisers, climate change and variability, land management, etc.) that collectively determine the net land
1701 CO_2 flux. Resolving the differences in the Northern Hemisphere land sink will require the consideration and
1702 inclusion of larger volumes of observations.

1703 We provide metrics for the evaluation of the ocean and land models and the atmospheric inversions (Figures B2
1704 to B4, Table S10). These metrics expand the use of observations in the global carbon budget, helping 1) to
1705 support improvements in the ocean and land carbon models that produce the sink estimates, and 2) to constrain
1706 the representation of key underlying processes in the models and to allocate the regional partitioning of the CO_2
1707 fluxes. The introduction of process-based metrics targeted to evaluate the simulation of SOCEAN in the ocean
1708 biogeochemistry models is an important addition to the evaluation based on ocean carbon observations. This is
1709 an initial step towards the introduction of a broader range of observations and more stringent model evaluation
1710 that we hope will support continued improvements in the annual estimates of the global carbon budget.

1711 We assessed before that a sustained decrease of -1% in global emissions could be detected at the 66%
1712 likelihood level after a decade only (Peters et al., 2017). Similarly, a change in behaviour of the land and/or
1713 ocean carbon sink would take as long to detect, and much longer if it emerges more slowly. To continue
1714 reducing the carbon imbalance on annual to decadal time scales, regionalising the carbon budget, and integrating
1715 multiple variables are powerful ways to shorten the detection limit and ensure the research community can
1716 rapidly identify issues of concern in the evolution of the global carbon cycle under the current rapid and
1717 unprecedented changing environmental conditions.

1718 **6 Conclusions**

1719 The estimation of global CO_2 emissions and sinks is a major effort by the carbon cycle research community that
1720 requires a careful compilation and synthesis of measurements, statistical estimates, and model results. The
1721 delivery of an annual carbon budget serves two purposes. First, there is a large demand for up-to-date
1722 information on the state of the anthropogenic perturbation of the climate system and its underpinning causes. A
1723 broad stakeholder community relies on the data sets associated with the annual carbon budget including
1724 scientists, policy makers, businesses, journalists, and non-governmental organisations engaged in adapting to
1725 and mitigating human-driven climate change. Second, over the last decades we have seen unprecedented
1726 changes in the human and biophysical environments (e.g., changes in the growth of fossil fuel emissions, impact
1727 of COVID-19 pandemic, Earth's warming, and strength of the carbon sinks), which call for frequent
1728 assessments of the state of the planet, a better quantification of the causes of changes in the contemporary global



1729 carbon cycle, and an improved capacity to anticipate its evolution in the future. Building this scientific
1730 understanding to meet the extraordinary climate mitigation challenge requires frequent, robust, transparent, and
1731 traceable data sets and methods that can be scrutinised and replicated. This paper via 'living data' helps to keep
1732 track of new budget updates.

1733 **Data availability**

1734 The data presented here are made available in the belief that their wide dissemination will lead to greater
1735 understanding and new scientific insights of how the carbon cycle works, how humans are altering it, and how
1736 we can mitigate the resulting human-driven climate change. Full contact details and information on how to cite
1737 the data shown here are given at the top of each page in the accompanying database and summarised in Table 2.

1738 The accompanying database includes three Excel files organised in the following spreadsheets:

1739 File `Global_Carbon_Budget_2023v0.1.xlsx` includes the following:

- 1740 1. Summary
- 1741 2. The global carbon budget (1959-2022);
- 1742 3. The historical global carbon budget (1750-2022);
- 1743 4. Global CO₂ emissions from fossil fuels and cement production by fuel type, and the per-capita emissions
1744 (1850-2022);
- 1745 5. CO₂ emissions from land-use change from the individual bookkeeping models (1959-2022);
- 1746 6. Ocean CO₂ sink from the individual global ocean biogeochemistry models and f CO₂-products (1959-
1747 2022);
- 1748 7. Terrestrial CO₂ sink from the individual DGVMs (1959-2022);
- 1749 8. Cement carbonation CO₂ sink (1959-2022).

1750 File `National_Fossil_Carbon_Emissions_2023v0.1.xlsx` includes the following:

- 1751 1. Summary
- 1752 2. Territorial country CO₂ emissions from fossil fuels and cement production (1850-2022);
- 1753 3. Consumption country CO₂ emissions from fossil fuels and cement production and emissions transfer from
1754 the international trade of goods and services (1990-2020) using CDIAC/UNFCCC data as reference;
- 1755 4. Emissions transfers (Consumption minus territorial emissions; 1990-2020);
- 1756 5. Country definitions.

1757 File `National_LandUseChange_Carbon_Emissions_2023v0.1.xlsx` includes the following:



1758 1. Summary

1759 2. Territorial country CO₂ emissions from Land Use Change (1850-2022) from three bookkeeping models;

1760 All three spreadsheets are published by the Integrated Carbon Observation System (ICOS) Carbon Portal and
1761 are available at <https://doi.org/10.18160/GCP-2023> (Friedlingstein et al., 2023). National emissions data are also
1762 available on Zenodo (Andrew and Peters, 2022), from the Global Carbon Atlas
1763 (<http://www.globalcarbonatlas.org/>, last access: 27 September 2023) and from Our World in Data
1764 (<https://ourworldindata.org/co2-emissions>, last access: 27 September 2023).

1765 **Author contributions**

1766 PF, MO, MWJ, RMA, DCEB, JH, PL, CLQ, ITL, GPP, WP, JP, CSc, and SSi designed the study, conducted the
1767 analysis, and wrote the paper with input from JGC, PCi and RBJ. RMA, GPP and JIK produced the fossil CO₂
1768 emissions and their uncertainties and analysed the emissions data. MH and GMa provided fossil fuel emission
1769 data. JP, TGa, CSc and RAH provided the bookkeeping land-use change emissions with synthesis by JP and
1770 CSc. FJo provided peat drainage emission estimates. SSm and CMP provided the estimates of non-vegetation
1771 CDR fluxes. LBo, MCh, ÖG, NG, TI, TJ, LR, JS, RS, and HiT provided an update of the global ocean
1772 biogeochemical models, TTTC, DF, LG, YI, AJ, GMc, ChR, and JZ provided an update of the ocean *f*CO₂-data
1773 products, with synthesis on both streams by JH, PL and NMa. SRA, LBa, NRB, MB, MCr, KE, WE, RAF, TGk,
1774 AK, NL, DRM, SN, AO, AMO, TO, MEP, DP, KP, GR, AJS, CSw, ST, BT, EvO, RW, and CWR provided
1775 ocean *f*CO₂ measurements for the year 2022, with synthesis by DCEB and KMO. PA, DB, SF, JG, HJ, AKJ,
1776 EK, DK, JK, GMe, LM, PM, MO, BP, TLS, QS, HTi, WY, XYua, XYue, and SZ provided an update of the
1777 Dynamic Global Vegetation Models, with synthesis by SSi and MO. HL, RSA, MW, and PCa provided
1778 estimates of land and ocean sinks from Earth System Models, as well as a projection of the atmospheric growth
1779 rate for 2023. FC, ITL, NC, LF, ARJ, FJi, JL, ZJin, ZLiu, YN, CR, DY, and BZ provided an updated
1780 atmospheric inversion, WP, FC, and ITL developed the protocol and produced the synthesis and evaluation of
1781 the atmospheric inversions. RMA provided projections of the 2023 fossil emissions and atmospheric CO₂
1782 growth rate. PL provided the predictions of the 2023 ocean and land sinks. IBMB, LPC, GCH, KKG, TMR, and
1783 GRvdW provided forcing data for land-use change. FT and GG provided data for the land-use change NGHGI
1784 harmonisation. RK provided key atmospheric CO₂ data. EJM and RFK provided the atmospheric oxygen
1785 constraint on surface net carbon sinks. XL, PPT and MWJ provided the historical atmospheric CO₂
1786 concentration and growth rate. MO and NB produced the aerosol diffuse radiative forcing for the DGVMs. IH
1787 provided the climate forcing data for the DGVMs. ER provided the evaluation of the DGVMs. MWJ provided



1788 the emissions prior for use in the inversion systems. XD provided seasonal emissions data for most recent years
1789 for the emission prior. PF, MO and MWJ coordinated the effort, revised all figures, tables, text and numbers to
1790 ensure the update was clear from the 2022 edition and in line with the globalcarbonatlas.org.

1791 **Competing interests.**

1792 At least one of the (co-)authors is a member of the editorial board of Earth System Science Data

1793 **Acknowledgements**

1794 We thank all people and institutions who provided the data used in this global carbon budget 2023 and the Global
1795 Carbon Project members for their input throughout the development of this publication. We thank Nigel Hawtin
1796 for producing Figure 2 and Figure 15. We thank Alex Vermeulen and Hanna Ritchie for respectively hosting the
1797 Global Carbon Budget datasets on the ICOS portal and the Our World in Data website. We thank Ian G. C. Ashton,
1798 Sebastian Brune, Fatemeh Cheginig, Sam Ditkovsky, Christian Ethé, Amanda R. Fay, Lonneke Goddijn-Murphy,
1799 T. Holding, Yawen Kong, Fabrice Lacroix, Yi Liu, Damian Loher, Naiqing Pan, Paridhi Rustogi, Shijie Shu, J.
1800 D. Shutler, Richard Sims, Phillip Townsend, Jing Wang, Andrew J. Watson, and David K. Woolf for their
1801 involvement in the development, use and analysis of the models and data-products used here. We thank Toste
1802 Tanhua, Marcos Fontela, Claire Lo Monaco and Nicolas Metzl who contributed to the provision of surface ocean
1803 CO₂ observations for the year 2022 (see Table S6). We also thank Stephen D. Jones of the Ocean Thematic Centre
1804 of the EU Integrated Carbon Observation System (ICOS) Research Infrastructure, Eugene Burger of NOAA's
1805 Pacific Marine Environmental Laboratory and Alex Kozyr of NOAA's National Centers for Environmental
1806 Information, for their contribution to surface ocean CO₂ data and metadata management. This is PMEL
1807 contribution 5550. We thank the scientists, institutions, and funding agencies responsible for the collection and
1808 quality control of the data in SOCAT as well as the International Ocean Carbon Coordination Project (IOCCP),
1809 the Surface Ocean Lower Atmosphere Study (SOLAS) and the Integrated Marine Biosphere Research (IMBeR)
1810 program for their support. We thank data providers ObsPack GLOBALVIEWplus v8.0 and NRT v8.1 for
1811 atmospheric CO₂ observations. We thank Fortunat Joos, Samar Khatiwala and Timothy DeVries for providing
1812 historical atmospheric and ocean data. Ingrid T Lujikx and Wouter Peters thank the CarbonTracker Europe team
1813 at Wageningen University, including Remco de Kok, Joram Hooghiem, Linda Kooijmans and Auke van der
1814 Woude. Daniel Kennedy thanks all the scientists, software engineers, and administrators who contributed to the
1815 development of CESM2. Josefine Ghattas thanks the whole ORCHIDEE group. Ian Harris thanks the Japan
1816 Meteorological Agency (JMA) for producing the Japanese 55-year Reanalysis (JRA-55). Reinel Sospedra-



1817 Alfonso thanks Barbara Winter, Woosung Lee, and William J. Merryfield for their contribution to the preparation
1818 and production of CanESM5 runs. Patricia Cadule thanks Olivier Torres, Juliette Mignot, Didier Swingedouw,
1819 and Laurent Bopp for contributions to the IPSL-CM6-LR-ESMCO2 simulations. Yosuke Niwa thanks CSIRO,
1820 EC, EMPA, FMI, IPEN, JMA, LSCE, NCAR, NIES, NILU, NIWA, NOAA, SIO, and TU/NIPR for providing
1821 data for NISMON-CO2. Zhe Jin thanks Xiangjun Tian, Yilong Wang, Hongqin Zhang, Min Zhao, Tao Wang,
1822 Jinzhi Ding and Shilong Piao for their contributions to the GONGGA inversion system. Bo Zheng thanks Yawen
1823 Kong for running the THU inversion system. Frédéric Chevallier thanks Zoé Lloret who maintained the
1824 atmospheric transport model for the CAMS inversions. Frédéric Chevallier and Thi-Tuyet-Trang Chau thank
1825 Marion Gehlen for her contribution to the CMEMS-LSCE-FFNNv2 product. Lian Fang thanks Paul I. Palmer and
1826 acknowledges ongoing support from the National Centre for Earth Observation. Junjie Liu thanks the Jet
1827 Propulsion Laboratory, California Institute of Technology. Zhiqiang Liu thanks Ning Zeng, Yun Liu, Eugenia
1828 Kalnay, and Gassem Asrar for their contributions to the COLA system. Fei Jiang acknowledges ongoing support
1829 from Frontiers Science Center for Critical Earth Material Cycling, Nanjing University. Andy Jacobson thanks the
1830 team at NOAA GML, Boulder, Colorado, USA, who provided the CarbonTracker CT2022 and CT-NRT.v2023-
1831 3 results from the website at <http://carbontracker.noaa.gov>. Meike Becker and Are Olsen thank Sparebanken Vest
1832 / Agenda Vestlandet for their support for the observations on the Statsraad Lehmkuhl. Margot Cronin thanks
1833 Anthony English, Clynt Gregory and Gordon Furey (P&O Maritime Services), Tobias Steinhoff and Aodhan
1834 Fitzgerald (Marine Institute) for their support. Wiley Evans and Katie Pockock thank the Tula Foundation for
1835 funding support. Thanos Gkritzalis and the VLIZ ICOS team are thankful to the crew of the research vessel Simon
1836 Stevin for all the support and help they provide. Data providers Nicolas Metzl and Claire LoMonaco thank the
1837 French Institut National des Sciences de l'Univers (INSU), Institut Polaire français, Paul-Emile Victor (IPEV),
1838 Observatoire des sciences de l'univers Ecce-Terra (OSU at Sorbonne Université), Institut de recherche français
1839 sur les ressources marines (IFREMER), French Oceanographic Fleet (FOF) for the Marion Dufresne data set
1840 (<http://dx.doi.org/10.17600/18001858>). Bronte Tilbrook and Erik van Ooijen thank Australia's Integrated Marine
1841 Observing System (IMOS) for sourcing of CO₂ data. IMOS is enabled by the National Collaborative Research
1842 Infrastructure Strategy (NCRIS). FAOSTAT is funded by FAO member states through their contributions to the
1843 FAO Regular Programme, data contributions by national experts are greatly acknowledged. The views expressed
1844 in this paper are the authors' only and do not necessarily reflect those of FAO. Finally, we thank all funders who
1845 have supported the individual and joint contributions to this work (see details below), as well as the reviewers of
1846 this manuscript and previous versions, and the many researchers who have provided feedback.



1847 **Financial and computing support**

1848 This research was supported by the following sources of funding: Integrated Marine Observing System (IMOS)
1849 [Australia]; ICOS Flanders [Belgium]; Research Foundation Flanders (grant no. I001821N) [Belgium]; Tula
1850 Foundation [Canada]; Chinese Academy of Science Project for Young Scientists in Basic Research (Grant No.
1851 YSBR-037) [China]; National Key R&D Program of China (Grant No: 2020YFA0607504); National Natural
1852 Science Foundation (grant no. 42141020, 42275128) [China]; National Natural Science Foundation (grant no.
1853 42275128) [China]; National Natural Science Foundation (grant no. 41921005) [China]; Scientific Research Start-
1854 up Funds (grant no. QD2021024C) from Tsinghua Shenzhen International Graduate School [China]; Second
1855 Tibetan Plateau Scientific Expedition and Research Program (Grant: 2022QZKK0101) [China]; Young Elite
1856 Scientists Sponsorship Program by CAST (grant no. YESS20200135) [China]; Copernicus Atmosphere
1857 Monitoring Service, implemented by ECMWF (Grant: CAMS2 55) [EC]; Copernicus Marine Environment
1858 Monitoring Service, implemented by MOi (Grant: CAMS2 55) [EC]; H2020 (Horizon 2020) 4C (grant no.
1859 821003) [European Commission, EC]; H2020 ESM2025 – Earth System Models for the Future (grant no.
1860 101003536) [European Commission, EC]; H2020 EuroSea (grant no. 862626) [EC]; H2020 GEORGE (grant no.
1861 101094716) [EC]; H2020 JERICO-S3 (grant no. 871153) [EC]; ICOS France [France]; Institut de Recherche pour
1862 le Développement (IRD) [France]; Federal Ministry of Education and Research (BMBF) (grant no. 03F0885AL1)
1863 [Germany]; Federal Ministry of Education and Research, collaborative project C-SCOPE (Towards Marine
1864 Carbon Observations 2.0: Socializing, COncnecting, Perfecting and Expanding, project no. 03F0877A) [Germany];
1865 Helmholtz Association ATMO programme [Germany]; Helmholtz Association of German Research Centres
1866 (project MOSES; Modular Observation Solutions for Earth Systems) [Germany]; ICOS (Integrated Carbon
1867 Observation System) Germany [Germany]; Ludwig-Maximilians-University Munich, Department of Geography
1868 [Germany]; Marine Institute [Ireland]; Arctic Challenge for Sustainability phase II project (ArCS-II; grant no. JP-
1869 MXD1420318865) [Japan]; Environment Research and Technology Development Fund (grant no. JP-
1870 MEERF21S20800) [Japan]; Fundamental Research Funds for the Central Universities (Grant No:
1871 090414380031); Global Environmental Research Coordination System, Ministry of the Environment (grant no.
1872 E2252) [Japan]; Japan Meteorological Agency [Japan]; Ministry of Education, Culture, Sports, Science and
1873 Technology, MEXT program for the advanced studies of climate change projection (SENTAN) (grant numbers
1874 JPMXD0722680395, JPMXD0722681344) [Japan]; Ministry of Environment, Environmental Restoration and
1875 Conservation Agency, Environment Research and Technology Development Fund (grant no.
1876 JPMEERF21S20810) [Japan]; Research Council of Norway (N-ICOS-2, grant no. 296012) [Norway]; Swiss



1877 National Science Foundation (grant no. 200020-200511) [Switzerland]; National Centre for Atmospheric Science
1878 [UK]; NERC (Natural Environment Research Council) Independent Research Fellowship (NE/V01417X/1) [UK];
1879 NERC (NE/R016518/1) [UK]; Royal Society (grant no. RP\R1\191063) [UK]; UK Research and Innovation
1880 (UKRI) for Horizon Europe (GreenFeedBack, grant no. 10040851) [UK]; NASA Carbon Monitoring System
1881 program (80NSSC21K1059) [USA]; NASA OCO Science team program (80NM0018F0583) [USA]; National
1882 Center for Atmospheric Research (NCAR) cooperative agreement (NSF No. 1852977) [USA]; National Oceanic
1883 and Atmospheric Administration (NOAA) cooperative agreement (NA22OAR4320151) [USA]; National Science
1884 Foundation (NSF- 831361857) [USA]; NOAA (NA20OAR4320278) [USA]; NOAA Cooperative Agreement,
1885 Cooperative Institute for Climate, Ocean, & Ecosystem Studies (CIOCES; NA20OAR4320271) [USA]; NOAA
1886 Cooperative Agreement, Cooperative Institute for Marine and Atmospheric Studies (CIMAS) / University of
1887 Miami (NA20OAR4320472) [USA]; NOAA Global Ocean Monitoring and Observing Program (grant no.
1888 100018302, 100007298, NA-03-AR4320179) [USA]; NOAA Ocean Acidification Program [USA]; National
1889 Science Foundation (OPP-1922922) [USA].

1890 We also acknowledge support from the following computing facilities: Adapter Allocation Scheme from the
1891 National Computational Infrastructure (NCI) [Australia]; High-Performance Computing Center (HPCC) of
1892 Nanjing University [China]; GENCI -TGCC (A0130102201, A0130106328, A0140107732 and A0130107403)
1893 [France], CCRT awarded by CEA/DRF (CCRT2023-p24cheva) [France]; HPC cluster Aether at the University
1894 of Bremen, financed by DFG within the scope of the Excellence Initiative [Germany], the State of Baden-
1895 Württemberg, through bwHPC [Germany]; Earth Simulator (ES4) at JAMSTEC [Japan], JAMSTEC's Super
1896 Computer system [Japan], NIES supercomputer system [Japan], NIES (SX-Aurora) and MRI (FUJITSU Server
1897 PRIMERGY CX2550M5) [Japan]; ADA HPC cluster at the University of East Anglia [UK], UK CEDA
1898 JASMIN supercomputer [UK]; Cheyenne NCAR HPC resources managed by CISL (doi:10.5065/D6RX99HX)
1899 [USA].

1900

1901



1902 **References**

- 1903 Ahlström, A., Raupach, M. R., Schurgers, G., Smith, B., Arneeth, A., Jung, M., Reichstein, M., Canadell, J. G.,
1904 Friedlingstein, P., Jain, A. K., Kato, E., Poulter, B., Sitch, S., Stocker, B. D., Viovy, N., Wang, Y. P., Wiltshire, A., Zaehle,
1905 S., and Zeng, N.: The dominant role of semi-arid ecosystems in the trend and variability of the land CO₂ sink, 348, 895–899,
1906 <https://doi.org/10.1126/science.aaa1668>, 2015.
- 1907 Amador-Jiménez, M., Millner, N., Palmer, C., Pennington, R. T., and Sileci, L.: The Unintended Impact of Colombia's
1908 Covid-19 Lockdown on Forest Fires, *Environ Resource Econ*, 76, 1081–1105, <https://doi.org/10.1007/s10640-020-00501-5>,
1909 2020.
- 1910 Andela, N., Morton, D. C., Giglio, L., Chen, Y., van der Werf, G. R., Kasibhatla, P. S., DeFries, R. S., Collatz, G. J.,
1911 Hantson, S., Kloster, S., Bachelet, D., Forrest, M., Lasslop, G., Li, F., Mangeon, S., Melton, J. R., Yue, C., and Randerson, J.
1912 T.: A human-driven decline in global burned area, *Science*, 356, 1356–1362, <https://doi.org/10.1126/science.aal4108>, 2017.
- 1913 Andrew, R. M.: A comparison of estimates of global carbon dioxide emissions from fossil carbon sources, *Earth Syst. Sci.*
1914 *Data*, 12, 1437–1465, <https://doi.org/10.5194/essd-12-1437-2020>, 2020a.
- 1915 Andrew, R. M.: Timely estimates of India's annual and monthly fossil CO₂ emissions, *Earth Syst. Sci. Data*, 12, 2411–2421,
1916 <https://doi.org/10.5194/essd-12-2411-2020>, 2020b.
- 1917 Andrew, R. M. and Peters, G. P.: The Global Carbon Project's fossil CO₂ emissions dataset (2022v27),
1918 <https://zenodo.org/record/7215364>, 2022.
- 1919 Angelsen, A. and Kaimowitz, D.: Rethinking the Causes of Deforestation: Lessons from Economic Models, *World Bank*
1920 *Res. Obs.*, 14, 73–98, <https://doi.org/10.1093/wbro/14.1.73>, 1999.
- 1921 Aragão, L. E. O. C., Anderson, L. O., Fonseca, M. G., Rosan, T. M., Vedovato, L. B., Wagner, F. H., Silva, C. V. J., Silva
1922 Junior, C. H. L., Arai, E., Aguiar, A. P., Barlow, J., Berenguer, E., Deeter, M. N., Domingues, L. G., Gatti, L., Gloor, M.,
1923 Malhi, Y., Marengo, J. A., Miller, J. B., Phillips, O. L., and Saatchi, S.: 21st Century drought-related fires counteract the
1924 decline of Amazon deforestation carbon emissions, *Nat Commun*, 9, 536, <https://doi.org/10.1038/s41467-017-02771-y>,
1925 2018.
- 1926 Archer, D., Eby, M., Brovkin, V., Ridgwell, A., Cao, L., Mikolajewicz, U., Caldeira, K., Matsumoto, K., Munhoven, G.,
1927 Montenegro, A., and Tokos, K.: Atmospheric Lifetime of Fossil Fuel Carbon Dioxide, *Annu. Rev. Earth Planet. Sci.*, 37,
1928 117–134, <https://doi.org/10.1146/annurev.earth.031208.100206>, 2009.
- 1929 Arneeth, A., Sitch, S., Pongratz, J., Stocker, B. D., Ciais, P., Poulter, B., Bayer, A. D., Bondeau, A., Calle, L., Chini, L. P.,
1930 Gasser, T., Fader, M., Friedlingstein, P., Kato, E., Li, W., Lindeskog, M., Nabel, J. E. M. S., Pugh, T. A. M., Robertson, E.,
1931 Viovy, N., Yue, C., and Zaehle, S.: Historical carbon dioxide emissions caused by land-use changes are possibly larger than
1932 assumed, *Nature Geosci*, 10, 79–84, <https://doi.org/10.1038/ngeo2882>, 2017.
- 1933 Asaadi, A., Arora, V. K., Melton, J. R., and Bartlett, P.: An improved parameterization of leaf area index (LAI) seasonality
1934 in the Canadian Land Surface Scheme (CLASS) and Canadian Terrestrial Ecosystem Model (CTEM) modelling framework,
1935 15, 6885–6907, <https://doi.org/10.5194/bg-15-6885-2018>, 2018.
- 1936 Aumont, O., Orr, J. C., Monfray, P., Ludwig, W., Amiotte-Suchet, P., and Probst, J.-L.: Riverine-driven interhemispheric
1937 transport of carbon, *Global Biogeochem. Cycles*, 15, 393–405, <https://doi.org/10.1029/1999GB001238>, 2001.



- 1938 Aumont, O., Ethé, C., Tagliabue, A., Bopp, L., and Gehlen, M.: PISCES-v2: an ocean biogeochemical model for carbon and
1939 ecosystem studies, 8, 2465–2513, <https://doi.org/10.5194/gmd-8-2465-2015>, 2015.
- 1940 Baccini, A., Walker, W., Carvalho, L., Farina, M., Sulla-Menashe, D., and Houghton, R. A.: Tropical forests are a net carbon
1941 source based on aboveground measurements of gain and loss, *Science*, 358, 230–234,
1942 <https://doi.org/10.1126/science.aam5962>, 2017.
- 1943 Bakker, D. C. E., Pfeil, B., Landa, C. S., Metzl, N., O'Brien, K. M., Olsen, A., Smith, K., Cosca, C., Harasawa, S., Jones, S.
1944 D., Nakaoka, S., Nojiri, Y., Schuster, U., Steinhoff, T., Sweeney, C., Takahashi, T., Tilbrook, B., Wada, C., Wanninkhof, R.,
1945 Alin, S. R., Balestrini, C. F., Barbero, L., Bates, N. R., Bianchi, A. A., Bonou, F., Boutin, J., Bozec, Y., Burger, E. F., Cai,
1946 W.-J., Castle, R. D., Chen, L., Chierici, M., Currie, K., Evans, W., Featherstone, C., Feely, R. A., Fransson, A., Goyet, C.,
1947 Greenwood, N., Gregor, L., Hankin, S., Hardman-Mountford, N. J., Harlay, J., Hauck, J., Hoppema, M., Humphreys, M. P.,
1948 Hunt, C. W., Huss, B., Ibáñez, J. S. P., Johannessen, T., Keeling, R., Kitidis, V., Körtzinger, A., Kozyr, A., Krasakopoulou,
1949 E., Kuwata, A., Landschützer, P., Lauvset, S. K., Lefèvre, N., Lo Monaco, C., Manke, A., Mathis, J. T., Merlivat, L.,
1950 Millero, F. J., Monteiro, P. M. S., Munro, D. R., Murata, A., Newberger, T., Omar, A. M., Ono, T., Paterson, K., Pearce, D.,
1951 Pierrot, D., Robbins, L. L., Saito, S., Salisbury, J., Schlitzer, R., Schneider, B., Schweitzer, R., Sieger, R., Skjelvan, I.,
1952 Sullivan, K. F., Sutherland, S. C., Sutton, A. J., Tadokoro, K., Telszewski, M., Tuma, M., van Heuven, S. M. A. C.,
1953 Vandemark, D., Ward, B., Watson, A. J., and Xu, S.: A multi-decade record of high-quality CO₂ data in version 3 of the
1954 Surface Ocean CO₂ Atlas (SOCAT), *Earth Syst. Sci. Data*, 8, 383–413, <https://doi.org/10.5194/essd-8-383-2016>, 2016.
- 1955 Bakker, Dorothee C. E.; Alin, Simone R.; Bates, Nicholas; Becker, Meike; Feely, Richard A.; Gkritzalis, Thanos; Jones,
1956 Steve D.; Kozyr, Alex; Lauvset, Siv K.; Metzl, Nicolas; Munro, David R.; Nakaoka, Shin-ichiro; Nojiri, Yukihiko; O'Brien,
1957 Kevin M.; Olsen, Are; Pierrot, Denis; Rehder, Gregor; Steinhoff, Tobias; Sutton, Adrienne J.; Sweeney, Colm; Tilbrook,
1958 Bronte; Wada, Chisato; Wanninkhof, Rik; Akl, John; Barbero, Leticia; Beatty, Cory M.; Berghoff, Carla F.; Bittig, Henry
1959 C.; Bott, Randy; Burger, Eugene F.; Cai, Wei-Jun; Castaño-Primo, Rocío; Corredor, Jorge E.; Cronin, Margot; De Carlo,
1960 Eric H.; DeGrandpre, Michael D.; Dietrich, Colin; Drennan, William M.; Emerson, Steven R.; Enochs, Ian C.; Enyo,
1961 Kazutaka; Epherra, Lucía; Evans, Wiley; Fiedler, Björn; Fontela, Marcos; Frangoulis, Constantin; Gehrung, Martina;
1962 Giannoudi, Louisa; Glockzin, Michael; Hales, Burke; Howden, Stephan D.; Ibáñez, J. Severino P.; Kamb, Linus;
1963 Körtzinger, Arne; Lefèvre, Nathalie; Lo Monaco, Claire; Lutz, Vivian A.; Macovei, Vlad A.; Maenner Jones, Stacy;
1964 Manalang, Dana; Manzello, Derek P.; Metzl, Nicolas; Mickett, John; Millero, Frank J.; Monacci, Natalie M.; Morell, Julio
1965 M.; Musielewicz, Sylvia; Neill, Craig; Newberger, Tim; Newton, Jan; Noakes, Scott; Ólafsdóttir, Sólveig Rósa; Ono,
1966 Tsuneo; Osborne, John; Padín, Xose A.; Paulsen, Melf; Perivoliotis, Leonidas; Petersen, Wilhelm; Petihakis, George;
1967 Plueddemann, Albert J.; Rodriguez, Carmen; Rutgersson, Anna; Sabine, Christopher L.; Salisbury, Joseph E.; Schlitzer,
1968 Reiner; Skjelvan, Ingunn; Stamatakis, Natalia; Sullivan, Kevin F.; Sutherland, Stewart C.; T'Jampens, Michiel; Tadokoro,
1969 Kazuaki; Tanhua, Toste; Telszewski, Maciej; Theetaert, Hannelore; Tomlinson, Michael; Vandemark, Douglas; Velo,
1970 Antón; Voynova, Yoana G.; Weller, Robert A.; Whitehead, Chris; Wimart-Rousseau, Cathy (2023). Surface Ocean CO₂
1971 Atlas Database Version 2023 (SOCATv2023) (NCEI Accession 0278913). [indicate subset used]. NOAA National Centers
1972 for Environmental Information. Dataset. <https://doi.org/10.25921/r7xa-bt92>, 2023.
- 1973 Ballantyne, A. P., Alden, C. B., Miller, J. B., Tans, P. P., and White, J. W. C.: Increase in observed net carbon dioxide
1974 uptake by land and oceans during the past 50 years, *Nature*, 488, 70–72, <https://doi.org/10.1038/nature11299>, 2012.
- 1975 Ballantyne, A. P., Andres, R., Houghton, R., Stocker, B. D., Wanninkhof, R., Anderegg, W., Cooper, L. A., DeGrandpre,
1976 M., Tans, P. P., Miller, J. B., Alden, C., and White, J. W. C.: Audit of the global carbon budget: estimate errors and their
1977 impact on uptake uncertainty, *Biogeosciences*, 12, 2565–2584, <https://doi.org/10.5194/bg-12-2565-2015>, 2015.



- 1978 Bastos, A., Hartung, K., Nützel, T. B., Nabel, J. E. M. S., Houghton, R. A., and Pongratz, J.: Comparison of uncertainties in
1979 land-use change fluxes from bookkeeping model parameterisation, *12*, 745–762, <https://doi.org/10.5194/esd-12-745-2021>,
1980 2021.
- 1981 Battle, M. O., Raynor, R., Kesler, S., and Keeling, R.: Technical Note: The impact of industrial activity on the amount of
1982 atmospheric O₂, *Atmospheric Chem. Phys. Discuss.*, 1–17, <https://doi.org/10.5194/acp-2022-765>, 2023.
- 1983 Beckman, J. and Countryman, A. M.: The Importance of Agriculture in the Economy: Impacts from COVID-19, *Am. J. Agr.*
1984 *Econ.*, 103, 1595–1611, <https://doi.org/10.1111/ajae.12212>, 2021.
- 1985 Bellenger, H., Bopp, L., Ethé, C., Ho, D., Duvel, J. P., Flavoni, S., Guez, L., Kataoka, T., Perrot, X., Parc, L., and Watanabe,
1986 M.: Sensitivity of the Global Ocean Carbon Sink to the Ocean Skin in a Climate Model, *J. Geophys. Res. Oceans*, 128,
1987 e2022JC019479, <https://doi.org/10.1029/2022JC019479>, 2023.
- 1988
- 1989 Bennington, V., Gloege, L., and McKinley, G. A.: Variability in the Global Ocean Carbon Sink From 1959 to 2020 by
1990 Correcting Models with Observations, *Geophys. Res. Lett.*, 49, e2022GL098632, <https://doi.org/10.1029/2022GL098632>,
1991 2022.
- 1992 Berthet, S., Sférian, R., Bricaud, C., Chevallier, M., Voltaire, A., and Ethé, C.: Evaluation of an Online Grid-Coarsening
1993 Algorithm in a Global Eddy-Admitting Ocean Biogeochemical Model, *J. Adv. Model Earth Sy.*, 11, 1759–1783,
1994 <https://doi.org/10.1029/2019MS001644>, 2019.
- 1995 Bloom, A. A. and Williams, M.: Constraining ecosystem carbon dynamics in a data-limited world: integrating ecological
1996 “common sense” in a model–data fusion framework, *Biogeosciences*, 12, 1299–1315, <https://doi.org/10.5194/bg-12-1299->
1997 2015, 2015.
- 1998
- 1999 Bloom, A. A., Exbrayat, J.-F., van der Velde, I. R., Feng, L., and Williams, M.: The decadal state of the terrestrial carbon
2000 cycle: Global retrievals of terrestrial carbon allocation, pools, and residence times, *Proc. Natl. Acad. Sci.*, 113, 1285–1290,
2001 <https://doi.org/10.1073/pnas.1515160113>, 2016.
- 2002
- 2003 Boer, G. J., Smith, D. M., Cassou, C., Doblas-Reyes, F., Danabasoglu, G., Kirtman, B., Kushnir, Y., Kimoto, M., Meehl, G.
2004 A., Msadek, R., Mueller, W. A., Taylor, K. E., Zwiers, F., Rixen, M., Ruprich-Robert, Y., and Eade, R.: The Decadal
2005 Climate Prediction Project (DCPP) contribution to CMIP6, *Geosci. Model Dev.*, 9, 3751–3777, <https://doi.org/10.5194/gmd->
2006 9-3751-2016, 2016.
- 2007
- 2008 Boucher, O., Servonnat, J., Albright, A. L., Aumont, O., Balkanski, Y., Bastrikov, V., Bekki, S., Bonnet, R., Bony, S., Bopp,
2009 L., Braconnot, P., Brockmann, P., Cadule, P., Caubel, A., Cheruy, F., Codron, F., Cozic, A., Cugnet, D., D’Andrea, F.,
2010 Davini, P., de Lavergne, C., Denvil, S., Deshayes, J., Devilliers, M., Ducharme, A., Dufresne, J.-L., Dupont, E., Ethé, C.,
2011 Fairhead, L., Falletti, L., Flavoni, S., Foujols, M.-A., Gardoll, S., Gastineau, G., Ghattas, J., Grandpeix, J.-Y., Guenet, B.,
2012 Guez, E., Lionel, Guilyardi, E., Guimberteau, M., Hauglustaine, D., Hourdin, F., Idelkadi, A., Joussaume, S., Kageyama, M.,
2013 Khodri, M., Krinner, G., Lebas, N., Levavasseur, G., Lévy, C., Li, L., Lott, F., Lurton, T., Luyssaert, S., Madec, G.,
2014 Madeleine, J.-B., Maignan, F., Marchand, M., Marti, O., Mellul, L., Meurdesoif, Y., Mignot, J., Musat, I., Ottlé, C., Peylin,
2015 P., Planton, Y., Polcher, J., Rio, C., Rochetin, N., Rousset, C., Sepulchre, P., Sima, A., Swingedouw, D., Thiéblemont, R.,
2016 Traore, A. K., Vancoppenolle, M., Vial, J., Vialard, J., Viovy, N., and Vuichard, N.: Presentation and Evaluation of the
2017 IPSL-CM6A-LR Climate Model, *J. Adv. Model. Earth Syst.*, 12, e2019MS002010, <https://doi.org/10.1029/2019MS002010>,
2018 2020.



- 2019 Bourgeois, T., Goris, N., Schwinger, J., and Tjiputra, J. F.: Stratification constrains future heat and carbon uptake in the
2020 Southern Ocean between 30°S and 55°S, *Nat. Commun.*, 13, 340, <https://doi.org/10.1038/s41467-022-27979-5>, 2022.
- 2021 Bray, E.: 2017 Minerals Yearbook: Aluminum [Advance Release], Tech. rep., U.S. Geological Survey, <https://d9-wret.s3-us-west-2.amazonaws.com/assets/palladium/production/atoms/files/myb1-2017-alumi.pdf>, 2020.
- 2023 Brancalion, P. H. S., Broadbent, E. N., de-Miguel, S., Cardil, A., Rosa, M. R., Almeida, C. T., Almeida, D. R. A.,
2024 Chakravarty, S., Zhou, M., Gamarra, J. G. P., Liang, J., Crouzeilles, R., Hérault, B., Aragão, L. E. O. C., Silva, C. A., and
2025 Almeyda-Zambrano, A. M.: Emerging threats linking tropical deforestation and the COVID-19 pandemic, *Perspectives in*
2026 *Ecology and Conservation*, 18, 243–246, <https://doi.org/10.1016/j.pecon.2020.09.006>, 2020.
- 2027 Brienen, R. J. W., Caldwell, L., Duchesne, L., Voelker, S., Barichivich, J., Baliva, M., Ceccantini, G., Di Filippo, A.,
2028 Helama, S., Locosselli, G. M., Lopez, L., Piovesan, G., Schöngart, J., Villalba, R., and Gloor, E.: Forest carbon sink
2029 neutralized by pervasive growth-lifespan trade-offs, *Nat. Commun.*, 11, 4241, <https://doi.org/10.1038/s41467-020-17966-z>,
2030 2020.
- 2031 Brienen, R. J. W., Phillips, O. L., Feldpausch, T. R., Gloor, E., Baker, T. R., Lloyd, J., Lopez-Gonzalez, G., Monteagudo-
2032 Mendoza, A., Malhi, Y., Lewis, S. L., Vásquez Martínez, R., Alexiades, M., Álvarez Dávila, E., Alvarez-Loayza, P.,
2033 Andrade, A., Aragão, L. E. O. C., Araujo-Murakami, A., Arets, E. J. M. M., Arroyo, L., Aymard C., G. A., Bánki, O. S.,
2034 Baraloto, C., Barroso, J., Bonal, D., Boot, R. G. A., Camargo, J. L. C., Castilho, C. V., Chama, V., Chao, K. J., Chave, J.,
2035 Comiskey, J. A., Cornejo Valverde, F., da Costa, L., de Oliveira, E. A., Di Fiore, A., Erwin, T. L., Fauset, S., Forsthofer, M.,
2036 Galbraith, D. R., Grahame, E. S., Groot, N., Hérault, B., Higuchi, N., Honorio Coronado, E. N., Keeling, H., Killeen, T. J.,
2037 Laurance, W. F., Laurance, S., Licona, J., Magnussen, W. E., Marimon, B. S., Marimon-Junior, B. H., Mendoza, C., Neill,
2038 D. A., Nogueira, E. M., Núñez, P., Pallqui Camacho, N. C., Parada, A., Pardo-Molina, G., Peacock, J., Peña-Claros, M.,
2039 Pickavance, G. C., Pitman, N. C. A., Poorter, L., Prieto, A., Quesada, C. A., Ramírez, F., Ramírez-Angulo, H., Restrepo, Z.,
2040 Roopsind, A., Rudas, A., Salomão, R. P., Schwarz, M., Silva, N., Silva-Espejo, J. E., Silveira, M., Stropp, J., Talbot, J., ter
2041 Steege, H., Teran-Aguilar, J., Terborgh, J., Thomas-Caesar, R., Toledo, M., Torello-Raventos, M., Umetzu, R. K., van der
2042 Heijden, G. M. F., van der Hout, P., Guimarães Vieira, I. C., Vieira, S. A., Vilanova, E., Vos, V. A., and Zagt, R. J.: Long-
2043 term decline of the Amazon carbon sink, 519, 344–348, <https://doi.org/10.1038/nature14283>, 2015.
- 2044 Bronselaer, B., Winton, M., Russell, J., Sabine, C. L., and Khatiwala, S.: Agreement of CMIP5 Simulated and Observed
2045 Ocean Anthropogenic CO₂ Uptake, *Geophys. Res. Lett.*, 44, 12,298–12,305, <https://doi.org/10.1002/2017GL074435>, 2017.
- 2046 Bruno, M. and Joos, F.: Terrestrial carbon storage during the past 200 years: A Monte Carlo Analysis of CO₂ data from ice
2047 core and atmospheric measurements, *Global Biogeochem. Cycles*, 11, 111–124, <https://doi.org/10.1029/96GB03611>, 1997.
- 2048 Burrows, S. M., Maltrud, M., Yang, X., Zhu, Q., Jeffery, N., Shi, X., Ricciuto, D., Wang, S., Bisht, G., Tang, J., Wolfe, J.,
2049 Harrop, B. E., Singh, B., Brent, L., Baldwin, S., Zhou, T., Cameron-Smith, P., Keen, N., Collier, N., Xu, M., Hunke, E. C.,
2050 Elliott, S. M., Turner, A. K., Li, H., Wang, H., Golaz, J.-C., Bond-Lamberty, B., Hoffman, F. M., Riley, W. J., Thornton, P.
2051 E., Calvin, K., and Leung, L. R.: The DOE E3SM v1.1 Biogeochemistry Configuration: Description and Simulated
2052 Ecosystem-Climate Responses to Historical Changes in Forcing, *J. Adv. Model. Earth Syst.*, 12, e2019MS001766,
2053 <https://doi.org/10.1029/2019MS001766>, 2020.
- 2054 Burton, C., Betts, R., Cardoso, M., Feldpausch, T. R., Harper, A., Jones, C. D., Kelley, D. I., Robertson, E., and Wiltshire,
2055 A.: Representation of fire, land-use change and vegetation dynamics in the Joint UK Land Environment Simulator vn4.9
2056 (JULES), *Geosci. Model Dev.*, 12, 179–193, <https://doi.org/10.5194/gmd-12-179-2019>, 2019.



- 2057 Burton, C. et al.: Global burned area increasingly explained by climate change, *under review*,
2058 <https://doi.org/10.21203/rs.3.rs-3168150/v1>, 2023.
- 2059 Bushinsky, S. M., Landschützer, P., Rödenbeck, C., Gray, A. R., Baker, D., Mazloff, M. R., Resplandy, L., Johnson, K. S.,
2060 and Sarmiento, J. L.: Reassessing Southern Ocean Air-Sea CO₂ Flux Estimates With the Addition of Biogeochemical Float
2061 Observations, *Global Biogeochem. Cycles*, 33, 1370–1388, <https://doi.org/10.1029/2019GB006176>, 2019.
- 2062 Canadell, J. G., Le Quere, C., Raupach, M. R., Field, C. B., Buitenhuis, E. T., Ciais, P., Conway, T. J., Gillett, N. P.,
2063 Houghton, R. A., and Marland, G.: Contributions to accelerating atmospheric CO₂ growth from economic activity, carbon
2064 intensity, and efficiency of natural sinks, *Proceedings of the National Academy of Sciences*, 104, 18866–18870,
2065 <https://doi.org/10.1073/pnas.0702737104>, 2007.
- 2066 Canadell, J. G., Monteiro, P. M. S., Costa, M. H., Cotrim da Cunha, L., Cox, P. M., Eliseev, A. V., Henson, S., Ishii, M.,
2067 Jaccard, S., Koven, C., Lohila, A., Patra, P. K., Piao, S., Rogelj, J., Syampungani, S., Zaehle, S., and Zickfeld, K.: Global
2068 Carbon and other Biogeochemical Cycles and Feedbacks. In: *Climate Change 2021: The Physical Science Basis*.
2069 Contribution of Working Group I to the Sixth Assessment Report of the Intergovernmental Panel on Climate Change
2070 [Masson-Delmotte, V., P. Zhai, A. Pirani, S. L. Connors, C. Péan, S. Berger, N. Caud, Y. Chen, L. Goldfarb, M. I. Gomis,
2071 M. Huang, K. Leitzell, E. Lonnoy, J.B.R. Matthews, T. K. Maycock, T. Waterfield, O. Yelekçi, R. Yu and B. Zhou (eds.)].
2072 Cambridge University Press, Cambridge, United Kingdom and New York, NY, USA, pp. 673–816, doi:
2073 [10.1017/9781009157896.007](https://doi.org/10.1017/9781009157896.007), 2021.
- 2074 Cao, Z., Myers, R. J., Lupton, R. C., Duan, H., Sacchi, R., Zhou, N., Reed Miller, T., Cullen, J. M., Ge, Q., and Liu, G.: The
2075 sponge effect and carbon emission mitigation potentials of the global cement cycle, *Nat Commun*, 11, 3777,
2076 <https://doi.org/10.1038/s41467-020-17583-w>, 2020.
- 2077 Céspedes, J., Sylvester, J. M., Pérez-Marulanda, L., Paz-García, P., Reymondin, L., Khodadadi, M., Tello, J. J., and Castro-
2078 Nunez, A.: Has global deforestation accelerated due to the COVID-19 pandemic?, *J. For. Res.*, 34, 1153–1165,
2079 <https://doi.org/10.1007/s11676-022-01561-7>, 2023.
- 2080 Chandra, N., Patra, P. K., Niwa, Y., Ito, A., Iida, Y., Goto, D., Morimoto, S., Kondo, M., Takigawa, M., Hajima, T., and
2081 Watanabe, M.: Estimated regional CO₂ flux and uncertainty based on an ensemble of atmospheric CO₂ inversions,
2082 *Atmospheric Chem. Phys.*, 22, 9215–9243, <https://doi.org/10.5194/acp-22-9215-2022>, 2022.
- 2083 Chatfield, C.: The Holt-Winters Forecasting Procedure, *J. Roy. Stat. Soc. C.*, 27, 264–279, <https://doi.org/10.2307/2347162>,
2084 1978.
- 2085 Chau, T. T. T., Gehlen, M., and Chevallier, F.: A seamless ensemble-based reconstruction of surface ocean pCO₂ and air–sea
2086 CO₂ fluxes over the global coastal and open oceans, *Biogeosciences*, 19, 1087–1109, [https://doi.org/10.5194/bg-19-1087-](https://doi.org/10.5194/bg-19-1087-2022)
2087 2022, 2022.
- 2088 Chevallier, F., Fisher, M., Peylin, P., Serran, S., Bousquet, P., Bréon, F.-M., Chédin, A., and Ciais, P.: Inferring CO₂
2089 sources and sinks from satellite observations: Method and application to TOVS data, *J. Geophys. Res.*, 110, D24309,
2090 <https://doi.org/10.1029/2005JD006390>, 2005.
- 2091 Ciais, P., Sabine, C., Bala, G., Bopp, L., Brovkin, V., Canadell, J. G., Chhabra, A., DeFries, R., Galloway, J., Heimann, M.,
2092 Jones, C., Le Quéré, C., Myneni, R., Piao, S., Thornton, P., Willem, J., Friedlingstein, P., and Munhoven, G.: Carbon and
2093 Other Biogeochemical Cycles, in *Climate Change 2013: The Physical Science Basis*, Contribution of Working Group I to the
2094 Fifth Assessment Report of the Intergovernmental Panel on Climate Change, edited by: Intergovernmental Panel on Climate



- 2095 Change, Cambridge University Press, Cambridge, United Kingdom and New York, NY, USA.
2096 doi:10.1017/CBO9781107415324.015, 2013.
- 2097 Ciais, P., Tan, J., Wang, X., Roedenbeck, C., Chevallier, F., Piao, S.-L., Moriarty, R., Broquet, G., Le Quéré, C., Canadell, J.
2098 G., Peng, S., Poulter, B., Liu, Z., and Tans, P.: Five decades of northern land carbon uptake revealed by the interhemispheric
2099 CO₂ gradient, *Nature*, 568, 221–225, <https://doi.org/10.1038/s41586-019-1078-6>, 2019.
- 2100 Ciais, P., Bastos, A., Chevallier, F., Lauerwald, R., Poulter, B., Canadell, P., Hugelius, G., Jackson, R. B., Jain, A., Jones,
2101 M., Kondo, M., Lujikx, I. T., Patra, P. K., Peters, W., Pongratz, J., Petrescu, A. M. R., Piao, S., Qiu, C., Von Randow, C.,
2102 Regnier, P., Saunois, M., Scholes, R., Shvidenko, A., Tian, H., Yang, H., Wang, X., and Zheng, B.: Definitions and methods
2103 to estimate regional land carbon fluxes for the second phase of the REgional Carbon Cycle Assessment and Processes
2104 Project (RECCAP-2), *Geosci. Model Dev.*, 15, 1289–1316, <https://doi.org/10.5194/gmd-15-1289-2022>, 2022.
- 2105 Collier, N., Hoffman, F. M., Lawrence, D. M., Keppel-Aleks, G., Koven, C. D., Riley, W. J., Mu, M., and Randerson, J. T.:
2106 The International Land Model Benchmarking (ILAMB) System: Design, Theory, and Implementation, *J. Adv. Model. Earth
2107 Syst.*, 10, 2731–2754, <https://doi.org/10.1029/2018MS001354>, 2018.
- 2108 Cox, P. M., Pearson, D., Booth, B. B., Friedlingstein, P., Huntingford, C., Jones, C. D., and Luke, C. M.: Sensitivity of
2109 tropical carbon to climate change constrained by carbon dioxide variability, *Nature*, 494, 341–344,
2110 <https://doi.org/10.1038/nature11882>, 2013.
- 2111 De Kauwe, M. G., Medlyn, B. E., Zachle, S., Walker, A. P., Dietze, M. C., Wang, Y.-P., Luo, Y., Jain, A. K., El-Masri, B.,
2112 Hickler, T., Wårlind, D., Weng, E., Parton, W. J., Thornton, P. E., Wang, S., Prentice, I. C., Asao, S., Smith, B., McCarthy,
2113 H. R., Iversen, C. M., Hanson, P. J., Warren, J. M., Oren, R., and Norby, R. J.: Where does the carbon go? A model–data
2114 intercomparison of vegetation carbon allocation and turnover processes at two temperate forest free-air CO₂ enrichment
2115 sites, *New Phytol.*, 203, 883–899, <https://doi.org/10.1111/nph.12847>, 2014.
- 2116 Delire, C., Séférian, R., Decharme, B., Alkama, R., Calvet, J.-C., Carrer, D., Gibelin, A.-L., Joetzjer, E., Morel, X., Rocher,
2117 M., and Tzanos, D.: The Global Land Carbon Cycle Simulated With ISBA-CTRIP: Improvements Over the Last Decade, *J.
2118 Adv. Model. Earth Syst.*, 12, e2019MS001886, <https://doi.org/10.1029/2019MS001886>, 2020.
- 2119 Denman, K. L., Brasseur, G., Chidthaisong, A., Ciais, P., Cox, P. M., Dickinson, R. E., Hauglustaine, D., Heinze, C.,
2120 Holland, E., Jacob, D., Lohmann, U., Ramachandran, S., Leite da Silva Dias, P., Wofsy, S. C., and Zhang, X.: Couplings
2121 Between Changes in the Climate System and Biogeochemistry, in: *Climate Change 2007: The Physical Science Basis.*
2122 Contribution of Working Group I to the Fourth Assessment Report of the Intergovernmental Panel on Climate Change,
2123 edited by: Solomon, S., Qin, D., Manning, M., Marquis, M., Averyt, K., Tignor, M. M. B., Miller, H. L., and Chen, Z. L.,
2124 Cambridge University Press, Cambridge, UK and New York, USA, 499–587, ISBN: 9780521705967, 2007.
- 2125 Denvil-Sommer, A., Gehlen, M., and Vrac, M.: Observation system simulation experiments in the Atlantic Ocean for
2126 enhanced surface ocean pCO₂ reconstructions, *Ocean Sci.*, 17, 1011–1030, <https://doi.org/10.5194/os-17-1011-2021>, 2021.
- 2127 DeVries, T., Holzer, M., and Primeau, F.: Recent increase in oceanic carbon uptake driven by weaker upper-ocean
2128 overturning, *Nature*, 542, 215–218, <https://doi.org/10.1038/nature21068>, 2017.
- 2129 DeVries, T., Quéré, C. L., Andrews, O., Berthet, S., Hauck, J., Ilyina, T., Landschützer, P., Lenton, A., Lima, I. D., Nowicki,
2130 M., Schwinger, J., and Séférian, R.: Decadal trends in the ocean carbon sink, *PNAS*, 116, 11646–11651,
2131 <https://doi.org/10.1073/pnas.1900371116>, 2019.



- 2132 DeVries, T., Yamamoto, K., Wanninkhof, R., Gruber, N., Hauck, J., Müller, J. D., Bopp, L., Carroll, D., Carter, B., Chau,
2133 T.-T.-T., Doney, S. C., Gehlen, M., Gloege, L., Gregor, L., Henson, S., Kim, J. H., Iida, Y., Ilyina, T., Landschützer, P., Le
2134 Quéré, C., Munro, D., Nissen, C., Patara, L., Pérez, F. F., Resplandy, L., Rodgers, K. B., Schwinger, J., Séférian, R., Sicardi,
2135 V., Terhaar, J., Triñanes, J., Tsujino, H., Watson, A., Yasunaka, S., and Zeng, J.: Magnitude, trends, and variability of the
2136 global ocean carbon sink from 1985–2018, *Glob. Biogeochem. Cycles*, n/a, e2023GB007780,
2137 <https://doi.org/10.1029/2023GB007780>, 2023.
- 2138
2139 Forster, P. M., Smith, C. J., Walsh, T., Lamb, W. F., Lamboll, R., Hauser, M., Ribes, A., Rosen, D., Gillett, N., Palmer, M.
2140 D., Rogelj, J., von Schuckmann, K., Seneviratne, S. I., Trewin, B., Zhang, X., Allen, M., Andrew, R., Birt, A., Borger, A.,
2141 Boyer, T., Broersma, J. A., Cheng, L., Dentener, F., Friedlingstein, P., Gutiérrez, J. M., Gütschow, J., Hall, B., Ishii, M.,
2142 Jenkins, S., Lan, X., Lee, J.-Y., Morice, C., Kadow, C., Kennedy, J., Killick, R., Minx, J. C., Naik, V., Peters, G. P., Pirani,
2143 A., Pongratz, J., Schleussner, C.-F., Szopa, S., Thorne, P., Rohde, R., Rojas Corradi, M., Schumacher, D., Vose, R.,
2144 Zickfeld, K., Masson-Delmotte, V., and Zhai, P.: Indicators of Global Climate Change 2022: annual update of large-scale
2145 indicators of the state of the climate system and human influence, *Earth Syst. Sci. Data*, 15, 2295–2327,
2146 <https://doi.org/10.5194/essd-15-2295-2023>, 2023.
- 2147 Doney, S. C., Lima, I., Feely, R. A., Glover, D. M., Lindsay, K., Mahowald, N., Moore, J. K., and Wanninkhof, R.:
2148 Mechanisms governing interannual variability in upper-ocean inorganic carbon system and air–sea CO₂ fluxes: Physical
2149 climate and atmospheric dust, *Deep Sea Research Part II: Topical Studies in Oceanography*, 56, 640–655,
2150 <https://doi.org/10.1016/j.dsr2.2008.12.006>, 2009.
- 2151 Dong, Y., Bakker, D. C. E., Bell, T. G., Huang, B., Landschützer, P., Liss, P. S., and Yang, M.: Update on the Temperature
2152 Corrections of Global Air–Sea CO₂ Flux Estimates, *Glob. Biogeochem. Cycles*, 36, e2022GB007360,
2153 <https://doi.org/10.1029/2022GB007360>, 2022.
- 2154
2155 Dou, X., Wang, Y., Ciais, P., Chevallier, F., Davis, S. J., Crippa, M., Janssens-Maenhout, G., Guizzardi, D., Solazzo, E.,
2156 Yan, F., Huo, D., Zheng, B., Zhu, B., Cui, D., Ke, P., Sun, T., Wang, H., Zhang, Q., Gentine, P., Deng, Z., and Liu, Z.: Near-
2157 real-time global gridded daily CO₂ emissions, *The Innovation*, 3, 100182, <https://doi.org/10.1016/j.xinn.2021.100182>, 2022.
- 2158 Edson, J. B., Jampana, V., Weller, R. A., Bigorre, S. P., Plueddemann, A. J., Fairall, C. W., Miller, S. D., Mahrt, L., Vickers,
2159 D., and Hersbach, H.: On the Exchange of Momentum over the Open Ocean, *J. Phys. Oceanogr.*, 43, 1589–1610,
2160 <https://doi.org/10.1175/JPO-D-12-0173.1>, 2013.
- 2161 EIA. Short-Term Energy Outlook: September 2023. U.S. Energy Information Administration. Available at:
2162 <http://www.eia.gov/forecasts/steo/outlook.cfm>, last access: 27 September 2023, 2023.
- 2163 Erb, K.-H., Kastner, T., Luyssaert, S., Houghton, R. A., Kuemmerle, T., Olofsson, P., and Haberl, H.: Bias in the attribution
2164 of forest carbon sinks, *Nature Clim Change*, 3, 854–856, <https://doi.org/10.1038/nclimate2004>, 2013.
- 2165 Erb, K.-H., Kastner, T., Plutzer, C., Bais, A. L. S., Carvalhais, N., Fetzel, T., Gingrich, S., Haberl, H., Lauk, C.,
2166 Niedertscheider, M., Pongratz, J., Thurner, M., and Luyssaert, S.: Unexpectedly large impact of forest management and
2167 grazing on global vegetation biomass, *Nature*, 553, 73–76, <https://doi.org/10.1038/nature25138>, 2018.
- 2168 Eskander, S. M. S. U. and Fankhauser, S.: Reduction in greenhouse gas emissions from national climate legislation, *Nat.*
2169 *Clim. Chang.*, 10, 750–756, <https://doi.org/10.1038/s41558-020-0831-z>, 2020.



- 2170 Etheridge, D. M., Steele, L. P., Langenfelds, R. L., Francey, R. J., Barnola, J.-M., and Morgan, V. I.: Natural and
2171 anthropogenic changes in atmospheric CO₂ over the last 1000 years from air in Antarctic ice and firn, *J. Geophys. Res.*,
2172 101, 4115–4128, <https://doi.org/10.1029/95JD03410>, 1996.
- 2173 Eyring, V., Bony, S., Meehl, G. A., Senior, C. A., Stevens, B., Stouffer, R. J., and Taylor, K. E.: Overview of the Coupled
2174 Model Intercomparison Project Phase 6 (CMIP6) experimental design and organization, *Geosci. Model Dev.*, 9, 1937–1958,
2175 <https://doi.org/10.5194/gmd-9-1937-2016>, 2016.
- 2176 FAO, Impact of the Ukraine-Russia conflict on global food security and related matters under the mandate of the Food and
2177 Agriculture Organization of the United Nations (FAO), Hundred and Seventieth Session of the Council,
2178 <https://www.fao.org/3/nj164en/nj164en.pdf>, last access: 27 September 2023, 2023.
- 2179 Fay, A. R., Gregor, L., Landschützer, P., McKinley, G. A., Gruber, N., Gehlen, M., Iida, Y., Laruelle, G. G., Rödenbeck, C.,
2180 Roobaert, A., and Zeng, J.: SeaFlux: harmonization of air–sea CO₂ fluxes from surface pCO₂ data products using a
2181 standardized approach, *Earth System Science Data*, 13, 4693–4710, <https://doi.org/10.5194/essd-13-4693-2021>, 2021.
- 2182 Feng, L., Palmer, P. I., Bösch, H., and Dance, S.: Estimating surface CO₂ fluxes from space-borne CO₂ dry air mole fraction
2183 observations using an ensemble Kalman Filter, *Atmospheric Chem. Phys.*, 9, 2619–2633, [https://doi.org/10.5194/acp-9-](https://doi.org/10.5194/acp-9-2619-2009)
2184 2619-2009, 2009.
- 2185 Feng, L., Palmer, P. I., Parker, R. J., Deutscher, N. M., Feist, D. G., Kivi, R., Morino, I., and Sussmann, R.: Estimates of
2186 European uptake of CO₂ inferred from GOSAT XCO₂ retrievals: sensitivity to measurement bias inside and outside Europe,
2187 *Atmos. Chem. Phys.*, 16, 1289–1302, <https://doi.org/10.5194/acp-16-1289-2016>, 2016.
- 2188 Flanagan, D.: 2017 Minerals Yearbook: Copper [Advance Release], Tech. rep., U.S. Geological Survey,
2189 <https://pubs.usgs.gov/myb/vol1/2017/myb1-2017-copper.pdf>, 2021.
- 2190 Friedlingstein, P., Houghton, R. A., Marland, G., Hackler, J., Boden, T. A., Conway, T. J., Canadell, J. G., Raupach, M. R.,
2191 Ciais, P., and Le Quéré, C.: Update on CO₂ emissions, *Nature Geosci.*, 3, 811–812, <https://doi.org/10.1038/ngeo1022>, 2010.
- 2192 Friedlingstein, P., Andrew, R. M., Rogelj, J., Peters, G. P., Canadell, J. G., Knutti, R., Luderer, G., Raupach, M. R.,
2193 Schaeffer, M., van Vuuren, D. P., and Le Quéré, C.: Persistent growth of CO₂ emissions and implications for reaching
2194 climate targets, *Nature Geosci.*, 7, 709–715, <https://doi.org/10.1038/ngeo2248>, 2014.
- 2195 Friedlingstein, P., Jones, M. W., O’Sullivan, M., Andrew, R. M., Hauck, J., Peters, G. P., Peters, W., Pongratz, J., Sitch, S.,
2196 Le Quéré, C., Bakker, D. C. E., Canadell, J. G., Ciais, P., Jackson, R. B., Anthoni, P., Barbero, L., Bastos, A., Bastrikov, V.,
2197 Becker, M., Bopp, L., Buitenhuis, E., Chandra, N., Chevallier, F., Chini, L. P., Currie, K. I., Feely, R. A., Gehlen, M.,
2198 Gilfillan, D., Gkritzalis, T., Goll, D. S., Gruber, N., Gutekunst, S., Harris, I., Haverd, V., Houghton, R. A., Hurtt, G., Ilyina,
2199 T., Jain, A. K., Joetzier, E., Kaplan, J. O., Kato, E., Klein Goldewijk, K., Korsbakken, J. I., Landschützer, P., Lauvset, S. K.,
2200 Lefèvre, N., Lenton, A., Lienert, S., Lombardozi, D., Marland, G., McGuire, P. C., Melton, J. R., Metzl, N., Munro, D. R.,
2201 Nabel, J. E. M. S., Nakaoka, S.-I., Neill, C., Omar, A. M., Ono, T., Pregon, A., Pierrot, D., Poulter, B., Rehder, G.,
2202 Resplandy, L., Robertson, E., Rödenbeck, C., Séférian, R., Schwinger, J., Smith, N., Tans, P. P., Tian, H., Tilbrook, B.,
2203 Tubiello, F. N., van der Werf, G. R., Wiltshire, A. J., and Zaehle, S.: Global Carbon Budget 2019, *Earth Syst. Sci. Data*, 11,
2204 1783–1838, <https://doi.org/10.5194/essd-11-1783-2019>, 2019.
- 2205 Friedlingstein, P., O’Sullivan, M., Jones, M. W., Andrew, R. M., Hauck, J., Olsen, A., Peters, G. P., Peters, W., Pongratz, J.,
2206 Sitch, S., Le Quéré, C., Canadell, J. G., Ciais, P., Jackson, R. B., Alin, S., Aragão, L. E. O. C., Armeth, A., Arora, V., Bates,
2207 N. R., Becker, M., Benoit-Cattin, A., Bittig, H. C., Bopp, L., Bultan, S., Chandra, N., Chevallier, F., Chini, L. P., Evans, W.,



- 2208 Florentie, L., Forster, P. M., Gasser, T., Gehlen, M., Gilfillan, D., Gkritzalis, T., Gregor, L., Gruber, N., Harris, I., Hartung,
2209 K., Haverd, V., Houghton, R. A., Ilyina, T., Jain, A. K., Joetzjer, E., Kadono, K., Kato, E., Kitidis, V., Korsbakken, J. I.,
2210 Landschützer, P., Lefèvre, N., Lenton, A., Lienert, S., Liu, Z., Lombardozi, D., Marland, G., Metzl, N., Munro, D. R.,
2211 Nabel, J. E. M. S., Nakaoka, S.-I., Niwa, Y., O'Brien, K., Ono, T., Palmer, P. I., Pierrot, D., Poulter, B., Resplandy, L.,
2212 Robertson, E., Rödenbeck, C., Schwinger, J., Séférian, R., Skjelvan, I., Smith, A. J. P., Sutton, A. J., Tanhua, T., Tans, P. P.,
2213 Tian, H., Tilbrook, B., van der Werf, G., Vuichard, N., Walker, A. P., Wanninkhof, R., Watson, A. J., Willis, D., Wiltshire,
2214 A. J., Yuan, W., Yue, X., and Zaehle, S.: Global Carbon Budget 2020, *Earth Syst. Sci. Data*, 12, 3269–3340,
2215 <https://doi.org/10.5194/essd-12-3269-2020>, 2020.
- 2216 Friedlingstein, P., Jones, M. W., O'Sullivan, M., Andrew, R. M., Bakker, D. C. E., Hauck, J., Le Quéré, C., Peters, G. P.,
2217 Peters, W., Pongratz, J., Sitch, S., Canadell, J. G., Ciais, P., Jackson, R. B., Alin, S. R., Anthoni, P., Bates, N. R., Becker, M.,
2218 Bellouin, N., Bopp, L., Chau, T. T. T., Chevallier, F., Chini, L. P., Cronin, M., Currie, K. I., Decharme, B., Djeutchouang, L.
2219 M., Dou, X., Evans, W., Feely, R. A., Feng, L., Gasser, T., Gilfillan, D., Gkritzalis, T., Grassi, G., Gregor, L., Gruber, N.,
2220 Gürses, Ö., Harris, I., Houghton, R. A., Hurtt, G. C., Iida, Y., Ilyina, T., Luijkx, I. T., Jain, A., Jones, S. D., Kato, E.,
2221 Kennedy, D., Klein Goldewijk, K., Knauer, J., Korsbakken, J. I., Körtzinger, A., Landschützer, P., Lauvset, S. K., Lefèvre,
2222 N., Lienert, S., Liu, J., Marland, G., McGuire, P. C., Melton, J. R., Munro, D. R., Nabel, J. E. M. S., Nakaoka, S.-I., Niwa,
2223 Y., Ono, T., Pierrot, D., Poulter, B., Rehder, G., Resplandy, L., Robertson, E., Rödenbeck, C., Rosan, T. M., Schwinger, J.,
2224 Schwingshackl, C., Séférian, R., Sutton, A. J., Sweeney, C., Tanhua, T., Tans, P. P., Tian, H., Tilbrook, B., Tubiello, F., van
2225 der Werf, G. R., Vuichard, N., Wada, C., Wanninkhof, R., Watson, A. J., Willis, D., Wiltshire, A. J., Yuan, W., Yue, C.,
2226 Yue, X., Zaehle, S., and Zeng, J.: Global Carbon Budget 2021, *Earth Syst. Sci. Data*, 14, 1917–2005,
2227 <https://doi.org/10.5194/essd-14-1917-2022>, 2022a.
- 2228 Friedlingstein, P. and co-authors of the current study, Supplemental data of the Global Carbon Budget 2023, ICOS-ERIC
2229 Carbon Portal, <https://doi.org/10.18160/GCP-2023>, 2023.
- 2230 Friedlingstein, P., O'Sullivan, M., Jones, M. W., Andrew, R. M., Gregor, L., Hauck, J., Le Quéré, C., Luijkx, I. T., Olsen,
2231 A., Peters, G. P., Peters, W., Pongratz, J., Schwingshackl, C., Sitch, S., Canadell, J. G., Ciais, P., Jackson, R. B., Alin, S. R.,
2232 Alkama, R., Arneeth, A., Arora, V. K., Bates, N. R., Becker, M., Bellouin, N., Bittig, H. C., Bopp, L., Chevallier, F., Chini, L.
2233 P., Cronin, M., Evans, W., Falk, S., Feely, R. A., Gasser, T., Gehlen, M., Gkritzalis, T., Gloege, L., Grassi, G., Gruber, N.,
2234 Gürses, Ö., Harris, I., Hefner, M., Houghton, R. A., Hurtt, G. C., Iida, Y., Ilyina, T., Jain, A. K., Jersild, A., Kadono, K.,
2235 Kato, E., Kennedy, D., Klein Goldewijk, K., Knauer, J., Korsbakken, J. I., Landschützer, P., Lefèvre, N., Lindsay, K., Liu,
2236 J., Liu, Z., Marland, G., Mayot, N., McGrath, M. J., Metzl, N., Monacchi, N. M., Munro, D. R., Nakaoka, S.-I., Niwa, Y.,
2237 O'Brien, K., Ono, T., Palmer, P. I., Pan, N., Pierrot, D., Pockock, K., Poulter, B., Resplandy, L., Robertson, E., Rödenbeck,
2238 C., Rodriguez, C., Rosan, T. M., Schwinger, J., Séférian, R., Shutler, J. D., Skjelvan, I., Steinhoff, T., Sun, Q., Sutton, A. J.,
2239 Sweeney, C., Takao, S., Tanhua, T., Tans, P. P., Tian, X., Tian, H., Tilbrook, B., Tsujino, H., Tubiello, F., van der Werf, G.
2240 R., Walker, A. P., Wanninkhof, R., Whitehead, C., Willstrand Wranne, A., et al.: Global Carbon Budget 2022, *Earth Syst.*
2241 *Sci. Data*, 14, 4811–4900, <https://doi.org/10.5194/essd-14-4811-2022>, 2022b.
- 2242 Ganzenmüller, R., Bultan, S., Winkler, K., Fuchs, R., Zabel, F., and Pongratz, J.: Land-use change emissions based on high-
2243 resolution activity data substantially lower than previously estimated, *Environ. Res. Lett.*, 17, 064050,
2244 <https://doi.org/10.1088/1748-9326/ac70d8>, 2022.
- 2245 Gasser, T., Crepin, L., Quilcaille, Y., Houghton, R. A., Ciais, P., and Obersteiner, M.: Historical CO₂ emissions from land
2246 use and land cover change and their uncertainty, *Biogeosciences*, 17, 4075–4101, <https://doi.org/10.5194/bg-17-4075-2020>,
2247 2020.



- 2248 Gaubert, B., Stephens, B. B., Basu, S., Chevallier, F., Deng, F., Kort, E. A., Patra, P. K., Peters, W., Rödenbeck, C., Saeki,
2249 T., Schimel, D., Van der Laan-Luijkx, I., Wofsy, S., and Yin, Y.: Global atmospheric CO₂ inverse models converging on
2250 neutral tropical land exchange, but disagreeing on fossil fuel and atmospheric growth rate, *Biogeosciences*, 16, 117–134,
2251 <https://doi.org/10.5194/bg-16-117-2019>, 2019.
- 2252 GCP: The Global Carbon Budget 2007, available at: <http://www.globalcarbonproject.org/carbonbudget/archive.htm>, last
2253 access: 27 September 2023, 2007.
- 2254 Giglio, L., Schroeder, W., and Justice, C. O.: The collection 6 MODIS active fire detection algorithm and fire products,
2255 *Remote Sensing of Environment*, 178, 31–41, <https://doi.org/10.1016/j.rse.2016.02.054>, 2016.
- 2256 Gilfillan, D. and Marland, G.: CDIAC-FF: global and national CO₂ emissions from fossil fuel combustion and cement
2257 manufacture: 1751–2017, 13, 1667–1680, <https://doi.org/10.5194/essd-13-1667-2021>, 2021.
- 2258 Gloege, L., McKinley, G. A., Landschützer, P., Fay, A. R., Frölicher, T. L., Fyfe, J. C., Ilyina, T., Jones, S., Lovenduski, N.,
2259 S., Rodgers, K. B., Schlunegger, S., and Takano, Y.: Quantifying Errors in Observationally Based Estimates of Ocean
2260 Carbon Sink Variability, *Global Biogeochem. Cy.*, 35, e2020GB006788, <https://doi.org/10.1029/2020GB006788>, 2021.
- 2261 Gloege, L., Yan, M., Zheng, T., and McKinley, G. A.: Improved Quantification of Ocean Carbon Uptake by Using Machine
2262 Learning to Merge Global Models and pCO₂ Data, *J. Adv. Model. Earth Syst.*, 14, e2021MS002620,
2263 <https://doi.org/10.1029/2021MS002620>, 2022.
- 2264 Golar, G., Malik, A., Muis, H., Herman, A., Nurudin, N., and Lukman, L.: The social-economic impact of COVID-19
2265 pandemic: implications for potential forest degradation, *Heliyon*, 6, e05354, <https://doi.org/10.1016/j.heliyon.2020.e05354>,
2266 2020.
- 2267 Goris, N., Tjiputra, J. F., Olsen, A., Schwinger, J., Lauvset, S. K., and Jeansson, E.: Constraining Projection-Based Estimates
2268 of the Future North Atlantic Carbon Uptake, *J. Clim.*, 31, 3959–3978, <https://doi.org/10.1175/JCLI-D-17-0564.1>, 2018.
- 2269 Grassi, G., House, J., Kurz, W. A., Cescatti, A., Houghton, R. A., Peters, G. P., Sanz, M. J., Viñas, R. A., Alkama, R.,
2270 Armeth, A., Bondeau, A., Dentener, F., Fader, M., Federici, S., Friedlingstein, P., Jain, A. K., Kato, E., Koven, C. D., Lee,
2271 D., Nabel, J. E. M. S., Nassikas, A. A., Perugini, L., Rossi, S., Sitch, S., Viogy, N., Wiltshire, A., and Zaehle, S.:
2272 Reconciling global-model estimates and country reporting of anthropogenic forest CO₂ sinks, *Nature Clim Change*, 8, 914–
2273 920, <https://doi.org/10.1038/s41558-018-0283-x>, 2018.
- 2274 Grassi, G., Stehfest, E., Rogelj, J., van Vuuren, D., Cescatti, A., House, J., Nabuurs, G.-J., Rossi, S., Alkama, R., Viñas, R.,
2275 A., Calvin, K., Ceccherini, G., Federici, S., Fujimori, S., Gusti, M., Hasegawa, T., Havlik, P., Humpenöder, F., Korosuo, A.,
2276 Perugini, L., Tubiello, F. N., and Popp, A.: Critical adjustment of land mitigation pathways for assessing countries' climate
2277 progress, *Nat. Clim. Chang.*, 11, 425–434, <https://doi.org/10.1038/s41558-021-01033-6>, 2021.
- 2278 Grassi, G., Schwingshackl, C., Gasser, T., Houghton, R. A., Sitch, S., Canadell, J. G., Cescatti, A., Ciais, P., Federici, S.,
2279 Friedlingstein, P., Kurz, W. A., Sanz Sanchez, M. J., Abad Viñas, R., Alkama, R., Bultan, S., Ceccherini, G., Falk, S., Kato,
2280 E., Kennedy, D., Knauer, J., Korosuo, A., Melo, J., McGrath, M. J., Nabel, J. E. M. S., Poulter, B., Romanovskaya, A. A.,
2281 Rossi, S., Tian, H., Walker, A. P., Yuan, W., Yue, X., and Pongratz, J.: Harmonising the land-use flux estimates of global
2282 models and national inventories for 2000–2020, *Earth Syst. Sci. Data*, 15, 1093–1114, [https://doi.org/10.5194/essd-15-1093-](https://doi.org/10.5194/essd-15-1093-2023)
2283 2023, 2023.



- 2284 Gregor, L. and Gruber, N.: OceanSODA-ETHZ: a global gridded data set of the surface ocean carbonate system for seasonal
2285 to decadal studies of ocean acidification, 13, 777–808, <https://doi.org/10.5194/essd-13-777-2021>, 2021.
- 2286 Gruber, N., Bakker, D. C. E., DeVries, T., Gregor, L., Hauck, J., Landschützer, P., McKinley, G. A., and Müller, J. D.:
2287 Trends and variability in the ocean carbon sink, *Nat. Rev. Earth Environ.*, 4, 119–134, [https://doi.org/10.1038/s43017-022-](https://doi.org/10.1038/s43017-022-00381-x)
2288 00381-x, 2023.
- 2289 Gruber, N., Clement, D., Carter, B. R., Feely, R. A., van Heuven, S., Hoppema, M., Ishii, M., Key, R. M., Kozyr, A.,
2290 Lauvset, S. K., Lo Monaco, C., Mathis, J. T., Murata, A., Olsen, A., Perez, F. F., Sabine, C. L., Tanhua, T., and Wanninkhof,
2291 R.: The oceanic sink for anthropogenic CO₂ from 1994 to 2007, 363, 1193–1199, <https://doi.org/10.1126/science.aau5153>,
2292 2019.
- 2293 Guan, D., Liu, Z., Geng, Y., Lindner, S., and Hubacek, K.: The gigatonne gap in China’s carbon dioxide inventories, *Nature*
2294 *Clim Change*, 2, 672–675, <https://doi.org/10.1038/nclimate1560>, 2012.
- 2295 Gulev, S. K., Thorne, P. W., Ahn, J., Dentener, F. J., Domingues, C. M., Gerland, S., Gong, D. S., Kaufman, S., Nnamchi,
2296 H. C., Quaas, J., Rivera, J. A., Sathyendranath, S., Smith, S. L., Trewin, B., von Shuckmann, K., and Vose, R. S.: Changing
2297 State of the Climate System. In: *Climate Change 2021: The Physical Science Basis. Contribution of Working Group I to the*
2298 *Sixth Assessment Report of the Intergovernmental Panel on Climate Change* [Masson-Delmotte, V., Zhai, P., Pirani, A.,
2299 Connors, S. L., Péan, C., Berger, S., Caud, N., Chen, Y., Goldfarb, L., Gomis, M. I., Huang, M., Leitzell, K., Lonnoy, E.,
2300 Matthews, J.B.R., Maycock, T.K., Waterfield, T., Yelekçi, O., Yu, R. and Zhou, B. (eds.)]. Cambridge University Press,
2301 Cambridge, United Kingdom and New York, NY, USA, pp. 287–422, doi:10.1017/9781009157896.004, 2021.
- 2302 Guo, R., Wang, J., Bing, L., Tong, D., Ciais, P., Davis, S. J., Andrew, R. M., Xi, F., and Liu, Z.: Global CO₂ uptake by
2303 cement from 1930 to 2019, 13, 1791–1805, <https://doi.org/10.5194/essd-13-1791-2021>, 2021.
- 2304 Gürses, Ö., Oziel, L., Karakuş, O., Sidorenko, D., Völker, C., Ye, Y., Zeising, M., Butzin, M., and Hauck, J.: Ocean
2305 biogeochemistry in the coupled ocean–sea ice–biogeochemistry model FESOM2.1–REcoM3, *Geosci. Model Dev.*, 16,
2306 4883–4936, <https://doi.org/10.5194/gmd-16-4883-2023>, 2023.
- 2307 Gütschow, J., Jeffery, M. L., Gieseke, R., Gebel, R., Stevens, D., Krapp, M., and Rocha, M.: The PRIMAP-hist national
2308 historical emissions time series, 8, 571–603, <https://doi.org/10.5194/essd-8-571-2016>, 2016.
- 2309 Gütschow, J., and Pflüger, M. (2023): The PRIMAP-hist national historical emissions time series v2.4.2 (1750-2021)
2310 [dataset]. <https://doi.org/10.5281/zenodo.7727475>, 2023.
- 2311 Hall, B. D., Crotwell, A. M., Kitzis, D. R., Mefford, T., Miller, B. R., Schibig, M. F., and Tans, P. P.: Revision of the World
2312 Meteorological Organization Global Atmosphere Watch (WMO/GAW) CO₂ calibration scale, 14, 3015–3032,
2313 <https://doi.org/10.5194/amt-14-3015-2021>, 2021.
- 2314 Hansis, E., Davis, S. J., and Pongratz, J.: Relevance of methodological choices for accounting of land use change carbon
2315 fluxes, *Global Biogeochem. Cycles*, 29, 1230–1246, <https://doi.org/10.1002/2014GB004997>, 2015.
- 2316 Hauck, J., Nissen, C., Landschützer, P., Rödenbeck, C., Bushinsky, S., and Olsen, A.: Sparse observations induce large
2317 biases in estimates of the global ocean CO₂ sink: an ocean model subsampling experiment, *Philos. Trans. R. Soc. Math.*
2318 *Phys. Eng. Sci.*, 381, 20220063, <https://doi.org/10.1098/rsta.2022.0063>, 2023.



- 2319 Hauck, J., Zeising, M., Le Quéré, C., Gruber, N., Bakker, D. C. E., Bopp, L., Chau, T. T. T., Gürses, Ö., Ilyina, T.,
2320 Landschützer, P., Lenton, A., Resplandy, L., Rödenbeck, C., Schwinger, J., and Séférian, R.: Consistency and Challenges in
2321 the Ocean Carbon Sink Estimate for the Global Carbon Budget, *Front. Mar. Sci.*, 7, 571720,
2322 <https://doi.org/10.3389/fmars.2020.571720>, 2020.
- 2323 Haverd, V., Smith, B., Nieradzik, L., Briggs, P. R., Woodgate, W., Trudinger, C. M., Canadell, J. G., and Cuntz, M.: A new
2324 version of the CABLE land surface model (Subversion revision r4601) incorporating land use and land cover change, woody
2325 vegetation demography, and a novel optimisation-based approach to plant coordination of photosynthesis, *Geosci. Model*
2326 *Dev.*, 11, 2995–3026, <https://doi.org/10.5194/gmd-11-2995-2018>, 2018.
- 2327 Heinke, J., Rolinski, S., and Müller, C.: Modelling the role of livestock grazing in C and N cycling in grasslands with
2328 LPJmL5.0-grazing, *Geosci. Model Dev.*, 16, 2455–2475, <https://doi.org/10.5194/gmd-16-2455-2023>, 2023.
- 2329 Hickler, T., Smith, B., Prentice, I. C., Mjöfors, K., Miller, P., Arneeth, A., and Sykes, M. T.: CO₂ fertilization in temperate
2330 FACE experiments not representative of boreal and tropical forests, *Glob. Change Biol.*, 14, 1531–1542,
2331 <https://doi.org/10.1111/j.1365-2486.2008.01598.x>, 2008.
- 2332 Hoesly, R. M., Smith, S. J., Feng, L., Klimont, Z., Janssens-Maenhout, G., Pitkanen, T., Seibert, J. J., Vu, L., Andres, R. J.,
2333 Bolt, R. M., Bond, T. C., Dawidowski, L., Kholod, N., Kurokawa, J., Li, M., Liu, L., Lu, Z., Moura, M. C. P., O'Rourke, P.
2334 R., and Zhang, Q.: Historical (1750–2014) anthropogenic emissions of reactive gases and aerosols from the Community
2335 Emissions Data System (CEDS), *Geosci. Model Dev.*, 11, 369–408, <https://doi.org/10.5194/gmd-11-369-2018>, 2018.
- 2336 Hong, C., Burney, J. A., Pongratz, J., Nabel, J. E. M. S., Mueller, N. D., Jackson, R. B., and Davis, S. J.: Global and regional
2337 drivers of land-use emissions in 1961–2017, *Nature*, 589, 554–561, <https://doi.org/10.1038/s41586-020-03138-y>, 2021.
- 2338 Holding, T., Ashton, I. G., Shutler, J. D., Land, P. E., Nightingale, P. D., Rees, A. P., Brown, I., Piolle, J.-F., Kock, A.,
2339 Bange, H. W., Woolf, D. K., Goddijn-Murphy, L., Pereira, R., Paul, F., Girard-Ardhuin, F., Chapron, B., Rehder, G.,
2340 Ardhuin, F., and Donlon, C. J.: The FluxEngine air–sea gas flux toolbox: simplified interface and extensions for in situ
2341 analyses and multiple sparingly soluble gases, *Ocean Sci.*, 15, 1707–1728, <https://doi.org/10.5194/os-15-1707-2019>, 2019.
- 2342 Houghton, R. A. and Castanho, A.: Annual emissions of carbon from land use, land-use change, and forestry from 1850 to
2343 2020, *Earth Syst. Sci. Data*, 15, 2025–2054, <https://doi.org/10.5194/essd-15-2025-2023>, 2023.
- 2344 Houghton, R. A., House, J. I., Pongratz, J., van der Werf, G. R., DeFries, R. S., Hansen, M. C., Le Quéré, C., and
2345 Ramankutty, N.: Carbon emissions from land use and land-cover change, *Biogeosciences*, 9, 5125–5142,
2346 <https://doi.org/10.5194/bg-9-5125-2012>, 2012.
- 2347 Hubau, W., Lewis, S.L., Phillips, O.L., Affum-Baffoe, K., Beeckman, H., Cuní-Sánchez, A., Daniels, A.K., Ewango, C.E.N.,
2348 Fauset, S., Mukinzi, J.M., Sheil, D., Sonké, B., Sullivan, M.J.P., Sunderland, T.C.H., Taedoum, H., Thomas, S.C., White,
2349 L.J.T., Abernethy, K.A., Adu-Bredu, S., Amani, C.A., Baker, T.R., Banin, L.F., Baya, F., Begne, S.K., Bennett, A.C.,
2350 Benedet, F., Bitariho, R., Bocko, Y.E., Boeckx, P., Boudjia, P., Brienen, R.J.W., Brncic, T., Chezeaux, E., Chuyong, G.B.,
2351 Clark, C.J., Collins, M., Comiskey, J.A., Coomes, D.A., Dargie, G.C., de Haulleville, T., Kamdem, M.N.D., Doucet, J.-L.,
2352 Esquivel-Muelbert, A., Feldpausch, T.R., Fofanah, A., Foli, E.G., Gilpin, M., Gloor, E., Gonmadje, C., Gourlet-Fleury, S.,
2353 Hall, J.S., Hamilton, A.C., Harris, D.J., Hart, T.B., Hockemba, M.B.N., Hladik, A., Ifo, S.A., Jeffery, K.J., Jucker, T.,
2354 Yakusu, E.K., Kearsley, E., Kenfack, D., Koch, A., Leal, M.E., Levesley, A., Lindsell, J.A., Lisingo, J., Lopez-Gonzalez, G.,
2355 Lovett, J.C., Makana, J.-R., Malhi, Y., Marshall, A.R., Martin, J., Martin, E.H., Mbayu, F.M., Medjibe, V.P., Mihindou, V.,
2356 Mitchard, E.T.A., Moore, S., Munishi, P.K.T., Bengone, N.N., Ojo, L., Ondo, F.E., Peh, K.S.-H., Pickavance, G.C., Poulsen,



- 2357 A.D., Poulsen, J.R., Qie, L., Reitsma, J., Rovero, F., Swaine, M.D., Talbot, J., Taplin, J., Taylor, D.M., Thomas, D.W.,
2358 Toirambe, B., Mukendi, J.T., Tuagben, D., Umunay, P.M., van der Heijden, G.M.F., Verbeeck, H., Vleminckx, J., Willcock,
2359 S., Wöll, H., Woods, J.T., Zemagho, L.: Asynchronous carbon sink saturation in African and Amazonian tropical forests,
2360 *Nature*, 579, 80–87, <https://doi.org/10.1038/s41586-020-2035-0>, 2020.
- 2361 Humphrey, V., Zscheischler, J., Ciais, P., Gudmundsson, L., Sitch, S., and Seneviratne, S. I.: Sensitivity of atmospheric CO₂
2362 growth rate to observed changes in terrestrial water storage, *Nature*, 560, 628–631, [https://doi.org/10.1038/s41586-018-](https://doi.org/10.1038/s41586-018-0424-4)
2363 0424-4, 2018.
- 2364 Humphrey, V., Berg, A., Ciais, P., Gentine, P., Jung, M., Reichstein, M., Seneviratne, S. I., and Frankenberg, C.: Soil
2365 moisture–atmosphere feedback dominates land carbon uptake variability, *Nature*, 592, 65–69,
2366 <https://doi.org/10.1038/s41586-021-03325-5>, 2021.
- 2367 Huntzinger, D. N., Michalak, A. M., Schwalm, C., Ciais, P., King, A. W., Fang, Y., Schaefer, K., Wei, Y., Cook, R. B.,
2368 Fisher, J. B., Hayes, D., Huang, M., Ito, A., Jain, A. K., Lei, H., Lu, C., Maignan, F., Mao, J., Parazoo, N., Peng, S., Poulter,
2369 B., Ricciuto, D., Shi, X., Tian, H., Wang, W., Zeng, N., and Zhao, F.: Uncertainty in the response of terrestrial carbon sink to
2370 environmental drivers undermines carbon-climate feedback predictions, *Sci Rep*, 7, 4765, [https://doi.org/10.1038/s41598-](https://doi.org/10.1038/s41598-017-03818-2)
2371 017-03818-2, 2017.
- 2372 Iida, Y., Takatani, Y., Kojima, A., and Ishii, M.: Global trends of ocean CO₂ sink and ocean acidification: an observation-
2373 based reconstruction of surface ocean inorganic carbon variables, *J Oceanogr*, 77, 323–358, [https://doi.org/10.1007/s10872-](https://doi.org/10.1007/s10872-020-00571-5)
2374 020-00571-5, 2021.
- 2375 Ilyina, T., Li, H., Spring, A., Müller, W. A., Bopp, L., Chikamoto, M. O., Danabasoglu, G., Dobrynin, M., Dunne, J.,
2376 Fransner, F., Friedlingstein, P., Lee, W., Lovenduski, N. S., Merryfield, W. J., Mignot, J., Park, J. Y., Séférian, R., Sospedra-
2377 Alfonso, R., Watanabe, M., and Yeager, S.: Predictable Variations of the Carbon Sinks and Atmospheric CO₂ Growth in a
2378 Multi-Model Framework, *Geophys. Res. Lett.*, 48, e2020GL090695, <https://doi.org/10.1029/2020GL090695>, 2021.
- 2379 IMF: International Monetary Fund: World Economic Outlook, available at: <http://www.imf.org>, last access: 27 September
2380 2023, 2022.
- 2381 IPCC: Annex II: Glossary [Möller, V, J.B.R. Matthews, R. van Diemen, C. Méndez, S. Semenov, J.S. Fuglestedt, A.
2382 Reisinger (eds.)]. In: *Climate Change 2022: Impacts, Adaptation, and Vulnerability. Contribution of Working Group II to the*
2383 *Sixth Assessment Report of the Intergovernmental Panel on Climate Change* [H.-O. Pörtner, D.C. Roberts, M. Tignor, E.S.
2384 Poloczanska, K. Mintenbeck, A. Alegría, M. Craig, S. Langsdorf, S. Lösschke, V. Möller, A. Okem, B. Rama (eds.)], in:
2385 *Climate Change 2022 – Impacts, Adaptation and Vulnerability: Working Group II Contribution to the Sixth Assessment*
2386 *Report of the Intergovernmental Panel on Climate Change* [Möller, V, J.B.R. Matthews, R. van Diemen, C. Méndez, S.
2387 Semenov, J.S. Fuglestedt, A. Reisinger (eds.)], Cambridge University Press, Cambridge, UK and New York, NY, 2897–
2388 2930, <https://doi.org/10.1017/9781009325844.029>, 2023.
- 2389 Ito, A. and Inatomi, M.: Use of a process-based model for assessing the methane budgets of global terrestrial ecosystems and
2390 evaluation of uncertainty, 9, 759–773, <https://doi.org/10.5194/bg-9-759-2012>, 2012.
- 2391 Jackson, R. B., Canadell, J. G., Le Quéré, C., Andrew, R. M., Korsbakken, J. I., Peters, G. P., and Nakicenovic, N.:
2392 Reaching peak emissions, *Nature Clim Change*, 6, 7–10, <https://doi.org/10.1038/nclimate2892>, 2016.



- 2393 Jackson, R. B., Le Quéré, C., Andrew, R. M., Canadell, J. G., Korsbakken, J. I., Liu, Z., Peters, G. P., and Zheng, B.: Global
2394 energy growth is outpacing decarbonization, *Environ. Res. Lett.*, 13, 120401, <https://doi.org/10.1088/1748-9326/aaf303>,
2395 2018.
- 2396 Jackson, R. B., Friedlingstein, P., Andrew, R. M., Canadell, J. G., Le Quéré, C., and Peters, G. P.: Persistent fossil fuel
2397 growth threatens the Paris Agreement and planetary health, *Environ. Res. Lett.*, 14, 121001, <https://doi.org/10.1088/1748-9326/ab57b3>, 2019.
- 2399 Jackson, R. B., Friedlingstein, P., Quéré, C. L., Abernethy, S., Andrew, R. M., Canadell, J. G., Ciais, P., Davis, S. J., Deng,
2400 Z., Liu, Z., Korsbakken, J. I., and Peters, G. P.: Global fossil carbon emissions rebound near pre-COVID-19 levels, *Environ.*
2401 *Res. Lett.*, 17, 031001, <https://doi.org/10.1088/1748-9326/ac55b6>, 2022.
- 2402 Jacobson, A. R., Schuldt, K. N., Tans, P., Arlyn Andrews, Miller, J. B., Oda, T., Mund, J., Weir, B., Ott, L., Aalto, T.,
2403 Abshire, J. B., Aikin, K., Aoki, S., Apadula, F., Arnold, S., Baier, B., Bartyzel, J., Beyersdorf, A., Biermann, T., Biraud, S.
2404 C., Boenisch, H., Brailsford, G., Brand, W. A., Chen, G., Huilin Chen, Lukasz Chmura, Clark, S., Colomb, A., Commane,
2405 R., Conil, S., Couret, C., Cox, A., Cristofanelli, P., Cuevas, E., Curcoll, R., Daube, B., Davis, K. J., De Wekker, S., Coletta,
2406 J. D., Delmotte, M., DiGangi, E., DiGangi, J. P., Di Sarra, A. G., Dlugokencky, E., Elkins, J. W., Emmenegger, L., Shuangxi
2407 Fang, Fischer, M. L., Forster, G., Frumau, A., Galkowski, M., Gatti, L. V., Gehrlein, T., Gerbig, C., Francois Gheusi, Gloor,
2408 E., Gomez-Trueba, V., Goto, D., Griffiths, T., Hammer, S., Hanson, C., Haszpra, L., Hatakka, J., Heimann, M., Heliasz, M.,
2409 Hensen, A., Hermansen, O., Hintsa, E., Holst, J., Ivakhov, V., Jaffé, D. A., Jordan, A., Joubert, W., Karion, A., Kawa, S. R.,
2410 Kazan, V., Keeling, R. F., Keronen, P., Kneuer, T., Kolari, P., Kateřina Komínková, Kort, E., Kozlova, E., Krummel, P.,
2411 Kubistin, D., Labuschagne, C., Lam, D. H. Y., Lan, X., Langenfelds, R. L., Laurent, O., Laurila, T., Lauvaux, T., Lavric, J.,
2412 Law, B. E., Lee, J., Lee, O. S. M., Lehner, I., Lehtinen, K., Leppert, R., et al.: CarbonTracker CT2022,
2413 <https://doi.org/10.25925/Z1GJ-3254>, 2023a.
- 2414 Jacobson, A. R., Schuldt, K. N., Tans, P., Arlyn Andrews, Miller, J. B., Oda, T., Mund, J., Weir, B., Ott, L., Aalto, T.,
2415 Abshire, J. B., Aikin, K., Aoki, S., Apadula, F., Arnold, S., Baier, B., Bartyzel, J., Beyersdorf, A., Biermann, T., Biraud, S.
2416 C., Boenisch, H., Brailsford, G., Brand, W. A., Chen, G., Huilin Chen, Lukasz Chmura, Clark, S., Colomb, A., Commane,
2417 R., Conil, S., Couret, C., Cox, A., Cristofanelli, P., Cuevas, E., Curcoll, R., Daube, B., Davis, K. J., De Wekker, S., Coletta,
2418 J. D., Delmotte, M., DiGangi, E., DiGangi, J. P., Di Sarra, A. G., Dlugokencky, E., Elkins, J. W., Emmenegger, L., Shuangxi
2419 Fang, Fischer, M. L., Forster, G., Frumau, A., Galkowski, M., Gatti, L. V., Gehrlein, T., Gerbig, C., Francois Gheusi, Gloor,
2420 E., Gomez-Trueba, V., Goto, D., Griffiths, T., Hammer, S., Hanson, C., Haszpra, L., Hatakka, J., Heimann, M., Heliasz, M.,
2421 Hensen, A., Hermansen, O., Hintsa, E., Holst, J., Ivakhov, V., Jaffé, D. A., Jordan, A., Joubert, W., Karion, A., Kawa, S. R.,
2422 Kazan, V., Keeling, R. F., Keronen, P., Kneuer, T., Kolari, P., Kateřina Komínková, Kort, E., Kozlova, E., Krummel, P.,
2423 Kubistin, D., Labuschagne, C., Lam, D. H. Y., Lan, X., Langenfelds, R. L., Laurent, O., Laurila, T., Lauvaux, T., Lavric, J.,
2424 Law, B. E., Lee, J., Lee, O. S. M., Lehner, I., Lehtinen, K., Leppert, R., et al.: CarbonTracker CT-NRT.v2023-3,
2425 <https://doi.org/10.25925/TTAF-J322>, 2023b.
- 2426 Janssens-Maenhout, G., Crippa, M., Guizzardi, D., Muntean, M., Schaaf, E., Dentener, F., Bergamaschi, P., Pagliari, V.,
2427 Olivier, J. G. J., Peters, J. A. H. W., van Aardenne, J. A., Monni, S., Doering, U., Petrescu, A. M. R., Solazzo, E., and
2428 Oreggioni, G. D.: EDGAR v4.3.2 Global Atlas of the three major greenhouse gas emissions for the period 1970–2012, *Earth*
2429 *Syst. Sci. Data*, 11, 959–1002, <https://doi.org/10.5194/essd-11-959-2019>, 2019.
- 2430 Jean-Michel, L., Eric, G., Romain, B.-B., Gilles, G., Angélique, M., Marie, D., Clément, B., Mathieu, H., Olivier, L. G.,
2431 Charly, R., Tony, C., Charles-Emmanuel, T., Florent, G., Giovanni, R., Mounir, B., Yann, D., and Pierre-Yves, L. T.: The
2432 Copernicus Global 1/12° Oceanic and Sea Ice GLORYS12 Reanalysis, *Front. Earth Sci.*, 9, 2021.



- 2433 Jiang, F., Ju, W., He, W., Wu, M., Wang, H., Wang, J., Jia, M., Feng, S., Zhang, L., and Chen, J. M.: A 10-year global
2434 monthly averaged terrestrial net ecosystem exchange dataset inferred from the ACOS GOSAT v9 XCO₂ retrievals
2435 (GCAS2021), *Earth Syst. Sci. Data*, 14, 3013–3037, <https://doi.org/10.5194/essd-14-3013-2022>, 2022.
- 2436 Jiang, F., Wang, H., Chen, J. M., Ju, W., Tian, X., Feng, S., Li, G., Chen, Z., Zhang, S., Lu, X., Liu, J., Wang, H., Wang, J.,
2437 He, W., and Wu, M.: Regional CO₂ fluxes from 2010 to 2015 inferred from GOSAT XCO₂ retrievals using a new version
2438 of the Global Carbon Assimilation System, *Atmospheric Chem. Phys.*, 21, 1963–1985, [https://doi.org/10.5194/acp-21-1963-](https://doi.org/10.5194/acp-21-1963-2021)
2439 2021, 2021.
- 2440
2441 Jin, Z., Wang, T., Zhang, H., Wang, Y., Ding, J., and Tian, X.: Constraint of satellite CO₂ retrieval on the global carbon
2442 cycle from a Chinese atmospheric inversion system, *Sci. China Earth Sci.*, 66, 609–618, [https://doi.org/10.1007/s11430-022-](https://doi.org/10.1007/s11430-022-1036-7)
2443 1036-7, 2023.
- 2444 Joos, F. and Spahni, R.: Rates of change in natural and anthropogenic radiative forcing over the past 20,000 years,
2445 *Proceedings of the National Academy of Sciences*, 105, 1425–1430, <https://doi.org/10.1073/pnas.0707386105>, 2008.
- 2446 Jones, C. D., Hickman, J. E., Rumbold, S. T., Walton, J., Lamboll, R. D., Skeie, R. B., Fiedler, S., Forster, P. M., Rogelj, J.,
2447 Abe, M., Botzet, M., Calvin, K., Cassou, C., Cole, J. N. S., Davini, P., Deushi, M., Dix, M., Fyfe, J. C., Gillett, N. P., Ilyina,
2448 T., Kawamiya, M., Kelley, M., Kharin, S., Koshiro, T., Li, H., Mackallah, C., Müller, W. A., Nabat, P., van Noije, T., Nolan,
2449 P., Ohgaito, R., Olivieri, D., Oshima, N., Parodi, J., Reerink, T. J., Ren, L., Romanou, A., Séférian, R., Tang, Y., Timmreck,
2450 C., Tjiputra, J., Tourigny, E., Tsigaridis, K., Wang, H., Wu, M., Wyser, K., Yang, S., Yang, Y., and Ziehn, T.: The Climate
2451 Response to Emissions Reductions Due to COVID-19: Initial Results From CovidMIP, *Geophys. Res. Lett.*, 48,
2452 e2020GL091883, <https://doi.org/10.1029/2020GL091883>, 2021a.
- 2453
2454 Jones, M. W., Abatzoglou, J. T., Veraverbeke, S., Andela, N., Lasslop, G., Forkel, M., Smith, A. J. P., Burton, C., Betts, R.
2455 A., van der Werf, G. R., Sitch, S., Canadell, J. G., Santin, C., Kolden, C., Doerr, S. H., and Le Quéré, C.: Global and
2456 Regional Trends and Drivers of Fire Under Climate Change, *Rev. Geophys.*, 60, e2020RG000726,
2457 <https://doi.org/10.1029/2020RG000726>, 2022.
- 2458 Jones, M. W., Andrew, R. M., Peters, G. P., Janssens-Maenhout, G., De-Gol, A. J., Ciais, P., Patra, P. K., Chevallier, F., and
2459 Le Quéré, C.: Gridded fossil CO₂ emissions and related O₂ combustion consistent with national inventories 1959–2018, *Sci*
2460 *Data*, 8, 2, <https://doi.org/10.1038/s41597-020-00779-6>, 2021b.
- 2461 Jones, M. W., Andrew, R. M., Peters, G. P., Janssens-Maenhout, G., De-Gol, A. J., Dou, X., Liu, Z., Pickers, P., Ciais, P.,
2462 Patra, P. K., Chevallier, F., and Le Quéré, C.: Gridded fossil CO₂ emissions and related O₂ combustion consistent with
2463 national inventories 1959–2022, Zenodo [dataset], <https://doi.org/10.5281/zenodo.8386803>, 2023.
- 2464 Jung, M., Reichstein, M., Schwalm, C. R., Huntingford, C., Sitch, S., Ahlström, A., Arneth, A., Camps-Valls, G., Ciais, P.,
2465 Friedlingstein, P., Gans, F., Ichii, K., Jain, A. K., Kato, E., Papale, D., Poulter, B., Raduly, B., Rödenbeck, C., Tramontana,
2466 G., Viovy, N., Wang, Y.-P., Weber, U., Zaehle, S., and Zeng, N.: Compensatory water effects link yearly global land CO₂
2467 sink changes to temperature, *Nature*, 541, 516–520, <https://doi.org/10.1038/nature20780>, 2017.
- 2468 Kaiser, J. W., Heil, A., Andreae, M. O., Benedetti, A., Chubarova, N., Jones, L., Morcrette, J.-J., Razinger, M., Schultz, M.
2469 G., Suttie, M., and van der Werf, G. R.: Biomass burning emissions estimated with a global fire assimilation system based
2470 on observed fire radiative power, *Biogeosciences*, 9, 527–554, <https://doi.org/10.5194/bg-9-527-2012>, 2012.



- 2471 Kato, E., Kinoshita, T., Ito, A., Kawamiya, M., and Yamagata, Y.: Evaluation of spatially explicit emission scenario of land-
2472 use change and biomass burning using a process-based biogeochemical model, *J. Land Use Sci.*, 8, 104–122,
2473 <https://doi.org/10.1080/1747423X.2011.628705>, 2013.
- 2474 Kawasaki, T., Hasumi, H., and Tanaka, Y.: Role of tide-induced vertical mixing in the deep Pacific Ocean circulation, *J.*
2475 *Oceanogr.*, 77, 173–184, <https://doi.org/10.1007/s10872-020-00584-0>, 2021.
- 2476 Keeley, J. E. and Pausas, J. G.: Distinguishing disturbance from perturbations in fire-prone ecosystems, *Int. J. Wildland Fire*,
2477 28, 282–287, <https://doi.org/10.1071/WF18203>, 2019.
- 2478 Keeling, C. D., Bacastow, R. B., Bainbridge, A. E., Ekdahl, C. A., Guenther, P. R., Waterman, L. S., and Chin, J. F. S.:
2479 Atmospheric carbon dioxide variations at Mauna Loa Observatory, Hawaii, *Tellus A.*, 28, 538–551,
2480 <https://doi.org/10.1111/j.2153-3490.1976.tb00701.x>, 1976.
- 2481 Keeling, R. F., Manning, A. C., Paplawsky, W. J., and Cox, A. C.: On the long-term stability of reference gases for
2482 atmospheric O₂/N₂ and CO₂ measurements, *Tellus B Chem. Phys. Meteorol.*, 59, 3–14, <https://doi.org/10.1111/j.1600-0889.2006.00196.x>, 2007.
- 2484 Keppler, L. and Landschützer, P.: Regional Wind Variability Modulates the Southern Ocean Carbon Sink, *Sci Rep*, 9, 7384,
2485 <https://doi.org/10.1038/s41598-019-43826-y>, 2019.
- 2486 Khatiwala, S., Primeau, F., and Hall, T.: Reconstruction of the history of anthropogenic CO₂ concentrations in the ocean,
2487 *Nature*, 462, 346–349, <https://doi.org/10.1038/nature08526>, 2009.
- 2488 Khatiwala, S., Tanhua, T., Mikaloff Fletcher, S., Gerber, M., Doney, S. C., Graven, H. D., Gruber, N., McKinley, G. A.,
2489 Murata, A., Ríos, A. F., and Sabine, C. L.: Global ocean storage of anthropogenic carbon, *Biogeosciences*, 10, 2169–2191,
2490 <https://doi.org/10.5194/bg-10-2169-2013>, 2013.
- 2491 Kong, Y., Zheng, B., Zhang, Q., and He, K.: Global and regional carbon budget for 2015–2020 inferred from OCO-2 based
2492 on an ensemble Kalman filter coupled with GEOS-Chem, *Atmospheric Chem. Phys.*, 22, 10769–10788,
2493 <https://doi.org/10.5194/acp-22-10769-2022>, 2022.
- 2494 Korsbakken, J. I., Peters, G. P., and Andrew, R. M.: Uncertainties around reductions in China’s coal use and CO₂ emissions,
2495 *Nature Clim Change*, 6, 687–690, <https://doi.org/10.1038/nclimate2963>, 2016.
- 2496 Krinner, G., Viovy, N., de Noblet-Ducoudré, N., Ogée, J., Polcher, J., Friedlingstein, P., Ciais, P., Sitch, S., and Prentice, I.
2497 C.: A dynamic global vegetation model for studies of the coupled atmosphere-biosphere system: DVGCM for coupled climate
2498 studies, *Global Biogeochem. Cycles*, 19, GB1015, <https://doi.org/10.1029/2003GB002199>, 2005.
- 2499 Lacroix, F., Ilyina, T., and Hartmann, J.: Oceanic CO₂ outgassing and biological production hotspots induced by pre-
2500 industrial river loads of nutrients and carbon in a global modeling approach, *Biogeosciences*, 17, 55–88,
2501 <https://doi.org/10.5194/bg-17-55-2020>, 2020.
- 2502 Lacroix, F., Ilyina, T., Mathis, M., Laruelle, G. G., and Regnier, P.: Historical increases in land-derived nutrient inputs may
2503 alleviate effects of a changing physical climate on the oceanic carbon cycle, *Glob Change Biol*, 27, 5491–5513,
2504 <https://doi.org/10.1111/gcb.15822>, 2021.



- 2505 Lan, X., Tans, P. and K.W. Thoning: Trends in globally-averaged CO₂ determined from NOAA Global Monitoring
2506 Laboratory measurements, Version 2023-09. National Oceanic and Atmospheric Administration, Global Monitoring
2507 Laboratory (NOAA/GML), available at: <https://gml.noaa.gov/ccgg/trends/global.html>, last access: 27 September 2023, 2023.
- 2508 Landschützer, P., Gruber, N., Haumann, F. A., Rödenbeck, C., Bakker, D. C. E., van Heuven, S., Hoppema, M., Metzl, N.,
2509 Sweeney, C., Takahashi, T., Tilbrook, B., and Wanninkhof, R.: The reinvigoration of the Southern Ocean carbon sink,
2510 *Science*, 349, 1221–1224, <https://doi.org/10.1126/science.aab2620>, 2015.
- 2511 Landschützer, P., Gruber, N., and Bakker, D. C. E.: Decadal variations and trends of the global ocean carbon sink: decadal
2512 air-sea CO₂ flux variability, *Global Biogeochem. Cycles*, 30, 1396–1417, <https://doi.org/10.1002/2015GB005359>, 2016.
- 2513 Law, R. M., Ziehn, T., Matear, R. J., Lenton, A., Chamberlain, M. A., Stevens, L. E., Wang, Y.-P., Srbinovsky, J., Bi, D.,
2514 Yan, H., and Vohralik, P. F.: The carbon cycle in the Australian Community Climate and Earth System Simulator
2515 (ACCESS-ESM1) – Part 1: Model description and pre-industrial simulation, *Geosci. Model Dev.*, 10, 2567–2590,
2516 <https://doi.org/10.5194/gmd-10-2567-2017>, 2017.
- 2517 Lawrence, D. M., Fisher, R. A., Koven, C. D., Oleson, K. W., Swenson, S. C., Bonan, G., Collier, N., Ghimire, B., van
2518 Kampenhout, L., Kennedy, D., Kluzek, E., Lawrence, P. J., Li, F., Li, H., Lombardozi, D., Riley, W. J., Sacks, W. J., Shi,
2519 M., Vertenstein, M., Wieder, W. R., Xu, C., Ali, A. A., Badger, A. M., Bisht, G., van den Broeke, M., Brunke, M. A., Burns,
2520 S. P., Buzan, J., Clark, M., Craig, A., Dahlin, K., Drewniak, B., Fisher, J. B., Flanner, M., Fox, A. M., Gentine, P., Hoffman,
2521 F., Keppel-Aleks, G., Knox, R., Kumar, S., Lenaerts, J., Leung, L. R., Lipscomb, W. H., Lu, Y., Pandey, A., Pelletier, J. D.,
2522 Perket, J., Randerson, J. T., Ricciuto, D. M., Sanderson, B. M., Slater, A., Subin, Z. M., Tang, J., Thomas, R. Q., Val Martin,
2523 M., and Zeng, X.: The Community Land Model Version 5: Description of New Features, Benchmarking, and Impact of
2524 Forcing Uncertainty, *J. Adv. Model Earth, Sy.*, 11, 4245–4287, <https://doi.org/10.1029/2018MS001583>, 2019.
- 2525 Le Quéré, C., Rödenbeck, C., Buitenhuis, E. T., Conway, T. J., Langenfelds, R., Gomez, A., Labuschagne, C., Ramonet, M.,
2526 Nakazawa, T., Metzl, N., Gillett, N., and Heimann, M.: Saturation of the Southern Ocean CO₂ Sink Due to Recent Climate
2527 Change, *Science*, 316, 1735–1738, <https://doi.org/10.1126/science.1136188>, 2007.
- 2528 Le Quéré, C., Raupach, M. R., Canadell, J. G., Marland, G., Bopp, L., Ciais, P., Conway, T. J., Doney, S. C., Feely, R. A.,
2529 Foster, P., Friedlingstein, P., Gurney, K., Houghton, R. A., House, J. I., Huntingford, C., Levy, P. E., Lomas, M. R., Majkut,
2530 J., Metzl, N., Ometto, J. P., Peters, G. P., Prentice, I. C., Randerson, J. T., Running, S. W., Sarmiento, J. L., Schuster, U.,
2531 Sitch, S., Takahashi, T., Viovy, N., van der Werf, G. R., and Woodward, F. I.: Trends in the sources and sinks of carbon
2532 dioxide, *Nature Geosci.*, 2, 831–836, <https://doi.org/10.1038/ngeo689>, 2009.
- 2533 Le Quéré, C., Andres, R. J., Boden, T., Conway, T., Houghton, R. A., House, J. I., Marland, G., Peters, G. P., van der Werf,
2534 G. R., Ahlström, A., Andrew, R. M., Bopp, L., Canadell, J. G., Ciais, P., Doney, S. C., Enright, C., Friedlingstein, P.,
2535 Huntingford, C., Jain, A. K., Jourdain, C., Kato, E., Keeling, R. F., Klein Goldewijk, K., Levis, S., Levy, P., Lomas, M.,
2536 Poulter, B., Raupach, M. R., Schwinger, J., Sitch, S., Stocker, B. D., Viovy, N., Zaehle, S., and Zeng, N.: The global carbon
2537 budget 1959–2011, *Earth Syst. Sci. Data*, 5, 165–185, <https://doi.org/10.5194/essd-5-165-2013>, 2013.
- 2538 Le Quéré, C., Peters, G. P., Andres, R. J., Andrew, R. M., Boden, T. A., Ciais, P., Friedlingstein, P., Houghton, R. A.,
2539 Marland, G., Moriarty, R., Sitch, S., Tans, P., Armeth, A., Arvanitis, A., Bakker, D. C. E., Bopp, L., Canadell, J. G., Chini, L.
2540 P., Doney, S. C., Harper, A., Harris, I., House, J. I., Jain, A. K., Jones, S. D., Kato, E., Keeling, R. F., Klein Goldewijk, K.,
2541 Körtzinger, A., Koven, C., Lefèvre, N., Maignan, F., Omar, A., Ono, T., Park, G.-H., Pfeil, B., Poulter, B., Raupach, M. R.,
2542 Regnier, P., Rödenbeck, C., Saito, S., Schwinger, J., Segsneider, J., Stocker, B. D., Takahashi, T., Tilbrook, B., van



- 2543 Heuven, S., Viovy, N., Wanninkhof, R., Wiltshire, A., and Zaehle, S.: Global carbon budget 2013, *Earth Syst. Sci. Data*, 6, 235–263, <https://doi.org/10.5194/essd-6-235-2014>, 2014.
- 2545 Le Quéré, C., Moriarty, R., Andrew, R. M., Peters, G. P., Ciais, P., Friedlingstein, P., Jones, S. D., Sitch, S., Tans, P.,
2546 Armeth, A., Boden, T. A., Bopp, L., Bozec, Y., Canadell, J. G., Chini, L. P., Chevallier, F., Cosca, C. E., Harris, I.,
2547 Hoppema, M., Houghton, R. A., House, J. I., Jain, A. K., Johannessen, T., Kato, E., Keeling, R. F., Kitidis, V., Klein
2548 Goldewijk, K., Koven, C., Landa, C. S., Landschützer, P., Lenton, A., Lima, I. D., Marland, G., Mathis, J. T., Metzl, N.,
2549 Nojiri, Y., Olsen, A., Ono, T., Peng, S., Peters, W., Pfeil, B., Poulter, B., Raupach, M. R., Regnier, P., Rödenbeck, C., Saito,
2550 S., Salisbury, J. E., Schuster, U., Schwinger, J., Séférian, R., Segsneider, J., Steinhoff, T., Stocker, B. D., Sutton, A. J.,
2551 Takahashi, T., Tilbrook, B., van der Werf, G. R., Viovy, N., Wang, Y.-P., Wanninkhof, R., Wiltshire, A., and Zeng, N.:
2552 Global carbon budget 2014, *Earth Syst. Sci. Data*, 7, 47–85, <https://doi.org/10.5194/essd-7-47-2015>, 2015a.
- 2553 Le Quéré, C., Moriarty, R., Andrew, R. M., Canadell, J. G., Sitch, S., Korsbakken, J. I., Friedlingstein, P., Peters, G. P.,
2554 Andres, R. J., Boden, T. A., Houghton, R. A., House, J. I., Keeling, R. F., Tans, P., Armeth, A., Bakker, D. C. E., Barbero,
2555 L., Bopp, L., Chang, J., Chevallier, F., Chini, L. P., Ciais, P., Fader, M., Feely, R. A., Gkritzalis, T., Harris, I., Hauck, J.,
2556 Ilyina, T., Jain, A. K., Kato, E., Kitidis, V., Klein Goldewijk, K., Koven, C., Landschützer, P., Lauvset, S. K., Lefèvre, N.,
2557 Lenton, A., Lima, I. D., Metzl, N., Millero, F., Munro, D. R., Murata, A., Nabel, J. E. M. S., Nakaoka, S., Nojiri, Y.,
2558 O'Brien, K., Olsen, A., Ono, T., Pérez, F. F., Pfeil, B., Pierrot, D., Poulter, B., Rehder, G., Rödenbeck, C., Saito, S.,
2559 Schuster, U., Schwinger, J., Séférian, R., Steinhoff, T., Stocker, B. D., Sutton, A. J., Takahashi, T., Tilbrook, B., van der
2560 Laan-Luijkx, I. T., van der Werf, G. R., van Heuven, S., Vandemark, D., Viovy, N., Wiltshire, A., Zaehle, S., and Zeng, N.:
2561 Global Carbon Budget 2015, *Earth Syst. Sci. Data*, 7, 349–396, <https://doi.org/10.5194/essd-7-349-2015>, 2015b.
- 2562 Le Quéré, C., Andrew, R. M., Canadell, J. G., Sitch, S., Korsbakken, J. I., Peters, G. P., Manning, A. C., Boden, T. A., Tans,
2563 P. P., Houghton, R. A., Keeling, R. F., Alin, S., Andrews, O. D., Anthoni, P., Barbero, L., Bopp, L., Chevallier, F., Chini, L.
2564 P., Ciais, P., Currie, K., Delire, C., Doney, S. C., Friedlingstein, P., Gkritzalis, T., Harris, I., Hauck, J., Haverd, V.,
2565 Hoppema, M., Klein Goldewijk, K., Jain, A. K., Kato, E., Körtzinger, A., Landschützer, P., Lefèvre, N., Lenton, A., Lienert,
2566 S., Lombardozi, D., Melton, J. R., Metzl, N., Millero, F., Monteiro, P. M. S., Munro, D. R., Nabel, J. E. M. S., Nakaoka, S.,
2567 O'Brien, K., Olsen, A., Omar, A. M., Ono, T., Pierrot, D., Poulter, B., Rödenbeck, C., Salisbury, J., Schuster, U., Schwinger,
2568 J., Séférian, R., Skjelvan, I., Stocker, B. D., Sutton, A. J., Takahashi, T., Tian, H., Tilbrook, B., van der Laan-Luijkx, I. T.,
2569 van der Werf, G. R., Viovy, N., Walker, A. P., Wiltshire, A. J., and Zaehle, S.: Global Carbon Budget 2016, *Earth Syst. Sci.*
2570 *Data*, 8, 605–649, <https://doi.org/10.5194/essd-8-605-2016>, 2016.
- 2571 Le Quéré, C., Andrew, R. M., Friedlingstein, P., Sitch, S., Pongratz, J., Manning, A. C., Korsbakken, J. I., Peters, G. P.,
2572 Canadell, J. G., Jackson, R. B., Boden, T. A., Tans, P. P., Andrews, O. D., Arora, V. K., Bakker, D. C. E., Barbero, L.,
2573 Becker, M., Betts, R. A., Bopp, L., Chevallier, F., Chini, L. P., Ciais, P., Cosca, C. E., Cross, J., Currie, K., Gasser, T.,
2574 Harris, I., Hauck, J., Haverd, V., Houghton, R. A., Hunt, C. W., Hurtt, G., Ilyina, T., Jain, A. K., Kato, E., Kautz, M.,
2575 Keeling, R. F., Klein Goldewijk, K., Körtzinger, A., Landschützer, P., Lefèvre, N., Lenton, A., Lienert, S., Lima, I.,
2576 Lombardozi, D., Metzl, N., Millero, F., Monteiro, P. M. S., Munro, D. R., Nabel, J. E. M. S., Nakaoka, S., Nojiri, Y., Padin,
2577 X. A., Peregon, A., Pfeil, B., Pierrot, D., Poulter, B., Rehder, G., Reimer, J., Rödenbeck, C., Schwinger, J., Séférian, R.,
2578 Skjelvan, I., Stocker, B. D., Tian, H., Tilbrook, B., Tubiello, F. N., van der Laan-Luijkx, I. T., van der Werf, G. R., van
2579 Heuven, S., Viovy, N., Vuichard, N., Walker, A. P., Watson, A. J., Wiltshire, A. J., Zaehle, S., and Zhu, D.: Global Carbon
2580 Budget 2017, *Earth Syst. Sci. Data*, 10, 405–448, <https://doi.org/10.5194/essd-10-405-2018>, 2018a.
- 2581 Le Quéré, C., Andrew, R. M., Friedlingstein, P., Sitch, S., Hauck, J., Pongratz, J., Pickers, P. A., Korsbakken, J. I., Peters, G.
2582 P., Canadell, J. G., Armeth, A., Arora, V. K., Barbero, L., Bastos, A., Bopp, L., Chevallier, F., Chini, L. P., Ciais, P., Doney,
2583 S. C., Gkritzalis, T., Goll, D. S., Harris, I., Haverd, V., Hoffman, F. M., Hoppema, M., Houghton, R. A., Hurtt, G., Ilyina, T.,



- 2584 Jain, A. K., Johannessen, T., Jones, C. D., Kato, E., Keeling, R. F., Klein Goldewijk, K., Landschützer, P., Lefèvre, N.,
2585 Lienert, S., Liu, Z., Lombardozi, D., Metzl, N., Munro, D. R., Nabel, J. E. M. S., Nakaoka, S., Neill, C., Olsen, A., Ono, T.,
2586 Patra, P., Peregón, A., Peters, W., Peylin, P., Pfeil, B., Pierrot, D., Poulter, B., Rehder, G., Resplandy, L., Robertson, E.,
2587 Rocher, M., Rödenbeck, C., Schuster, U., Schwinger, J., Séférian, R., Skjelvan, I., Steinhoff, T., Sutton, A., Tans, P. P.,
2588 Tian, H., Tilbrook, B., Tubiello, F. N., van der Laan-Luijkx, I. T., van der Werf, G. R., Viovy, N., Walker, A. P., Wiltshire,
2589 A. J., Wright, R., Zaehle, S., and Zheng, B.: Global Carbon Budget 2018, *Earth Syst. Sci. Data*, 10, 2141–2194,
2590 <https://doi.org/10.5194/essd-10-2141-2018>, 2018b.
- 2591 Le Quéré, C., Korsbakken, J. I., Wilson, C., Tosun, J., Andrew, R., Andres, R. J., Canadell, J. G., Jordan, A., Peters, G. P.,
2592 and van Vuuren, D. P.: Drivers of declining CO₂ emissions in 18 developed economies, *Nat. Clim. Chang.*, 9, 213–217,
2593 <https://doi.org/10.1038/s41558-019-0419-7>, 2019.
- 2594 Le Quéré, C., Peters, G. P., Friedlingstein, P., Andrew, R. M., Canadell, J. G., Davis, S. J., Jackson, R. B., and Jones, M. W.:
2595 Fossil CO₂ emissions in the post-COVID-19 era, *Nat. Clim. Chang.*, 11, 197–199, [https://doi.org/10.1038/s41558-021-](https://doi.org/10.1038/s41558-021-01001-0)
2596 01001-0, 2021.
- 2597 Levitus, S., Antonov, J. I., Boyer, T. P., Baranova, O. K., Garcia, H. E., Locarnini, R. A., Mishonov, A. V., Reagan, J. R.,
2598 Seidov, D., Yarosh, E. S., and Zweng, M. M.: World ocean heat content and thermocline sea level change (0–2000 m),
2599 1955–2010, *Geophys. Res. Lett.*, 39, <https://doi.org/10.1029/2012GL051106>, 2012.
2600
- 2601 Li, H., Ilyina, T., Müller, W. A., and Sienz, F.: Decadal predictions of the North Atlantic CO₂ uptake, *Nat. Commun.*, 7,
2602 11076, <https://doi.org/10.1038/ncomms11076>, 2016.
2603
- 2604 Li, H., Ilyina, T., Müller, W. A., and Landschützer, P.: Predicting the variable ocean carbon sink, *Sci. Adv.*, 5, eaav6471,
2605 <https://doi.org/10.1126/sciadv.aav6471>, 2019.
2606
- 2607 Li, H., Ilyina, T., Loughran, T., Spring, A., and Pongratz, J.: Reconstructions and predictions of the global carbon budget
2608 with an emission-driven Earth system model, *Earth Syst. Dyn.*, 14, 101–119, <https://doi.org/10.5194/esd-14-101-2023>, 2023.
- 2609 Li, W., Ciais, P., Peng, S., Yue, C., Wang, Y., Thurner, M., Saatchi, S. S., Armeth, A., Avitabile, V., Carvalhais, N., Harper,
2610 A. B., Kato, E., Koven, C., Liu, Y. Y., Nabel, J. E. M. S., Pan, Y., Pongratz, J., Poulter, B., Pugh, T. A. M., Santoro, M.,
2611 Sitch, S., Stocker, B. D., Viovy, N., Wiltshire, A., Yousefpour, R., and Zaehle, S.: Land-use and land-cover change carbon
2612 emissions between 1901 and 2012 constrained by biomass observations, *Biogeosciences*, 14, 5053–5067,
2613 <https://doi.org/10.5194/bg-14-5053-2017>, 2017.
- 2614 Liao, E., Resplandy, L., Liu, J., and Bowman, K. W.: Amplification of the Ocean Carbon Sink During El Niños: Role of
2615 Poleward Ekman Transport and Influence on Atmospheric CO₂, *Global Biogeochem. Cy.*, 34, e2020GB006574,
2616 <https://doi.org/10.1029/2020GB006574>, 2020.
- 2617 Lienert, S. and Joos, F.: A Bayesian ensemble data assimilation to constrain model parameters and land-use carbon
2618 emissions, *Biogeosciences*, 15, 2909–2930, <https://doi.org/10.5194/bg-15-2909-2018>, 2018.
- 2619 Liu, J., Baskaran, L., Bowman, K., Schimel, D., Bloom, A. A., Parazoo, N. C., Oda, T., Carroll, D., Menemenlis, D., Joiner,
2620 J., Commane, R., Daube, B., Gatti, L. V., McKain, K., Miller, J., Stephens, B. B., Sweeney, C., and Wofsy, S.: Carbon
2621 Monitoring System Flux Net Biosphere Exchange 2020 (CMS-Flux NBE 2020), 13, 299–330, [https://doi.org/10.5194/essd-](https://doi.org/10.5194/essd-13-299-2021)
2622 13-299-2021, 2021.



- 2623 Liu, Z., Guan, D., Wei, W., Davis, S. J., Ciais, P., Bai, J., Peng, S., Zhang, Q., Hubacek, K., Marland, G., Andres, R. J.,
2624 Crawford-Brown, D., Lin, J., Zhao, H., Hong, C., Boden, T. A., Feng, K., Peters, G. P., Xi, F., Liu, J., Li, Y., Zhao, Y.,
2625 Zeng, N., and He, K.: Reduced carbon emission estimates from fossil fuel combustion and cement production in China,
2626 *Nature*, 524, 335–338, <https://doi.org/10.1038/nature14677>, 2015.
- 2627 Liu, Z., Zeng, N., Liu, Y., Kalnay, E., Asrar, G., Wu, B., Cai, Q., Liu, D., and Han, P.: Improving the joint estimation of
2628 CO₂ and surface carbon fluxes using a constrained ensemble Kalman filter in COLA (v1.0), *Geosci. Model Dev.*, 15, 5511–
2629 5528, <https://doi.org/10.5194/gmd-15-5511-2022>, 2022.
- 2630
2631 Lovenduski, N. S., Bonan, G. B., Yeager, S. G., Lindsay, K., and Lombardozzi, D. L.: High predictability of terrestrial
2632 carbon fluxes from an initialized decadal prediction system, *Environ. Res. Lett.*, 14, 124074, [https://doi.org/10.1088/1748-](https://doi.org/10.1088/1748-9326/ab5c55)
2633 [9326/ab5c55](https://doi.org/10.1088/1748-9326/ab5c55), 2019a.
- 2634
2635 Lovenduski, N. S., Yeager, S. G., Lindsay, K., and Long, M. C.: Predicting near-term variability in ocean carbon uptake,
2636 *Earth Syst. Dyn.*, 10, 45–57, <https://doi.org/10.5194/esd-10-45-2019>, 2019b.
- 2637 Lutz, F., Herzfeld, T., Heinke, J., Rolinski, S., Schaphoff, S., von Bloh, W., Stoorvogel, J. J., and Müller, C.: Simulating the
2638 effect of tillage practices with the global ecosystem model LPJmL (version 5.0-tillage), *Geosci. Model Dev.*, 12, 2419–2440,
2639 <https://doi.org/10.5194/gmd-12-2419-2019>, 2019.
- 2640 Ma, L., Hurr, G., Ott, L., Sahajpal, R., Fisk, J., Lamb, R., Tang, H., Flanagan, S., Chini, L., Chatterjee, A., and Sullivan, J.:
2641 Global evaluation of the Ecosystem Demography model (ED v3.0), *Geosci. Model Dev.*, 15, 1971–1994,
2642 <https://doi.org/10.5194/gmd-15-1971-2022>, 2022.
- 2643
2644 Magi, B. I., Rabin, S., Shevliakova, E., and Pacala, S.: Separating agricultural and non-agricultural fire seasonality at
2645 regional scales, *Biogeosciences*, 9, 3003–3012, <https://doi.org/10.5194/bg-9-3003-2012>, 2012.
- 2646 Masarie, K. A. and Tans, P. P.: Extension and integration of atmospheric carbon dioxide data into a globally consistent
2647 measurement record, *J. Geophys. Res.*, 100, 11593, <https://doi.org/10.1029/95JD00859>, 1995.
- 2648 Mather, A. S.: The transition from deforestation to reforestation in Europe, in: *Agricultural technologies and tropical*
2649 *deforestation* (eds. Angelsen, A.; Kaimowitz, D.), CABI in association with centre for international Forestry Research, 35–
2650 52, 2001.
- 2651 Mauritsen, T., Bader, J., Becker, T., Behrens, J., Bittner, M., Brokopf, R., Brovkin, V., Claussen, M., Crueger, T., Esch, M.,
2652 Fast, I., Fiedler, S., Fläschner, D., Gayler, V., Giorgetta, M., Goll, D. S., Haak, H., Hagemann, S., Hedemann, C.,
2653 Hohenegger, C., Ilyina, T., Jahns, T., Jimenez-de-la-Cuesta, D., JungCLAUS, J., Kleinen, T., Kloster, S., Kracher, D., Kinne,
2654 S., Kleberg, D., Lasslop, G., Kornbluh, L., Marotzke, J., Matei, D., Meraner, K., Mikolajewicz, U., Modali, K., Möbis, B.,
2655 Müller, W. A., Nabel, J. E. M. S., Nam, C. C. W., Notz, D., Nyawira, S.-S., Paulsen, H., Peters, K., Pincus, R., Pohlmann,
2656 H., Pongratz, J., Popp, M., Raddatz, T. J., Rast, S., Redler, R., Reick, C. H., Rohrschneider, T., Schemann, V., Schmidt, H.,
2657 Schnur, R., Schulzweida, U., Six, K. D., Stein, L., Stemmler, I., Stevens, B., von Storch, J.-S., Tian, F., Voigt, A., Vrese, P.,
2658 Wieners, K.-H., Wilkenskjaeld, S., Winkler, A., and Roeckner, E.: Developments in the MPI-M Earth System Model version
2659 1.2 (MPI-ESM1.2) and Its Response to Increasing CO₂, *J. Adv. Model Earth Sy.*, 11, 998–1038,
2660 <https://doi.org/10.1029/2018MS001400>, 2019.



- 2661 McGrath, M. J., Luysaert, S., Meyfroidt, P., Kaplan, J. O., Bürgi, M., Chen, Y., Erb, K., Gimmi, U., McInerney, D., Naudts,
2662 K., Otto, J., Pasztor, F., Ryder, J., Schelhaas, M.-J., and Valade, A.: Reconstructing European forest management from 1600
2663 to 2010, 12, 4291–4316, <https://doi.org/10.5194/bg-12-4291-2015>, 2015.
- 2664 McKinley, G. A., Fay, A. R., Eddebbar, Y. A., Gloege, L., and Lovenduski, N. S.: External Forcing Explains Recent
2665 Decadal Variability of the Ocean Carbon Sink, *AGU Advances*, 1, e2019AV000149,
2666 <https://doi.org/10.1029/2019AV000149>, 2020.
- 2667 McKinley, G. A., Fay, A. R., Lovenduski, N. S., and Pilcher, D. J.: Natural Variability and Anthropogenic Trends in the
2668 Ocean Carbon Sink, *Annu. Rev. Mar. Sci.*, 9, 125–150, <https://doi.org/10.1146/annurev-marine-010816-060529>, 2017.
- 2669 Meiyappan, P., Jain, A. K., and House, J. I.: Increased influence of nitrogen limitation on CO₂ emissions from future land
2670 use and land use change, *Global Biogeochem. Cycles*, 29, 1524–1548, <https://doi.org/10.1002/2015GB005086>, 2015.
- 2671 Melton, J. R., Arora, V. K., Wisernig-Cojoc, E., Seiler, C., Fortier, M., Chan, E., and Teckentrup, L.: CLASSIC v1.0: the
2672 open-source community successor to the Canadian Land Surface Scheme (CLASS) and the Canadian Terrestrial Ecosystem
2673 Model (CTEM) – Part 1: Model framework and site-level performance, *Geosci. Model Dev.*, 13, 2825–2850,
2674 <https://doi.org/10.5194/gmd-13-2825-2020>, 2020.
- 2675 Mercado, L. M., Bellouin, N., Sitch, S., Boucher, O., Huntingford, C., Wild, M., and Cox, P. M.: Impact of changes in
2676 diffuse radiation on the global land carbon sink, *Nature*, 458, 1014–1017, <https://doi.org/10.1038/nature07949>, 2009.
- 2677 Merchant, C. J., Embury, O., Bulgin, C. E., Block, T., Corlett, G. K., Fiedler, E., Good, S. A., Mittaz, J., Rayner, N. A.,
2678 Berry, D., Eastwood, S., Taylor, M., Tsushima, Y., Waterfall, A., Wilson, R., and Donlon, C.: Satellite-based time-series of
2679 sea-surface temperature since 1981 for climate applications, *Sci. Data*, 6, 223, <https://doi.org/10.1038/s41597-019-0236-x>,
2680 2019.
- 2681 Moorcroft, P. R., Hurtt, G. C., and Pacala, S. W.: A Method for Scaling Vegetation Dynamics: The Ecosystem Demography
2682 Model (ed), *Ecol. Monogr.*, 71, 557–586, [https://doi.org/10.1890/0012-9615\(2001\)071\[0557:AMFSVD\]2.0.CO;2](https://doi.org/10.1890/0012-9615(2001)071[0557:AMFSVD]2.0.CO;2), 2001.
- 2683 Müller, J. D., Gruber, N., Carter, B., Feely, R., Ishii, M., Lange, N., Lauvset, S. K., Murata, A., Olsen, A., Pérez, F. F.,
2684 Sabine, C., Tanhua, T., Wanninkhof, R., and Zhu, D.: Decadal Trends in the Oceanic Storage of Anthropogenic Carbon
2685 From 1994 to 2014, *AGU Adv.*, 4, e2023AV000875, <https://doi.org/10.1029/2023AV000875>, 2023.
- 2686 Nakano, H., Tsujino, H., Hirabara, M., Yasuda, T., Motoi, T., Ishii, M., and Yamanaka, G.: Uptake mechanism of
2687 anthropogenic CO₂ in the Kuroshio Extension region in an ocean general circulation model, *J. Oceanogr.*, 67, 765–783,
2688 <https://doi.org/10.1007/s10872-011-0075-7>, 2011.
- 2689 NCEP: National Centers for Environmental Prediction. ONI Index. Cold & Warm Episodes by Season, available at:
2690 https://origin.cpc.ncep.noaa.gov/products/analysis_monitoring/ensostuff/ONI_v5.php, last access: 27 September 2023, 2023.
- 2691 Niu, G.-Y., Yang, Z.-L., Mitchell, K. E., Chen, F., Ek, M. B., Barlage, M., Kumar, A., Manning, K., Niyogi, D., Rosero, E.,
2692 Tewari, M., and Xia, Y.: The community Noah land surface model with multiparameterization options (Noah-MP): 1. Model
2693 description and evaluation with local-scale measurements, *J. Geophys. Res. Atmospheres*, 116,
2694 <https://doi.org/10.1029/2010JD015139>, 2011.



- 2695 Niwa, Y., Ishijima, K., Ito, A., and Iida, Y.: Toward a long-term atmospheric CO₂ inversion for elucidating natural carbon
2696 fluxes: technical notes of NISMOM-CO₂ v2021.1, *Prog. Earth Planet Sci.*, 9, 42, [https://doi.org/10.1186/s40645-022-00502-](https://doi.org/10.1186/s40645-022-00502-6)
2697 6, 2022.
- 2698 Niwa, Y., Langenfelds, R., Krummel, P., Loh, Zoe, Worthy, Doug, Hatakka, Juha, Aalto, Tuula, Ramonet, Michel,
2699 Delmotte, Marc, Schmidt, Martina, Gheusi, Francois, Mihalopoulos, N., Morgui, J.A., Andrews, Arlyn, Dlugokencky, Ed,
2700 Lee, John, Sweeney, Colm, Thoning, Kirk, Tans, Pieter, De Wekker, Stephan, Fischer, Marc L., Jaffe, Dan, McKain,
2701 Kathryn, Viner, Brian, Miller, John B., Karion, Anna, Miller, Charles, Sloop, Christopher D., Saito, Kazuyuki, Aoki, Shuji,
2702 Morimoto, Shinji, Goto, Daisuke, Steinbacher, Martin, Myhre, Cathrine Lund, Hermanssen, Ove, Stephens, Britton, Keeling,
2703 Ralph, Afshar, Sara, Paplawsky, Bill, Cox, Adam, Walker, Stephen, Schuldt, Kenneth, Mukai, Hitoshi, Machida, Toshinobu,
2704 Sasakawa, Motoki, Nomura, Shohei, Ito, Akihiko, Iida, Yosuke, and Jones, Matthew W.: Long-term global CO₂ fluxes
2705 estimated by NICAM-based Inverse Simulation for Monitoring CO₂ (NISMOM-CO₂) (ver.2022.1), National Institute for
2706 Environmental Studies Japan [dataset], <https://doi.org/10.17595/20201127.001>, 2020.
- 2707 Obermeier, W. A., Nabel, J. E. M. S., Loughran, T., Hartung, K., Bastos, A., Havermann, F., Anthoni, P., Arneeth, A., Goll,
2708 D. S., Lienert, S., Lombardozzi, D., Luysaert, S., McGuire, P. C., Melton, J. R., Poulter, B., Sitch, S., Sullivan, M. O., Tian,
2709 H., Walker, A. P., Wiltshire, A. J., Zaehle, S., and Pongratz, J.: Modelled land use and land cover change emissions – a
2710 spatio-temporal comparison of different approaches, 12, 635–670, <https://doi.org/10.5194/esd-12-635-2021>, 2021.
- 2711 O'Rourke, P. R., Smith, S. J., Mott, A., Ahsan, H., McDuffie, E. E., Crippa, M., Klimont, Z., McDonald, B., Wang, S.,
2712 Nicholson, M. B., Feng, L., and Hoesly, R. M.: CEDS v_2021_04_21 Release Emission Data,
2713 <https://doi.org/10.5281/zenodo.4741285>, 2021.
- 2714 O'Sullivan, M., Zhang, Y., Bellouin, N., Harris, I., Mercado, L. M., Sitch, S., Ciais, P., and Friedlingstein, P.: Aerosol–light
2715 interactions reduce the carbon budget imbalance, *Environ. Res. Lett.*, 16, 124072, <https://doi.org/10.1088/1748-9326/ac3b77>,
2716 2021.
- 2717 O'Sullivan, M., Friedlingstein, P., Sitch, S., Anthoni, P., Arneeth, A., Arora, V. K., Bastrikov, V., Delire, C., Goll, D. S., Jain,
2718 A., Kato, E., Kennedy, D., Knauer, J., Lienert, S., Lombardozzi, D., McGuire, P. C., Melton, J. R., Nabel, J. E. M. S.,
2719 Pongratz, J., Poulter, B., Séférian, R., Tian, H., Vuichard, N., Walker, A. P., Yuan, W., Yue, X., and Zaehle, S.: Process-
2720 oriented analysis of dominant sources of uncertainty in the land carbon sink, *Nat. Commun.*, 13, 4781,
2721 <https://doi.org/10.1038/s41467-022-32416-8>, 2022.
- 2722 O'Sullivan, M., Spracklen, D. V., Batterman, S. A., Arnold, S. R., Gloor, M., and Buermann, W.: Have Synergies Between
2723 Nitrogen Deposition and Atmospheric CO₂ Driven the Recent Enhancement of the Terrestrial Carbon Sink?, *Glob.*
2724 *Biogeochem. Cycles*, 33, 163–180, <https://doi.org/10.1029/2018GB005922>, 2019.
- 2725 Palmer, P. I., Feng, L., Baker, D., Chevallier, F., Bösch, H., and Somkuti, P.: Net carbon emissions from African biosphere
2726 dominate pan-tropical atmospheric CO₂ signal, *Nat Commun*, 10, 3344, <https://doi.org/10.1038/s41467-019-11097-w>, 2019.
- 2727 Pan, Y., Birdsey, R. A., Fang, J., Houghton, R., Kauppi, P. E., Kurz, W. A., Phillips, O. L., Shvidenko, A., Lewis, S. L.,
2728 Canadell, J. G., Ciais, P., Jackson, R. B., Pacala, S. W., McGuire, A. D., Piao, S., Rautiainen, A., Sitch, S., and Hayes, D.: A
2729 Large and Persistent Carbon Sink in the World's Forests, *Science*, 333, 988–993, <https://doi.org/10.1126/science.1201609>,
2730 2011.



- 2731 Pendrill, F., Persson, U. M., Godar, J., Kastner, T., Moran, D., Schmidt, S., and Wood, R.: Agricultural and forestry trade
2732 drives large share of tropical deforestation emissions, *Global Environmental Change*, 56, 1–10,
2733 <https://doi.org/10.1016/j.gloenvcha.2019.03.002>, 2019.
- 2734 Peters, G. P., Minx, J. C., Weber, C. L., and Edenhofer, O.: Growth in emission transfers via international trade from 1990 to
2735 2008, *Proceedings of the National Academy of Sciences*, 108, 8903–8908, <https://doi.org/10.1073/pnas.1006388108>, 2011a.
- 2736 Peters, G. P., Marland, G., Le Quéré, C., Boden, T., Canadell, J. G., and Raupach, M. R.: Rapid growth in CO₂ emissions
2737 after the 2008–2009 global financial crisis, *Nature Clim Change*, 2, 2–4, <https://doi.org/10.1038/nclimate1332>, 2012a.
- 2738 Peters, G. P., Andrew, R. M., Boden, T., Canadell, J. G., Ciais, P., Le Quéré, C., Marland, G., Raupach, M. R., and Wilson,
2739 C.: The challenge to keep global warming below 2 °C, *Nature Clim Change*, 3, 4–6, <https://doi.org/10.1038/nclimate1783>,
2740 2013.
- 2741 Peters, G. P., Le Quéré, C., Andrew, R. M., Canadell, J. G., Friedlingstein, P., Ilyina, T., Jackson, R. B., Joos, F.,
2742 Korsbakken, J. I., McKinley, G. A., Sitch, S., and Tans, P.: Towards real-time verification of CO₂ emissions, *Nature Clim
2743 Change*, 7, 848–850, <https://doi.org/10.1038/s41558-017-0013-9>, 2017.
- 2744 Peters, G. P., Andrew, R. M., Canadell, J. G., Friedlingstein, P., Jackson, R. B., Korsbakken, J. I., Le Quéré, C., and
2745 Peregón, A.: Carbon dioxide emissions continue to grow amidst slowly emerging climate policies, *Nat. Clim. Chang.*, 10, 3–
2746 6, <https://doi.org/10.1038/s41558-019-0659-6>, 2020.
- 2747 Peters, W., Miller, J. B., Whitaker, J., Denning, A. S., Hirsch, A., Krol, M. C., Zupanski, D., Bruhwiler, L., and Tans, P. P.:
2748 An ensemble data assimilation system to estimate CO₂ surface fluxes from atmospheric trace gas observations, *J. Geophys.
2749 Res. Atmospheres*, 110, <https://doi.org/10.1029/2005JD006157>, 2005.
- 2750 Peters W, Woude Avd, Luijkx I, Joetzjer E, Lafont S, Loubet B, Herig-Coimbra P, Loustau D, Koren G, Ciais P, Ramonet
2751 M, Xu Y, Bastos A, Sitch S, Kneuer T, Kubistin D, De Kok R, Botía S. Temperature extremes of 2022 reduced carbon
2752 uptake by forests in Europe. doi:10.21203/rs.3.rs-2841861/v1. PPR:PPR653515, 2023.
- 2753 Petrescu, A. M. R., Peters, G. P., Janssens-Maenhout, G., Ciais, P., Tubiello, F. N., Grassi, G., Nabuurs, G.-J., Leip, A.,
2754 Carmona-García, G., Winiwarter, W., Höglund-Isaksson, L., Günther, D., Solazzo, E., Kiesow, A., Bastos, A., Pongratz, J.,
2755 Nabel, J. E. M. S., Conchedda, G., Pilli, R., Andrew, R. M., Schelhaas, M.-J., and Dolman, A. J.: European anthropogenic
2756 AFOLU greenhouse gas emissions: a review and benchmark data, *Earth Syst. Sci. Data*, 12, 961–1001,
2757 <https://doi.org/10.5194/essd-12-961-2020>, 2020.
- 2758 Pfeil, B., Olsen, A., Bakker, D. C. E., Hankin, S., Koyuk, H., Kozyr, A., Malczyk, J., Manke, A., Metzl, N., Sabine, C. L.,
2759 Akl, J., Alin, S. R., Bates, N., Bellerby, R. G. J., Borges, A., Boutin, J., Brown, P. J., Cai, W.-J., Chavez, F. P., Chen, A.,
2760 Cosca, C., Fassbender, A. J., Feely, R. A., González-Dávila, M., Goyet, C., Hales, B., Hardman-Mountford, N., Heinze, C.,
2761 Hood, M., Hoppema, M., Hunt, C. W., Hydes, D., Ishii, M., Johannessen, T., Jones, S. D., Key, R. M., Körtzinger, A.,
2762 Landschützer, P., Lauvset, S. K., Lefèvre, N., Lenton, A., Lourantou, A., Merlivat, L., Midorikawa, T., Mintrop, L.,
2763 Miyazaki, C., Murata, A., Nakadate, A., Nakano, Y., Nakaoka, S., Nojiri, Y., Omar, A. M., Padin, X. A., Park, G.-H.,
2764 Paterson, K., Perez, F. F., Pierrot, D., Poisson, A., Ríos, A. F., Santana-Casiano, J. M., Salisbury, J., Sarma, V. V. S. S.,
2765 Schlitzer, R., Schneider, B., Schuster, U., Sieger, R., Skjelvan, I., Steinhoff, T., Suzuki, T., Takahashi, T., Tedesco, K.,
2766 Telszewski, M., Thomas, H., Tilbrook, B., Tjiputra, J., Vandemark, D., Veness, T., Wanninkhof, R., Watson, A. J., Weiss,
2767 R., Wong, C. S., and Yoshikawa-Inoue, H.: A uniform, quality controlled Surface Ocean CO₂ Atlas (SOCAT), *Earth Syst.
2768 Sci. Data*, 5, 125–143, <https://doi.org/10.5194/essd-5-125-2013>, 2013.



- 2769 Piao, S., Ciais, P., Friedlingstein, P., de Noblet-Ducoudré, N., Cadule, P., Viovy, N., and Wang, T.: Spatiotemporal patterns
2770 of terrestrial carbon cycle during the 20th century, *Global Biogeochem. Cy.*, 23, GB4026,
2771 <https://doi.org/10.1029/2008GB003339>, 2009.
- 2772 Piao, S., Huang, M., Liu, Z., Wang, X., Ciais, P., Canadell, J. G., Wang, K., Bastos, A., Friedlingstein, P., Houghton, R. A.,
2773 Le Quéré, C., Liu, Y., Myneni, R. B., Peng, S., Pongratz, J., Sitch, S., Yan, T., Wang, Y., Zhu, Z., Wu, D., and Wang, T.:
2774 Lower land-use emissions responsible for increased net land carbon sink during the slow warming period, *Nature Geosci.*, 11,
2775 739–743, <https://doi.org/10.1038/s41561-018-0204-7>, 2018.
- 2776 Pongratz, J., Reick, C. H., Houghton, R. A., and House, J. I.: Terminology as a key uncertainty in net land use and land
2777 cover change carbon flux estimates, *Earth Syst. Dynam.*, 5, 177–195, <https://doi.org/10.5194/esd-5-177-2014>, 2014.
- 2778 Poulter, B., Frank, D. C., Hodson, E. L., and Zimmermann, N. E.: Impacts of land cover and climate data selection on
2779 understanding terrestrial carbon dynamics and the CO₂ airborne fraction, *Biogeosciences*, 8, 2027–2036,
2780 <https://doi.org/10.5194/bg-8-2027-2011>, 2011.
- 2781 Poulter, B., Freeborn, P. H., Jolly, W. M., and Varner, J. M.: COVID-19 lockdowns drive decline in active fires in
2782 southeastern United States, *PNAS*, 118, e2105666118, <https://doi.org/10.1073/pnas.2105666118>, 2021.
- 2783 Powis, C. M., Smith, S. M., Minx, J. C., and Gasser, T.: Quantifying global carbon dioxide removal deployment, *Environ.*
2784 *Res. Lett.*, 18, 024022, <https://doi.org/10.1088/1748-9326/acb450>, 2023.
- 2785 Prentice, I. C., Farquhar, G. D., Fasham, M. J. R., Goulden, M. L., Heimann, M., Jaramillo, V. J., Kheshgi, H. S., Le Quéré,
2786 C., Scholes, R. J., and Wallace, D. W. R.: The Carbon Cycle and Atmospheric Carbon Dioxide, in *Climate Change 2001:
2787 The Scientific Basis. Contribution of Working Group I to the Third Assessment Report of the Intergovernmental Panel on
2788 Climate Change*, edited by: Houghton, J. T., Ding, Y., Griggs, D. J., Noguer, M., van der Linden, P. J., Dai, X., Maskell, K.,
2789 and Johnson, C. A., Cambridge University Press, Cambridge, United Kingdom and New York, NY, USA, 183–237, ISBN:
2790 978-0521014953, 2001.
- 2791 Price, J. T. and Warren, R.: Literature Review of the Potential of “Blue Carbon” Activities to Reduce Emissions, available
2792 at: [https://avoid-net-uk.cc.ic.ac.uk/wp-content/uploads/delightful-downloads/2016/03/Literature-review-of-the-potential-of-
2793 blue-carbon-activities-to-reduce-emissions-AVOID2-WPE2.pdf](https://avoid-net-uk.cc.ic.ac.uk/wp-content/uploads/delightful-downloads/2016/03/Literature-review-of-the-potential-of-blue-carbon-activities-to-reduce-emissions-AVOID2-WPE2.pdf), last access: 27 September 2023, 2016.
- 2794 Qin, Y., Xiao, X., Wigneron, J.-P., Ciais, P., Brandt, M., Fan, L., Li, X., Crowell, S., Wu, X., Doughty, R., Zhang, Y., Liu,
2795 F., Sitch, S., and Moore, B.: Carbon loss from forest degradation exceeds that from deforestation in the Brazilian Amazon,
2796 *Nat. Clim. Chang.*, 11, 442–448, <https://doi.org/10.1038/s41558-021-01026-5>, 2021.
- 2797 Randerson, J. T., Chen, Y., van der Werf, G. R., Rogers, B. M., and Morton, D. C.: Global burned area and biomass burning
2798 emissions from small fires: BURNED AREA FROM SMALL FIRES, *J. Geophys. Res. Biogeosciences*, 117, n/a–n/a,
2799 <https://doi.org/10.1029/2012JG002128>, 2012.
- 2800 Raupach, M. R., Marland, G., Ciais, P., Le Quere, C., Canadell, J. G., Klepper, G., and Field, C. B.: Global and regional
2801 drivers of accelerating CO₂ emissions, *Proceedings of the National Academy of Sciences*, 104, 10288–10293,
2802 <https://doi.org/10.1073/pnas.0700609104>, 2007.
- 2803 Regnier, P., Resplandy, L., Najjar, R. G., and Ciais, P.: The land-to-ocean loops of the global carbon cycle, *Nature*, 603,
2804 401–410, <https://doi.org/10.1038/s41586-021-04339-9>, 2022.



- 2805 Reick, C. H., Gayler, V., Goll, D., Hagemann, S., Heidkamp, M., Nabel, J. E. M. S., Raddatz, T., Roeckner, E., Schnur, R.,
2806 110 and Wilkenskjeld, S.: JSBACH 3 – The land component of the MPI Earth System Model: documentation of version 3.2,
2807 available at: <https://doi.org/10.17617/2.3279802>, 2021.
- 2808 Remaud, M., Chevallier, F., Cozic, A., Lin, X., and Bousquet, P.: On the impact of recent developments of the LMDz
2809 atmospheric general circulation model on the simulation of CO₂ transport, 11, 4489, [https://doi.org/10.5194/gmd-11-4489-](https://doi.org/10.5194/gmd-11-4489-2018)
2810 2018, 2018.
- 2811 Resplandy, L., Keeling, R. F., Rödenbeck, C., Stephens, B. B., Khatiwala, S., Rodgers, K. B., Long, M. C., Bopp, L., and
2812 Tans, P. P.: Revision of global carbon fluxes based on a reassessment of oceanic and riverine carbon transport, *Nature*
2813 *Geosci.*, 11, 504–509, <https://doi.org/10.1038/s41561-018-0151-3>, 2018.
- 2814 Rodenbeck, C., Houweling, S., Gloor, M., and Heimann, M.: CO₂ flux history 1982–2001 inferred from atmospheric data
2815 using a global inversion of atmospheric transport, *Atmos Chem Phys*, 3, 1919–1964, 2003.
- 2816 Rödenbeck, C., Bakker, D. C. E., Metzl, N., Olsen, A., Sabine, C., Cassar, N., Reum, F., Keeling, R. F., and Heimann, M.:
2817 Interannual sea–air CO₂ flux variability from an observation-driven ocean mixed-layer scheme, 11, 4599–4613,
2818 <https://doi.org/10.5194/bg-11-4599-2014>, 2014.
- 2819 Rödenbeck, C., Zaehle, S., Keeling, R., and Heimann, M.: History of El Niño impacts on the global carbon cycle 1957–
2820 2017: a quantification from atmospheric CO₂ data, 373, 20170303, <https://doi.org/10.1098/rstb.2017.0303>, 2018.
- 2821 Rödenbeck, C., DeVries, T., Hauck, J., Le Quéré, C., and Keeling, R. F.: Data-based estimates of interannual sea–air CO₂
2822 flux variations 1957–2020 and their relation to environmental drivers, *Biogeosciences*, 19, 2627–2652,
2823 <https://doi.org/10.5194/bg-19-2627-2022>, 2022.
- 2824 Rosan, T. M., Klein Goldewijk, K., Ganzenmüller, R., O’Sullivan, M., Pongratz, J., Mercado, L. M., Aragao, L. E. O. C.,
2825 Heinrich, V., Randow, C. V., Wiltshire, A., Tubiello, F. N., Bastos, A., Friedlingstein, P., and Sitch, S.: A multi-data
2826 assessment of land use and land cover emissions from Brazil during 2000–2019, *Environ. Res. Lett.*, 16, 074004,
2827 <https://doi.org/10.1088/1748-9326/ac08c3>, 2021.
- 2828 Sakamoto, K., H. Nakano, S. Urakawa, T. Toyoda, Y. Kawakami, H. Tsujino, G. Yamanaka, 2023: Reference manual for the
2829 Meteorological Research Institute Community Ocean Model version 5 (MRI.COMv5), Technical Reports of the
2830 Meteorological Research Institute, No.87, <https://doi.org/10.11483/mritechrepo.87>.
- 2831 Sarma, V. V. S. S., Sridevi, B., Metzl, N., Patra, P. K., Lachkar, Z., Chakraborty, K., Goyet, C., Levy, M., Mehari, M., and
2832 Chandra, N.: Air-Sea Fluxes of CO₂ in the Indian Ocean Between 1985 and 2018: A Synthesis Based on Observation-Based
2833 Surface CO₂, Hindcast and Atmospheric Inversion Models, *Glob. Biogeochem. Cycles*, 37, e2023GB007694,
2834 <https://doi.org/10.1029/2023GB007694>, 2023.
- 2835 Schaphoff, S., von Bloh, W., Rammig, A., Thonicke, K., Biemans, H., Forkel, M., Gerten, D., Heinke, J., Jägermeyr, J.,
2836 Knauer, J., Langerwisch, F., Lucht, W., Müller, C., Rolinski, S., and Waha, K.: LPJmL4 – a dynamic global vegetation
2837 model with managed land – Part 1: Model description, *Geosci. Model Dev.*, 11, 1343–1375, [https://doi.org/10.5194/gmd-11-](https://doi.org/10.5194/gmd-11-1343-2018)
2838 1343-2018, 2018.
- 2839 Schimel, D., Alves, D., Enting, I. G., Heimann, M., Joos, F., Raynaud, D., Wigley, T., Prater, M., Derwent, R., Ehalt, D.,
2840 Fraser, P., Sanhueza, E., Zhou, X., Jonas, P., Charlson, R., Rodhe, H., Sadasivan, S., Shine, K. P., Fouquart, Y.,



- 2841 Ramaswamy, V., Solomon, S., Srinivasan, J., Albritton, D., Derwent, R., Isaksen, I., Lal, M., and Wuebbles, D.: Radiative
2842 Forcing of Climate Change, in: *Climate Change 1995: The Science of Climate Change*, Contribution of Working Group I to
2843 the Second Assessment Report of the Intergovernmental Panel on Climate Change [Houghton, J. T., Meira Rillo, L. G.,
2844 Callander, B. A., Harris, N., Kattenberg, A., and Maskell, K. (eds.)], Cambridge University Press, Cambridge, United
2845 Kingdom and New York, NY, USA, ISBN: 978-0521559621, 1995.
- 2846 Schimel, D., Stephens, B. B., and Fisher, J. B.: Effect of increasing CO₂ on the terrestrial carbon cycle, *Proc Natl Acad Sci*
2847 *USA*, 112, 436–441, <https://doi.org/10.1073/pnas.1407302112>, 2015.
- 2848 Schuh, A. E., Jacobson, A. R., Basu, S., Weir, B., Baker, D., Bowman, K., Chevallier, F., Crowell, S., Davis, K. J., Deng, F.,
2849 Denning, S., Feng, L., Jones, D., Liu, J., and Palmer, P. I.: Quantifying the Impact of Atmospheric Transport Uncertainty on
2850 CO₂ Surface Flux Estimates, *Global Biogeochem. Cycles*, 33, 484–500, <https://doi.org/10.1029/2018GB006086>, 2019.
- 2851 Schwinger, J., Goris, N., Tjiputra, J. F., Kriest, I., Bentsen, M., Bethke, I., Ilicak, M., Assmann, K. M., and Heinze, C.:
2852 Evaluation of NorESM-OC (versions 1 and 1.2), the ocean carbon-cycle stand-alone configuration of the Norwegian Earth
2853 System Model (NorESM1), *Geosci. Model Dev.*, 9, 2589–2622, <https://doi.org/10.5194/gmd-9-2589-2016>, 2016.
- 2854 Schwingshackl, C., Obermeier, W. A., Bultan, S., Grassi, G., Canadell, J. G., Friedlingstein, P., Gasser, T., Houghton, R. A.,
2855 Kurz, W. A., Sitch, S., and Pongratz, J.: Differences in land-based mitigation estimates reconciled by separating natural and
2856 land-use CO₂ fluxes at the country level, *One Earth*, 5, 1367–1376, <https://doi.org/10.1016/j.oneear.2022.11.009>, 2022.
- 2857 Séférian, R., Nabat, P., Michou, M., Saint-Martin, D., Voldoire, A., Colin, J., Decharme, B., Delire, C., Berthet, S.,
2858 Chevallier, M., Sénési, S., Franchisteguy, L., Vial, J., Mallet, M., Joetzjer, E., Geoffroy, O., Guérémy, J.-F., Moine, M.-P.,
2859 Msadek, R., Ribes, A., Rocher, M., Roehrig, R., Salas-y-Méllia, D., Sanchez, E., Terray, L., Valcke, S., Waldman, R.,
2860 Aumont, O., Bopp, L., Deshayes, J., Éthé, C., and Madec, G.: Evaluation of CNRM Earth System Model, CNRM-ESM2-1:
2861 Role of Earth System Processes in Present-Day and Future Climate, *Journal of Advances in Modeling Earth Systems*, 11,
2862 4182–4227, <https://doi.org/10.1029/2019MS001791>, 2019.
- 2863 Seiler, C., Melton, J. R., Arora, V. K., Sitch, S., Friedlingstein, P., Anthoni, P., Goll, D., Jain, A. K., Joetzjer, E., Lienert, S.,
2864 Lombardozi, D., Luyssaert, S., Nabel, J. E. M. S., Tian, H., Vuichard, N., Walker, A. P., Yuan, W., and Zaehle, S.: Are
2865 Terrestrial Biosphere Models Fit for Simulating the Global Land Carbon Sink?, *J. Adv. Model. Earth Syst.*, 14,
2866 e2021MS002946, <https://doi.org/10.1029/2021MS002946>, 2022.
- 2867 Sellar, A. A., Jones, C. G., Mulcahy, J. P., Tang, Y., Yool, A., Wiltshire, A., O'Connor, F. M., Stringer, M., Hill, R.,
2868 Palmieri, J., Woodward, S., Mora, L., Kuhlbrodt, T., Rumbold, S. T., Kelley, D. I., Ellis, R., Johnson, C. E., Walton, J.,
2869 Abraham, N. L., Andrews, M. B., Andrews, T., Archibald, A. T., Berthou, S., Burke, E., Blockley, E., Carslaw, K., Dalvi,
2870 M., Edwards, J., Folberth, G. A., Gedney, N., Griffiths, P. T., Harper, A. B., Hendry, M. A., Hewitt, A. J., Johnson, B.,
2871 Jones, A., Jones, C. D., Keeble, J., Liddicoat, S., Morgenstern, O., Parker, R. J., Predoi, V., Robertson, E., Siahhaan, A.,
2872 Smith, R. S., Swaminathan, R., Woodhouse, M. T., Zeng, G., and Zerroukat, M.: UKESM1: Description and Evaluation of
2873 the U.K. Earth System Model, *J. Adv. Model. Earth Syst.*, 11, 4513–4558, <https://doi.org/10.1029/2019MS001739>, 2019.
- 2874 Shu, S., Jain, A. K., Koven, C. D., and Mishra, U.: Estimation of Permafrost SOC Stock and Turnover Time Using a Land
2875 Surface Model With Vertical Heterogeneity of Permafrost Soils, *Global Biogeochem. Cy.*, 34, e2020GB006585,
2876 <https://doi.org/10.1029/2020GB006585>, 2020.



- 2877 Shutler, J. D., Land, P. E., Piolle, J.-F., Woolf, D. K., Goddijn-Murphy, L., Paul, F., Girard-Ardhuin, F., Chapron, B., and
2878 Donlon, C. J.: FluxEngine: A Flexible Processing System for Calculating Atmosphere–Ocean Carbon Dioxide Gas Fluxes
2879 and Climatologies, *J. Atmospheric Ocean. Technol.*, 33, 741–756, <https://doi.org/10.1175/JTECH-D-14-00204.1>, 2016.
- 2880 Sitch, S., Huntingford, C., Gedney, N., Levy, P. E., Lomas, M., Piao, S. L., Betts, R., Ciais, P., Cox, P., Friedlingstein, P.,
2881 Jones, C. D., Prentice, I. C., and Woodward, F. I.: Evaluation of the terrestrial carbon cycle, future plant geography and
2882 climate-carbon cycle feedbacks using five Dynamic Global Vegetation Models (DGVs): Uncertainty In Land Carbon
2883 Cycle Feedbacks, *Glob. Change Biol.*, 14, 2015–2039, <https://doi.org/10.1111/j.1365-2486.2008.01626.x>, 2008.
- 2884 Smallman, T. L., Milodowski, D. T., Neto, E. S., Koren, G., Ometto, J., and Williams, M.: Parameter uncertainty dominates
2885 C-cycle forecast errors over most of Brazil for the 21st century, *Earth Syst. Dyn.*, 12, 1191–1237,
2886 <https://doi.org/10.5194/esd-12-1191-2021>, 2021.
- 2887 Smith, B., Wårlind, D., Arneth, A., Hickler, T., Leadley, P., Siltberg, J., and Zaehle, S.: Implications of incorporating N
2888 cycling and N limitations on primary production in an individual-based dynamic vegetation model, *Biogeosciences*, 11,
2889 2027–2054, <https://doi.org/10.5194/bg-11-2027-2014>, 2014.
- 2890 Smith, S., Geden, O., Nemet, G., Gidden, M., Lamb, W., Powis, C., Bellamy, R., Callaghan, M., Cowie, A., Cox, E. and
2891 Fuss, S., 2023. The State of Carbon Dioxide Removal—1st Edition, <http://dx.doi.org/10.17605/OSF.IO/W3B4Z>, 2023.
- 2892 Sospedra-Alfonso, R., Merryfield, W. J., Boer, G. J., Kharin, V. V., Lee, W.-S., Seiler, C., and Christian, J. R.: Decadal
2893 climate predictions with the Canadian Earth System Model version 5 (CanESM5), *Geosci. Model Dev.*, 14, 6863–6891,
2894 <https://doi.org/10.5194/gmd-14-6863-2021>, 2021.
- 2895 Stephens, B. B., Gurney, K. R., Tans, P. P., Sweeney, C., Peters, W., Bruhwiler, L., Ciais, P., Ramonet, M., Bousquet, P.,
2896 Nakazawa, T., Aoki, S., Machida, T., Inoue, G., Vinnichenko, N., Lloyd, J., Jordan, A., Heimann, M., Shibistova, O.,
2897 Langenfelds, R. L., Steele, L. P., Francey, R. J., and Denning, A. S.: Weak Northern and Strong Tropical Land Carbon
2898 Uptake from Vertical Profiles of Atmospheric CO₂, *Science*, 316, 1732–1735, <https://doi.org/10.1126/science.1137004>,
2899 2007.
- 2900 Stephens, B. B., Keeling, R. F., Heimann, M., Six, K. D., Murnane, R., and Caldeira, K.: Testing global ocean carbon cycle
2901 models using measurements of atmospheric O₂ and CO₂ concentration, *Glob. Biogeochem. Cycles*, 12, 213–230,
2902 <https://doi.org/10.1029/97GB03500>, 1998.
- 2903 Stocker, T., Qin, D., and Platner, G.-K.: Climate Change 2013: The Physical Science Basis. Contribution of Working Group
2904 I to the Fifth Assessment Report of the Intergovernmental Panel on Climate Change [Intergovernmental Panel on Climate
2905 Change (eds.)], Cambridge University Press, Cambridge, ISBN: 9789291691388, 2013.
- 2906 Swart, N. C., Cole, J. N. S., Kharin, V. V., Lazare, M., Scinocca, J. F., Gillett, N. P., Anstey, J., Arora, V., Christian, J. R.,
2907 Hanna, S., Jiao, Y., Lee, W. G., Majaess, F., Saenko, O. A., Seiler, C., Seinen, C., Shao, A., Sigmond, M., Solheim, L., von
2908 Salzen, K., Yang, D., and Winter, B.: The Canadian Earth System Model version 5 (CanESM5.0.3), *Geosci. Model Dev.*, 12,
2909 4823–4873, <https://doi.org/10.5194/gmd-12-4823-2019>, 2019.
- 2910 SX Coal: Monthly coal consumption estimates, <http://www.sxcoal.com/>, last access: 27 September 2023, 2022.
- 2911 Takahashi, T., Sutherland, S. C., Wanninkhof, R., Sweeney, C., Feely, R. A., Chipman, D. W., Hales, B., Friederich, G.,
2912 Chavez, F., Sabine, C., Watson, A., Bakker, D. C. E., Schuster, U., Metzl, N., Yoshikawa-Inoue, H., Ishii, M., Midorikawa,



- 2913 T., Nojiri, Y., Körtzinger, A., Steinhoff, T., Hoppema, M., Olafsson, J., Arnarson, T. S., Tilbrook, B., Johannessen, T.,
2914 Olsen, A., Bellerby, R., Wong, C. S., Delille, B., Bates, N. R., and de Baar, H. J. W.: Climatological mean and decadal
2915 change in surface ocean pCO₂, and net sea–air CO₂ flux over the global oceans, *Deep Sea Research Part II: Topical Studies*
2916 in *Oceanography*, 56, 554–577, <https://doi.org/10.1016/j.dsr2.2008.12.009>, 2009.
- 2917 Terhaar, J., Frölicher, T. L., and Joos, F.: Southern Ocean anthropogenic carbon sink constrained by sea surface salinity, *Sci.*
2918 *Adv.*, 7, eabd5964, <https://doi.org/10.1126/sciadv.abd5964>, 2021.
- 2919 Terhaar, J., Frölicher, T. L., and Joos, F.: Observation-constrained estimates of the global ocean carbon sink from Earth
2920 system models, *Biogeosciences*, 19, 4431–4457, <https://doi.org/10.5194/bg-19-4431-2022>, 2022.
- 2921 Tian, H., Xu, X., Lu, C., Liu, M., Ren, W., Chen, G., Melillo, J., and Liu, J.: Net exchanges of CO₂, CH₄, and N₂O between
2922 China’s terrestrial ecosystems and the atmosphere and their contributions to global climate warming, *J. Geophys. Res.*
2923 *Biogeosciences*, 116, G02011, <https://doi.org/10.1029/2010JG001393>, 2011.
- 2924 Tian, H., Chen, G., Lu, C., Xu, X., Hayes, D. J., Ren, W., Pan, S., Huntzinger, D. N., and Wofsy, S. C.: North American
2925 terrestrial CO₂ uptake largely offset by CH₄ and N₂O emissions: toward a full accounting of the greenhouse gas budget,
2926 *Climatic Change*, 129, 413–426, <https://doi.org/10.1007/s10584-014-1072-9>, 2015.
- 2927 Tubiello, F. N., Conchedda, G., Wanner, N., Federici, S., Rossi, S., and Grassi, G.: Carbon emissions and removals from
2928 forests: new estimates, 1990–2020, *Earth Syst. Sci. Data*, 13, 1681–1691, <https://doi.org/10.5194/essd-13-1681-2021>, 2021.
- 2929 Tuck, C.: 2022 Mineral Commodity Summary: Iron Ore, Tech. rep., U.S. Geological Survey,
2930 <https://pubs.usgs.gov/periodicals/mcs2022/mcs2022-iron-ore.pdf>, 2022.
- 2931 UNFCCC: Synthesis report for the technical assessment component of the first global stocktake, available at:
2932 <https://unfccc.int/documents/461466>, last access: 27 September 2023, 2022
- 2933 Urakawa, L. S., Tsujino, H., Nakano, H., Sakamoto, K., Yamanaka, G., and Toyoda, T.: The sensitivity of a depth-
2934 coordinate model to diapycnal mixing induced by practical implementations of the isopycnal tracer diffusion scheme, *Ocean*
2935 *Model.*, 154, 101693, <https://doi.org/10.1016/j.ocemod.2020.101693>, 2020.
- 2936 Vale, M. M., Berenguer, E., Argollo de Menezes, M., Viveiros de Castro, E. B., Pugliese de Siqueira, L., and Portela, R. de
2937 C. Q.: The COVID-19 pandemic as an opportunity to weaken environmental protection in Brazil, *Biological Conservation*,
2938 255, 108994, <https://doi.org/10.1016/j.biocon.2021.108994>, 2021.
- 2939 van der Laan-Luijkx, I. T., van der Velde, I. R., van der Veen, E., Tsuruta, A., Stanislawski, K., Babenhausserheide, A.,
2940 Zhang, H. F., Liu, Y., He, W., Chen, H., Masarie, K. A., Krol, M. C., and Peters, W.: The CarbonTracker Data Assimilation
2941 Shell (CTDAS) v1.0: implementation and global carbon balance 2001–2015, *Geosci. Model Dev.*, 10, 2785–2800,
2942 <https://doi.org/10.5194/gmd-10-2785-2017>, 2017.
- 2943 van der Velde, I. R., van der Werf, G. R., Houweling, S., Maasackers, J. D., Borsdorff, T., Landgraf, J., Tol, P., van
2944 Kempen, T. A., van Hees, R., Hoogeveen, R., Veefkind, J. P., and Aben, I.: Vast CO₂ release from Australian fires in 2019–
2945 2020 constrained by satellite, *Nature*, 597, 366–369, <https://doi.org/10.1038/s41586-021-03712-y>, 2021.
- 2946 van der Werf, G. R., Randerson, J. T., Giglio, L., Collatz, G. J., Mu, M., Kasibhatla, P. S., Morton, D. C., DeFries, R. S., Jin,
2947 Y., and van Leeuwen, T. T.: Global fire emissions and the contribution of deforestation, savanna, forest, agricultural, and
2948 peat fires (1997–2009), *Atmospheric Chem. Phys.*, 10, 11707–11735, <https://doi.org/10.5194/acp-10-11707-2010>, 2010.



- 2949 van der Werf, G. R., Randerson, J. T., Giglio, L., van Leeuwen, T. T., Chen, Y., Rogers, B. M., Mu, M., van Marle, M. J. E.,
2950 Morton, D. C., Collatz, G. J., Yokelson, R. J., and Kasibhatla, P. S.: Global fire emissions estimates during 1997–2016,
2951 *Earth Syst. Sci. Data*, 9, 697–720, <https://doi.org/10.5194/essd-9-697-2017>, 2017.
- 2952 van Wees, D., van der Werf, G. R., Randerson, J. T., Andela, N., Chen, Y., and Morton, D. C.: The role of fire in global
2953 forest loss dynamics, *Glob. Change Biol.*, 27, 2377–2391, <https://doi.org/10.1111/gcb.15591>, 2021.
- 2954 von Bloh, W., Schaphoff, S., Müller, C., Rolinski, S., Waha, K., and Zaehle, S.: Implementing the nitrogen cycle into the
2955 dynamic global vegetation, hydrology, and crop growth model LPJmL (version 5.0), *Geosci. Model Dev.*, 11, 2789–2812,
2956 <https://doi.org/10.5194/gmd-11-2789-2018>, 2018.
- 2957 Vaittinada Ayar, P., Bopp, L., Christian, J. R., Ilyina, T., Krasting, J. P., Séférian, R., Tsujino, H., Watanabe, M., Yool, A.,
2958 and Tjiputra, J.: Contrasting projections of the ENSO-driven CO₂ flux variability in the equatorial Pacific under high-
2959 warming scenario, *Earth Syst. Dynam.*, 13, 1097–1118, <https://doi.org/10.5194/esd-13-1097-2022>, 2022.
- 2960 Vuichard, N., Messina, P., Luysaert, S., Guenet, B., Zaehle, S., Ghattas, J., Bastrikov, V., and Peylin, P.: Accounting for
2961 carbon and nitrogen interactions in the global terrestrial ecosystem model ORCHIDEE (trunk version, rev 4999): multi-scale
2962 evaluation of gross primary production, *Geosci. Model Dev.*, 12, 4751–4779, <https://doi.org/10.5194/gmd-12-4751-2019>,
2963 2019.
- 2964 Walker, A. P., Quaife, T., Bodegom, P. M., De Kauwe, M. G., Keenan, T. F., Joiner, J., Lomas, M. R., MacBean, N., Xu, C.,
2965 Yang, X., and Woodward, F. I.: The impact of alternative trait-scaling hypotheses for the maximum photosynthetic
2966 carboxylation rate (V_{cmax}) on global gross primary production, *New Phytol.*, 215, 1370–1386,
2967 <https://doi.org/10.1111/nph.14623>, 2017.
- 2968 Walker, A. P., De Kauwe, M. G., Bastos, A., Belmecheri, S., Georgiou, K., Keeling, R. F., McMahon, S. M., Medlyn, B. E.,
2969 Moore, D. J. P., Norby, R. J., Zaehle, S., Anderson-Teixeira, K. J., Battipaglia, G., Brienen, R. J. W., Cabugao, K. G.,
2970 Cailleret, M., Campbell, E., Canadell, J. G., Ciais, P., Craig, M. E., Ellsworth, D. S., Farquhar, G. D., Fatichi, S., Fisher, J.
2971 B., Frank, D. C., Graven, H., Gu, L., Haverd, V., Heilman, K., Heimann, M., Hungate, B. A., Iversen, C. M., Joos, F., Jiang,
2972 M., Keenan, T. F., Knauer, J., Körner, C., Leshyk, V. O., Leuzinger, S., Liu, Y., MacBean, N., Malhi, Y., McVicar, T. R.,
2973 Penuelas, J., Pongratz, J., Powell, A. S., Riutta, T., Sabot, M. E. B., Schleucher, J., Sitoh, S., Smith, W. K., Sulman, B.,
2974 Taylor, B., Terrer, C., Torn, M. S., Treseder, K. K., Trugman, A. T., Trumbore, S. E., van Mantgem, P. J., Voelker, S. L.,
2975 Whelan, M. E., and Zuidema, P. A.: Integrating the evidence for a terrestrial carbon sink caused by increasing atmospheric
2976 CO₂, *New Phytol.*, 229, 2413–2445, <https://doi.org/10.1111/nph.16866>, 2021.
- 2977 Watanabe, M., Tatebe, H., Koyama, H., Hajima, T., Watanabe, M., and Kawamiya, M.: Importance of El Niño
2978 reproducibility for reconstructing historical CO₂ flux variations in the equatorial Pacific, *Ocean Sci.*, 16, 1431–1442,
2979 <https://doi.org/10.5194/os-16-1431-2020>, 2020.
- 2980 Watson, A. J., Schuster, U., Shutler, J. D., Holding, T., Ashton, I. G. C., Landschützer, P., Woolf, D. K., and Goddijn-
2981 Murphy, L.: Revised estimates of ocean-atmosphere CO₂ flux are consistent with ocean carbon inventory, *Nat Commun*, 11,
2982 4422, <https://doi.org/10.1038/s41467-020-18203-3>, 2020.
- 2983 Watson, R. T., Rohde, H., Oeschger, H., and Siegenthaler, U.: Greenhouse Gases and Aerosols, in: *Climate Change: The*
2984 *IPCC Scientific Assessment. Intergovernmental Panel on Climate Change (IPCC)*, edited by: Houghton, J. T., Jenkins, G. J.,
2985 and Ephraums, J. J., Cambridge University Press, Cambridge, ISBN: 978-0521403603, 1990.



- 2986 Wenzel, S., Cox, P. M., Eyring, V., and Friedlingstein, P.: Projected land photosynthesis constrained by changes in the
2987 seasonal cycle of atmospheric CO₂, *Nature*, 538, 499–501, <https://doi.org/10.1038/nature19772>, 2016.
- 2988 Wilkenskjeld, S., Kloster, S., Pongratz, J., Raddatz, T., and Reick, C. H.: Comparing the influence of net and gross
2989 anthropogenic land-use and land-cover changes on the carbon cycle in the MPI-ESM, *Biogeosciences*, 11, 4817–4828,
2990 <https://doi.org/10.5194/bg-11-4817-2014>, 2014.
- 2991 Wiltshire, A. J., Burke, E. J., Chadburn, S. E., Jones, C. D., Cox, P. M., Davies-Barnard, T., Friedlingstein, P., Harper, A. B.,
2992 Liddicoat, S., Sitch, S., and Zaehle, S.: JULES-CN: a coupled terrestrial carbon–nitrogen scheme (JULES vn5.1), 14, 2161–
2993 2186, <https://doi.org/10.5194/gmd-14-2161-2021>, 2021.
- 2994 Winkler, K., Yang, H., Ganzenmüller, R., Fuchs, R., Ceccherini, G., Duveiller, G., Grassi, G., Pongratz, J., Bastos, A.,
2995 Shvidenko, A., Araza, A., Herold, M., Wigneron, J.-P., and Ciais, P.: Changes in land use and management led to a decline
2996 in Eastern Europe’s terrestrial carbon sink, *Commun. Earth Environ.*, 4, 1–14, <https://doi.org/10.1038/s43247-023-00893-4>,
2997 2023.
- 2998 Woodward, F. I. and Lomas, M. R.: Vegetation dynamics – simulating responses to climatic change, *Biol. Rev.*, 79, 643–
2999 670, <https://doi.org/10.1017/S1464793103006419>, 2004.
- 3000 Wright, R. M., Le Quéré, C., Buitenhuis, E., Pitois, S., and Gibbons, M. J.: Role of jellyfish in the plankton ecosystem
3001 revealed using a global ocean biogeochemical model, 18, 1291–1320, <https://doi.org/10.5194/bg-18-1291-2021>, 2021.
- 3002 Wunder, S., Kaimowitz, D., Jensen, S., and Feder, S.: Coronavirus, macroeconomy, and forests: What likely impacts?, *For.*
3003 *Policy Econ.*, 131, 102536, <https://doi.org/10.1016/j.forpol.2021.102536>, 2021.
- 3004 Xi, F., Davis, S. J., Ciais, P., Crawford-Brown, D., Guan, D., Pade, C., Shi, T., Syddall, M., Lv, J., Ji, L., Bing, L., Wang, J.,
3005 Wei, W., Yang, K.-H., Lagerblad, B., Galan, I., Andrade, C., Zhang, Y., and Liu, Z.: Substantial global carbon uptake by
3006 cement carbonation, *Nature Geosci*, 9, 880–883, <https://doi.org/10.1038/ngeo2840>, 2016.
- 3007 Xia, J., Chen, Y., Liang, S., Liu, D., and Yuan, W.: Global simulations of carbon allocation coefficients for deciduous
3008 vegetation types, *Tellus B*, 67, 28016, <https://doi.org/10.3402/tellusb.v67.28016>, 2015.
- 3009 Yang, D., Liu, Y., Feng, L., Wang, J., Yao, L., Cai, Z., Zhu, S., Lu, N., and Lyu, D.: The First Global Carbon Dioxide Flux
3010 Map Derived from TanSat Measurements, *Adv. Atmospheric Sci.*, 38, 1433–1443, <https://doi.org/10.1007/s00376-021-1179-7>, 2021.
- 3012 Yang, X., Thornton, P., Ricciuto, D., Wang, Y., and Hoffman, F.: Global evaluation of terrestrial biogeochemistry in the
3013 Energy Exascale Earth System Model (E3SM) and the role of the phosphorus cycle in the historical terrestrial carbon
3014 balance, *Biogeosciences*, 20, 2813–2836, <https://doi.org/10.5194/bg-20-2813-2023>, 2023.
- 3015 Yu, Z., Ciais, P., Piao, S., Houghton, R. A., Lu, C., Tian, H., Agathokleous, E., Kattel, G. R., Sitch, S., Goll, D., Yue, X.,
3016 Walker, A., Friedlingstein, P., Jain, A. K., Liu, S., and Zhou, G.: Forest expansion dominates China’s land carbon sink since
3017 1980, *Nat. Commun.*, 13, 5374, <https://doi.org/10.1038/s41467-022-32961-2>, 2022.
- 3018 Yue, X. and Unger, N.: The Yale Interactive terrestrial Biosphere model version 1.0: description, evaluation and
3019 implementation into NASA GISS ModelE2, *Geosci. Model Dev.*, 8, 2399–2417, <https://doi.org/10.5194/gmd-8-2399-2015>,
3020 2015.



- 3021 Yuan, W., Liu, D., Dong, W., Liu, S., Zhou, G., Yu, G., Zhao, T., Feng, J., Ma, Z., Chen, J., Chen, Y., Chen, S., Han, S.,
3022 Huang, J., Li, L., Liu, H., Liu, S., Ma, M., Wang, Y., Xia, J., Xu, W., Zhang, Q., Zhao, X., and Zhao, L.: Multiyear
3023 precipitation reduction strongly decreases carbon uptake over northern China, *J. Geophys. Res.-Biogeo.*, 119, 881–896,
3024 <https://doi.org/10.1002/2014JG002608>, 2014.
- 3025 Yue, C., Ciais, P., Zhu, D., Wang, T., Peng, S. S., and Piao, S. L.: How have past fire disturbances contributed to the current
3026 carbon balance of boreal ecosystems?, *Biogeosciences*, 13, 675–690, <https://doi.org/10.5194/bg-13-675-2016>, 2016.
- 3027 Zaehle, S. and Friend, A. D.: Carbon and nitrogen cycle dynamics in the O-CN land surface model: 1. Model description,
3028 site-scale evaluation, and sensitivity to parameter estimates: Site-scale evaluation of a C-N model, *Global Biogeochem.*
3029 *Cycles*, 24, GB1005, <https://doi.org/10.1029/2009GB003521>, 2010.
- 3030 Zaehle, S., Ciais, P., Friend, A. D., and Prieur, V.: Carbon benefits of anthropogenic reactive nitrogen offset by nitrous oxide
3031 emissions, *Nature Geosci.*, 4, 601–605, <https://doi.org/10.1038/ngeo1207>, 2011.
- 3032 Zaehle, S., Medlyn, B. E., De Kauwe, M. G., Walker, A. P., Dietze, M. C., Hickler, T., Luo, Y., Wang, Y.-P., El-Masri, B.,
3033 Thornton, P., Jain, A., Wang, S., Warlind, D., Weng, E., Parton, W., Iversen, C. M., Gallet-Budynek, A., McCarthy, H.,
3034 Finzi, A., Hanson, P. J., Prentice, I. C., Oren, R., and Norby, R. J.: Evaluation of 11 terrestrial carbon–nitrogen cycle models
3035 against observations from two temperate Free-Air CO₂ Enrichment studies, *New Phytol.*, 202, 803–822,
3036 <https://doi.org/10.1111/nph.12697>, 2014.
- 3037 Zeng, J., Iida, Y., Matsunaga, T., and Shirai, T.: Surface ocean CO₂ concentration and air-sea flux estimate by machine
3038 learning with modelled variable trends, *Front. Mar. Sci.*, 9, <https://doi.org/10.3389/fmars.2022.989233>, 2022.
- 3039 Zheng, B., Ciais, P., Chevallier, F., Chuvieco, E., Chen, Y., and Yang, H.: Increasing forest fire emissions despite the
3040 decline in global burned area, *Sci. Adv.*, 7, eabh2646, <https://doi.org/10.1126/sciadv.abh2646>, 2021.
- 3041 Zou, Y., Wang, Y., Ke, Z., Tian, H., Yang, J., and Liu, Y.: Development of a REgion-Specific Ecosystem Feedback Fire
3042 (RESFire) Model in the Community Earth System Model, *J. Adv. Model. Earth Syst.*, 11, 417–445,
3043 <https://doi.org/10.1029/2018MS001368>, 2019.
- 3044 Zscheischler, J., Mahecha, M. D., Avitabile, V., Calle, L., Carvalhais, N., Ciais, P., Gans, F., Gruber, N., Hartmann, J.,
3045 Herold, M., Ichii, K., Jung, M., Landschützer, P., Laruelle, G. G., Lauerwald, R., Papale, D., Peylin, P., Poulter, B., Ray, D.,
3046 Regnier, P., Rödenbeck, C., Roman-Cuesta, R. M., Schwalm, C., Tramontana, G., Tyukavina, A., Valentini, R., van der
3047 Werf, G., West, T. O., Wolf, J. E., and Reichstein, M.: Reviews and syntheses: An empirical spatiotemporal description of
3048 the global surface–atmosphere carbon fluxes: opportunities and data limitations, *Biogeosciences*, 14, 3685–3703,
3049 <https://doi.org/10.5194/bg-14-3685-2017>.
- 3050
- 3051



3052 **Tables**

3053

3054

Unit 1	Unit 2	Conversion	Source
GtC (gigatonnes of carbon)	ppm (parts per million) (a)	2.124 (b)	Ballantyne et al. (2012)
GtC (gigatonnes of carbon)	PgC (petagrams of carbon)		1 SI unit conversion
GtCO ₂ (gigatonnes of carbon dioxide)	GtC (gigatonnes of carbon)	3.664	44.01/12.011 in mass equivalent
GtC (gigatonnes of carbon)	MtC (megatonnes of carbon)	1000	SI unit conversion
(a) Measurements of atmospheric CO ₂ concentration have units of dry-air mole fraction. ‘ppm’ is an abbreviation for micromole/mol, dry air.			
(b) The use of a factor of 2.124 assumes that all the atmosphere is well mixed within one year. In reality, only the troposphere is well mixed and the growth rate of CO ₂ concentration in the less well-mixed stratosphere is not measured by sites from the NOAA network. Using a factor of 2.124 makes the approximation that the growth rate of CO ₂ concentration in the stratosphere equals that of the troposphere on a yearly basis.			

3055 **Table 1.** Factors used to convert carbon in various units (by convention, Unit 1 = Unit 2 × conversion).

3056

3057



3058

Component	Primary reference
Global fossil CO ₂ emissions (EFOS), total and by fuel type	Updated from Andrew and Peters (2022)
National territorial fossil CO ₂ emissions (EFOS)	Gilfillan and Marland (2021), UNFCCC (2022)
National consumption-based fossil CO ₂ emissions (EFOS) by country (consumption)	Peters et al. (2011a) updated as described in this paper
Net land-use change flux (ELUC)	This paper (see Table 4 for individual model references).
Growth rate in atmospheric CO ₂ concentration (GATM)	Lan et al. (2023)
Ocean and land CO ₂ sinks (SOCEAN and SLAND)	This paper (see Table 4 for individual model and data products references).

3059

3060

3061

Table 2. How to cite the individual components of the global carbon budget presented here.



3062

Publication year	Fossil fuel emissions		LUC emissions	Reservoirs			Other changes
	Global	Country (territorial)		Atmosphere	Ocean	Land	
2019	Global emissions calculated as sum of all countries plus bunkers, rather than taken directly from CDIAC.		Average of two bookkeeping models; use of 15 DGVMs	Use of three atmospheric inversions	Based on nine models	Based on 16 models	
Friedlingstein et al. (2019) GCB2019							
2020	Cement carbonation now included in the EFOS estimate, reducing EFOS by about 0.2GtC yr-1 for the last decade	India's emissions from Andrew (2020: India); Corrections to Netherland Antilles and Aruba and Soviet emissions before 1950 as per Andrew (2020: CO2); China's coal emissions in 2019 derived from official statistics, emissions now shown for EU27 instead of EU28. Projection for 2020 based on assessment of four approaches.	Average of three bookkeeping models; use of 17 DGVMs. Estimate of gross land use sources and sinks provided	Use of six atmospheric inversions	Based on nine models. River flux revised and partitioned NH, Tropics, SH	Based on 17 models	
Friedlingstein et al. (2020) GCB2020							
2021	Projections are no longer an assessment of four approaches.	Official data included for a number of additional countries, new estimates for South Korea, added emissions from lime	ELUC estimate compared to the estimates adopted in national GHG inventories (NGHGI)		Average of means of eight models and means of seven data-products. Current year prediction of SOCEAN using a feed-forward	Current year prediction of SLAND using a feed-forward neural network method	
Friedlingstein et al. (2022a) GCB2021							



		production in China.			neural network method		
2022			ELUC provided at country level. Revised components decomposition of ELUC fluxes. Revision of LUC maps for Brazil. New datasets for peat drainage.		Average of means of ten models and means of seven data-products	Based on 16 models. Revision of LUC maps for Brazil.	
Friedlingstein et al. (2022) GCB2022				Use of nine atmospheric inversions			
2023			Refined components decomposition of ELUC. Revision of LUC maps for Indonesia. Use of updated peat drainage estimates.	Use of 14 atmospheric inversions. Additional use of 4 Earth System Models to estimate current year CO2	Additional use of 4 Earth System Models and atmospheric oxygen method to assess SOCEAN. Regional distribution of river flux adjustment revised.	Based on 20 models. Additional use of 4 Earth System Models and atmospheric oxygen method to assess the net atmosphere-land flux.	Inclusion of an estimate of Carbon Dioxide Removal (CDR)
This study							

3063 **Table 3.** Main methodological changes in the global carbon budget since 2019. Methodological changes
 3064 introduced in one year are kept for the following years unless noted. Empty cells mean there were no
 3065 methodological changes introduced that year. Table S8 lists methodological changes from the first global carbon
 3066 budget publication up to 2018.

3067

3068



3069

Model/data name	Reference	Change from Global Carbon Budget 2022 (Friedlingstein et al., 2022b)
<i>Bookkeeping models for land-use change emissions</i>		
BLUE	Hansis et al. (2015)	No change to model, but simulations performed with LUH2-GCB2023 forcing. Update in added peat drainage emissions.
H&C2023	Houghton and Castanho (2023)	H&C2023 replaces the formerly used H&N2017 model. Minor bug fix in fuel harvest estimates. Update in added peat drainage emissions.
OSCAR	Gasser et al. (2020)	No change to model, but land-use forcing changed to LUH2-GCB2023 and FRA2020 (extrapolated to 2022). Constraining based on GCB2022 data for SLAND over 1960-2021. Update in added peat drainage emissions.
<i>Dynamic global vegetation models</i>		
CABLE-POP	Haverd et al. (2018)	Improved representation of nitrogen retranslocation and plant uptake, minor bug fixes, parameter changes
CLASSIC	Melton et al. (2020), Asaadi et al. (2018)	Bug fixes, correct allocation of leaves after summer solstice for latitudes higher than 45°N, improved phenology for several PFTs
CLM5.0	Lawrence et al. (2019)	No change.
DLEM	Tian et al. (2011, 2015)	No change.
EDv3	Moorcroft et al. (2001), Ma et al. (2022)	New this year.
ELM	Yang et al.(2023), Burrows et al.(2020)	New this year.
IBIS	Yuan et al. (2014)	Changes in parameterisation and new module of soil nitrogen dynamics (Ma et al., 2022)
ISAM	Jain et al. (2013), Meiyappan et al. (2015), Shu et al. (2020)	Vertically resolved soil biogeochemistry (carbon and nitrogen) module, following Shu et al. (2020),
ISBA-CTRIP	Delire et al. (2020)	No change.
JSBACH	Mauritsen et al. (2019), Reick et al. (2021)	No change.
JULES-ES	Wiltshire et al. (2021), Sellar et al. (2019), Burton et al. (2019)	Minor bug fixes. (Using JULES v6.3, suite u-co002)
LPJ-GUESS	Smith et al. (2014)	Minor bug fixes.



LPJml	Schaphoff et al., 2018, von Bloh et al., 2018, Lutz et al., 2019 (tillage), Heinke et al., 2023 (livestock grazing)	New this year.
LPJwsl	Poulter et al. (2011) (d)	No change.
LPX-Bern	Lienert and Joos (2018)	No change.
OCN	Zaehle and Friend (2010), Zaehle et al. (2011)	Minor bug fixes
ORCHIDEEv3	Krinner et al. (2005), Zaehle and Friend (2010), Vuichard et al. (2019)	Small update for leaf senescence (ORCHIDEE - V3; revision 8119)
SDGVM	Woodward and Lomas (2004), Walker et al. (2017)	implement gross land-use transitions, to track carbon from wood & crop harvest, and to track primary & secondary vegetation.
VISIT	Ito and Inatomi (2012), Kato et al. (2013)	No change.
YIBs	Yue and Unger (2015)	Inclusion of process-based water cycle from Noah-MP (Niu et al., 2011)
Intermediate complexity land carbon cycle model		
CARDAMOM	Bloom et al. (2016), Smallman et al. (2021)	New this year
Global ocean biogeochemistry models		
NEMO3.6-PISCESv2-gas (CNRM)	Berthet et al. (2019), Séférian et al. (2019)	No change.
FESOM-2.1-REcoM2	Gürses et al. (2023)	No change
NEMO-PISCES (IPSL)	Aumont et al. (2015)	No change.
MOM6-COBALT (Princeton)	Liao et al. (2020)	No change
MRI-ESM2-2	Nakano et al. (2011)	The ocean model has been updated to MRI.COMv5 (Sakamoto et al. 2023). The distribution of background vertical diffusivity is changed to the one proposed by Kawasaki et al. (2021). Model was spun-up with a preindustrial xCO ₂ of 278 ppm.
MICOM-HAMOCC (NorESM-OCv1.2)	Schwinger et al. (2016)	No change.
NEMO-PlankTOM12	Wright et al. (2021)	Minor bug fixes, switch to ERA5 forcing, salinity restoring
CESM-ETHZ	Doney et al. (2009)	Model was spun-up with a preindustrial xCO ₂ of 278 ppm.



MPIOM-HAMOCC6	Lacroix et al. (2021)	No change.
ACCESS (CSIRO)	Law et al. (2017)	Minor bug fixes, extended spinup since last participation 2020.
fCO₂-products		
CMEMS-LSCE-FFNNv2	Chau et al. (2022)	Update to SOCATv2023 measurements and time period 1985-2022. The mapping approach by Chau et al (2022) has been upgraded by increasing spatial resolution from 1° to 0.25°.
JMA-MLR	Iida et al. (2021)	Updated to SOCATv2023
LDEO-HPD	Gloege et al. (2022), Bennington et al. (2022)	Updated with SOCATv2023. Updated with current GCB2023 models and extending back in time using Bennington et al. (2022) method.
MPI-SOMFFN	Landschützer et al. (2016)	update to SOCATv2023. Since GCB2022, fluxes cover open ocean and coastal domains as well as the Arctic Ocean extension.
NIES-ML3	Zeng et al. (2022)	New this year
OS-ETHZ-GRaCER	Gregor et al. (2021)	Updated to SOCATv2023
Jena-MLS	Rödenbeck et al. (2014, 2022)	update to SOCATv2023 measurements, time period extended to 1957-2022
UOEx-Watson	Watson et al. (2020)	Updated to SOCAT v2023. fCO ₂ (sw) corrected to CCI SST v2.1 (Merchant et al. 2019) instead of OI SST v2.1. Updated interpolation datasets to CCI SST v2.1, CMEMS SSS and MLD (Jean-Michel et al. 2021). Monthly cool skin difference calculated using NOAA COARE 3.5 (Edson et al. 2013). CO ₂ flux computed using FluxEngine (Holding et al., 2019; Shutler et al., 2016).
Atmospheric inversions		
Jena CarboScope	Rödenbeck et al. (2003, 2018)	Extension to 2022, re-addition of a 2.5-year relaxation term.
CAMS	Chevallier et al. (2005), Remaud et al. (2018)	Increase of the 3D resolution (4.5 times more 3D cells than the previous submission); extension to year 2022; update of the prior fluxes.
CarbonTracker Europe (CTE)	van der Laan-Luijkx et al. (2017)	Extension to 2022, update of prior fluxes.
NISMOM-CO ₂	Niwa et al. (2020, 2022)	Prior terrestrial fluxes include minor fluxes (BVOC and CH ₄) in addition to GPP, RE and LUC.
CT-NOAA	Peters et al. (2005), Jacobson et al. (2023a, 2023b)	New this year.
CMS-Flux	Liu et al. (2021)	Update of OCO-2 observations and prior fluxes.



CAMS-Satellite	Chevallier et al. (2005), Remaud et al. (2018)	Increase of the 3D resolution, extension to year 2022 and the first months of 2023; removal of the pre-OCO-2 period (2010-2014 with GOSAT); update of the prior fluxes.
GONGGA	Jin et al. (2023)	Update of OCO-2 observations and prior fluxes.
THU	Kong et al. (2022)	Updates to the OCO-2 product and the fossil fuel data.
COLA	Liu et al. (2022)	New this year.
GCASv2	Jiang et al. (2021, 2022)	New this year.
UoE in-situ	Feng et al. (2009), Feng et al. (2016), Palmer et al. (2019)	Update of the inversion system by using new version of GEOS-Chem
IAPCAS	Feng et al. (2016), Yang et al. (2021)	New this year.
MIROC4-ACTM	Chandra et al. (2022)	New this year
Earth System Models		
CanESM5	Swart et al. (2019), Sospedra-Alfonso et al. (2021)	New this year.
IPSL-CM6a-CO2-LR	Boucher et al. (2020)	New this year.
MIROC-ES2L	Watanabe et al. (2020)	New this year.
MPI-ESM1-2-LR	Mauritsen et al. (2019), Li et al. (2023)	New this year.

3070

3071 **Table 4.** References for the process models, bookkeeping models, ocean data products, and atmospheric
 3072 inversions. All models and products are updated with new data to the end of year 2022, and the atmospheric
 3073 forcing for the DGVMs has been updated as described in Section C.2.2 and C.4.1.

3074



	1960s	1970s	1980s	1990s	2000s	2013-2022	2022	
Land-use change emissions (ELUC)	Bookkeeping (BK) Net flux (1a)	1.5±0.7	1.3±0.7	1.4±0.7	1.6±0.7	1.4±0.7	1.2±0.7	
	BK - deforestation (total)	1.7 [1.3,2.1]	1.6 [1.2,1.9]	1.7 [1.3,2.1]	1.9 [1.6,2.2]	2 [1.6,2.4]	1.9 [1.5,2.4]	1.9 [1.4,2.5]
	BK - forest regrowth (total)	-0.8 [-1.1,-0.6]	-0.9 [-1.1,-0.7]	-0.9 [-1.1,-0.7]	-1 [-1.2,-0.7]	-1.1 [-1.3,-0.8]	-1.3 [-1.5,-0.9]	-1.3 [-1.6,-1]
	BK - other transitions	0.4 [0.3,0.4]	0.2 [0.1,0.3]	0.2 [0.2,0.3]	0.1 [0,0.2]	0.1 [0,0.2]	0.1 [0,0.3]	0.1 [0,0.2]
	BK - peat drainage & peat fires	0.2 [0.1,0.2]	0.2 [0.1,0.2]	0.2 [0.2,0.3]	0.3 [0.3,0.3]	0.3 [0.2,0.3]	0.3 [0.3,0.3]	0.2 [0.2,0.3]
	BK - wood harvest & forest management	0.2 [-0.2,0.6]	0.2 [-0.2,0.6]	0.2 [-0.2,0.6]	0.2 [-0.1,0.6]	0.2 [-0.1,0.6]	0.2 [0,0.6]	0.2 [0,0.7]
	DGVMs-net flux (1b)	1.5±0.5	1.3±0.5	1.6±0.6	1.8±0.6	1.8±0.7	1.7±0.6	1.7±0.6
Terrestrial sink (SLAND)	Residual sink from global budget (E _{FOS} +E _{ELUC} (1a)-G _{ATM} → _{OCEAN}) (2a)	1.7±0.8	1.8±0.8	1.7±0.9	2.7±0.9	2.9±0.9	2.9±0.9	3.7±1
	DGVMs (2b)	1.3±0.5	2±0.7	1.9±0.8	2.5±0.6	2.9±0.7	3.3±0.8	3.8±0.8
Net land fluxes (SLAND-ELUC)	GCB2023 Budget (2b-1a)	-0.2±0.8	0.8±1	0.5±1	0.9±0.9	1.4±1	2.1±1.1	2.6±1.1
	Atmospheric O ₂	---	---	---	1.2±1	1.1±1.1	1.1±1.3	-
	DGVMs-net (2b-1b)	-0.2±0.4	0.7±0.7	0.3±0.6	0.7±0.5	1.1±0.4	1.7±0.6	2.1±0.6
	Inversions ^a	- [-,-]	- [-,-]	0.5 [0.4,0.6] (2)	0.9 [0.6,1.3] (3)	1.3 [0.7,2] (4)	1.6 [0.5,2.3] (8)	2.7 [1.4-3.8] (13)
	ESMs	---	---	0.6 [0.1,1]	1.7 [1.3,2]	2 [1.4,2.7]	2.4 [1.8,3.3]	3.9 [2.8-5.5]

3075

3076 *Estimates are adjusted for the pre-industrial influence of river fluxes, for the cement carbonation sink, and
 3077 adjusted to common E_{FOS} (Sect. 2.7). The ranges given include varying numbers (in parentheses) of inversions
 3078 in each decade (Table S4).

3079 **Table 5.** Comparison of results from the bookkeeping method and budget residuals with results from the
 3080 DGVMs, as well as additional estimates from atmospheric oxygen, atmospheric inversions and Earth System
 3081 Models (ESMs) for different periods, the last decade, and the last year available. All values are in GtCyr⁻¹. See
 3082 Figure 7 for explanation of the bookkeeping component fluxes. The DGVM uncertainties represent ±1σ of the
 3083 decadal or annual (for 2022) estimates from the individual DGVMs: for the inverse systems the mean and range
 3084 of available results is given. All values are rounded to the nearest 0.1 GtC and therefore columns do not
 3085 necessarily add to zero.

3086

3087

3088



3089

Product	1960s	1970s	1980s	1990s	2000s	2013-2022	2022
$f\text{CO}_2$ -products	---	---	---	2.3 [2,2.9]	2.4 [2.2,2.7]	3.1 [2.6,3.3]	3.1 [2.5,3.3]
GOBMs	1±0.3	1.2±0.3	1.7±0.3	2±0.3	2.1±0.4	2.6±0.4	2.5±0.4
GCB2023 Budget	1.1±0.4	1.4±0.4	1.9±0.4	2.1±0.4	2.3±0.4	2.8±0.4	2.8±0.4
Atmospheric O ₂	---	---	---	2±0.7	2.6±0.6	3.3±0.6	-
Inversions	- [-,-]	- [-,-]	1.7 [1.6,1.8] (2)	2.2 [1.9,2.5] (3)	2.4 [1.8,3.1] (4)	3 [2.4,4.1] (8)	3 [2.2-4.2] (13)
ESMs	---	---	1.6 [0.7,2.4]	1.8 [1.1,2.5]	2.1 [1.5,2.8]	2.6 [2.2,3.4]	2.7 [2.3-3.5]

3090

3091 **Table 6:** Comparison of results for the ocean sink from the $f\text{CO}_2$ -products, from global ocean biogeochemistry
 3092 models (GOBMs), the best estimate for GCB2023 as calculated from $f\text{CO}_2$ -products and GOBMs that is used in
 3093 the budget Table 7, as well as additional estimates from atmospheric oxygen, atmospheric inversions and Earth
 3094 System Models (ESMs) for different periods, the last decade, and the last year available. All values are in
 3095 GtCyr⁻¹. Uncertainties represent $\pm 1\sigma$ of the estimates from the GOBMs ($N > 10$) and range of ensemble
 3096 members is given for ensembles with $N < 10$ ($f\text{CO}_2$ -products, inversions, ESMs). The uncertainty of the
 3097 GCB2023 budget estimate is based on expert judgement (Section 2 and Supplementary S1 to S4) and for
 3098 oxygen it is the standard deviation of a Monte Carlo ensemble (Section 2.8).

3099



		1960s	1970s	1980s	1990s	2000s	2013-2022	2022	2023 (Projection)
Total emissions (EFOS + ELUC)	Fossil CO ₂ emissions (EFOS) [*]	3±0.2	4.7±0.2	5.5±0.3	6.4±0.3	7.8±0.4	9.6±0.5	9.9±0.5	10±0.5
	Land-use change emissions (ELUC)	1.5±0.7	1.3±0.7	1.4±0.7	1.6±0.7	1.4±0.7	1.3±0.7	1.2±0.7	1.1±0.7
	Total emissions	4.6±0.7	6±0.7	6.9±0.8	7.9±0.8	9.2±0.8	10.9±0.8	11.1±0.9	11.2±0.9
Growth rate in atmos CO ₂ (GATM)		1.7±0.07	2.8±0.07	3.4±0.02	3.1±0.02	4±0.02	5.2±0.02	4.6±0.2	4±0.4
Partitioning	Ocean sink (SOCEAN)	1.1±0.4	1.4±0.4	1.9±0.4	2.1±0.4	2.3±0.4	2.8±0.4	2.8±0.4	2.9±0.4
	Terrestrial sink (SLAND)	1.3±0.5	2±0.7	1.9±0.8	2.5±0.6	2.9±0.7	3.3±0.8	3.8±0.8	3±1
Budget Imbalance	BIM=EFOS+ELUC-(GATM+SOCEAN+SLAND)	0.4	-0.2	-0.2	0.2	0	-0.4	-0.1	1.2

3100

3101 **Table 7:** Decadal mean in the five components of the anthropogenic CO₂ budget for different periods, and last
 3102 year available. All values are in GtC yr⁻¹, and uncertainties are reported as ±1σ. Fossil CO₂ emissions include
 3103 cement carbonation. The table also shows the budget imbalance (B_{IM}), which provides a measure of the
 3104 discrepancies among the nearly independent estimates. A positive imbalance means the emissions are
 3105 overestimated and/or the sinks are too small. All values are rounded to the nearest 0.1 GtC and therefore
 3106 columns do not necessarily add to zero.

3107



		1750-2022	1850-2014	1850-2022	1960-2022	1850-2023
Emissions	Fossil CO ₂ emissions (EFOS)	480±25	400±20	475±25	395±20	485±25
	Land-use change emissions (ELUC)	250±75	210±65	220±65	90±45	220±65
	Total emissions	730±80	610±65	695±70	485±50	705±70
Partitioning	Growth rate in atmos CO ₂ (GATM)	300±5	235±5	280±5	215±5	280±5
	Ocean sink (SOCEAN)	190±40	155±30	180±35	125±25	180±35
	Terrestrial sink (SLAND)	245±60	200±50	225±55	150±35	225±55
Budget imbalance	BIM=EFOS+ELUC-(GATM+SOCEAN+SLAND)	-5	20	15	-5	15

3108

3109 **Table 8.** Cumulative CO₂ for different time periods in gigatonnes of carbon (GtC). Fossil CO₂ emissions
 3110 include cement carbonation. The budget imbalance (BIM) provides a measure of the discrepancies among the
 3111 nearly independent estimates. All values are rounded to the nearest 5 GtC and therefore columns do not
 3112 necessarily add to zero. Uncertainties are reported as follows: EFOS is 5% of cumulative emissions; ELUC prior to
 3113 1959 is 1σ spread from the DGVMs, ELUC post-1959 is 0.7*number of years (where 0.7 GtC/yr is the
 3114 uncertainty on the annual ELUC flux estimate); GATM uncertainty is held constant at 5 GtC for all time periods;
 3115 SOCEAN uncertainty is 20% of the cumulative sink (20% relates to the annual uncertainty of 0.4 GtC/yr, which is
 3116 ~20% of the current ocean sink); and SLAND is the 1σ spread from the DGVMs estimates.

3117



3118

	2003-2012	2013-2022
ELUC from bookkeeping estimates (from Table 5)	1.4	1.3
SLAND on non-intact forest from DGVMs	1.9	2.0
ELUC subtract SLAND on non-intact forests	-0.5	-0.8
National Greenhouse Gas Inventories	-0.4	-0.7

3119 **Table 9:** Translation of global carbon cycle models' land flux definitions to the definition of the LULUCF net
3120 flux used in national Greenhouse Gas Inventories reported to UNFCCC. See Sec. C.2.3 and Table S9 for detail
3121 on methodology and comparison to other datasets. Units are GtC yr⁻¹.

3122



3123

Source of uncertainty	Time scale (years)	Location	Evidence
Fossil CO₂ emissions (EFOS; Section 2.1)			
energy statistics	annual to decadal	global, but mainly China & major developing countries	(Korsbakken et al., 2016, Guan et al., 2012)
carbon content of coal	annual to decadal	global, but mainly China & major developing countries	(Liu et al., 2015)
system boundary	annual to decadal	all countries	(Andrew, 2020a)
Net land-use change flux (ELUC; section 2.2)			
land-cover and land-use change statistics	continuous	global; in particular tropics	(Houghton et al., 2012, Gasser et al., 2020, Ganzenmüller et al., 2022, Yu et al. 2022)
sub-grid-scale transitions	annual to decadal	global	(Wilkenskjeld et al., 2014)
vegetation biomass	annual to decadal	global; in particular tropics	(Houghton et al., 2012, Bastos et al., 2021)
forest degradation (fire, selective logging)	annual to decadal	tropics	(Aragão et al., 2018, Qin et al., 2021)
wood and crop harvest	annual to decadal	global; SE Asia	(Arneth et al., 2017, Erb et al., 2018)
peat burning	multi-decadal trend	global	(van der Werf et al., 2010, 2017)
loss of additional sink capacity	multi-decadal trend	global	(Pongratz et al, 2014, Gasser et al, 2020; Obermeier et al., 2021)
Atmospheric growth rate (GATM; section 2.4) no demonstrated uncertainties larger than ± 0.3 GtC yr ⁻¹ . The uncertainties in GATM have been estimated as ± 0.2 GtC yr ⁻¹ , although the conversion of the growth rate into a global annual flux assuming instantaneous mixing throughout the atmosphere introduces additional errors that have not yet been quantified.			
Ocean sink (SOCEAN; section 2.5)			
sparsity in surface fCO ₂ observations	mean, decadal variability and trend	global, in particular southern hemisphere	(Gloege et al., 2021, Denvil-Sommer et al., 2021, Hauck et al., 2023)



riverine carbon outgassing and its anthropogenic perturbation	annual to decadal	global, in particular partitioning between Tropics and South	(Aumont et al., 2001, Lacroix et al., 2020, Cris et al., 2022)
Models underestimate interior ocean anthropogenic carbon storage	annual to decadal	global	(Friedlingstein et al., 2021, this study, DeVries et al., 2023, see also Terhaar et al., 2022)
near-surface temperature and salinity gradients	mean on all time-scales	global	(Watson et al., 2020, Dong et al., 2022, Bellenger et al., 2023)
Land sink (SLAND; section 2.6)			
strength of CO ₂ fertilisation	multi-decadal trend	global	(Wenzel et al., 2016; Walker et al., 2021)
response to variability in temperature and rainfall	annual to decadal	global; in particular tropics	(Cox et al., 2013; Jung et al., 2017; Humphrey et al., 2018; 2021)
nutrient limitation and supply	annual to decadal	global	(Zaehle et al., 2014)
carbon allocation and tissue turnover rates	annual to decadal	global	(De Kauwe et al., 2014; O'Sullivan et al., 2022)
tree mortality	annual	global in particular tropics	(Hubau et al., 2021; Brienen et al., 2020)
response to diffuse radiation	annual	global	(Mercado et al., 2009; O'Sullivan et al., 2021)

3124

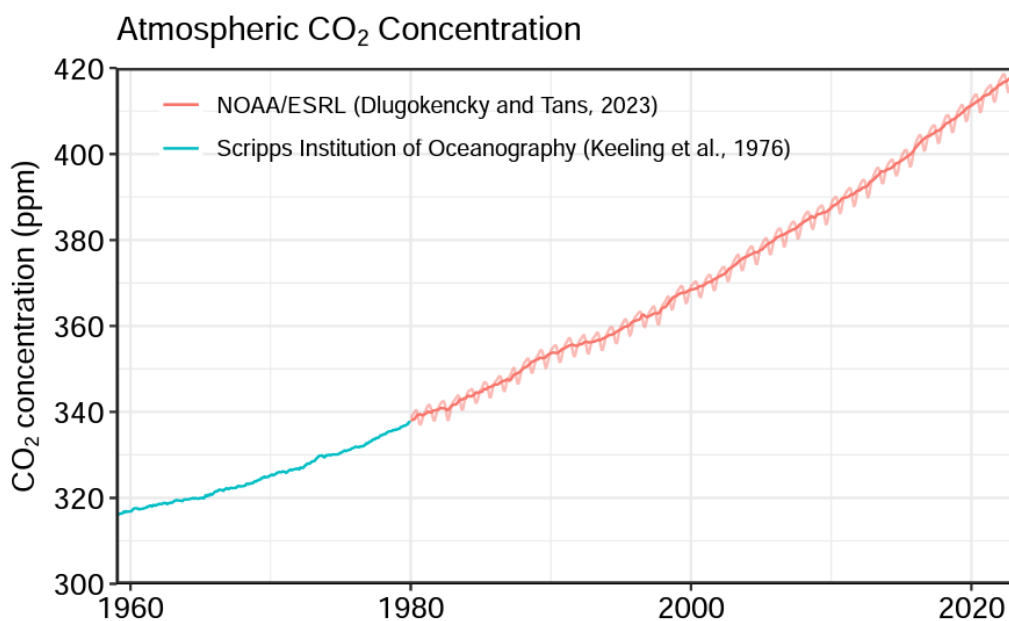
3125 **Table 10.** Major known sources of uncertainties in each component of the Global Carbon Budget, defined as
 3126 input data or processes that have a demonstrated effect of at least ± 0.3 GtC yr⁻¹.

3127

3128



3129 **Figures and Captions**



3130

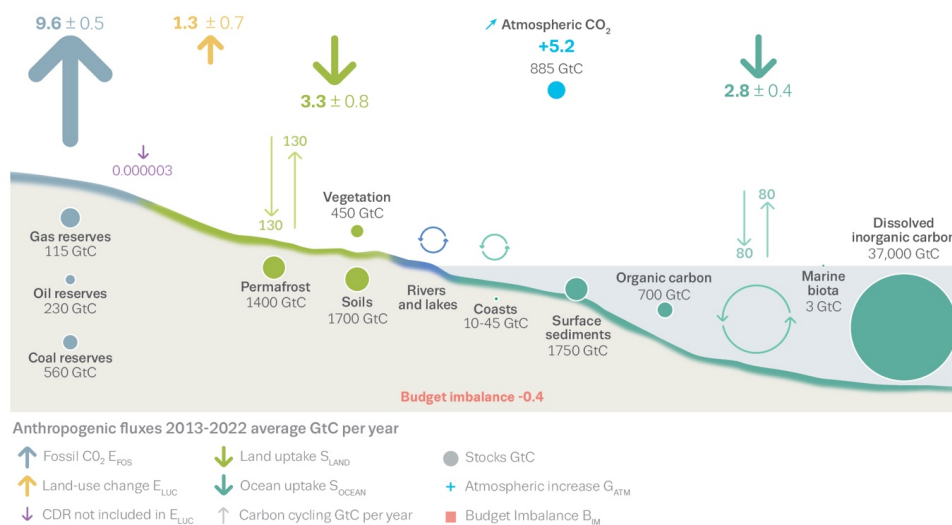
3131 **Figure 1.** Surface average atmospheric CO₂ concentration (ppm). Since 1980, monthly data are from
3132 NOAA/GML (Lan et al., 2023) and are based on an average of direct atmospheric CO₂ measurements from
3133 multiple stations in the marine boundary layer (Masarie and Tans, 1995). The 1958-1979 monthly data are from
3134 the Scripps Institution of Oceanography, based on an average of direct atmospheric CO₂ measurements from the
3135 Mauna Loa and South Pole stations (Keeling et al., 1976). To account for the difference of mean CO₂ and
3136 seasonality between the NOAA/GML and the Scripps station networks used here, the Scripps surface average
3137 (from two stations) was de-seasonalised and adjusted to match the NOAA/GML surface average (from multiple
3138 stations) by adding the mean difference of 0.667 ppm, calculated here from overlapping data during 1980-2012.

3139

3140



The global carbon cycle



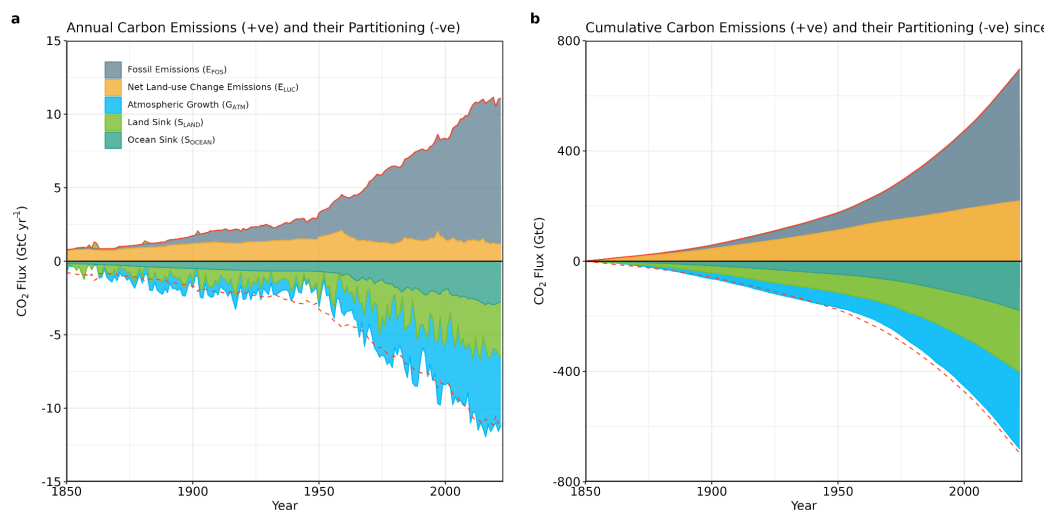
3141

3142

3143 **Figure 2.** Schematic representation of the overall perturbation of the global carbon cycle caused by
 3144 anthropogenic activities, averaged globally for the decade 2013-2022. See legends for the corresponding arrows
 3145 and units. The uncertainty in the atmospheric CO₂ growth rate is very small (± 0.02 GtC yr⁻¹) and is neglected
 3146 for the figure. The anthropogenic perturbation occurs on top of an active carbon cycle, with fluxes and stocks
 3147 represented in the background and taken from Canadell et al. (2021) for all numbers, except for the carbon
 3148 stocks in coasts which is from a literature review of coastal marine sediments (Price and Warren, 2016).

3149

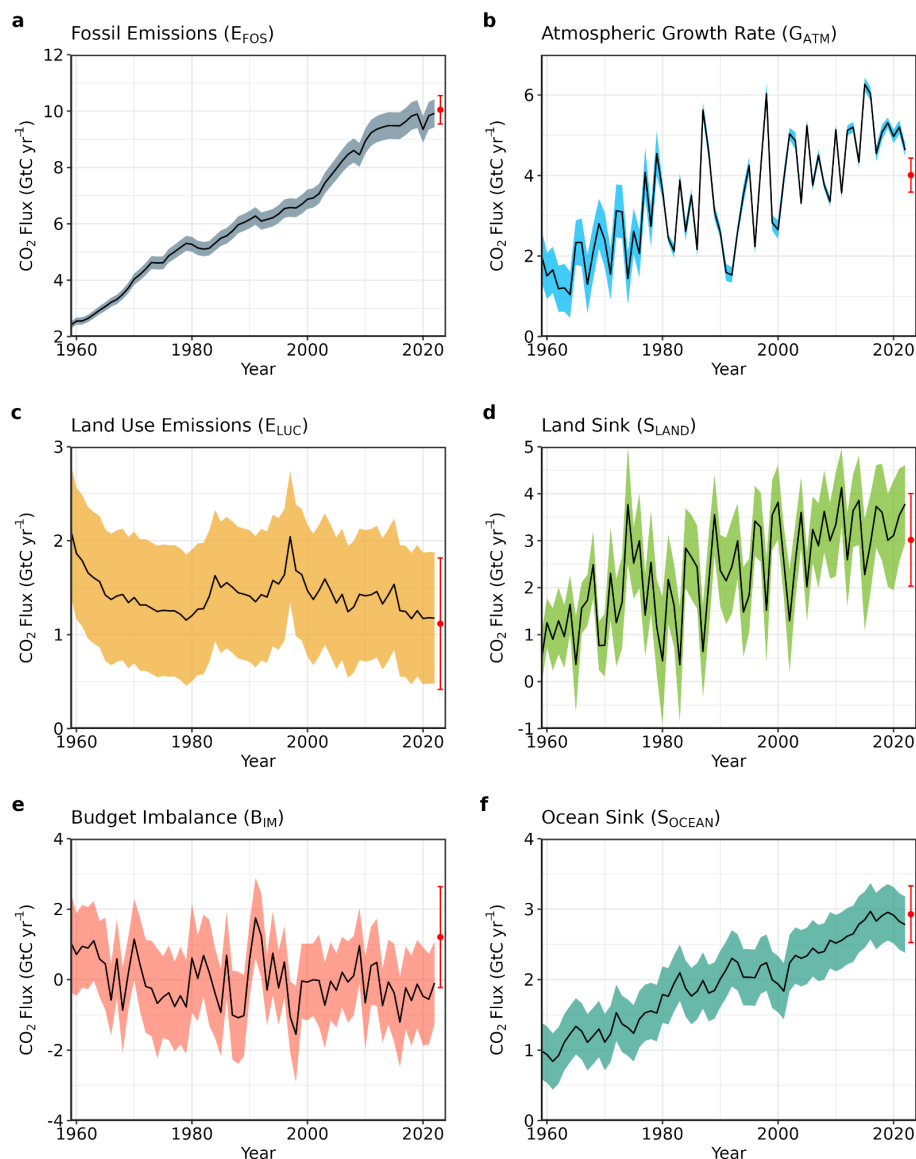
3150



3151

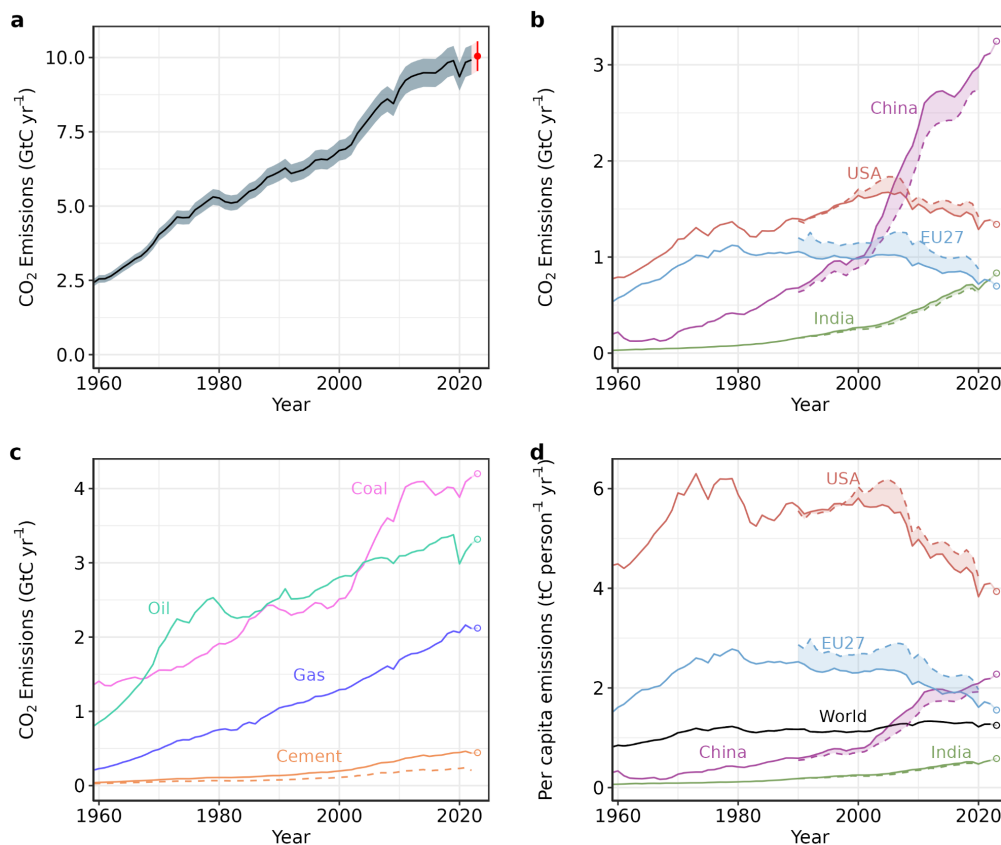
3152 **Figure 3.** Combined components of the global carbon budget as a function of time, for fossil CO₂ emissions
3153 (EFOS, including a small sink from cement carbonation; grey) and emissions from land-use change (ELUC;
3154 brown), as well as their partitioning among the atmosphere (GATM; cyan), ocean (SOCEAN; blue), and land
3155 (SLAND; green). Panel (a) shows annual estimates of each flux and panel (b) the cumulative flux (the sum of all
3156 prior annual fluxes) since the year 1850. The partitioning is based on nearly independent estimates from
3157 observations (for GATM) and from process model ensembles constrained by data (for SOCEAN and SLAND)
3158 and does not exactly add up to the sum of the emissions, resulting in a budget imbalance (BIM) which is
3159 represented by the difference between the bottom red line (mirroring total emissions) and the sum of carbon
3160 fluxes in the ocean, land, and atmosphere reservoirs. All data are in GtC yr⁻¹ (panel a) and GtC (panel b). The
3161 EFOS estimate is based on a mosaic of different datasets, and has an uncertainty of $\pm 5\%$ ($\pm 1\sigma$). The ELUC
3162 estimate is from three bookkeeping models (Table 4) with uncertainty of ± 0.7 GtC yr⁻¹. The GATM estimates
3163 prior to 1959 are from Joos and Spahni (2008) with uncertainties equivalent to about ± 0.1 - 0.15 GtC yr⁻¹ and
3164 from Lan et al. (2023) since 1959 with uncertainties of about ± 0.07 GtC yr⁻¹ during 1959-1979 and ± 0.02 GtC
3165 yr⁻¹ since 1980. The SOCEAN estimate is the average from Khatiwala et al. (2013) and DeVries (2014) with
3166 uncertainty of about $\pm 30\%$ prior to 1959, and the average of an ensemble of models and an ensemble of fCO₂-
3167 products (Table 4) with uncertainties of about ± 0.4 GtC yr⁻¹ since 1959. The SLAND estimate is the average of
3168 an ensemble of models (Table 4) with uncertainties of about ± 1 GtC yr⁻¹. See the text for more details of each
3169 component and their uncertainties.

3170



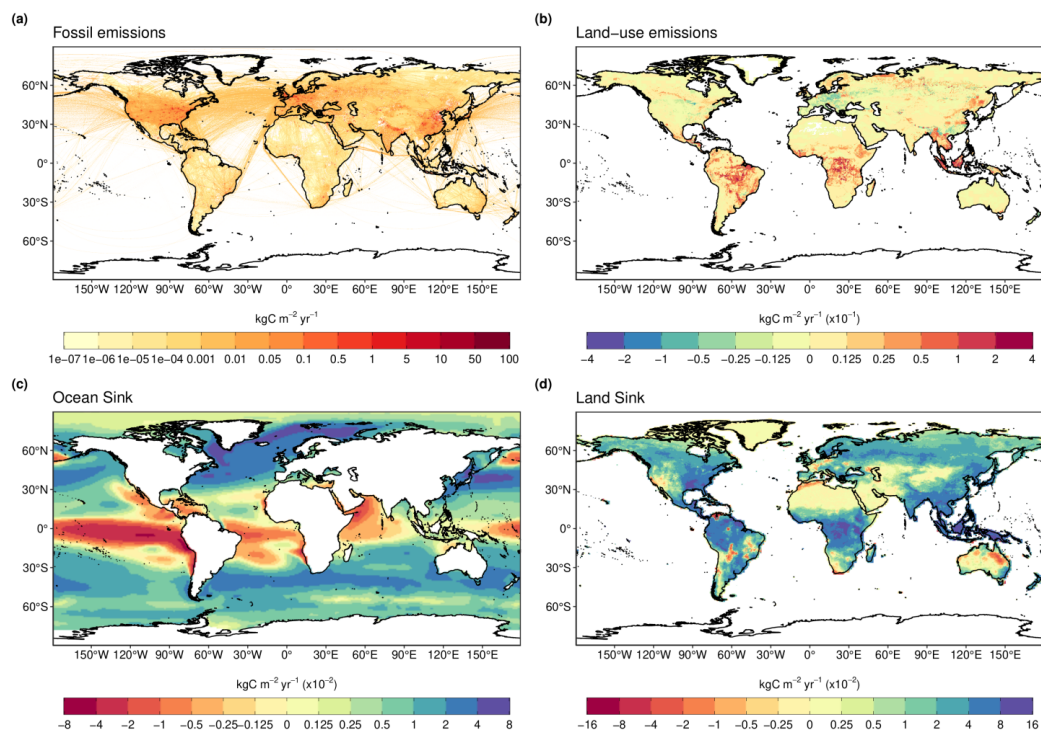
3171

3172 **Figure 4.** Components of the global carbon budget and their uncertainties as a function of time, presented
 3173 individually for (a) fossil CO₂ and cement carbonation emissions (E_{FOS}), (b) growth rate in atmospheric CO₂
 3174 concentration (G_{ATM}), (c) emissions from land-use change (E_{LUC}), (d) the land CO₂ sink (S_{LAND}), (e) the ocean
 3175 CO₂ sink (S_{OCEAN}), (f) the budget imbalance that is not accounted for by the other terms. Positive values of
 3176 S_{LAND} and S_{OCEAN} represent a flux from the atmosphere to land or the ocean. All data are in GtC yr⁻¹ with the
 3177 uncertainty bounds representing ± 1 standard deviation in shaded colour. Data sources are as in Figure 3. The red
 3178 dots indicate our projections for the year 2023 and the red error bars the uncertainty in the projections (see
 3179 methods).



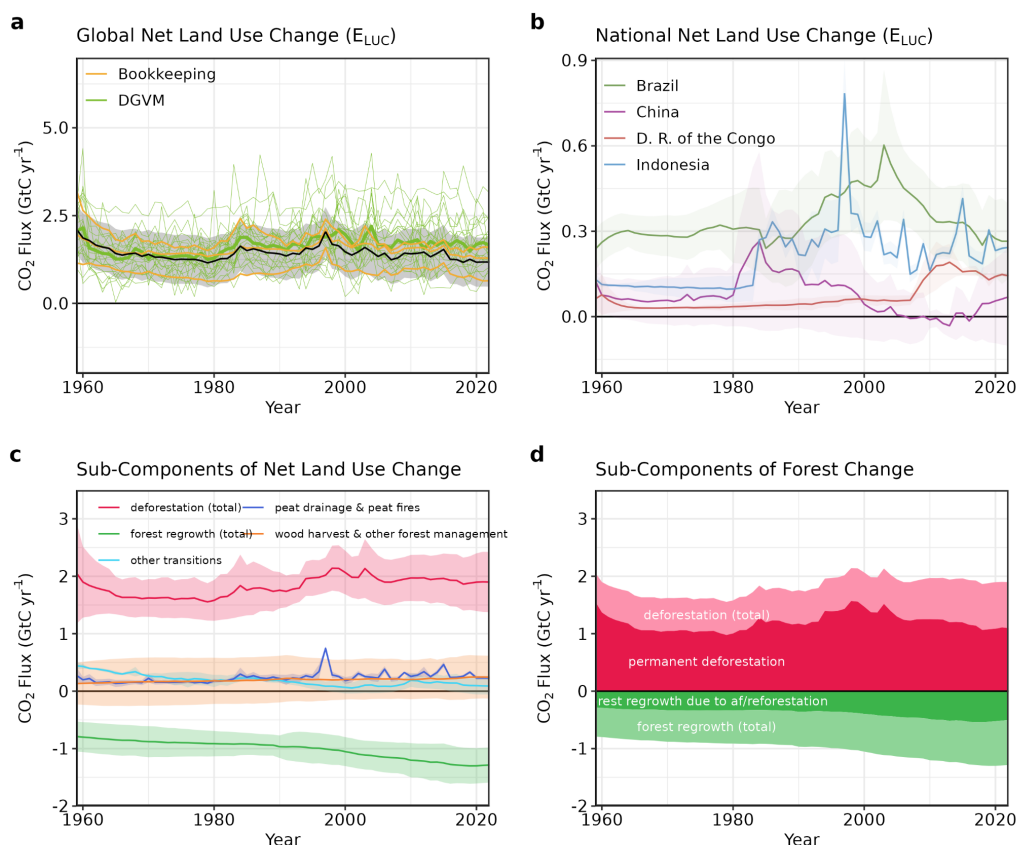
3180
3181 **Figure 5.** Fossil CO₂ emissions for (a) the globe, including an uncertainty of $\pm 5\%$ (grey shading) and a
3182 projection through the year 2023 (red dot and uncertainty range), (b) territorial (solid lines) and consumption
3183 (dashed lines) emissions for the top three country emitters (USA, China, India) and for the European Union
3184 (EU27), (c) global emissions by fuel type, including coal, oil, gas, and cement, and cement minus cement
3185 carbonation (dashed), and (d) per-capita emissions the world and for the large emitters as in panel (b). Territorial
3186 emissions are primarily from a draft update of Gilfillan and Marland (2021) except for national data for Annex I
3187 countries for 1990–2021, which are reported to the UNFCCC as detailed in the text, as well as some
3188 improvements in individual countries, and extrapolated forward to 2022 using data from Energy Institute.
3189 Consumption-based emissions are updated from Peters et al. (2011a). See Section 2.1 and Supplement S.1 for
3190 details of the calculations and data sources.

3191
3192

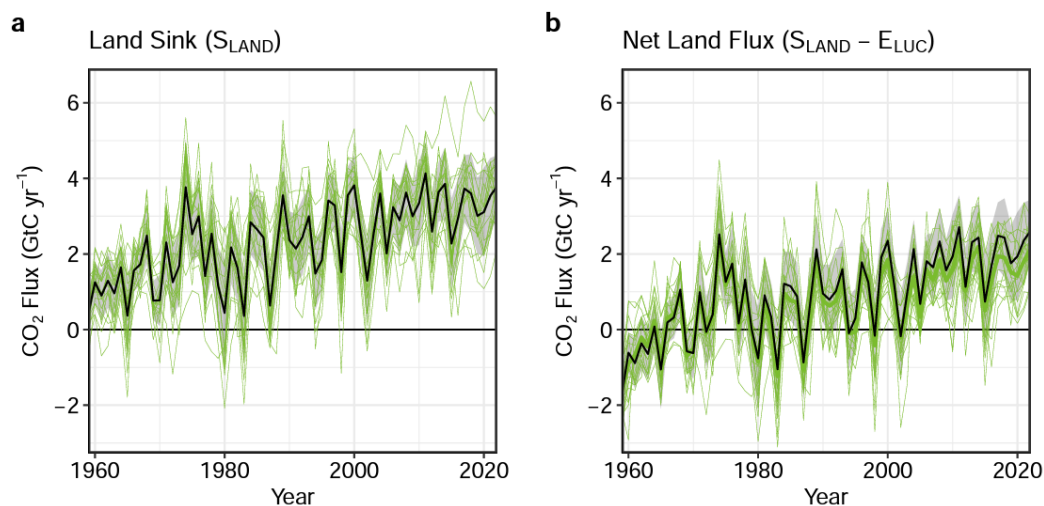


3193
 3194
 3195
 3196
 3197
 3198
 3199
 3200
 3201
 3202
 3203
 3204
 3205
 3206
 3207
 3208
 3209

Figure 6. The 2013–2022 decadal mean components of the global carbon budget, presented for (a) fossil CO₂ emissions (E_{FOS}), (b) land-use change emissions (E_{LUC}), (c) the ocean CO₂ sink (S_{OCEAN}), and (d) the land CO₂ sink (S_{LAND}). Positive values for E_{FOS} and E_{LUC} represent a flux to the atmosphere, whereas positive values of S_{OCEAN} and S_{LAND} represent a flux from the atmosphere to the ocean or the land (carbon sink). In all panels, yellow/red colours represent a source (flux from the land/ocean to the atmosphere), green/blue colours represent a sink (flux from the atmosphere into the land/ocean). All units are in $\text{kgC m}^{-2} \text{yr}^{-1}$. Note the different scales in each panel. E_{FOS} data shown is from GCP-GridFEDv2023.1. The E_{LUC} map shows the average E_{LUC} from the three bookkeeping models plus emissions from peat drainage and peat fires. Gridded E_{LUC} estimates for H&C2023 and OSCAR are derived by spatially distributing their national data based on the spatial patterns of BLUE gross fluxes in each country (see Schwingshackl et al., 2022, for more details about the methodology). S_{OCEAN} data shown is the average of GOBMs and data-products means, using GOBMs simulation A, no adjustment for bias and drift applied to the gridded fields (see Section 2.5). S_{LAND} data shown is the average of the DGVMS for simulation S2 (see Section 2.6).



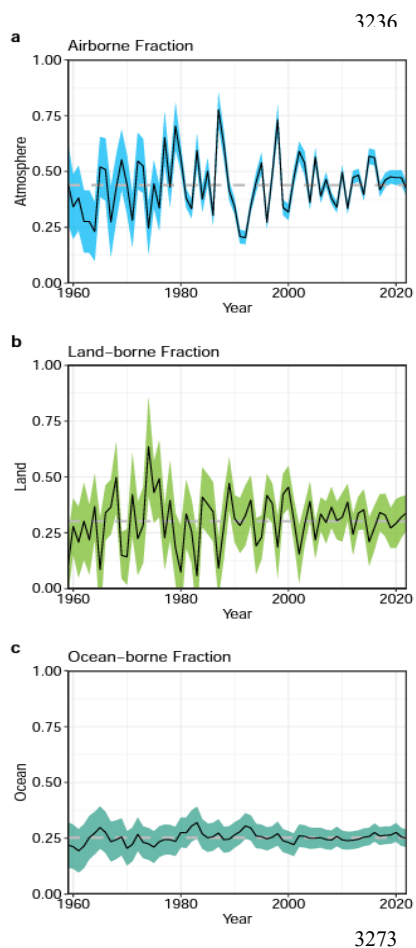
3210
 3211 **Figure 7.** Net CO₂ exchanges between the atmosphere and the terrestrial biosphere related to land use change.
 3212 (a) Net CO₂ emissions from land-use change (E_{LUC}) with estimates from the three bookkeeping models (yellow
 3213 lines) and the budget estimate (black with $\pm 1\sigma$ uncertainty), which is the average of the three bookkeeping
 3214 models. Estimates from individual DGVMs (narrow green lines) and the DGVM ensemble mean (thick green
 3215 line) are also shown. (b) Net CO₂ emissions from land-use change from the four countries with largest
 3216 cumulative emissions since 1959. Values shown are the average of the three bookkeeping models, with shaded
 3217 regions as $\pm 1\sigma$ uncertainty. (c) Sub-components of E_{LUC} : (i) emissions from deforestation (including permanent
 3218 deforestation and deforestation in shifting cultivation cycles), (ii) emissions from peat drainage & peat fires, (iii)
 3219 removals from forest (re-)growth (including forest (re-)growth due to afforestation and reforestation and forest
 3220 regrowth in shifting cultivation cycles), (iv) fluxes from wood harvest and other forest management (comprising
 3221 slash and product decay following wood harvest, regrowth after wood harvest, and fire suppression), and (v)
 3222 emissions and removals related to other land-use transitions. The sum of the five components is E_{LUC} shown in
 3223 panel (a). (d) Sub-components of ‘deforestation (total)’ and of ‘forest (re-)growth (total)’: (i) deforestation in
 3224 shifting cultivation cycles, (ii) permanent deforestation, (iii) forest (re-)growth due to afforestation and/or
 3225 reforestation, and (iv) forest regrowth in shifting cultivation cycles.
 3226



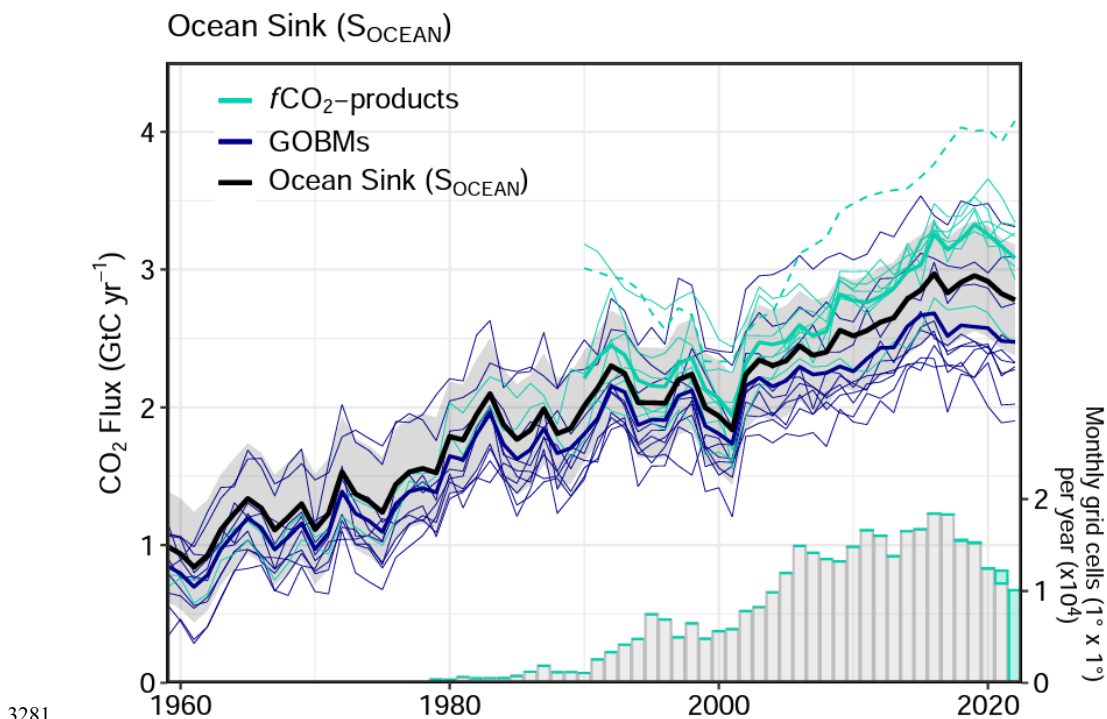
3227

3228 **Figure 8:** (a) The land CO₂ sink (S_{LAND}) estimated by individual DGVMs (green), as well as the budget estimate
3229 (black with $\pm 1\sigma$ uncertainty), which is the average of all DGVMs. (b) Net atmosphere-land CO₂ fluxes ($S_{\text{LAND}} -$
3230 E_{LUC}). The budget estimate of the net land flux (black with $\pm 1\sigma$ uncertainty) combines the DGVM estimate of
3231 S_{LAND} from panel (a) with the bookkeeping estimate of E_{LUC} from Figure 7a. Uncertainties are similarly
3232 propagated in quadrature. DGVMs also provide estimates of E_{LUC} (see Figure 7a), which can be combined with
3233 their own estimates of the land sink. Hence panel (b) also includes an estimate for the net land flux for
3234 individual DGVMs (thin green lines) and their multi-model mean (thick green line).

3235



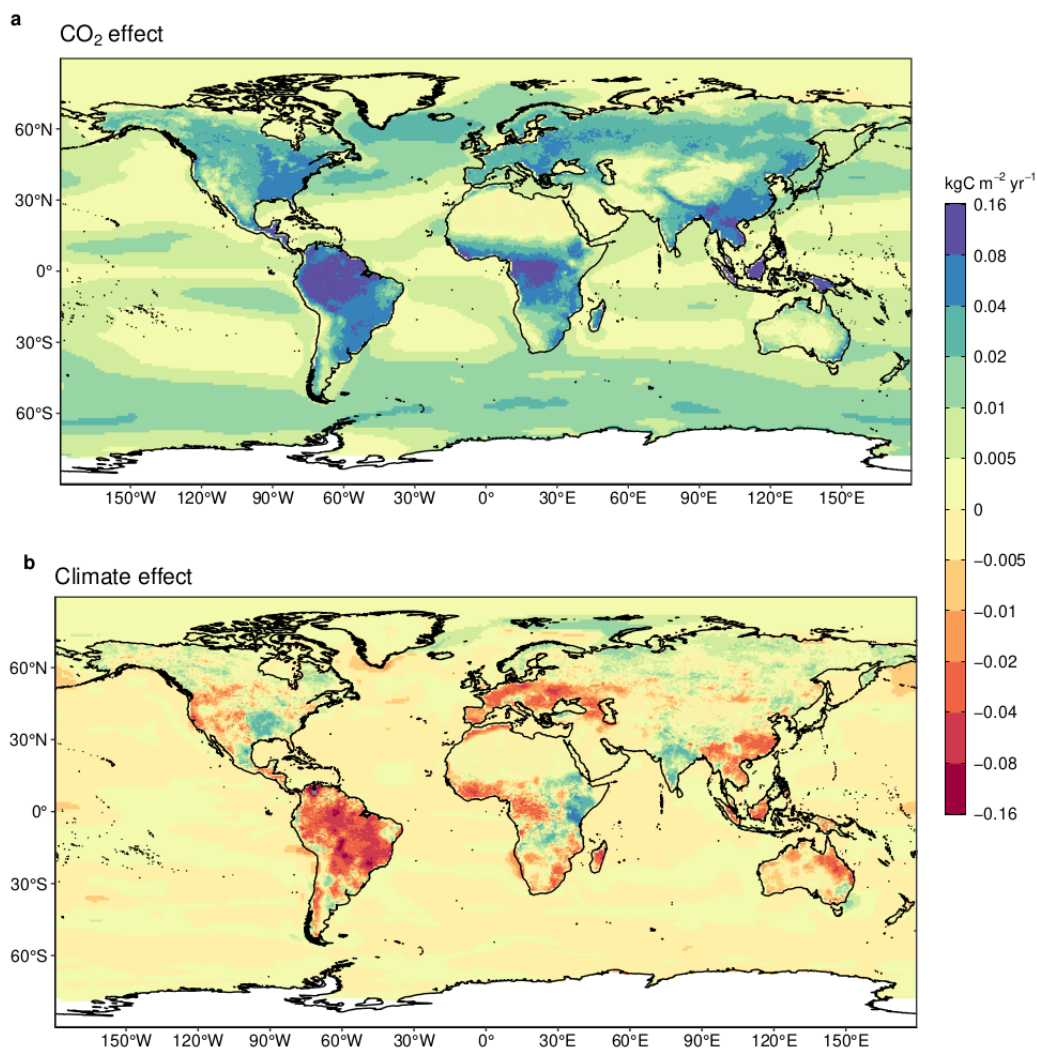
3274
3275 **Figure 9.** The partitioning of total anthropogenic CO₂ emissions ($E_{FOS} + E_{LUC}$) across (a) the atmosphere
3276 (airborne fraction), (b) land (land-borne fraction), and (c) ocean (ocean-borne fraction). Black lines represent the
3277 central estimate, and the coloured shading represents the uncertainty. The grey dashed lines represent the long-
3278 term average of the airborne (44%), land-borne (30%) and ocean-borne (25%) fractions during 1960-2022 (with
3279 a BIM of 1%).
3280



3281

3282 **Figure 10.** Comparison of the anthropogenic atmosphere-ocean CO_2 flux showing the budget values of S_{OCEAN}
3283 (black; with the uncertainty in grey shading), individual ocean models (royal blue), and the ocean fCO_2 -products
3284 (cyan; with Watson et al. (2020) in dashed line as not used for ensemble mean). Only one fCO_2 -product (Jena-
3285 MLS) extends back to 1959 (Rödenbeck et al., 2022). The fCO_2 -products were adjusted for the pre-industrial
3286 ocean source of CO_2 from river input to the ocean, by subtracting a source of $0.65\ GtC\ yr^{-1}$ to make them
3287 comparable to S_{OCEAN} (see Section 2.5). Bar-plot in the lower right illustrates the number of fCO_2 observations
3288 in the SOCAT v2023 database (Bakker et al., 2023). Grey bars indicate the number of data points in SOCAT
3289 v2022, and coloured bars the newly added observations in v2023.

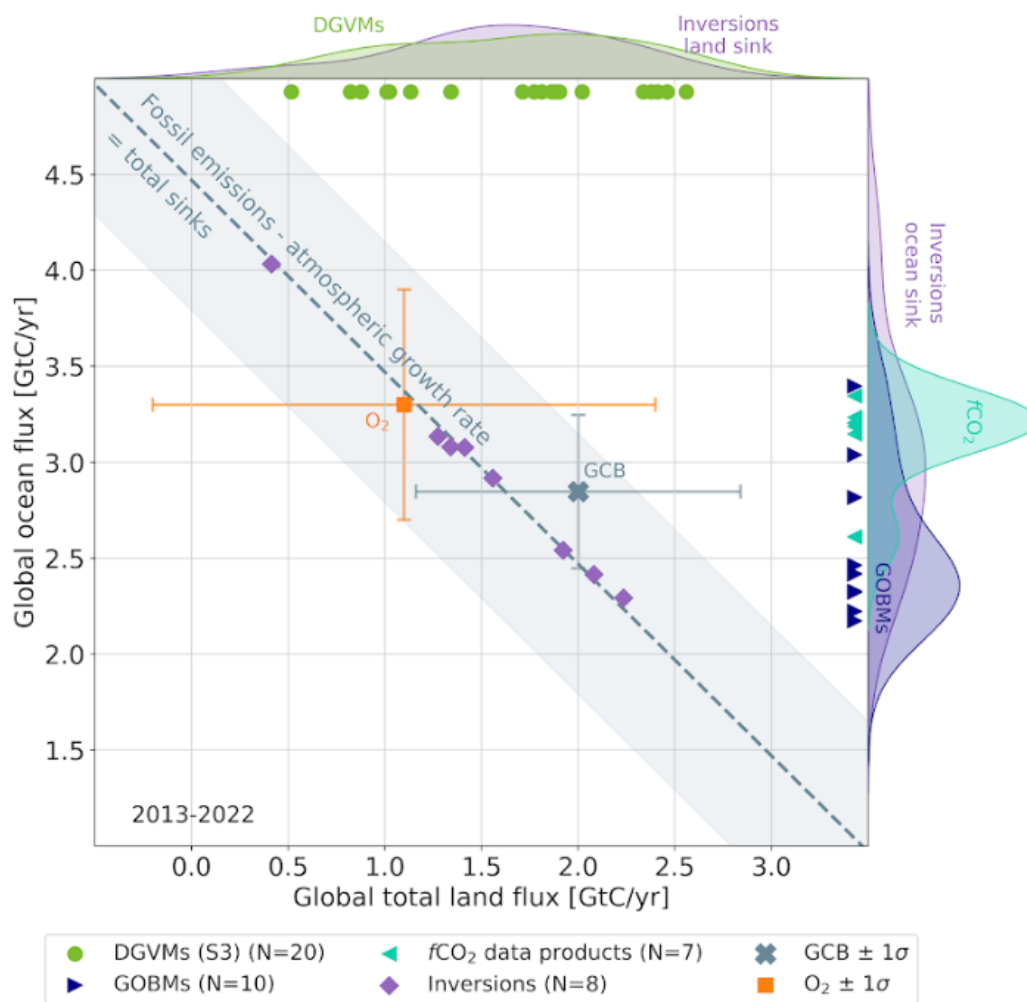
3290



3291

3292 **Figure 11.** Attribution of the atmosphere-ocean (S_{OCEAN}) and atmosphere-land (S_{LAND}) CO₂ fluxes to (a)
3293 increasing atmospheric CO₂ concentrations and (b) changes in climate, averaged over the previous decade 2013-
3294 2022. All data shown is from the processed-based GOBMs and DGVMs. Note that the sum of ocean CO₂ and
3295 climate effects shown here will not equal the ocean sink shown in Figure 6 which includes the f_{CO_2} -products.
3296 See Supplement S.3.2 and S.4.1 for attribution methodology. Units are in kgC m⁻² yr⁻¹ (note the non-linear
3297 colour scale).

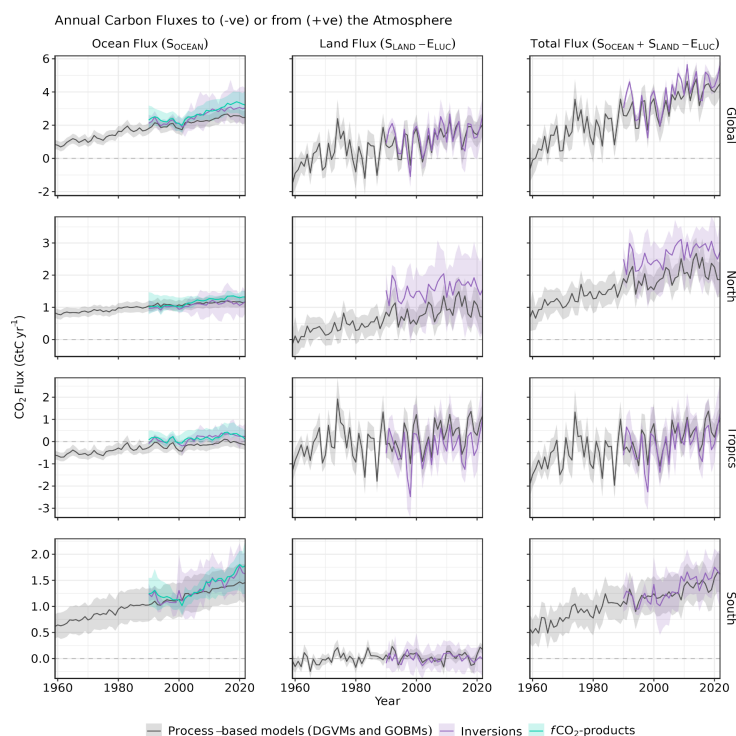
3298



3299

3300 **Figure 12.** The 2013-2022 decadal mean net atmosphere-ocean and atmosphere-land fluxes derived from the
 3301 ocean models and $f\text{CO}_2$ products (y-axis, right and left pointing blue triangles respectively), and from the
 3302 DGVMs (x-axis, green symbols), and the same fluxes estimated from the inversions (purple symbols). The
 3303 shaded distributions show the densities of the ensembles of individual estimates. The grey central cross is the
 3304 mean ($\pm 1\sigma$) of S_{OCEAN} and $(S_{\text{LAND}} - E_{\text{LUC}})$ as assessed in this budget. The grey diagonal line represents the
 3305 global land + ocean net flux, i.e. global fossil fuel emissions minus the atmospheric growth rate from this budget
 3306 ($E_{\text{FOS}} - G_{\text{ATM}}$). The orange square represents the ocean and land sink as estimated from the atmospheric O_2
 3307 constraint. Positive values are CO_2 sinks. Note that the inverse estimates have been scaled for a minor difference
 3308 between E_{FOS} and GridFEDv2023.1 (Jones et al., 2023).

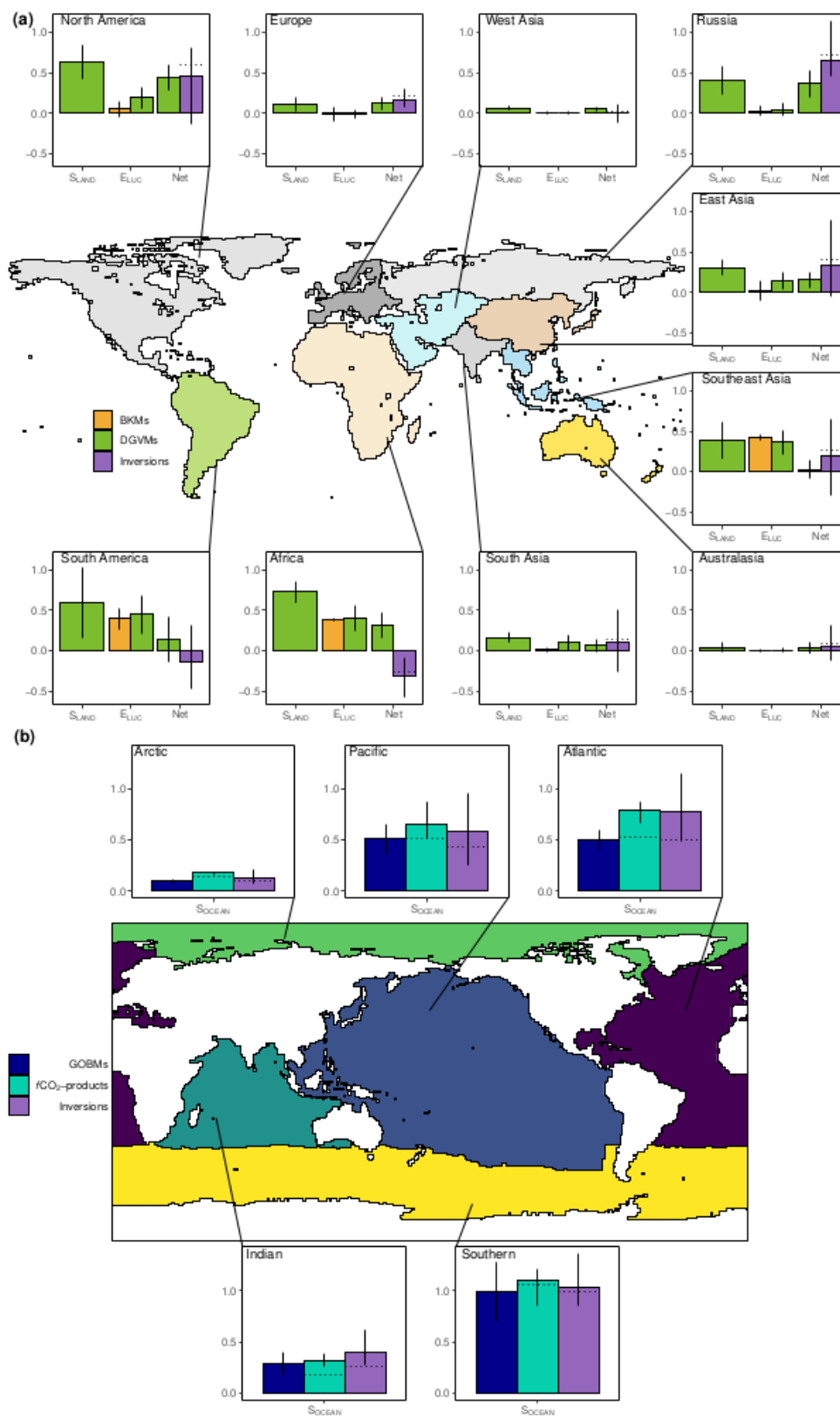
3309



3310

3311 **Figure 13.** CO₂ fluxes between the atmosphere and the Earth's surface separated between land and oceans,
 3312 globally and in three latitude bands. The ocean flux is S_{OCEAN} and the land flux is the net atmosphere-land fluxes
 3313 from the DGVMs. The latitude bands are (top row) global, (2nd row) north (>30°N), (3rd row) tropics (30°S-
 3314 30°N), and (bottom row) south (<30°S), and over ocean (left column), land (middle column), and total (right
 3315 column). Estimates are shown for: process-based models (DGVMs for land, GOBMs for oceans); inversion
 3316 systems (land and ocean); and fCO_2 -products (ocean only). Positive values are CO₂ sinks. Mean estimates from
 3317 the combination of the process models for the land and oceans are shown (black line) with ± 1 standard deviation
 3318 (1σ) of the model ensemble (grey shading). For the total uncertainty in the process-based estimate of the total
 3319 sink, uncertainties are summed in quadrature. Mean estimates from the atmospheric inversions are shown
 3320 (purple lines) with their full spread (purple shading). Mean estimates from the fCO_2 -products are shown for the
 3321 ocean domain (light blue lines) with full model spread (light blue shading). The global S_{OCEAN} (upper left) and
 3322 the sum of S_{OCEAN} in all three regions represents the anthropogenic atmosphere-to-ocean flux based on the
 3323 assumption that the preindustrial ocean sink was 0 GtC yr⁻¹ when riverine fluxes are not considered. This
 3324 assumption does not hold at the regional level, where preindustrial fluxes can be significantly different from
 3325 zero. Hence, the regional panels for S_{OCEAN} represent a combination of natural and anthropogenic fluxes. Bias-
 3326 correction and area-weighting were only applied to global S_{OCEAN} ; hence the sum of the regions is slightly
 3327 different from the global estimate (<0.05 GtC yr⁻¹).

3328





3330 **Figure 14.** Decadal mean (a) land and (b) ocean fluxes for RECCAP-2 regions over 2013-2022. For land fluxes,
3331 S_{LAND} is estimated by the DGVMs (green bars), with the error bar as $\pm 1\sigma$ spread among models. A positive
3332 S_{LAND} is a net transfer of carbon from the atmosphere to the land. E_{LUC} fluxes are shown for both DGVMs
3333 (green) and bookkeeping models (orange), again with the uncertainty calculated as the $\pm 1\sigma$ spread. Note, a
3334 positive E_{LUC} flux indicates a loss of carbon from the land. The net land flux is shown for both DGVMs (green)
3335 and atmospheric inversions (purple), including the full model spread for inversions. The net ocean sink (S_{OCEAN})
3336 is estimated by GOBMs (royal blue), $f\text{CO}_2$ -products (cyan), and atmospheric inversions (purple). Uncertainty is
3337 estimated as the $\pm 1\sigma$ spread for GOBMs, and the full model spread for the other two products. The dotted lines
3338 show the $f\text{CO}_2$ -products and inversion results without river flux adjustment. Positive values are CO_2 sinks.

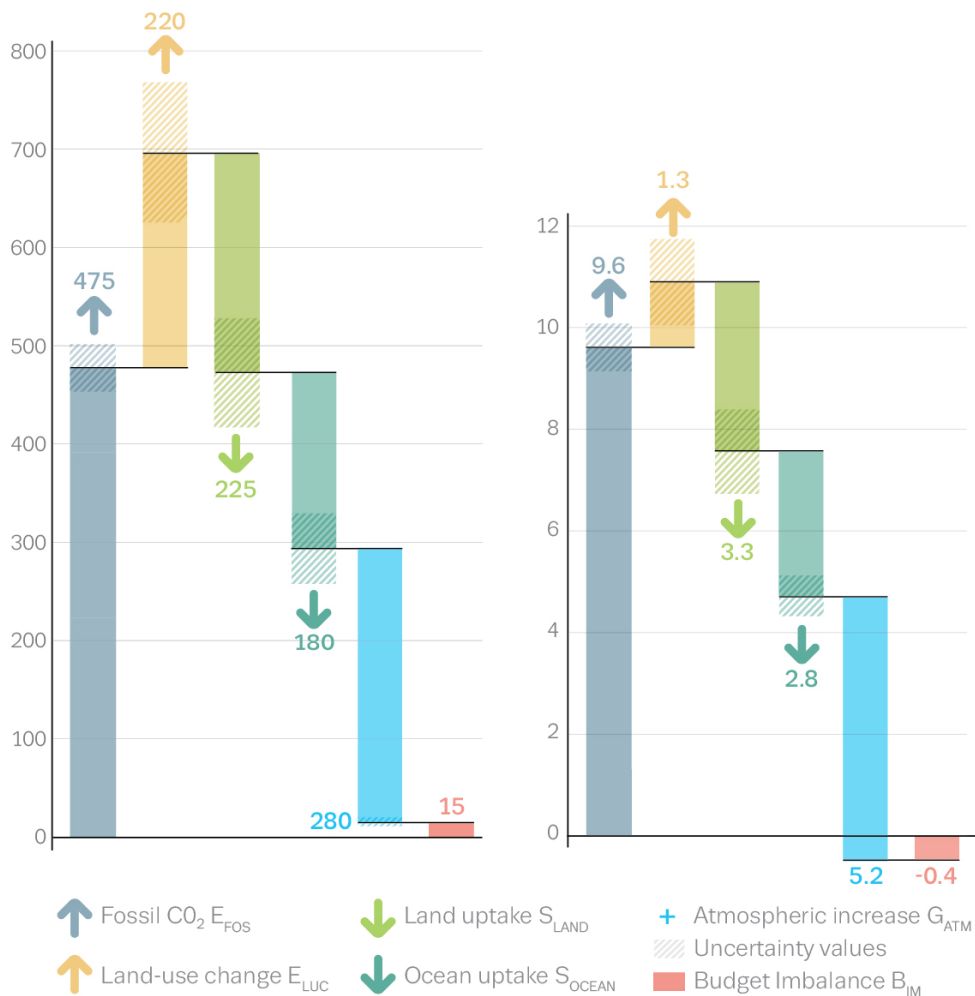
3339



Anthropogenic carbon flows

Cumulative changes 1850-2022 GtC

Mean fluxes 2013-2022 GtC per year



3340

3341 **Figure 15.** Cumulative changes over the 1850-2022 period (left) and average fluxes over the 2013-2022 period
 3342 (right) for the anthropogenic perturbation of the global carbon cycle. See the caption of Figure 3 for key
 3343 information and the methods in text for full details.

3344



3345

3346 **Figure 16.** Kaya decomposition of the main drivers of fossil CO₂ emissions, considering population, GDP per
3347 person, Energy per GDP, and CO₂ emissions per energy, for China (top left), USA (top right), EU27 (middle
3348 left), India (middle right), Rest of the World (bottom left), and World (bottom right). Black dots are the annual
3349 fossil CO₂ emissions growth rate, coloured bars are the contributions from the different drivers. A general trend
3350 is that population and GDP growth put upward pressure on emissions, while energy per GDP and, more
3351 recently, CO₂ emissions per energy put downward pressure on emissions. Both the COVID-19 induced changes
3352 during 2020 and the recovery in 2021 led to a stark contrast to previous years, with different drivers in each
3353 region. The EU27 had strong Energy/GDP improvements in 2022.

3354